# Modulation of polycyclic aromatic hydrocarbon toxicity by the human skin microbiome

**Inaugural-Dissertation**

**to obtain the academic degree**

**Doctor rerum naturalium (Dr. rer. nat.)**

**submitted to the Department of Biology, Chemistry, Pharmacy**

**of Freie Universität Berlin**

**by**

**Lisa Lemoine**

**from Berlin**

**2021**

This thesis was carried out at the Federal Institute for Risk Assessment (BfR) in Berlin under the supervision of Prof. Dr. Dr. Andreas Luch.

1st Reviewer: Prof. Dr. Dr. Andreas Luch

2nd Reviewer: Prof. Dr. Burkhard Kleuser

Date of defense: 09.12.2021

## Erklärung

Hiermit versichere ich, die vorliegende Dissertation mit dem Titel “ Modulation of polycyclic aromatic hydrocarbon toxicity by the human skin microbiome” ohne Benutzung anderer als der zugelassenen Hilfsmittel selbstständig angefertigt zu haben. Alle angeführten Zitate sind als solche kenntlich gemacht. Die vorliegende Arbeit wurde in keinem früheren Promotionsverfahren angenommen oder als ungenügend beurteilt.

Berlin, den 14.09.2021

Lisa Lemoine

Die Dissertation wurde in englischer Sprache verfasst.

## Danksagung

Ich möchte mich auf diesem Wege bei Prof. Dr. Dr. Luch für die Möglichkeit bedanken, meine Doktorarbeit am BfR mit dem Thema Hautmikrobiom in seiner Abteilung durchzuführen. Herr Luch hat mich stets bei meiner Arbeit unterstützt und mir Inspiration für weitere interessante Forschungsansätze gegeben.
Herrn Prof. Dr. Burkhard Kleuser danke ich für die Übernahme des Zweitgutachtens meiner Dissertation und seine Unterstützung.
Einen großen Dank möchte ich zudem Herrn Dr. Tralau aussprechen, der mich mit seinem Zuspruch und seiner großen fachlichen Kompetenz stets motiviert hat, auch in schweren Zeiten weiter fokussiert an meiner Dissertation zu arbeiten. Er hat mit seinen Ideen gerade in der Anfangsphase dieser Arbeit zu einem erfolgreichen Verlauf verholfen.
Auch Herrn Dr. Hutzler und Herrn Dr. Roloff möchte ich danken für die Einarbeitung in die gaschromatographische Analytik und Massenspektrometrie, sowie die Interpretation der resultierenden Datensätze.
Karsten Schön, Bettina Hoffman, Nils Dommershausen und Julian Tharmann möchte ich für die Hilfe im Labor sowie für die gute Zusammenarbeit danken.
Ich danke auch der gesamten Abteilung 7 für die spannenden und hilfreichen Diskussionen und allgemein für die motivierende Arbeitsatmosphäre am Institut. Ein besonderer Dank geht zudem an alle Weggefährten aus dem Großraumbüro, die sowohl fachlich als auch menschlich immer an meiner Seite standen. Im Besonderen möchte ich mich bei Tessa Höper bedanken, die durch Ihre Durchsicht meiner Präsentation und finale Korrektur vieler meiner Texte immer eine riesige Stütze für mich war. Auch Florian Padberg, Tony Bewersdorff, Rashad Haidar und Susanne Linke haben dazu beigetragen, dass ich immer gerne zur Arbeit gekommen bin. Zudem möchte ich mich bei den Praktikanten und Studenten bedanken, die mit ihrer wertvollen Arbeit das Projekt entscheidend vorangetrieben haben.

Zu guter Letzt war außerhalb der Wissenschaft auch mein Freund, Christoph Zimmer und meine gesamte Familie immer für mich da. Ihre Unterstützung bedeutet mir sehr viel. Insbesondere meine Mutter, Annegret Jatzkewitz, hat mir in den letzten Zügen der Anfertigung dieser Arbeit sehr geholfen.

# Table of contents

# Abstract

With approximately 2 $m^2$ the human skin is one of our largest organs and serves as the primary barrier against the external environment. As such, it is subject to environmental impacts and xenobiotic exposures. These include polycyclic aromatic hydrocarbons (PAH). Their ubiquitous occurrence results in constant human exposure, with many PAHs being suspected or established carcinogens. The best characterized model substance is benzo[*a*]pyrene (B[*a*]P) which is metabolized by eukaryotic cytochrome P450 dependent monooxygenases (CYPs) to form the highly mutagenic B[*a*]P-7,8-diol-9,10-epoxide (BPDE). Being environmental and industrial contaminants PAHs are predominantly addressed either for their environmental or toxicological fate. This includes their potential toxification and metabolism in eukaryotes as well as their microbial degradation in the environment. Yet, the latter is often driven by the PAHs potential to serve as a source of carbon and energy for microbial growth. With a plethora of underlying pathways this is as such of course also relevant for the human microbiome and the question of potential microbiome-mediated substance toxification. In preliminary work at the German Federal Institute for Risk Assessment (BfR), it could be shown that PAH-metabolism is indeed a ubiquitous feature of the human skin microbiome. Using batch enrichment and skin swabs from 11 volunteers a total of 21 pure cultures were isolated, all of which used B[*a*]P as their sole source of carbon and energy. Building on these results this thesis subsequently investigated the respective microbial PAH-metabolism and –toxification *in vitro* as well as assessing the potential host-impact and related microbiome-host interactions *in situ*.

To address these questions in more detail a total of 4 skin isolates were examined further. These included two representatives of *M. luteus*, one *B. licheniformis* and one *P. oleovorans*, respectively. Using carbon-limited cultures, we could show that these skin commensals convert B[*a*]P into a number of highly cyto- and genotoxic metabolites that are excreted in toxicologically relevant concentrations during growth. The respective bacterial supernatants contained a mixture of eukaryotic and prokaryotic metabolites, the combination of which led to synergistic cyto- and genotoxicity at levels clearly exceeding of what was induced by either the substances alone or a mixture thereof, respectively.

In order to assess the potential impact of this commensally triggered toxification on the human host we established a microbial competent skin tissue co-culture system. Being the first of its kind to investigate microbial substance toxification and its longer term effects on the skin and its commensals in a highly standardized manner under near *in vivo* conditions the prototype of this model consisted of MatTek's 3-D skin model EpidermFT™ colonized with *M. luteus*, *P. oleovorans* or a mixture thereof. The model was shown to maintain stable colony counts for prolonged periods of time, allowing the reliable study of

substance induced microbe-host effects. It could be shown that microbe-host interaction as such resulted in strong changes in the skin with regard to CYP-expression, microbiota-related expression of immunomodulatory domains, as well as cell growth, cell proliferation and skin differentiation. Altogether these and further results suggest commensal colonization to induce strengthening of the epidermal barrier.

Application of B[*a*]P to commensally colonized models led to the formation and accumulation of B[*a*]P-metabolites on the skin. The metabolites matched those previously identified in the respective carbon limited batch cultures with the most predominant one being the genotoxic B[*a*]P-7,8-dione. However, notably unmetabolized B[*a*]P as well as its metabolites penetrated the skin layers of the commensally competent models to a lesser extent due to a microbial- induced strengthening of tight junctions (TJ) and increased epidermal differentiation. Most importantly, the formation and penetration of the ultimate carcinogen BPDE was greatly reduced in the colonized models, which consequently led to lower formation of BPDE-DNA adducts.

Altogether the results demonstrate that albeit there is a high potential for microbial-induced PAH-toxification, further assessment of its respective effects on host biology and wellbeing requires complex model systems. Given the high species specificity of microbiomes any such systems have to be sufficiently species relevant as to avoid false predictions. Only few such systems exist with those available predominantly covering the gut. For skin this thesis is the first work that established a standardized and widely applicable commensal 3D-skin co-culture model to study microbiome-induced substance toxicity, using PAH as a proof of concept.

# Zusammenfassung

Die menschliche Haut ist mit ca. 2 $m^2$ eines unserer größten Organe und dient als primäre Barriere gegenüber unserer Außenwelt. Als solche ist sie Umwelteinflüssen sowie Xenobiotika direkt ausgesetzt. Zu Letzteren gehören polyzyklische aromatische Kohlenwasserstoffe (PAK), deren ubiquitäres Vorkommen zu einer konstanten Exposition des Menschen führt und von denen viele potentielle oder bestätigte Kanzerogene sind. Die am besten charakterisierte Modellsubstanz ist Benzo[*a*]pyren (B[*a*]P), das von eukaryotischen Cytochrom P450-abhängigen Monooxygenasen (CYPs) zu dem stark mutagenen B[*a*]P-7,8-diol-9,10-epoxid (BPDE) metabolisiert wird. Als Umwelt- und Industriekontaminanten werden PAKs überwiegend entweder auf ihr Umwelt- oder ihr toxikologisches Verhalten hin untersucht. Dies umfasst sowohl ihre potentielle Toxifizierung und ihren Metabolismus in Eukaryoten als auch ihren mikrobiellen Abbau in der Umwelt. Letzteres wird oft durch das Potenzial der PAKs, als Kohlenstoff- und Energiequelle für mikrobielles Wachstum zu dienen, angetrieben. Mit einer Fülle von zugrundeliegenden Stoffwechselwegen ist dies natürlich auch für das menschliche Mikrobiom und die Frage nach einer möglichen Mikrobiom-vermittelten Substanztoxifizierung relevant. In Vorarbeiten am Bundesinstitut für Risikobewertung (BfR) konnte gezeigt werden, dass der PAK-Metabolismus tatsächlich ein ubiquitäres Merkmal des menschlichen Hautmikrobioms darstellt. Mittels Batch-Anreicherung und Hautabstrichen von 11 Probanden wurden insgesamt 21 Reinkulturen isoliert, die B[*a*]P als alleinige Kohlenstoff- und Energiequelle nutzen können. Aufbauend auf diesen Ergebnissen untersuchte diese Arbeit den jeweiligen mikrobiellen PAK-Metabolismus und die Toxifizierung *in vitro* sowie die potenzielle Auswirkung auf den Wirt und die damit verbundenen Mikrobiom-Wirt-Interaktionen *in situ*.

Um diese Fragestellungen zu klären wurden vier repräsentative Hautisolate weiterführend toxikologisch untersucht. Darunter waren zwei Vertreter von *M. luteus*, ein *B. licheniformis* und ein *P. oleovorans*. Mit Hilfe von kohlenstofflimitierten Kulturen konnten gezeigt werden, dass diese Hautkommensalen B[*a*]P in eine Reihe hochzyto- und genotoxischer Metaboliten umwandeln, die während des Wachstums in toxikologisch relevanten Konzentrationen ausgeschieden werden. Die jeweiligen bakteriellen Überstände enthielten ein Gemisch aus eukaryotischen und prokaryotischen Metaboliten, deren Kombination zu einer synergistischen Zyto- und Genotoxizität führte, die deutlich über derjenigen lag, die durch die Substanzen allein bzw. deren Gemisch induziert wurde.

Um die potentiellen Auswirkungen dieser kommensal-induzierten Toxizität auf den menschlichen Wirt zu untersuchen, haben wir eine mikrobiell kompetente Hautgewebe-Co-kultur etabliert. Als eines der ersten seiner Art, um längerfristige Effekte des menschlichen Hautmikrobioms in einer hoch standardisierten Weise unter nahezu *in vivo* Bedingungen zu untersuchen, bestand der Prototyp dieses Modells aus

MatTek's 3-D-Hautmodell EpidermFT™, besiedelt jeweils mit *M. luteus*, *P. oleovorans* oder einem Gemisch aus beiden Organismen. Es wurde gezeigt, dass das Modell über längere Zeiträume stabile Koloniezahlen aufrechterhält, was die zuverlässige Untersuchung von substanzinduzierten Mikroben-Wirt-Effekten ermöglicht. Zudem konnte gezeigt werden, dass die Mikroben-Wirt-Interaktion als solche zu starken Veränderungen in der Haut hinsichtlich der CYP-Expression, der mikrobiotabezogenen Expression immunmodulatorischer Domänen sowie des Zellwachstums, der Zellproliferation und der Hautdifferenzierung führte. Insgesamt deuten diese und weitere Ergebnisse auf eine kommensal bedingte Stärkung der epidermalen Barriere hin.

Die Applikation von B[*a*]P auf die kommensal besiedelten Modelle führte zur Bildung und Akkumulation von B[*a*]P-Metaboliten auf der Hautoberfläche. Die Metaboliten stimmten mit denen überein, die zuvor in den jeweiligen kohlenstofflimitierten Batch-Kulturen identifiziert worden waren, wobei das genotoxische B[*a*]P-7,8-Dion vorherrschte. Allerdings drangen vor allem das unmetabolisierte B[*a*]P sowie dessen Metaboliten nur in geringerem Maße in die Hautschichten der kommensal kompetenten Modelle ein, was auf eine mikrobiell induzierte Stärkung der Tight Junctions (TJ) und eine erhöhte epidermale Differenzierung zurückzuführen ist. Besonders bedeutsam war die stark verminderte Bildung und Penetration des ultimativen Karzinogens BPDE was in der Konsequenz zu einer geringeren Bildung von BPDE-DNA-Addukten führte.

Insgesamt zeigen die Ergebnisse, dass es zwar ein hohes Potenzial für eine mikrobiell-induzierte PAK-Toxifizierung gibt, die weitere Bewertung der jeweiligen Auswirkungen auf die Wirtsbiologie und –Gesundheit jedoch komplexe Modellsysteme erfordert. Angesichts der hohen Speziesspezifität von Mikrobiomen müssen solche Systeme ausreichend speziesrelevant sein, um falsche Vorhersagen zu vermeiden. Es existieren nur wenige solcher Systeme, wobei die vorhandenen vorwiegend den Darm abdecken. Für die Haut ist diese Doktorarbeit die erste Studie, die ein standardisiertes und breit anwendbares kommensales 3D-Haut-Kokulturmodell zur Untersuchung der Mikrobiom-induzierten Substanztoxizität etabliert hat, wobei PAKs für den „Proof of Concept“ verwendet wurden.

# Abbreviations

All abbreviations occurring in the text, except for those used in the articles in Chapter 2, are listed in the following table.

| | |
|---|---|
| 2D | Two-dimensional |
| 3D | Three-dimensional |
| 5-FU | 5-fluorouracil |
| ACE-2 | Angiotensin-converting enzyme 2 |
| AhR | Aryl hydrocarbon receptor |
| AMP | Antimicrobial peptides |
| ARNT | Aryl hydrocarbon receptor nuclear translocator |
| B[*a*]P | B[a]P: Benzo[a]pyrene |
| B[*a*]P-tetrol | B[a]P-tetrol: B[a]P-r-7,t-8,t-9,c-10-tetrahydrotetrol |
| BfR | German Federal Institute for Risk Assessment (Bundesinstitut für Risikobewertung) |
| BPDE | Benzo[a]pyrene-7,8-diol-9,10-epoxide |
| BSTFA | N,O-bis(trimethylsilyl)-trifluoracetamide |
| CAMP | Cathelicidin-related antimicrobial peptides |
| CAR | Constitutive androstane receptor |
| CFU | Colony forming unit |
| COVID-19 | Coronavirus disease 2019 |
| CYP | Cytochromes P450 |
| DCM | Diclormethane |
| DMSO | Dimethyl sulfoxide |
| EDC | Epidermal differentiation complex |
| EPHX | Epoxide hydrolases |
| ERK | Extracellular signal–regulated kinase |
| EtOH | Ethanol |
| FGF | Fibroblast growth factors |
| FLG | Filaggrin |
| GAPDH | Glyceraldehyde 3-phosphate dehydrogenase |

| | |
|---|---|
| GC/MS | Gas chromatography–mass spectrometry |
| GI | Gastrointestinal |
| GST | Glutathione transferases |
| HEPES | 4-(2-hydroxyethyl)-1-piper-azineethanesulfonic acid |
| HGF | Hepatocyte growth factor |
| HMP | Human Microbiome Project |
| IGFBP | Insulin-like growth factor-binding protein family |
| IF | Intermediate filament |
| IL | Interleukin |
| INF | Interferon |
| IVL | Involucrin |
| JNK | C-Jun N-terminal kinase |
| LB | Lysogeny broth |
| MCP | Monocyte chemoattractant protein |
| MM | Minimal medium |
| NER | Nucleotide excision repair |
| PAH | Polycyclic aromatic hydrocarbons |
| PXR | Pregnane X receptor |
| REACH | Registration, Evaluation, Authorisation & restriction of Chemicals |
| reverse-BPDE | Benzo[a]pyrene-9,10-diol-7,8-epoxide |
| RIN | RNA-integrity |
| SARS-CoV-2 | Severe acute respiratory syndrome coronavirus 2 |
| SC | Stratum corneum |
| SULT | Sulfotransferases |
| TJs | Tight junctions |
| TLR | Toll-like Receptor |
| TAC | Transcriptome Analysis Console |
| XPC | Xeroderma pigmentosum, complementation group C |
| XPG | Xeroderma pigmentosum, complementation group G |

# 1. Introduction

## 1.1. The human skin

The human skin is one of our largest organs, covering an area of ~2 $m^2$. It is one of the few organs with large scale contact external environment and as such of particular importance as physical and metabolic barrier[1]. As such it protects us against dehydration, invasion by pathogens; UV radiation, chemicals, and mechanical injury.[2]. It comprises three layers, the epidermis, dermis, and the hypodermis, all of which vary significantly in terms of anatomy and function.

### 1.1.1. Epidermis

The epidermis is the external tissue layer providing a physical and permeability barrier, which is essential for survival of higher eukaryotes[3]. The epidermis mainly consists of keratinocytes in various stages of differentiation but also comprises non-epithelial cells, including antigen-presenting dendritic Langerhans cells as well as melanocytes and Merkel cells. Through the process of proliferation and differentiation, distinct layers are formed, the stratum basale, stratum spinosum, stratum granulosum, stratum lucidum, and stratum corneum (SC). The latter is the outermost layer of the epidermis, consisting of 10–30 layers of keratinized cell envelopes (corneocytes). The cornified envelope (CE) replaces the plasma membrane of differentiating keratinocytes and consists of keratins that are enclosed within an insoluble amalgam of proteins, which are cross-linked by transglutaminases and surrounded by a lipid envelope[3]. The latter is attached to the outer surface of the plasma membrane, which consists of a lipid-hydrophobic layer. Here, barrier lipids derived from lamellar bodies form an occlusive matrix between the corneocytes[4,5]. Deeper epidermal layers, including the stratum granulosum and stratum spinosum, are major producers of keratin filaments that provide structural support for the epidermis. Finally, the basal layer of the epidermis contains stem cells that proliferate under homeostatic conditions. The epidermis has no blood supply which is why its cells solely rely on intercellular diffusion for their nutritional support[6].

In this highly organized differentiation process the keratinocytes in the basal layer move to the spinous and granular layers, ultimately forming a tough multilayer of corneocytes. At the end of the keratinization process, keratinocytes can be found flat, nucleus-free and as highly keratinized squamous cells at the SC [4]. This terminal differentiation is driven by various cytokines and growth factors[7]. The complete turnover process takes about 28 days in total. Each of the different epidermal layers has different gene expression profiles leading to the expression of distinctive markers[8]. These proteins are part of the CE, which is formed

by cross-linking of soluble precursor proteins such as loricrin, involucrin (IVL), envoplakin and periplakin and filaggrin (FLG), that aggregates keratin Ifs forming a scaffold[3] (Figure 1).

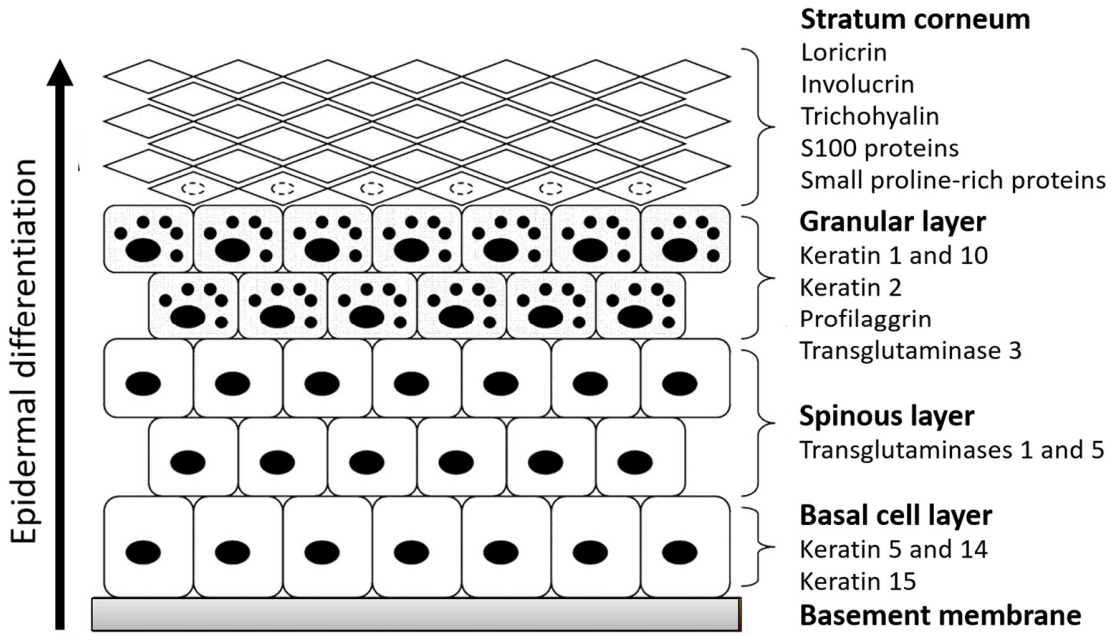


**Figure 1:** During epidermal differentiation keratinocytes progress upwards through the different epidermal layers (the spinous layer, granular layer and SC), becoming a nucleated and increasingly compacted in size. Each stage of epidermal differentiation is characterized by the expression of specific proteins, and examples of these are listed in the figure (modified from Sandilands, et al. [9]).

Keratins are the main components of the intermediate filament (IF) cytoskeleton of epithelial cells. The human genome contains 54 keratin genes which are arranged in two clusters. These are type I proteins which tend to be smaller and acidic and type II proteins which are larger and tend to be basic-neutral [10]. Pairs of a type I and a type II keratin are co-expressed in different epithelial cell types and differentiation stages, allowing heterodimerization and subsequent formation of cell type- and differentiation-specific supramolecular filaments. The type I K14 and type II K5 co-polymerize to form the prominent IF apparatus that occurs in the basal layer and related complex epithelia[11,12]. The pair of K1 and K10 form the main part of the cytoskeleton in the outer (suprabasal) layers of the epidermis [13]. Further essential skin barrier components are keratin-linked desmosomal junctions and tight junctions (TJs) between the cells, proteins cross-linked by transglutamination and protein-bound ceramides at the cell surface[14]. The stratified squamous epithelial cells in each layer are connected to each other via desmosomes and adherens[15]. In

addition to the physical protection of the skin barrier, TJ proteins, such as cadherin adhesion molecules and occludin proteins, play a role in the proliferation and differentiation of keratinocytes[16-18].

Futhermore, the lipids of the cornification layer play a significant role as gateway for the absorption of chemicals from the skin surface[19]. The most important pathway is selective absorption by the epidermis, where the lamellar, bilayer structure with opposite electrical charge of the extracellular lipids facilitates the dissolution of lipophilic substances. Nonpolar compounds with molecular weights below 500 Da readily penetrate the epidermis. The second but less frequently used route is the uptake of substances by skin appendages called the fast permeation pathway[20]. Notably this is also the entry point for many carcinogenic substances. The uptake of which can result in malignant degeneration. The ubiquitous and frequent exposure to such substances, together with direct UV radiation, makes the skin the most common site for tumor formation in the body[21].

### 1.1.2. Dermis and Hypodermis (Subcutis)

The dermis is a connective tissue layer located between the epidermis and the subcutaneous fat layer (subcutis)[5]. The dermis has a fibrous structure consisting of collagen, elastic tissue and other extracellular components, and contains vessels, nerve endings, hair follicles and eccrine sweat glands, apocrine sweat glands, and sebaceous glands. The role of the dermis is to support the skin and deeper layers, as well as to support heat balance and promote sensation. Fibroblasts are the primary cells within the dermis, but histiocytes, mast cells and adipocytes also play an important role in maintaining the normal structure and function of the dermis[22]. The latter is divided into two layers: the papillary dermis and the reticular dermis. The papillary dermis is the superficial layer that lies beneath the epidermis. It consists of loose connective tissue that is highly vascularized. The reticular layer is thicker and consists of dense connective tissue and contains blood vessels, nerve endings and skin appendages[23]. The collagen bundles and other connective tissue elements of the dermis blend with those of the hypodermis, creating an unclear boundary[24].

The hypodermis, also known as the subcutaneous tissue (adipocytes, nerves and blood vessels), is located under the reticular layer of the dermis and consists of a looser connective tissue. Generally, it merges with subcutaneous adipose tissue. Adipose cells form a layer of varying thickness depending on their location in the body, gender and nutritional status. The adipose tissue contributes to heat insulation and energy storage and acts as a shock absorber[24].

### 1.1.3. Skin models

Following the complete ban on animal testing for cosmetic ingredients in 2013, efforts to further develop and validate *in vitro* models for human skin have increased[25]. The simplest *in vitro* skin models are immortalized cell lines. The "Human adult low Calcium high Temperature" (HaCaT) cell line has been used extensively to study skin function and toxicity[26]. In contrast to other permanent cell lines, the spontaneously immortalized HaCaT cells from adult skin show a comparatively normal differentiation capacity and high immortality, which facilitates their experimental handling[27]. The cell line exhibits normal morphogenesis and functional activities of isolated keratinocytes[28]. On stimulation, it differentiates with the expression of specific markers. However, its gene transcriptional profile of CE-associated proteins is generally different from that of normal human keratinocytes (NHKs) which limits the use as a model system for skin development[29]. In contrast NHKs are isolated from normal human epidermis and exhibit the endogenous biochemical processes used *in vivo* by keratinocytes. However, in the two methods mentioned above the complexity of the skin is simplified as these are two-dimensional (2D) cell cultures, in which keratinocytes are grown as monolayers on solid flat surfaces covered by a cell culture medium. Yet, it is precisely this simplicity that makes such single well-defined cell type so attractive for cyto- and genotoxicity testing of substances, as they allow direct detection of cellular behavior using luminescence or fluorescence detection methods[30].

The complete structure and function of the skin as an organ depends on all layers and as such not all results and conclusions of 2D cell culture experiments are transferable to *in vivo* systems[31,32]. There is a lack of many features of a fully stratified epidermis that are important for physiologically relevant cell functions. This affects cellular responses ranging from morphology, proliferation, migration and differentiation to biochemical signaling as well as the underlying gene and protein expression[33]. The development and use of complex *in vitro* 3D tissue cultures thus becomes increasingly important for skin research. This applies in particular to complex issues such as regulation of wound healing, skin barrier function and skin-microbiome interactions.

While there is a long history of studying these aspects it is only since recently that sufficiently complex models for addressing questions of complex skin biology *in vitro* have become commercially available[34]. The simplest form of a 3D skin model is a model of an epidermis consisting of keratinocytes cultured on a membrane. Such systems are referred to as reconstructed human epidermis (RHE), with the most commonly used commercially available models being EpiDerm™ (MatTek Corp), EpiSkin™ and SkinEthic™ (a subsidiary of L'Oreal)[35]. These RHEs are already much more realistic than simple cell cultures although

still lacking cross-talk between fibroblasts and keratinocytes which is fundamental for promoting proper epidermal stratification, homeostasis, inflammatory response and wound healing[36].

More advanced full thickness skin models have an additional compartment, the dermal layer, generally formed by proteins from the extracellular matrix, such as collagen type I, and fibroblasts[37]. These *in vitro* models show a highly organized skin structure similar to that observed *in vivo.* Among the most widely used (and for regulatory purposes also partly pre-validated) full thickness models are the EpiDermFT™ (MatTek Corp.) and Phenion®FT (Henkel), which have been used for various applications, including: skin penetration[38,39]; effects of UV irradiation[40,41]; skin metabolism[42,43]; genotoxicity[44-46]; wound healing[47,48] and skin sensitisation[49].

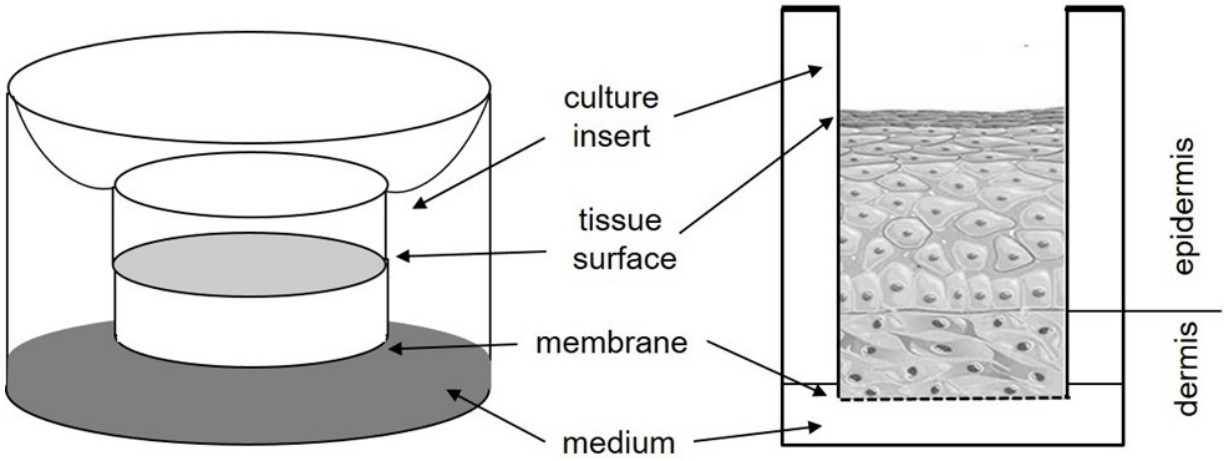


**Figure 2:** Schematic structure of the full-thickness skin model EpidermFT™ from MatTek**.** (modified from Kubilus, et al. [50] and Sanches, et al. [51])

MatTek's EpiDermFT™ system consists of normal, human epidermal keratinocytes (NHEK) and normal, human dermal fibroblasts (NHFB) derived from human neonatal foreskin cultured to form a multilayered, highly differentiated model of the human dermis and epidermis. The dermal compartment is composed of a collagen matrix containing viable human dermal fibroblasts, with keratinocytes cultured atop the dermal component to form the epidermis[52] (Figure 2). Both the epidermal and dermal layer are mitotically and metabolically active and exhibit *in vivo*-like morphological and growth characteristics which are uniform and highly reproducible. The cultivation at an air-liquid interface allows the application of cosmetics, drugs and chemicals to a dry surface. Furthermore it mimics an *in vivo* skin-like environment for microorganisms.

## 1.2. The human skin microbiome

Like any other part of our body that is exposed to the external environment, the human skin is harboring a diverse microbiota, consisting of bacteria, fungi and phages with mostly commensal properties. The composition and stability of the microbial community depends on the specific characteristics of the colonized skin region[53]. The skin offers a variety of distinct ecosystems, which create conditions conducive to different subsets of organisms [54].

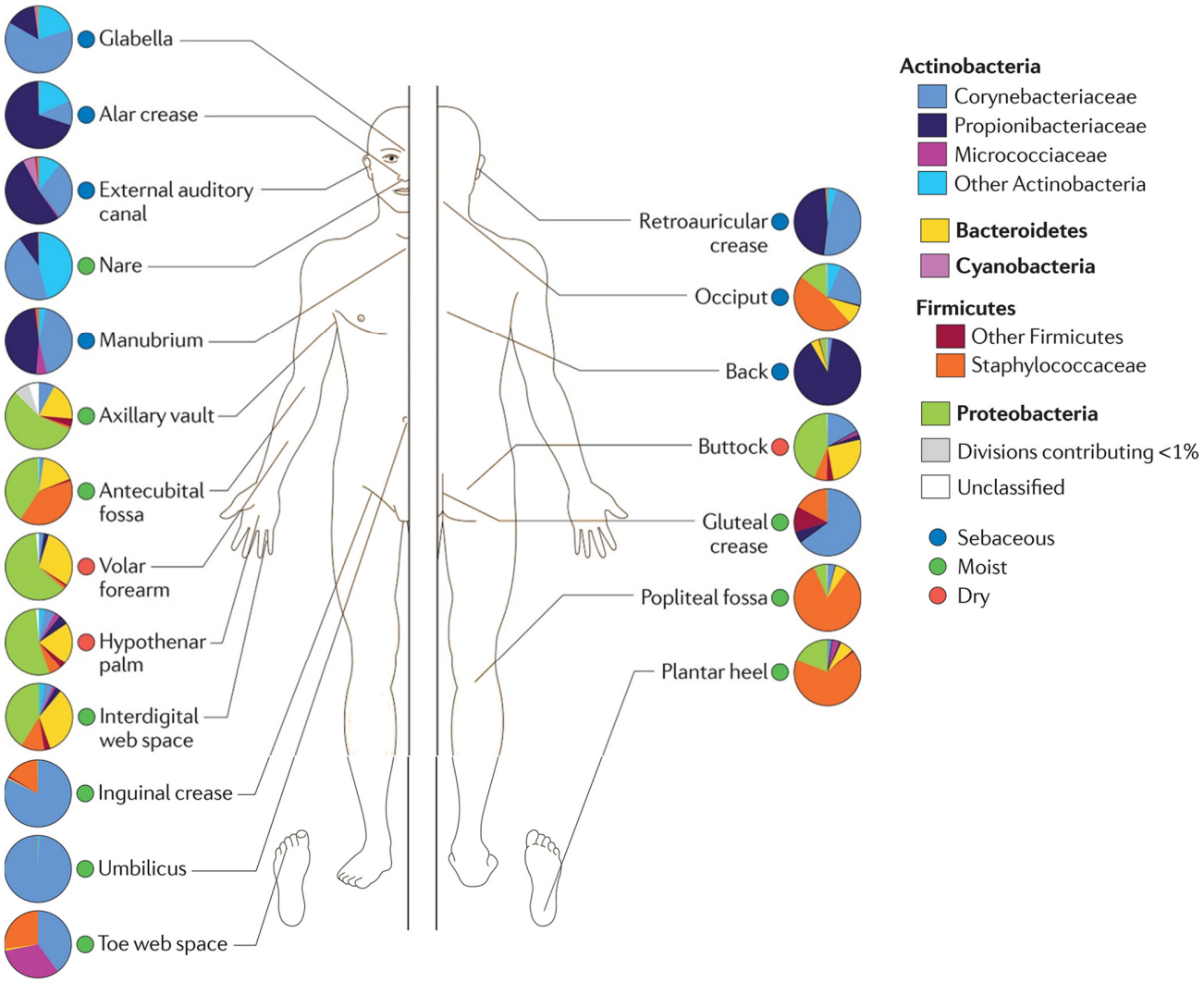


**Figure 3:** Topographical distribution of bacteria on skin sites (modified from Grice and Segre [55]).

The particularity of the skin as an ecosystem is that ecologically very different areas are located in the immediate vicinity, such as the hairy moist armpit and the mostly hairless dry upper arm. Depending on

the nature of a skin region, the species present are similar in nature, with Cutibacterium, Staphylococcus and Corynebacterium predominating in seborrheic areas. In moist areas, Proteobacterium and Staphylococcus are most abundant, and in dry areas the species are most diverse[53]. The majority of the skin microbiota can be assigned to the four phyla Actinobacteria, Firmicutes, Proteobacteria, and Bacteroidetes, with the number of species being identified increasing steadily[55]. This is mainly due to the late improvement of sequencing strategies and cultivation-based approaches [56].

Depending on their residential status the skin microbiota can be divided into two groups. The resident microbiota is a conserved microbial community which resides permanently on the host and will reestablish itself when disturbed. These organisms are often commensal and as such often beneficial for the host. Contrastingly transient microbes often do not establish permanently on the surface but originate from the environment and will only persist from hours to days [57]. While the vast majority of these transient co-habitants will be non-pathogenic some species can become harmful to the host, for example if skin barrier function is disrupted or in case of compromised immuncompetence[58].

Significant variability has been observed between different individual's microbiomes[59]. Many factors, including age, diet, antibiotic use, geographical location and host genetic constitution, contribute to this variability[60-63]. Poor diet and antibiotic use mostly decrease microbiomes diversity, especially in elder people. In addition, the amount of beneficial gut bacteria is reduced with consumption of low-fiber diets[64]. Reduction in microbiome diversity or dysbiosis can lead to compositional alteration at various taxonomic levels that have been associated with inflammatory bowel disease, Crohn's disease, asthma, rheumatoid arthritis, multiple sclerosis, obesity, metabolic syndrome, cardiovascular diseases, cancer, neurodegenerative and neuropsychiatric diseases[65]. This also applies to popular skin diseases[66].

The majority of the skin microbiota colonizes the surface of the skin[67]. However more and more studies show a colonization of deeper layers as well, indicating a well-conserved dermal community that is functionally distinct from the epidermal community[68,69]. Notably skin is a rather nutrient-scarce habitat, with amino acids, steroids, lipids and sugars from the SC being the only available sources for carbon and energy, though tightly controlled. As in soil and other nutrient poor-ecosystems this situation selects for the use of external sources for microbial growth such as xenobiotics [56].

### 1.2.1. Role of the skin microbiome in human immune function

The rise of new techniques such as 16S and whole genome metagenomic shotgun sequencing and culture-independent approaches has provided a deeper understanding of the composition of our microbiome and its contribution to health and disease[70-72]. These analysis have shown that commensal microbes play a

pivotal role in the regulation of metabolic, endocrine and immune function[73]. They provide essential capacities for the fermentation of undigested polysaccharides and are important for the synthesis of essential vitamins (e.g., vitamins B3, B5, B6, B12, K and biotin) as well as amino acids (e.g., methionine or tryptophan)[74]. In addition, the presence of commensal bacteria is crucial for maintaining a healthy environment: in the skin, this is firstly due to the production of antimicrobial factors important for immune tolerance and defense against microbial pathogens[75,76]. The phenol-soluble modulins secreted by the commensal *S. epidermidis*, for example, have an antibiotic effect on *S. aureus*[77]. Commensals can also hydrolyze lipids that are secreted from sebum glands to free fatty acids. The latter have an intrinsic antibacterial effect against various gram-positive bacteria[78].

On the other hand skin commensals stimulate hosts adaptive immune response. This occurs through commensals control of the expression of various innate immune factors, including antimicrobial peptides (AMPs), as it has been shown for the best characterized commensal bacteria, *S. epidermidis*[79-82]. Major AMPs in the skin are β-defensins and cathelicidin which are released by keratinocytes to kill or inactivate a diverse range of skin pathogens[83-86]. However, for the resident epithelial and immune cells, it is difficult to distinguish between dangerous pathogens and commensals and to react accordingly. Therefore, complex regulatory mechanisms have evolved to enable delicate coordination between host tissues and their resident microbiota (immune tolerance)[18].

The development of immune tolerance of the skin already begins in the postnatal period when T-reg cells start to express the pathogen-specific transcription factor FOXP3, which coincides with colonization by commensals[87]. Later in development, SCFAs can act on the skin-resident T-reg pool, leading to increased numbers of skin-resident IL-10-producing Foxp3+ T-regs, similar to what is known for the gut[88]. More importantly, the continued presence of skin commensals promotes the induction of homeostatic immune responses dominated by the accumulation interferon (IFN)-γ- and interleukin (IL)-17A-producing T cells[89,90]. The IL-17A secretion can be both beneficial for skin homeostasis and host defence, but is also considered as a major player in the etiology of skin inflammatory disorders including psoriasis[91,92]. This increased ability of T-cells to release IL-17A is dependent on the interleukin IL-1α and IL-1β[93]. These cytokines are able to induce the expression of AMPs, as well as activate dendritic cells (DC) and promote B-cell maturation and clonal expansion[94-98]. In healthy skin, keratinocytes constitutively synthesize both pro-IL-1α and pro-IL-1β but cannot process or secrete them in their active form. The activation depends on the microbiota, that is, the sensing of pathogen-associated molecular patterns (PAMPs) such as bacterial flagellin or host-derived danger-associated molecular pattern (DAMP) including

lipopolysaccharides (LPS) from the cell wall of gram negative organisms[99]. These structurally conserved molecules derived from microbes are recognized by pattern recognition receptors (PRRs) including toll-like receptors (TLRs), which are expressed on the surface of many cells[100]. Concomitantly to this above mentioned indirect AMP induction, commensal microbes secrete molecules which act directly as TLR ligands. For example, *S. epidermidis* secretes several small molecules that act as TLR2 and EGFR agonists and stimulate the production of AMPs that are effective against group A. Streptococcus and *S. aureus*[80]. Lai, et al. [79] found an additional mechanisms by which commensals reduce inflammation during wound healing by regulating TLR3-dependent inflammation. Additionally, wound healing may be promoted by commensals through the induction of tissue repair genes such as VEGFA, FGF and PDGF of $CD8^+$ T-cells[89].

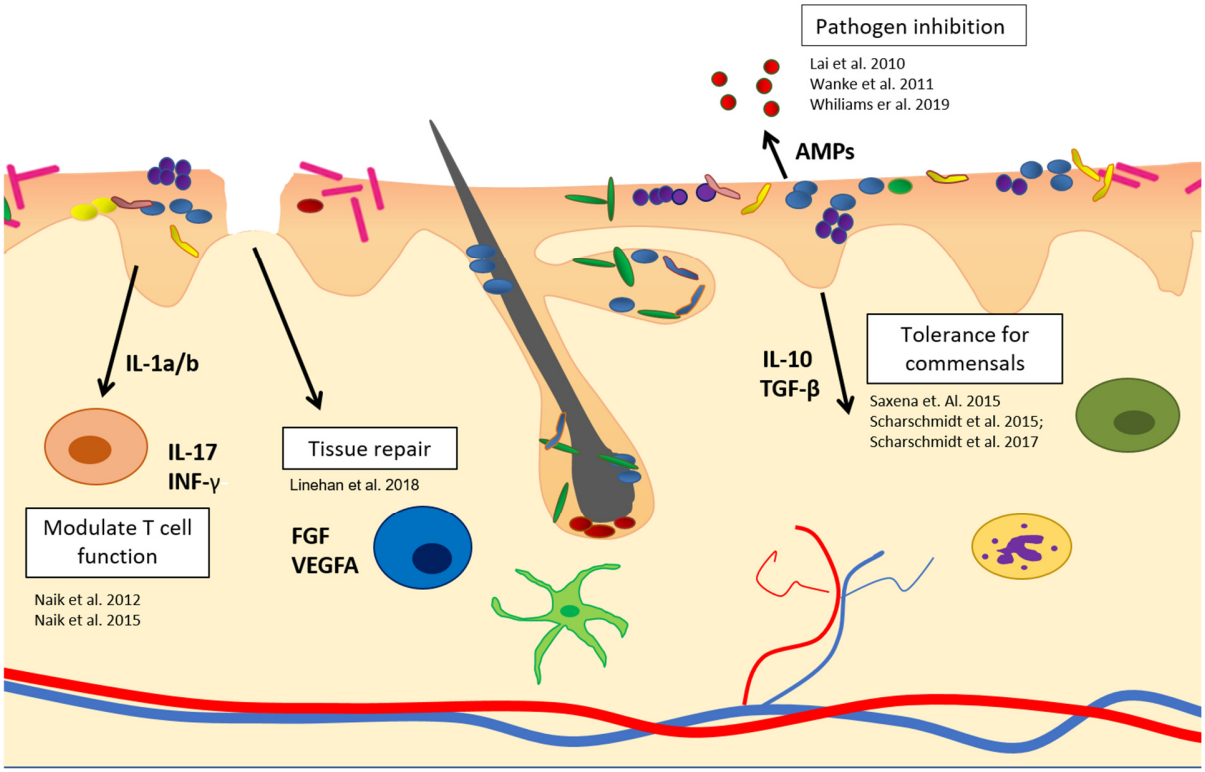


**Figure 4:** Summary of the influence of the skin commensal on cutaneous immunity described in this section. The brown cell represents an IL-17-producing T cell, the blue a CD8+ T cell and the green a T-reg cell. The green cell with the cell extensions represents a DC and the cell with the inclusions represents a Langerhanz cell. In addition, various skin bacteria and a wound in the skin are shown as examples (modified from a presentation of Elizabeth Grice 2019 at the Society for Investigative Dermatology; and Linehan, et al. [89]).

As summarized by Belkaid and Segre [101] the skin microbiota can also increase the expression of components of the complement system, which is composed of a large number of proteins that react with

one another to opsonize pathogens. Remarkably, AMPs, the complement system and IL-1 all represent ancient arms of the innate immune system, suggesting that these pathways may have originated as early mediators of skin-host interaction[101].

TLRs are a class of proteins that play a key role in the innate immune system consisting of 10 subclasses in humans TLR1 to TLR10. TLRs initiate a series of downstream signal cascades that activate cellular processes including the production of cytokines, chemokines, and other inflammatory mediators[102]. All TLRs activate a common signalling pathway that drives the activation of nuclear factor–κB (NF-κB) transcription factors, as well as the mitogen-activated protein kinases (MAPKs) extracellular signal–regulated kinase (ERK), p38, and c-Jun N-terminal kinase (JNK) [103]. In contrast to an inflammatory TLR response after pathogen colonization, recognition of commensal bacteria by TLRs is important for limiting inflammation. In fact, this interaction plays a crucial role in resistance to epithelial injury[104,105].

Overall, commensal bacteria exhibit both pro-inflammatory and anti-inflammatory activities, either being important for maintaining host-microbe homeostasis[106]. Through these mechanisms, commensals help keratinocytes to respond more efficiently to pathogenic invasion and thus play an important role in the defense against bacterial and viral infections[107].

### 1.2.2. The microbiome in xenobiotic metabolism

Chemicals and particularly xenobiotics including environmental pollutants can be harmful to human health and in the long term contribute to the development of diseases such as cancer[108]. However, the extent of impairment varies for each individual. This is also observed epidemiologically. Notably with regard to xenobiotic metabolism and detoxification the observed variability cannot be explained by genetic inter- and intraindividuality alone[109]. The Human Microbiome Project (HMP) has shown that this differences can be additionally influenced by the human microbiota. This impact may occur directly through transformation of xenobiotics or their metabolites by microbial enzymes or indirectly by affecting the expression of host metabolic genes, interference with the host's detoxification mechanisms and changing the xenobiotic bioavailability[109,110].

Direct biotransformation of xenobiotics often occurs through flavoreductases, oxidoreductases, mono- and dioxygenases as well as dehalogenases, hydrolases, azoreductases, nitroreductases, glucuronidases, sulfatases, and lyases[74,111]. Gut microbial xenobiotic metabolites are known to have altered bioactivity, bioavailability, and toxicity[112]. Additionally, they can interfere with the activities of human xenobiotic-metabolizing enzymes thus affecting the fate of other molecules[109,113]. The majority of human microbiota-

xenobiotic interactions occur within the gastrointestinal (GI) tract. Given the immense metabolic versatility of the gut microbiome it hence comes as little surprise that some reports point out that the intestinal microbiota metabolizes xenobiotics to a greater extent than any human organ[112].

Historically, studies have focused on the microbial metabolism of pharmaceuticals, with an emphasis on its influence on drug efficacy[74,114]. In this regard, some studies have shown a microbe-induced increase in drug toxicity[110]. According to AstraZeneca, up to 37 % of drug candidates are susceptible to microbial metabolism and recent research indicates that intestinal microbes are able to metabolize more than 170 orally administered drugs[115-117]. Pharmaceuticals toxified by microbes include acetaminophen, balsalazide, chloramphenicol, indomethacin, irinotecan, nitrazepam, olsalazine, phenacetin, risperidone, sorivudine, brivudine and sulfasalazine (nicely summarized by Koontz, et al. [110]). The antiviral drug brivudine, for example, is metabolized by both the host and its gut microbiota to bromovinyluracil, the latter exerting hepatic toxicity. Using germ-free mice Zimmermann, et al. [118] found that 70 % of brivudine toxicity is due to the gut microbiota. In the 1990s this strong influence of microbial metabolism on the detoxification of brivudine proved to be tragically fatal for 18 cancer patients relying on the analog antiviral drug sorivudine in combination with the anticancer prodrug of 5-fluorouracil (5-FU) for treatment. Later studies showed that the combination of these two drugs leads to a fatal accumulation of 5-FU. The likely cause for this is block of 5-FU detoxifying liver enzymes microbial sorivudine metabolites[119].

However, the course of the currently rampant coronavirus infection (COVID-19) caused by severe acute respiratory syndrome coronavirus 2 (SARS-CoV-2) is also suspected to be influenced by the human microbiome[120]. The GI tract has been shown to influence the propensity for COVID-19 infection and possibly its severity[121]. The protein angiotensin-converting enzyme 2 (ACE-2) is a key receptor for COVID-19 virus entry. Studies in mice have shown that the gut microbiome can influence the expression of the ACE-2 receptor and that the presence of certain species correlates with the severity of infection[122,123]. Consequently, the infection progression of COVID-19 may also be impacted by intestinal microbiome dysbiosis, which is common in older, obese people and those with underlying chronic diseases[124].

### 1.2.3. The microbiome and the skin barrier

Over the past decade, researchers have uncovered evidence of extensive communication between bacteria and skin cells. These interactions help to reinforce, repair but also destroy the barrier formed by the skin. Functionally this barrier consists of four different compartments: the physical, chemical, immunological and microbial skin barrier[125]. The three latter are described in detail in Chapter 1.2.1. In short the microbial barrier represents a barrier for pathogenic microorganisms[101]. By releasing of AMPs,

SCFAs, and polyamines the skin microbiota influences and primes the immune barrier. The skin´s chemical barrier depends on its acidic surface pH, which is affected by bacterial lipases creating free fatty acids[126]. Changes in the skin microbiota are associated with various skin diseases such as atopic dermatitis, acne, and psoriasis[127-130]. Many of these diseases are related to a disturbed physical skin barrier[131]. Recent studies show an important role of commensals in epidermal differentiation, which highly influences the skin's physical barrier strength [132]. Such a microbiota-associated modulation of epidermal differentiation has been examined by Meisel, et al. [133] using animal experiments that have shown strong alterations of gene expressions of the epidermal differentiation complex (EDC). More recently, Uberoi, et al. [134] discovered that the microbiota is required for proper epidermal barrier differentiation and repair in an AHR-dependent manner. This agrees with results from Landemaine, et al. [135], who showed, using 3D skin models with cells of human origin, that skin barrier strengthening is caused by *S. epidermidis* colonization, the effect was further enhanced by the use of a multiple commensal. In a similar experimental design Loomis, et al. [136] confirmed the latter results and further demonstrated that the mixture of selected commensals influences the thickness of the epidermal layer, the number of actively proliferating cells and the FLG expression.

Add to that, an increasing number of experiments found out that bacteria, more familiar from the intestine, are also able to reinforce the skin barrier[137-139]. This implies that living organisms, their lysates and their culture supernatants are becoming increasingly popular in the cosmetics industry as ingredients in products for the treatment of skin diseases or for normal skin care[140-142]. Among others, a Berlin-based company called BELANO Medical AG produces microbiotic skin care products.

### 1.2.4. Microbiota-skin models

The skin surface and associated appendages are home to a significant biomass of colonizing micro-organisms, with each square centimeter being home to ~$10^8$ metabolically active microbes[55,143]. Although there is more and more evidence that this colonization plays an important role in various aspects of skin functions, sterile skin models are still largely used to investigate biological processes of the skin as well as in skin toxicity studies[74,144]. This is mainly due to the lack of suitable models commercially available[125].

So far, our knowledge of the critical functional role of the microbiota in skin homeostasis has mainly been derived from animal experiments. The recolonization of germ-free mice with various commensals has highlighted the importance of an intact microbiota for the barrier function of the skin[133,134,145]. However, the available animal models are scarce, ethically questionable, difficult to handle, and suffer from questionable transferability[146,147]. The latter is due, among others, to strong differences in gene expression

and composition of barrier-related structural proteins in humans and mice, species specificity of the microbiota, and marked variations between skin-derived mouse and human AMPs[146,148,149]. This highlights the need for the use of *in vitro* models of human origin.

Since the turn of the century, many *in vitro* studies have been conducted on the influence of the microbiota on the skin, primarily focusing on the mechanism of microbial pathogeneses. In the simplest of these models, bacterial inversions were simulated by the use of endotoxins. In some cases, more complex models were used, in which living pathogens were applied into the culture medium of human cell lines[150,151]. A step closer to *in vivo* skin was the SC model from van der Krieken, et al. [152] in which the skin microbes are cultivated on dead corneocytes. This model comes closer to the *in vivo* situation, at least structurally, but lacks the interaction of the microbes with the living keratinocytes and fibroblasts.

So far there are only few studies relying on 3D skin models for studying aspects of microbiome biology and those that do usually address very specific aspects of microbial pathogenicity, e.g. with regard to wound healing[153,154]. One of the first studies reported that *Candida albicans* strains penetrate the protective layer of keratinocytes in *in vitro* reconstructed human skin and invade through the epithelial cell layers[155]. Further studies integrated individual commensals to determine their influence on pathogens. These studies used 3D skin models colonized with skin commensals (e. g. S. epidermidis) and bacterial pathogens (e. g. S. aureus) for up to 72 hours, revealing that commensal and pathogens initiate differential innate immune responses[154,156,157]. However, studies focusing on the role of commensals are still much rarer, although commensals have been shown to be crucial for the homeostasis of cutaneous immunity, and the overall cutaneous gene transcription[133,158]. One of the first studies of this type was the colonization of a tissue engineered human skin equivalent with predominant commensal members of the cutaneous microbiota by Holland, et al. [156]. Like a later study from Bojar [143], who colonized a 3D skin model with complex skin swabs, the bacterial cultures were stable, however, no further attention was paid to possible resultant changes in the skin or microbial-host interactions.

## 1.3. Polycyclic aromatic hydrocarbons

Epidemiological as well as toxicological evidence indicates that exposure to environmental pollutants and xenobiotics is one of the many factors contributing to the development of various health disorders in humans [111]. The toxicity of such pollutants can be altered by microorganisms. This is also true for polycyclic aromatic hydrocarbons (PAHs)[159]. The latter form a group of planar organic compounds consisting of two or more condensed benzene rings. These rings can be linear, angular, or arranged in clusters [160]. There are more than 100 different PAH compounds formed by incomplete combustion of organic matter[161]. PAHs occur naturally in the environment in fossil fuels such as coal, oil, and tar, or can be man-made from the extraction of coke and gas from coal, wood treatment processes, and the combustion of fuels and wastes[162,163]. Additionally, tobacco smoke is a significant source of PAH exposure for smokers and passive smokers[164]. However, PAHs are also found in consumer products (various rubber and plastic products, toys, or cosmetics) and in smoked, grilled, and fried foods[165,166]. With deposition, they are carried onto and into the soil, where they can be detected over large areas. This results in continuous human exposure to low to moderate levels of PAHs through the respiratory tract, digestive system and skin. The latter is a major absorption pathway due to direct contact with PAH-containing materials or indirect contact with contaminated work clothing or particulate skin debris[167].

The physical and chemical properties of PAHs vary depending on the number of benzene rings. Chemical reactivity, water solubility, and volatility decrease as the number of condensed benzene rings increases[168]. As a result, PAHs vary in transport, distribution, and fate in the environment and in their effects on biological systems. Their persistence in the environment is primarily due to their low water solubility and adsorption to solid particles. Moreover, higher molecular weight PAHs, which include compounds such as B[*a*]P with more than four benzene rings, tend to be potentially genotoxic [169,170]. The United States Environmental Protection Agency (EPA) has classified 16 PAHs as priority pollutants based on their cytotoxicity and genotoxicity[171] (Figure 5). The classification ranges from confirmed to probable to possible human carcinogens[172]. Because of their carcinogenic effects, many PAHs are classified as CMR (carcinogenic, mutagenic, reprotoxic) substances according to the European Chemicals Legislation “Registration, Evaluation, Authorisation & restriction of Chemicals” (REACH). The best studied model substance of a carcinogenic PAH is B[*a*]P[173].

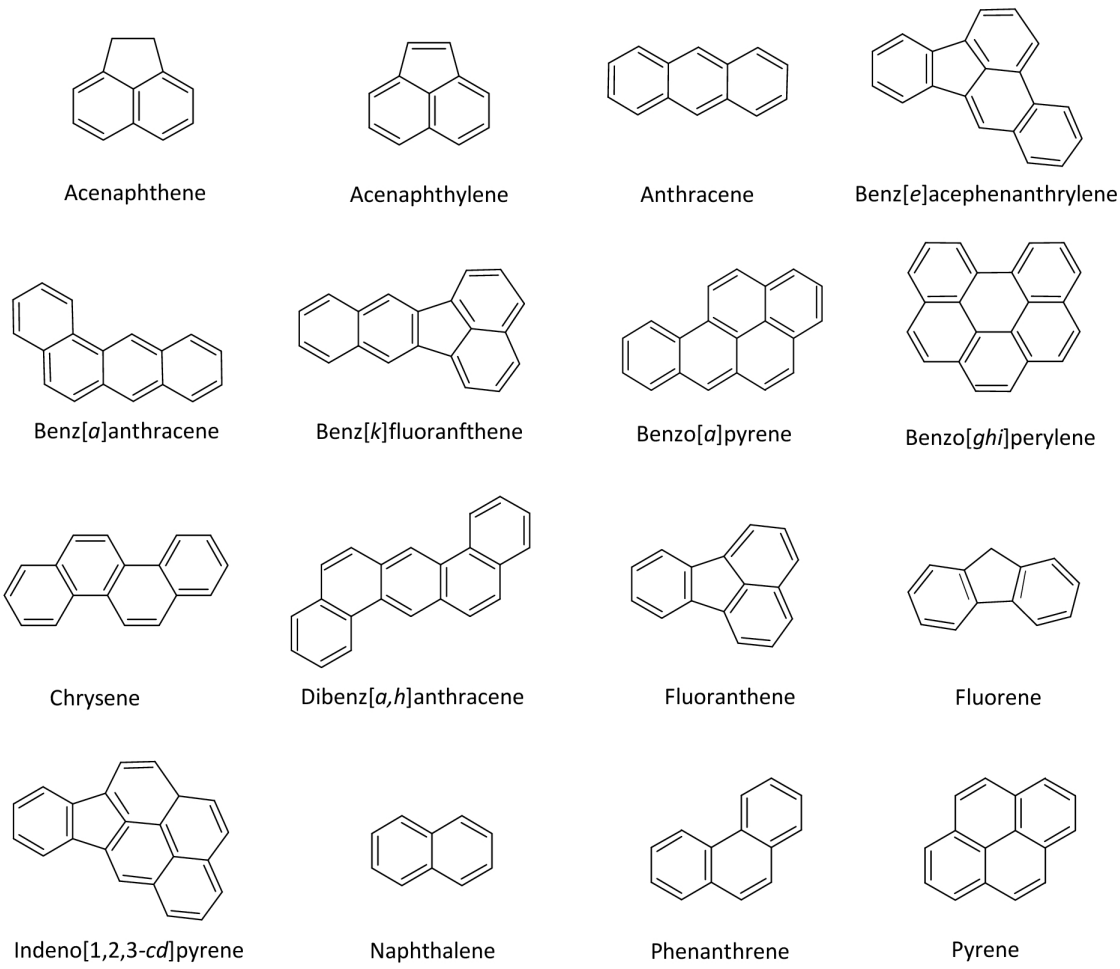


**Figure 5:** Chemical structure of the 16 representative polycyclic aromatic hydrocarbons (PAHs) in alphabetical order classified as priority pollutants based on their cytotoxicity and genotoxicity by the United States Environmental Protection Agency (EPA) (modified from Honda and Suzuki [174])

Early indications of the genotoxic and carcinogenic potential being relevant for humans go back as far as 1775, where an increased incidence of testicular cancer was recorded in chimney sweeps[175]. In the early 20th century a human epidemiological study reported increased lung cancer mortality among workers in coal coking and gasification processes with high PAH exposure[176]. Later studies in the United States and the Netherlands in the 1970s and 80s confirmed this for coal miners and tile roofers[177,178]. Today, the industries with the highest dermal B[*a*]P exposition are the primary aluminum sector and coke oven workers with exposures of 2 to 34 ng/cm² and 55 ng/cm$^2$ to 106 ng/cm$^2$, respectively [179,180].

In 1991, the long-term average daily intake of B[*a*]P across all possible intake routes by the general population in the United States was approximately 2.2 µg per day[181].

In the environment, PAHs typically occur as mixtures covering a spectrum from non-toxic compounds to potent carcinogens which makes attributing health risk to a specific PAH in epidemiological studies is very difficult[173]. In contrast, the carcinogenicity of certain PAHs in laboratory animals is well established. Increased incidences of skin, liver, lung, breast, ovaries, hematopoietic tissue, stomach and sarcomas occur in experimental animals at the respective injection sites or after oral administration[182-186]. Some PAHs also affect the hematopoietic and immune systems and may have reproductive, neurological, and developmental effects[187-190].

### 1.3.1. Eukaryotic metabolism of polycyclic aromatic hydrocarbons

PAHs are highly lipid-soluble and thus readily absorbed from the skin and the GI tract of mammals depending on the route of exposure[180]. They are rapidly distributed in a wide variety of tissues with a marked tendency for accumulation in body fat[191]. Most of the PAHs are not carcinogenic themselves, but are activated in the eukaryotic metabolism, so that they exert toxic effects[192].

In general, biotransformation can be divided into two phases[193]. In phase-I, polar functional groups (e.g., -OH, -SH, or -$NH_2$) are introduced into the substrate by oxidation, reduction, or hydrolysis, or existing functional groups are modified so that the substrate becomes hydrophilic. In phase-II the corresponding molecules/metabolites are conjugated via functional groups to form more water-soluble molecules[194]. The respective functional groups are usually added by transferases and comprise glucuronyl, methyl, acetyl, sulfonyl, and glutathione groups[195]. The stepwise transformation facilitates the elimination of the respective substrates. Among the most important representatives of phase-I metabolism are the CYPs, which catalyze the oxidation of many endogenous and exogenous compounds[196]. Almost all cells in the human body are capable of metabolizing xenobiotics. This includes the skin, which plays a crucial role in detoxifying xenobiotics, but also activating of pro-toxic substances due to its direct contact with the environment[197]. Human skin is known to express several CYPs (e.g., CYP1B1, CYP1A1, CYP2B6, CYP2D6, CYP2E1, CYP3A4, and CYP2S1). The corresponding metabolism occurs in the epidermis, i.e., epidermal keratinocytes[198].

The activation of PAHs is catalyzed mainly by CYPs[199]. In particular, B[*a*]P is metabolized primarily by CYP1A1, CYP1B1 and to some extent by CYP1A2, , CYP2C9, and CYP3A4[200,201]. There are several nuclear receptors that lead to activation of CYPs by binding of various chemicals. These include, the aryl hydrocarbon receptor (AHR), the pregnane X receptor (PXR), and the constitutive androstane receptor

(CAR), which belong to the nuclear receptor superfamily[202]. Although originally characterized in the liver, the AHR pathway has been shown to also play an important role in regulating xenobiotic responses in extrahepatic tissues such as the skin[203]. The AHR is a ligand-activated transcription factor that dimerizes with its DNA-binding partner AHR nuclear translocator (ARNT) to regulate a number of xenobiotic metabolizing genes such as CYPs and UDP-glucuronosyltransferases (UGTs)[204].

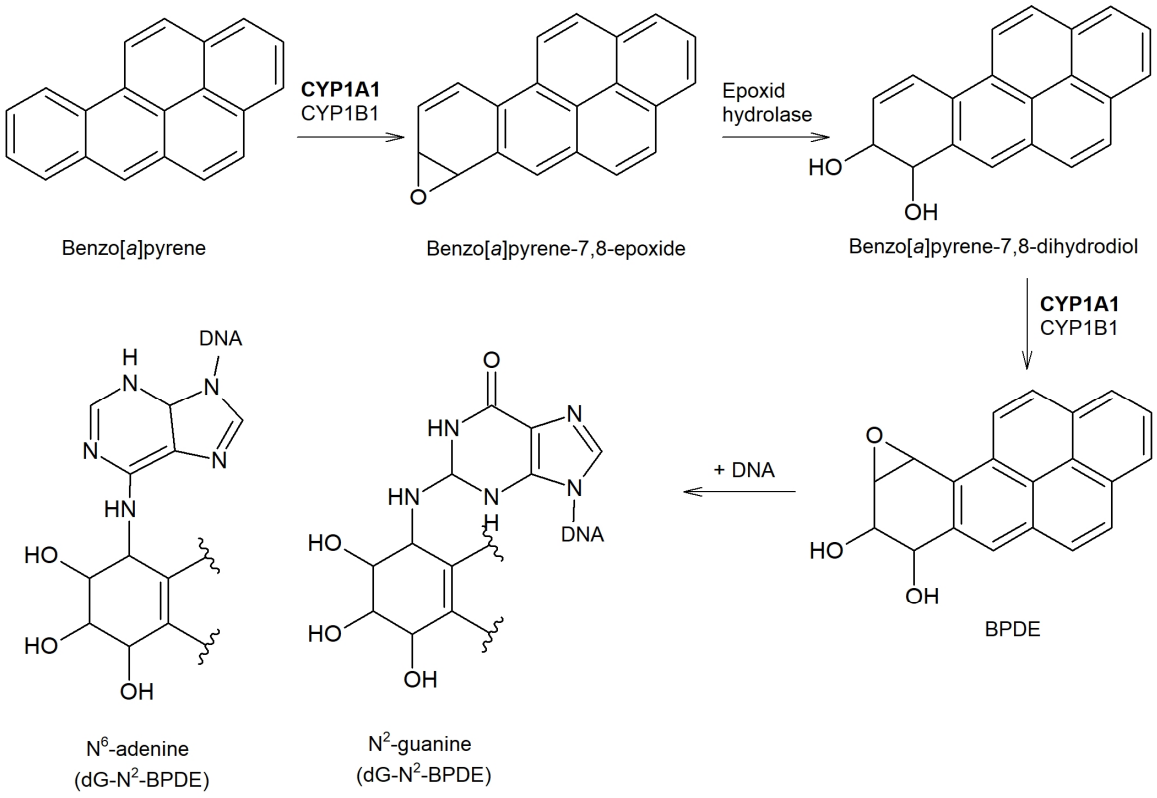


**Figure 6:** Eukaryotic metabolism for the activation of B[*a*]P (modified from Moserova, et al. [205]).

In human B[*a*]P metabolism, various phenols, dihydrodiols, diones as well as diolepoxides are formed enzymatically in a stepwise manner. The bioactivation can either begun with the formation of unstable arene oxides, which can be converted to the phenols 3-, 7-, 9-OH-B[*a*]P or with its oxidation to B[*a*]P-2,3-, 4,5-, 7,8- and 9,10-epoxides by CYP1A1 and CYP1B1[46]. These epoxides can be further metabolized by the microsomal epoxide hydrolase (mEH) to the corresponding B[*a*]P-4,5-, 7,8- and 9,10-dihydrodiols. The epoxidation of the B[*a*]P-7,8-dihydrodiol leads to the formation of the ultimately reactive species B[*a*]P-7,8-dihydrodiol-9,10-epoxide (BPDE) (Figure 6)[192,206] . In human metabolism, about 10 % of the B[*a*]P is metabolized to BPDE[207]. This so called "bay region" epoxide is highly active and can react with DNA,

forming adducts preferentially at guanine residues, namely 10-(deoxyguanosin- N2 -yl)-7,8,9-trihydroxy-7,8,9,10-tetrahydrobenzo[a]pyrene (dG- N2 -BPDE)[208,209]. In this regard, cis- or trans-opening of the epoxide ring of BPDE by the amino group N6 of adenine or N2 of guanine leads to the formation of covalent DNA adducts[210,211]. Unrepaired or false repaired DNA adducts interfere with replication and transcription, leading to either mutations and cancer, or senescence and cell death[212].

Nucleophilic B[*a*]P metabolites such as phenols or dihydrodiols can also be subjected to enzymatic detoxification by conjugation to glucuronic acid or sulfate[192], with UDP-glucuronosyltransferases (UGTs) playing a particularly important role[213]. This process leading to water-soluble and, thus, excretable derivatives.

### 1.3.2. Repair of PAH-DNA adducts

The genotoxicity of PAHs depends on different factors such as its metabolic activation, the detoxification of reactive metabolites and the rate of repair of DNA adducts[214]. The nucleotide excision repair (NER) is the main pathway used by mammals to remove chemical carcinogen-induced bulky DNA adducts such as those formed by PAHs[215]. The NER can be divided into two subpathways, the global genomic NER (GG-NER) and the transcription coupled NER (TC-NER). These two pathways differ in how they recognize DNA damage but share the same process for lesion, incision, repair, and ligation (Figure 7). While the GG-NER ensures DNA repair in non-transcribed genome regions, the TC-NER is responsible for the accelerated repair of lesions in the transcribed strand of active genes[216]. Approximately 30 different proteins are involved in NER. Two of them, XPA and XPC, are involved in damage recognition, with XPA contributing to both pathways of the NER. The XPC-HR23B heterodimer performs the initial damage recognition of BPDE-DNA adducts during the GG-NER[217]. This complex initiates the recruitment of other NER factors that are essential for ultimately stimulating the dual incisions of the damaged strand. The recruited helicases XPB and XPD cause the unwinding of the site of the lesion[218]. Factor XPA then binds to this complex, stabilizing the bubble-like structure and allowing the release of XPC/HR23B[219]. A single-stranded binding protein, RPA, further stabilizes this nucleoprotein complex. Subsequently, the structure-specific endonucleases XPG and XPF/ERCC1 bind to the complex and nick the damaged strand releasing the 24-32 nucleotide long fragments[220]. In contrast, TC-NER is initiated by RNA polymerase stalled at a lesion with the help of TC-NER specific factors CSA, CSB, and XAB2[216] (Figure 7).

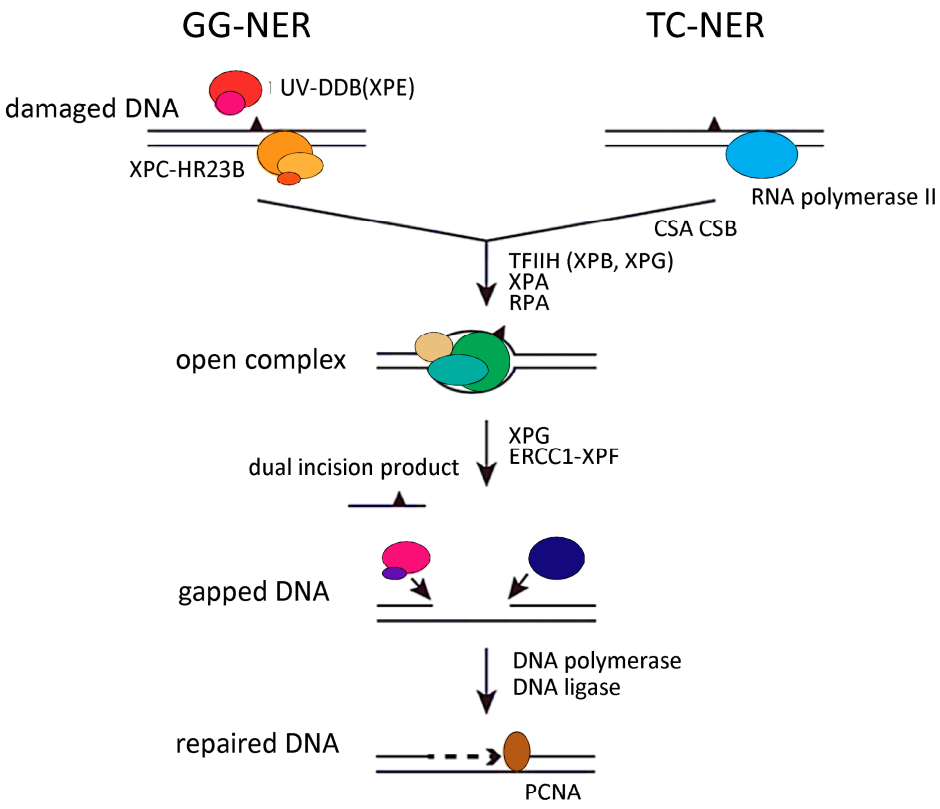


**Figure 7**: Schematic diagram of proteins involved in NER (TC-NER and GG-NER). Different recognition complexes operate during TC-NER and GG-NER (modified from Araujo and Kuraoka [221])

### 1.3.3. Microbial PAH metabolism

Prokaryotic metabolism of PAHs has been studied primarily in contaminated soil[222,223]. Different bacterial species, consortia and fungi are able to metabolize both low and high molecular weight PAHs [224]. PAHs degrading bacteria and fungi are ubiquitously distributed in the natural environment and can utilize it both anaerobically and aerobically[225,226]. The initial catabolic step in aerobic oxidation of a PAHs mostly occurs via formation of dihydrodiols by a multicomponent dioxygenase enzyme system[227]. Subsequent metabolism is generally slow and forms hydroxylated and epoxidized intermediates, as well as aldehydes[228-230]. A large proportion of the studies on biodegradation of PAHs focus on the microbial catabolism of lower molecular weight PAHs, such as naphthalene, phenanthrene, anthracene, and acenaphthene[231-239]. In contrast, limited work has yet been carried out on these processes of PAHs with high molecular weight[240]. Their low bioavailability makes them less attractive as a nutrient source for microorganisms, since a large amount of energy is required to break the carbon-carbon bonds[240].

Nevertheless, there are some microorganisms that are able to degrade B[*a*]P such as *Mycobacterium sp.*, *Stenotrophomonas maltophilia*, *Bacillus subtilis*, *Pseudomonas saccharophila*, *Staphylococcus haemoliticus* and *Sphingomonas yanoikuyae (formerly Beijerinckia sp. strain B8/36)*[241-248]. The bacterial degradation of B[*a*]P predominantly occurs via oxygenase-mediated metabolism, with the involvement of both dioxygenase and monooxygenase[223,249]. They transfer oxygen to the B[*a*]P, forming dihydrodiols as initial ring cleavage products, at the B[*a*]P-4,5-, 7,8-, 9,10- and 11,12-positions[241,243,248]. The first ring oxidation metabolites include hydroxylated B[*a*]Ps such as 3-OH-B[*a*]P or 9-OH-B[*a*]P and B[*a*]P-diones such as B[*a*]P-1,6-dione, B[*a*]P-3,6-dione as well as other uncharacterized B[*a*]P-diones[248,250,251]. The resulting diones are further metabolized to intermediates such as 10-oxabenzo-[*def*] chrysen-9-one, and hydroxymethoxy and dimethoxy derivatives of B[*a*]P. 4,5-chrysene-dicarboxylic acid, cis-4-(8hydroxypyrene-7-yl)-2-oxobut-3-enoic acid or cis-4-(7-hydroxypyrene-8-yl)-2-oxobut-3-enoic acid, and 7,8-dihydro-pyrene-7-carboxylic acid or 7,8-dihydro-pyrene-8-carboxylic acid.

However, complete detoxification in the form of B[*a*]P mineralization to $CO_2$ is usually only possible through the combination of bacterial and fungal metabolism[240,252].

In contrast, an incomplete microbial B[*a*]P degradation can generate toxification of the parent substance, as shown within the scope of this doctoral thesis on skin isolates[253].

## 1.4. Human skin microbiome and PAHs

This thesis builds upon some preliminary work done at BfR, particularly the enrichment and initial characterization of PAH-degrading skin commensals as a perquisite for the proof of concept *in vitro* [254]. In this work human skin was sampled from a group of 11 healthy volunteers. These included subjects of both sexes as well as of different age groups and people with different B[*a*]P pre-exposure.

All subjects were sampled on both the forearms and the neck. The elected regions are representative of a dry and a sebum-rich, moist habitat, respectively. The studies yielded 21 pure cultures that were able to utilize B[*a*]P as their sole source of energy and carbon, 10 of which came from the forearm and 11 from the neck. The microorganisms were identified based on the sequence of their 16S rRNA genes, and their phylogeny was determined using maximum likelihood and ARB. The most frequently isolated microorganisms were species closely related to *Micrococcus luteus*. Identification of the other forearm isolates revealed high similarities to *Staphylococcus capareae*, *Staphylococcus* sp., *Bacillus licheniformis*, *Paracoccus yeei*, *Pseudomonas oleovorans*, and *Acinetobacter lwoffii*, whereas species from the neck had high sequence similarities to *Bacillus pumilus*, *Straphylococcus aureus*, and *Pantonea agglomerans* (Figure 8). From each subject, at least one species could be isolated that can use B[*a*]P as the sole source of carbon and energy, independent of sex, age, or B[*a*]P pre-exposure. This is indicative of high selective pressure for the corresponding degradation pathway, presumably as a consequence of long-term exposure. With doubling times ranging from 13 h to 3 days, the growth rate of the isolates on B[*a*]P is slow. This may be due to both limited transport and slow metabolism. With molar growth yields approaching 6 g protein per mole of carbon *Micrococcus luteus* (3A), *Staphylococcus caprae* (3B), *Micrococcus luteus* (1D), and *Staphylococcus* epidermides (2D) metabolize B[*a*]P completely. The other isolates partially degrade it, presumably to the stage of a three- or four-ring system. Subsequent characterization of the substrate spectrum of the forearm isolates showed that they are also capable of metabolizing other higher molecular weight PAHs. These include possible intermediates of the B[*a*]P degradation pathway, such as pyrene or fluoranthene.

| Area sampled | Volunteer | Age [years] | B[a]P exposure | Isolate | ID | Sequence identity |
|---|---|---|---|---|---|---|
| *volar forearm* | A (♂) | 30 – 40 | medium | 1A | *Paracoccus yeei* | 99 % |
| | | | | 2A | *Acinetobacter lwofii* | 99 % |
| | | | | 3A | *Micrococcus luteus* | 99 % |
| | B (♀) | 20 – 30 | average | 1B | *Micrococcus luteus* | 99 % |
| | | | | 2B | *Micrococcus luteus* | 99 % |
| | | | | 3B | *Staphylococcus caprae* | 99 % |
| | C (♂) | 40 – 50 | average | 1C | *Pseudomonas oleovorans* | 99 % |
| | | | | 2C | *Bacillus licheniformis* | 99 % |
| | D (♂) | 0 – 10 | low | 1D | *Micrococcus luteus* | 99 % |
| | | | | 2D | *Staphylococcus (epidermis)** | 99 % |
| *neck* | E (♀) | 20 – 30 | average | 1E | *Micrococcus luteus* | 99 % |
| | F (♀) | 20 – 30 | average | 1F | *Micrococcus luteus* | 99 % |
| | | | | 2F | *Micrococcus luteus* | 99 % |
| | | | | 3F | *Micrococcus luteus* | 99 % |
| | G (♂) | 20 – 30 | high | 1G | *Pantoea agglomerans* | 100 % |
| | H (♂) | 20 – 30 | average | 1H | *Bacillus pumilus* | 99 % |
| | K (♂) | 50 – 60 | medium | 1K | *Micrococcus luteus* | 99 % |
| | L (♂) | 30 – 40 | medium | 1L | *Pantoea agglomerans* | 99 % |
| | | | | 2L | *Micrococcus luteus* | 99 % |
| | | | | 3L | *Micrococcus luteus* | 99 % |
| | M (♂) | 0-10 | low | 1M | *Staphylococcus aureus* | 99 % |

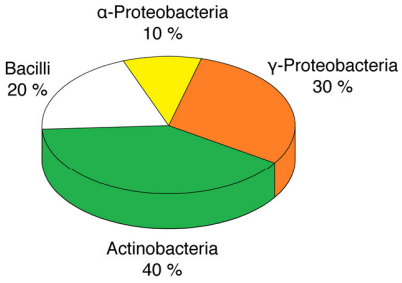


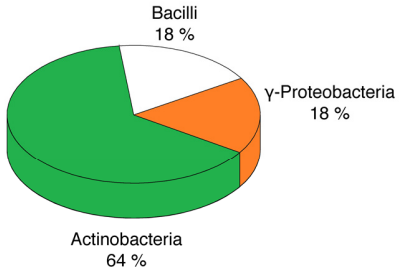


**Figure 8:** List of B[*a*]P-degrading isolates from the forearm and neck of 10 healthy volunteers. Bacteria were identified by the sequence of their 16S rRNA genes. The asterisk indicates isolates that could not be clearly identified. The pie charts indicate the % belonging to different organism classes. The PAH exposure of the subjects was estimated as average, medium, and high based on their lifestyle and work environment. Here, "average" corresponds to the PAH exposure of an average office worker, while the designations "medium" and "high" were used for subjects whose occupation involves frequent contact with PAHs, such as car mechanics or construction workers who work with tar (modified from Sowada, et al. [254]).

Aerobic bacteria generally degrade B[*a*]P via stepwise oxidation, as described at length in section 1.3.3. However, information on the particular mechanism is often scarce. To better understand the degradation

reactions, primers belonging to conserved sequences of known or suspected degradation pathways of various higher molecular weight PAHs/pollutants were derived. Two transcripts were identified that are specifically induced during growth on B[*a*]P. One is a previously uncharacterized flavin-dependent monooxygenase with sequence similarities to DszA/NtaA and the other is a NifH-like reductase. The former is likely required for the degradation of monocyclic aromatic compounds. In *Rhodococcus jostii* RHA1, for example, the respective gene is part of an operon required for the degradation of cyclic terpenes, such as limonene. Likewise for the NifH-like reductase a function in the late phase of B[*a*]P degradation seems likely, analogous to the degradation of the carbon skeleton of chloroalkanes in *Rhodopseudomonas palustris* CGA 009 (pathway rpa00625 of the KEGG database)[255].

# 2. Aim of this thesis

The skin serves as a physical barrier between the human body and the external environment. It provides protection against both dehydration and pathogen invasion. At the same time it is host to a substantial microbial community. Due to the high colonization density of the skin, there is strong competition for the available carbon sources. Since the skin is permanently exposed to low to moderate doses of PAHs through air, consumer products and cosmetics, its utilization as a growth substrate for skin bacteria may provide a selection advantage. Bacterial growth and metabolism on the skin are relatively slow due to low temperature, resulting in a prolonged residence time of metabolites on human skin, making their potential toxicity a high health risk[256]. Commensal B[*a*]P metabolism on human skin has not been studied in detail, so that no analysis on possible intermediates/metabolites has taken place.

With mounting evidence that the human microbiota can modulate the toxicity of environmental pollutants, a central goal of my work was to investigate this influence on B[*a*]P as an exemplary PAH. For this purpose, the bacterial supernatants were examined according to the formation of toxicologically relevant B[*a*]P intermediates by characterizing culture supernatants in more detail with regard to cyto- and genotoxicity using different human cell lines as well as primary keratinocytes (Chapter 3.1). Toxicologically relevant culture supernatants were furthermore analytically examined for the presence of microbial metabolites. The aim of the work was to identify these B[*a*]P metabolites formed by skin commensals by establishing and optimizing chemical analysis (Chapter 3.1).

In addition to direct chemical modification of xenobiotic, host-microbiota interaction can indirectly alter the toxicity for the host. The latter include alteration of host's endogenous detoxification enzymes, changes of xenobiotic absorption and bioavailability e.g. through regulation of the epithelial barrier. While this clearly highlights the need to be more alert towards our commensal`s toxicological potential, efforts to study such interactions are still hampered by a lack of suitable experimental systems. Developing such systems is in fact a challenge since the human microbiome is not only complex but highly species specific, thus making animal testing second choice. Therefore, the aim of this work was to establish a system that allows to overcome this species specificity and at the same time allow for sufficient complexity. Our novel co-culture model should therefore consist of cells and selected commensals of human skin origin arranged in a 3-D structure (Chapter 3.2). This model was to be characterized with regard to its microbial influence on skin physiology and xenobiotic metabolism. These microbial-induced changes should correspond to those of commensal-induced changes *in vivo* to subsequently enable to evaluate its influence on the toxicity of B[*a*]P *in situ* (Chapter 3.2 and 3.3). Such a model allows for the first time to study the impact of the skin´s microbiome on the toxicity of environmental chemicals in a high-throughput system in an

environment similar to *in vivo* without ethical issues due to human experimentation or the use of laboratory animals.

Such a model further allows to elucidate microbiome-induced changes in the distribution, absorption, and uptake of B[*a*]P in human skin. In addition, such a model allows to investigate whether commensals actually metabolize B[*a*]P on the skin despite the presence of other nutrient alternatives or whether they influence its toxicity to humans via indirect mechanisms (Chapter 3.3). It further allows the identification of possible mechanisms behind such modulations in the toxicity of chemicals and thus helps to evaluate them in their biological context, thus helping to identify and minimize future risks to human health.

# 3. Results

Publications are displayed chronologically and contain a section “author contributions” to distinguish individual involvement in the manuscripts.

The resulting chapters each feature independent units. Therefore, abbreviations and references are defined within each chapter.

## 3.1. Toxification of polycyclic aromatic hydrocarbons by commensal bacteria from human skin

Juliane Sowada, **Lisa Lemoine,** Karsten Schön, Christoph Hutzler, Andreas Luch & Tewes Tralau

This chapter was published on 04 April 2017:

Archives of Toxicology 91, 2331–2341 (2017)

DOI: 10.1007/s00204-017-1964-3

Link: https://doi.org/10.1007/s00204-017-1964-3

Involvement of the author within this publication: Project planning (20%), project execution (45%), data analysis (30%), writing of the manuscript (20%).

Supplementary materials for the following publication are detailed in Annex I.

TOXICOKINETICS AND METABOLISM
DOI 10.1007/s00204-017-1964-3

# Toxification of polycyclic aromatic hydrocarbons by commensal bacteria from human skin

**Juliane Sowada[1] · Lisa Lemoine[1] · Karsten Schön[1] · Christoph Hutzler[1] · Andreas Luch[1] · Tewes Tralau[1]**

Received: 6 July 2016 / Accepted: 21 March 2017 / Published online: 4 April 2017


**Abstract** The ubiquitous occurrence of polycyclic aromatic hydrocarbons (PAHs) leads to constant human exposure at low levels. Toxicologically relevant are especially the high-molecular weight substances due to their (pro-) carcinogenic potential. Following ingestion or uptake, the eukaryotic phase I metabolism often activates these substances to become potent DNA binders, and unsurpris-ingly metabolism and DNA-adduct formation of modelsubstances such as benzo[*a*]pyrene (B[*a*]P) are well stud- ied. However, apart from being subjected to eukaryotic transformations PAHs are also carbon and energy sources for the myriads of commensal microbes inhabiting man's every surface. Yet, we know little about the microbiome's PAH-metabolism capacity and its potentially adverseimpact on the human host. This study now shows that read-ily isolable skin commensals transform B[*a*]P into a range of highly cyto- and genotoxic metabolites that are excreted in toxicologically relevant concentrations during growth. The respective bacterial supernatants contain a mixture of established eukaryotic as well as hitherto unknown prokaryotic metabolites, the combination of which leads to an increased toxicity. Altogether we show that PAH metabolism of the microbiome has to be considered a potential hazard.

**Keywords** Microbiome · Polycyclic aromatic hydrocarbons · PAHs · Benzo[*a*]pyrene · Toxification · Genotoxicity · Cytotoxicity

## Introduction

With a surface of nearly 2 $m^2$ the skin is our largest although toxicologically often less appreciated organ. Its protective function is essential, be it for mitigating exog- enous impacts or by acting as physical and metabolic bar- rier against chemicals. Unsurprisingly, skin biology usually focuses on this very barrier function together with skin immunology (Veiga-Fernandes and Mucida 2016). This rather "eukaryo-centric" perspective has in recent yearsbeen complemented by the realisation that the skin also harbours a most diverse microbiome comprising more than200 niche-specific genera (Clemente et al. 2012; Costelloet al. 2009, 2013; Grice et al. 2009). However, the corre- sponding microbial populations are still primarily seen as atrait with immunological or olfactoric consequences at best(Clemente et al. 2012; El Aidy et al. 2012; Kerr et al. 2015;SanMiguel and Grice 2015).

Nevertheless, akin to the gut with its well-documented microbe–drug interactions the skin's microbiome harbours a metabolic potential far exceeding that of its host. With a genome 100-fold the size of ours this includes the degradation and modification of ubiquitous xenobiotic substances such as polycyclic aromatic hydrocarbons (PAHs) (Tralau et al. 2015; Wallace and Redinbo 2013). Apart from constituting the majority of airborne pollutants (e.g. exhaust fumes, cigarette smoke, volcanic emissions), PAHs also occur in many consumer products, including cosmetics, tools and toys (Commins 1969; Lin et al. 2016; Morillo et al. 2007; Souza et al. 2016; Tarnow et al. 2016). Skin

**Electronic supplementary material** The online version of this article (doi:10.1007/s00204-017-1964-3) contains supplementary material, which is available to authorised users.

✉ Tewes Tralau
tewes.tralau@bfr.bund.de

[1] Department of Chemical and Product Safety, German Federal Institute for Risk Assessment (BfR), Max-Dohrn-Strasse 8-10, 10589 Berlin, Germany

exposure is thus frequent with many of these substances being potentially harmful. Benzo[*a*]pyrene (B[*a*]P),for example, is subject to cytochrome P450-dependent monooxygenase (CYP)-mediated epoxidation in keratinocytes and other skin cells, leading to the formation of B[*a*]P-7,8-dihydrodiol-9,10-epoxide (Dekant 2009; Luch 2005; Shimada 2006). Unless eliminated via conjugation and excretion, the latter is a highly efficient DNA alkylat- ing agent and as such a most potent carcinogen (Luch2005; Luch and Baird 2010). At the same time, B[*a*]P is a potential substrate for skin bacteria, and although oxidative transformations are likely to occur, we know little about the corresponding metabolites or their toxicological potential for the human host (Sowada et al. 2014).

Previous data show the ability for commensal degradation of B[*a*]P and other PAHs not only to be widespread but to occur irrespective of age, gender or occupational pre-exposure (Sowada et al. 2014). Degradation was found to be partial as well as complete with the respective isolates presumably using different pathways for the degradation of B[*a*]P as sole source of carbon and energy. Microbial pathways need selective pressure to be maintained. The ready isolation of B[*a*]P-degrading organisms from skin therefore not only confirms permanent exposure but indicates biological relevance of this metabolism. We now report on the identification and toxicological characterisation of someof the corresponding excreted metabolites, several of them being cyto- and genotoxic.

**Table 1** List of reference substances used for metabolite identification and quantification

| | rt/min | Quantifier m/z | Qualifier m/z |
|---|---|---|---|
| $D_{12}$-B[*a*]P | 18.36 | 406 | 316 |
| B[*a*]P-3-ol | 20.19 | 340 | 341 |
| B[*a*]P-7-ol | 19.90 | 340 | 341 |
| B[*a*]P-8-ol | 20.37 | 340 | 341 |
| B[*a*]P-12-ol | 19.54 | 340 | 341 |
| B[*a*]P-1,6-dione | 21.69 | 428 | 429 |
| B[*a*]P-6,12-dione | 20.51 | 428 | 429 |
| B[*a*]P-11,12-dione | 19.07 | 428 | 429 |
| B[*a*]P-7,8-dione | 21.57 | 428 | 429 |
| B[*a*]P-9,10-diol | 18.35 | 430 | 340 |
| B[*a*]P-7,8-diol | 21.35 | 430 | 340 |
| B[*a*]P-4,5-diol | 18.20 | 430 | 340 |
| B[*a*]A | 16.24 | 228 | 226 |
| B[*a*]A-2-ol | 17.87 | 316 | 301 |
| B[*a*]A-4-ol | 18.01 | 316 | 301 |
| B[*a*]A-5-ol | 17.76 | 316 | 301 |
| B[*a*]A-9-ol | 18.16 | 316 | 301 |
| B[*a*]A-11-ol | 17.53 | 316 | 301 |
| B[*a*]A-3,4-diol | 18.33 | 406 | 316 |
| B[*a*]A-5,6-diol | 16.65 | 406 | 316 |
| B[*a*]A-8,9-diol | 18.13 | 406 | 316 |
| B[*a*]A-10,11-diol | 17.75 | 406 | 316 |
| Phe-4-$CO_2$H | 14.75 | 294 | 205 |
| Pyrene | 14.14 | 202 | 200 |
| Anthracene | 11.94 | 178 | 176 |

*B[a]P* benzo[*a*]pyrene, *B[a]A* benz[*a*]anthracene, *Phe* phenanthrene, *rt* retention time

## Materials and methods

### Chemicals and media

If not mentioned otherwise chemicals were purchased from Sigma-Aldrich (Taufkirchen, Germany) or Carl Roth (Karlsruhe, Germany) with the purity of chemicals used for enrichment cultures being greater than 98%. Media for cell lines and primary cells were sourced from PAN Biotech (Aidenbach, Germany) and Promocell (Heidelberg, Germany), respectively. Analytical reference substances (Table 1) were bought at the highest purity available from MRIGlobal Research (Kansas City, USA) and the PAH Research Institute (Igling-Holzhausen, Germany). Molecular reagents and kits were obtained from Qiagen (Hilden, Germany).

### Bacterial growth

Bacterial growth was routinely estimated using optical density (OD, $\lambda$ = 600 nm). Cultures for toxicity testing and metabolite analysis were set up as batch cultures at volumes of 150–250 ml using minimal growth medium with 100 µM B[*a*]P as sole source of carbon and energy (Sowada et al. 2014). Shake flasks were cultivated at 30 °C at 200 rpm with samples of 2 ml for supernatant testing and 2 × 25 ml for metabolite analysis taken every second day. Centrifuga-tion for 10 min at 1000 rpm was used to separate the super-natant from cells as required and samples stored at −25 °C until further usage. Bacterial flask cultures were incubated for up to 4 weeks with non-inoculated mock cultures serv- ing as negative controls for contaminations.

### Cell and tissue culture

The human immortal keratinocyte cell line HaCaT was cultivated in Dulbecco's Modified Eagle's Medium (DMEM) supplemented with 10% foetal calf serum (FCS) and 5 mg/ml penicillin/streptomycin at 37 °C in a humidified atmosphere with 5% $CO_2$. Similar culture conditions were applied for HepG2 cells using Roswell Park Memorial Institute (RPMI) medium instead of full DMEM. Primary normal human epidermal keratinocytes (NHEK) from

**Table 2** Primers used for quantitative RT-PCR

| Primer | Sequence |
|---|---|
| CYP1A1 forward | 5′-TCC AAG AGT CCA CCC TTC C-3′ |
| CYP1A1 reverse | 5′-AAG CAT GAT CAG TGT AGG GAT CT-3′ |
| HPRT forward | 5′-GTT CTG TGG CCA TCT GCT TAG-3′ |
| HPRT reverse | 5′-GCC CAA AGG GAA CTG ATA GTC-3′ |

juvenile foreskin were obtained and isolated as described previously (Brinkmann et al. 2013).

### Cytotoxicity assays

Cytotoxicity was assayed in cellular assays based on glycolytic activity in at least three biological replicates. Assays were carried out using a 96-well microtitre format with $1 \times 10^5$ cells per ml. Cells were subjected to substance treatment after an initial 24-h resting phase by adding 4 µl of bacterial supernatants or control substances, respectively. After 48 h of incubation, the assay was stopped by addition of 3-(4,5-dimethylthiazole-2-yl)-2,5-diphenyltetrazoliumbromide (MTT) at a final concentration of 500 µg/ml. Formation of formazan commenced for another 3 h. Following media removal and addition of DMSO (100 µl/well), the solubilised salt was then quantified in a "Genios Infinite M1000pro" microtitre plate reader (Tecan, Mainz-Kastel, Germany) based on its absorbance at $\lambda = 595$ nm.

### Single-cell electrophoresis assay (comet assay) and mutagenicity testing according to Ames

Analysis for genotoxic effects was done by using a modified comet assay as described previously (Brinkmannet al. 2013; Tarnow et al. 2016). Briefly, $1 \times 10^5$ cells/ml were seeded into 24-well plates and left to rest for 24 h before being challenged with test substances as indicated. Methyl methanesulfonate (MMS, 80 µM) and B[*a*]P (2 mM) were routinely used as positive controls. While the first induces DNA damage directly, the lat- ter requires oxidative activation and is thus indicative ofthe cellular phase I activity. Exposure to test substances lasted for 24 or 48 h. To increase the assay's sensitivity DNA repair was inhibited by addition of 5 µg/ml aphidi- colin being added after 2 h. For scoring, DNA was vis- ualised using SYPBR Gold (Thermo Fisher Scientific, Darmstadt, Germany) and any comets quantified using the Image-Analyser Comet-Assay II software (Perceptive Instruments, Bury St Edmunds, UK). All experiments were performed as biological duplicates at least, scor- ing 50 cells per slide and using a call cut-off of 50 cellsper slide. A concomitant bacterial reverse mutation assay (Ames test) was performed according to OECD guide-line 471 as described previously by Buhrke et al. (Buhrkeet al. 2013).

### Quantitative RT-PCR

Expression of selected CYP transcripts was analysedby quantitative RT-PCR using gene-specific prim-ers (Table 2) and the "QuantiTect SYBR® Green Kit" from Qiagen (Hilden, Germany). Cells were seeded into 6-well plates at a concentration of $1 \times 10^5$ cells per mland left to rest for 24 h before being subjected to sub- stance treatment as indicated. Subsequent to cell harvest by trypsinisation extraction and reverse transcription ofRNA was performed using "Omniscript Reverse Tran- scription Kit" (Qiagen, Hilden, Germany) as instructed by the manufacturer. In brief, 200 ng of mRNA was reversely transcribed using oligo-dT primers, followed by a gene-specific PCR for *CYP1A1* or the house-keeping control hypoxanthine–guanine phosphoribosyltransferase (*HPRT*), respectively. All experiments were performed as biological triplicates using an "Applied Biosystems 7500 Fast Real-time PCR System" (Thermo Fisher Scientific, Darmstadt, Germany) and relative transcript levels were calculated based on the $c_T$ values as determined by the manufacturer's "7500 Fast SDS Software" (Applied Bio- systems, Thermo Fisher Scientific, Darmstadt, Germany).

### Gas chromatography coupled to mass spectrometry (GC-MS)

Metabolite analyses were performed using GC-MS. For each analysis, a total of 25 ml of bacterial super- natant were mixed with a mixture of internal standards (Table 3, 500 ng/ml in ethyl acetate) and subjected to extraction with 5 ml ethyl acetate. The extraction was repeated, collected, concentrated and transferred into fresh vials using methanol. The latter was subsequently removed by evaporation using a TurboVap system (Bio- tage, Uppsala, Sweden) at 40 °C and a gentle nitrogen air flow. The samples were then directly dissolved in 20 µl

**Table 3** Internal standards used for verification of metabolite extraction and silylation, respectively

| | Retention time/min | Quantifier m/z | Qualifier m/z |
|---|---|---|---|
| $D_{12}$-B[*a*]A | 16.12 | 240 | 120 |
| 9-Fluorenone | 13.31 | 254 | 239 |
| Pyrene-1-ol | 16.30 | 290 | 275 |

*N,O*-bis(trimethylsilyl)-trifluoracetamide (BSTFA) as derivatisation agent followed by silylation at 60 °C for 90 min and 120 rpm in a water bath. Sample injection used splitless mode technique to inject 1 µl of the silylated mixture into a gas chromatograph 6890 (Agilent Technologies, Waldronn, Germany) equipped with an HP-5MS capillary column (Agilent, 30 m × 0.25 mm × 0.25 µm) and coupled to a 5975 mass spectrometric detector (Agilent, sim/scan mode) operated in electron impact ionisa- tion mode at 70 eV. The data acquisition was performedin combined mode of full-scan analysis and single-ion monitoring (SIM) mode, in order to achieve the highest sensitivity for analytes for which standard compounds are available while at the same time avoiding loss of information for unknown metabolites which might be not detected in the SIM mode. The column was operated in constant flow mode (1 ml/min) with helium 5.0 as carrier gas and an oven program ranging from 60 °C (for 1 min) to 320 °C (ramped at 15 °C/min, hold for 10 min). The transfer temperature was set at 295 °C. The injector was a cold injection system (Gerstel, Mülheim, Germany) starting at 45 °C, ramping to 300 °C at a rate of 12 °C/s. Metabolites were quantified using "GC/MSD ChemSta-tion Software" (Agilent). Values from non-inoculated day 0 samples were used as blanks for background subtraction as necessary. Calibration series for all standards were prepared by dilution of stock solutions, for every sequence of real samples in *n*-hexane containing 5–500 ng/ml of the standard compounds and 500 ng/ml of the internal standards. Calibration curves were checked for linearity and used for quantification of the analytes.

## Results

### Human skin commensals excrete cytotoxic and genotoxic B[*a*]P metabolites

Aerobic bacterial degradation of PAHs such as B[*a*]P often involves dioxygenases (Brezna et al. 2003; Haritash and Kaushik 2009; Peng et al. 2008). The respective intermediates comprise epoxides as well as diols, aldehydes or carboxylic acids. These are similar but not necessarily identical to those known from eukaryotic metabolism (Brezna et al. 2006; Luch 2009; Peng et al. 2008). Yet, there are hardly any analytical or toxicological data available for metabolites that result from the bacterial degradation of B[*a*]P or other high-molecular weight PAHs.

Out of the 21 B[*a*]P-degrading isolates obtained previously, we selected three for further analytical and toxicological characterisation, namely *Micrococcus luteus* 1D, *Micrococcus luteus* 1B and *Bacillus licheniformis* 2C (Sowada et al. 2014). Their physiological parameters (i.e. substrate usage, growth rates and carbon yield) indicate these organisms to use different degradation pathways with *M. luteus* 1D being a total and *M. luteus* 1B or *B. licheniformis* 2C being partial degraders, respectively. Excretion of potentially cytotoxic metabolites was analysed in a cellu-lar MTT assay and complementary microscopy by supplementing HaCaT cells, HepG2 cells or primary NHEK cells with supernatants from bacterial batch cultures grown on B[*a*]P as sole source of carbon and energy (Fig. 1).

The data show all strains to excrete cytotoxic metabolites, reducing cell viability down to 40%. Cytotoxic effects were recorded typically concomitant with the beginning of early exponential growth and were found to be transient for the complete degrader *M. luteus* 1D, while the other two isolates apparently accumulated cytotoxic end products. Effects were found to be more pronounced in HepG2 cells, probably as a result of additional phase I activation. Compared to skin cells, liver cell lines typically show higher levels of basal CYP expression. Yet RT-PCR nevertheless showed potential for further metabolic activation with extracts from the late exponential phase leading to a 70- to 100-fold induction of *CYP1A1* transcripts in HaCaT and NHEK cells, respectively (data not shown). Notably, this is in a range similar to the 122-fold induction observed with 2 mM B[*a*]P.

In addition, a comet assay showed the respective supernatants to also feature genotoxic potential with the two *M. lutei* inducing higher amounts of DNA damage than *B. licheniformis* 2D (Fig. 2). Compared to the positive control, the two *Micrococci* induced 42 and 51% of relative DNA damage, contrastingly to the *Bacillus* with 27%. In addition, pre-screens showed the effects to be dose-dependent, again with the toxic potential ranging between 40 and 80% of what is seen with 1 mM B[*a*]P. However, at this late exponential phase B[*a*]P has already been used as growth substrate and the DNA damage is induced by the bacterial metabolites. The potential mutagenicity of the supernatants was confirmed further in a reverse mutation assay (Table S1). For *B. licheniformis* 2C, the Ames test recorded S9-dependent base-pair substitutions, while frame shiftsand base-pair substitutions induced by *M. luteus* 1B did not require any metabolic activation.

### Metabolite identification and toxicity

Supernatant composition was subsequently analysed using GC-MS (Table 4). The data confirm all three iso- lates to have different metabolite patterns with the fulldegrader *M. luteus* 1D showing prominent excretion ofB[*a*]P-1,6-dione, while the metabolite pattern of the partial degrader *M. luteus* 1B is dominated by B[*a*]P-7,8-dioneand B[*a*]P-6,12-dione. Moreover, all isolates produced intermediates not found in eukaryotic metabolism. Again

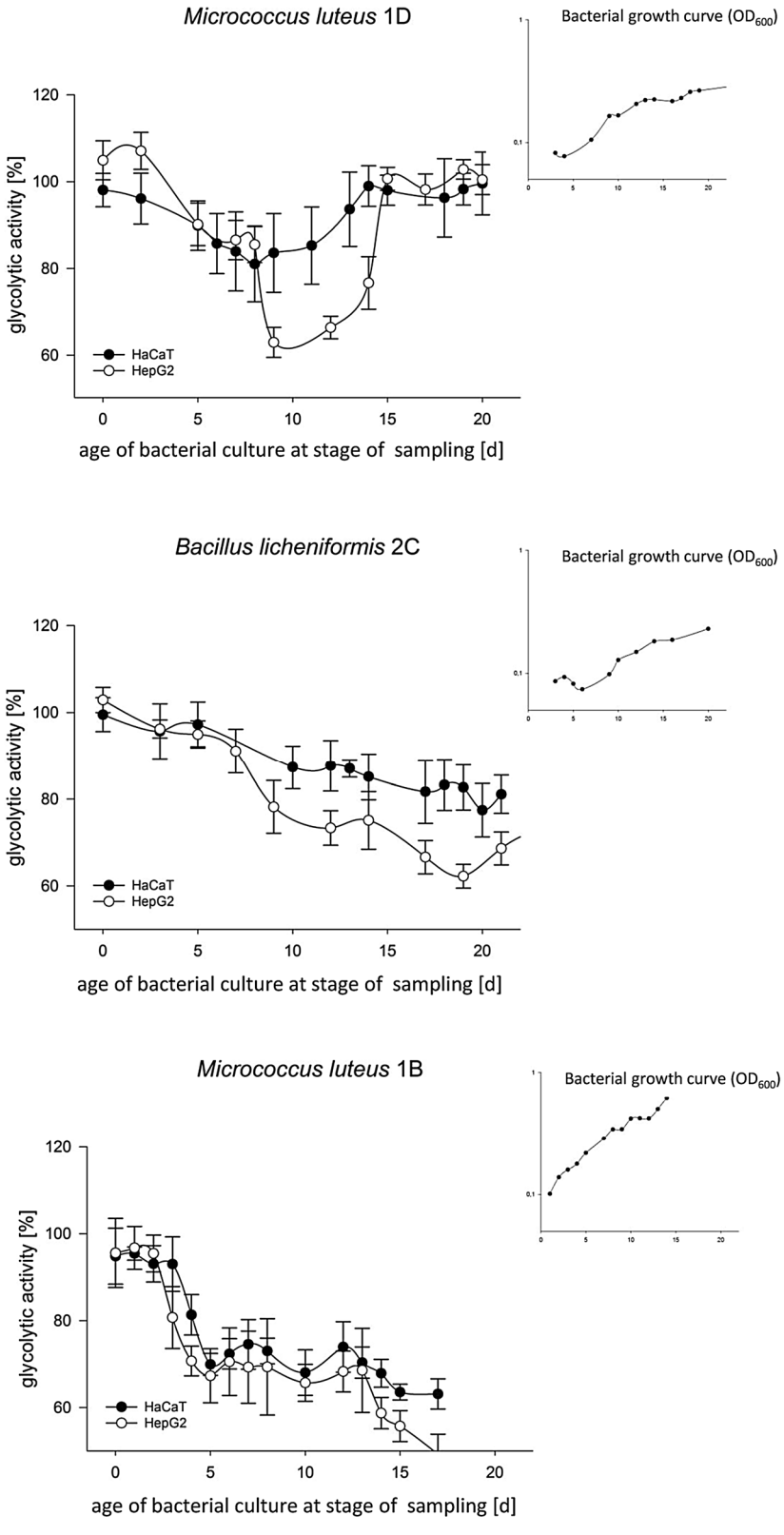


**Fig. 1** Cytotoxicity of metabolites as excreted by *M. luteus* 1D (**a**), *B. licheniformis* 2C (**b**) and *M. luteus* 1B (**c**) during growth on 100 µM B[*a*]P as sole source of carbon and energy. Batch cultures (inlets) were sampled as indicated and the supernatants added to cultures with HaCaT and HepG2 cells. Following 48 h of incubation cellular glycolytic activity was then recorded using an MTT assay as primary readout and microscopy for confirmation (data not shown, refer to suppl. Fig. S1). All data shown represent the mean of six biological replicates with $p < 0.01$. Negative controls comprised assays with bacterial minimal medium or cultures grown in lysogeny broth, all of which failed to induce signs of cytotoxicity (suppl. Fig. S2). Screens with NHEK cells produced similar results (data not shown, please refer to suppl. Fig. S3 for an exemplary plot)

the corresponding patterns and peak excretions differed between the various organisms. Differences included, for example, varying concentrations of B[*a*]P-12-ol in all three isolates or the presence or absence of metabolites such as benz[*a*]anthracene (B[*a*]A), B[*a*]A-11-ol and phenanthrene (Phe)-4-$CO_2H$ in the supernatants of *B. licheniformis*

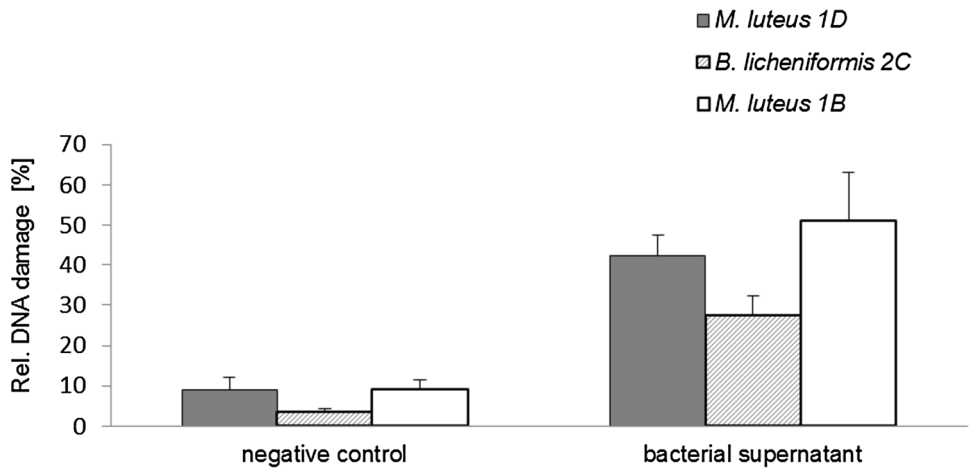


**Fig. 2** Genotoxicity of selected bacterial supernatants. Supernatants used had previously been tested positive for cytotoxicity before being assayed in a comet assay using HaCaT cells and 48 h of incubation. The results show levels of DNA damage relative to methyl methanesulfonate (MMS), using minimal medium without B[*a*]P as negative control. The data shown represent the mean of three biological replicates with $p < 0.01$. Similar levels of DNA damage were observed with NHEK cells or with B[*a*]P (data not shown)

**Table 4** Quantities of metabolites identified in bacterial supernatants tested positive for toxicity (all values given are in nM)

| | *M. luteus* 1D | *B. licheni-formis* 2C | *M. luteus* 1B |
|---|---|---|---|
| B[*a*]P-9,10-diol | 42 | | |
| B[*a*]P-1,6-dione | 2050 | 56 | 277 |
| B[*a*]P-6,12-dione | | | 961 |
| B[*a*]P-7,8-dione | 41 | 220 | >10,000[a] |
| B[*a*]P-3-ol | 177 | 14 | 31 nM |
| B[*a*]P-7-ol | 89 | 24 | n.q |
| B[*a*]P-12-ol* | 4 | | |
| B[*a*]A* | 5 | 29 | |
| B[*a*]A-11-ol* | 26 | | |
| Phe-4-$CO_2$H* | 5 | | |

The asterisk denotes metabolites not known to occur in eukaryotes

*B[a]P* benzo[*a*]pyrene, *B[a]A* benz[*a*]anthracene, *Phe* phenanthrene, *n.q*. not quantifiable

[a]Value of 16,948 nM is outside the linear range

2C and *M. luteus* 1B. The identification of metaboli- cally formed B[*a*]A in cultures of *B. licheniformis* 2C is illustrated in Fig. 3. Another unidentified B[*a*]A-diol was detected in the supernatant of *M. luteus* 1D (Fig. 4). In addition, the extracts contained several metabolites at low concentrations which could neither be qualified nor quantified unambiguously (data not shown, for an example please refer to Fig. 4a). Based on their chromatographic behaviour and properties, they are likely B[*a*]P-1-ol or B[*a*]P-2-ol, B[*a*]P-4-ol, or B[*a*]P-10-ol and B[*a*]A-1-ol (Grova et al. 2011).

The identified metabolites and selected combinations thereof were subsequently tested for cytotoxicity (Fig. 5).

Generally, effects of the single substances on glycolytic activity were found to be weak. Only B[*a*]P-7,8-dione and B[*a*]P-1,6-dione and the two hydroxylated B[*a*]P metabolites showed some moderate effects. However, cytotoxicity was more pronounced following metabolite application as organism-specific mixture for *M. luteus* 1D or *M. luteus* 1B. Similarly, in the comet assay the genotoxic potential was more pronounced for the mixtures than for the single substances (Fig. 6).

## Discussion

Bacterial degradation of B[*a*]P has been observed before, although mostly in an environmental context (Cerniglia and Heitkamp 1990; Haritash and Kaushik 2009; Peng et al. 2008). The observation that B[*a*]P-degrading isolates can readily be isolated from human skin isolates thus came as a surprise (Sowada et al. 2014). Given the potential toxicity of oxidative B[*a*]P-metabolites, the wide occurrence of this phenomenon quickly leads to questions of metabolite identity and toxicity.

Analysing three of the previously obtained isolates, this study quantitatively identified a total of ten excreted metabolites (Table 4). Only six of these have previously been shown to also occur in eukaryotes (i.e. B[*a*]P-9,10-diol, B[*a*]P-1,6-dione, B[*a*]P-6,12-dione, B[*a*]P-7,8-dione, B[*a*]P-3-ol and B[*a*]P-7-ol), while B[*a*]P-12-ol, B[*a*]A, B[*a*]A-11-ol and Phe-4-$CO_2$H seem to be specific for prokaryotic metabolism (Baird et al. 2005; Dekant 2009; Lin et al. 2016; Lorentzen and Ts'o 1977; Luch 2009; Shimada 2006; Souza et al. 2016; Sulc et al. 2016). Moreover, only three of these metabolites, namely B[*a*]P-1,6-dione,

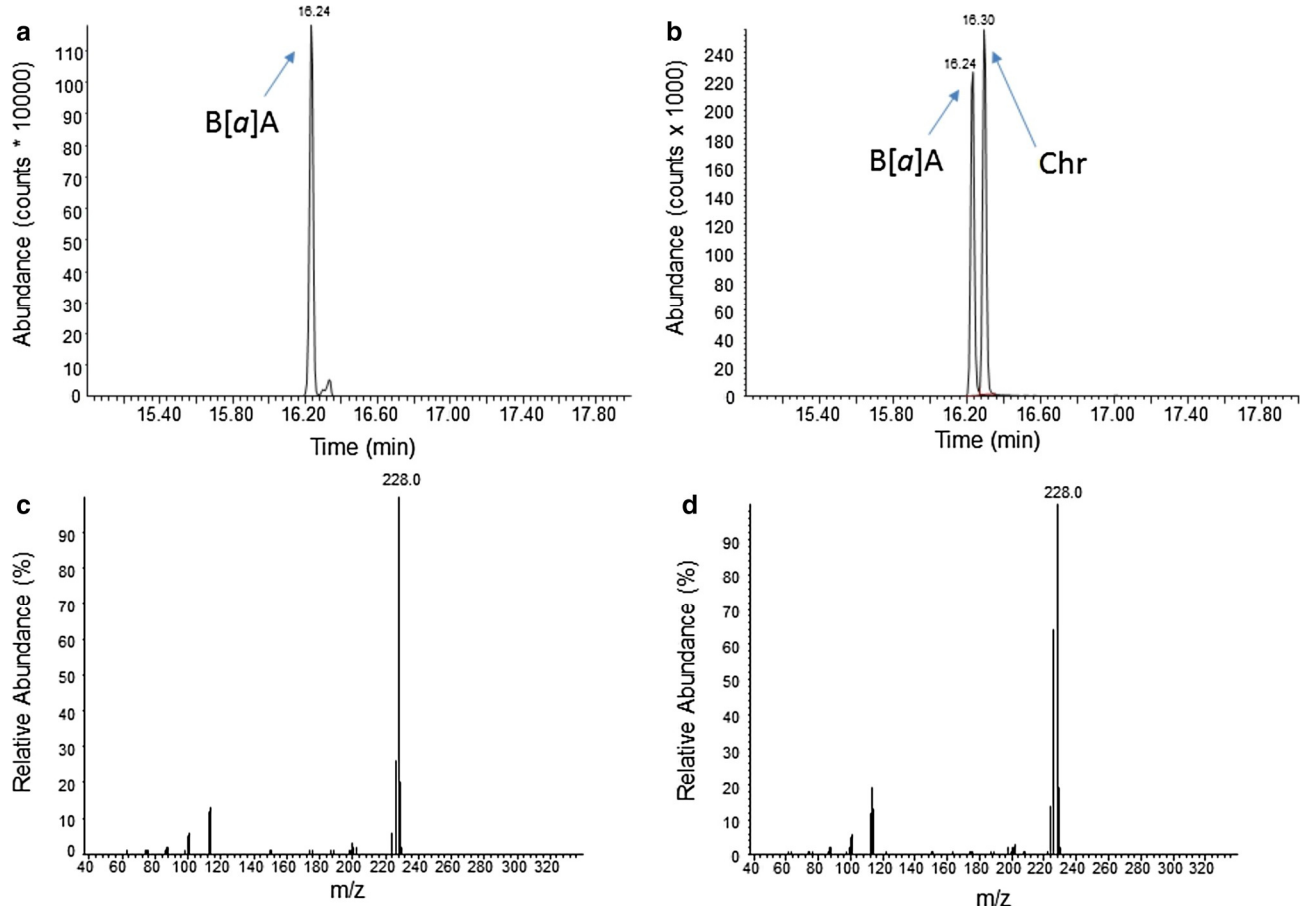


**Fig. 3** GC-MS chromatograms and corresponding full-scan mass spectra of benz[*a*]anthracene (B[*a*]A; m/z = 228; retention time = 16.24 min) as metabolite formed by *B. licheniformis* 2 C (**a, c**) and as synthetic compound (**b, d**). The reference chromatogram (**b**) also shows chrysene (Chr)

B[*a*]P-3-ol and B[*a*]P-7-ol, are also formed by the only B[*a*]P-degrading model organism, that is the environmental isolate *Mycobacterium vanbaalenii* PYR-1 (data not shown). The metabolite patterns of the three isolates confirmed the use of different degradation pathways, as also suggested by their substrate usage (Sowada et al. 2014). Befittingly the only three-ring metabolite (i.e. Phe-4-$CO_2$) was detected in the supernatants of the fully degrading *M. luteus* 1D (Fig. S4), while the two partial degraders *B. licheniformis* 2C and *M. luteus* 1B only featured four- and five-ring systems. While this matches the expecta- tions from the corresponding growth yields (i.e. 6.4, 1.6and 2.9 g protein per mol carbon) (Sowada et al. 2014),it should be noted that the list of identified metabolites is not comprehensive. Although all major metabolites have been identified, the identification of some others remains ambiguous. This comprises the aforementioned B[*a*]A-diol from *M. luteus* 1D, as well as those that were only analysed qualitatively based on their chromatographic properties (i.e. B[*a*]P-1-ol or B[*a*]P-2-ol, B[*a*]P-4-ol, B[*a*]P-10-ol and B[*a*]A-1-ol) (Grova et al. 2011). Limiting factors are the transient metabolite formation together with low levels of excretion as well as chromatographic ambiguity. For example, distinction of some of the hydroxylated B[*a*]A derivatives from chrysenes requires the presence of the parent compound or extensive reference compound libraries, not all of which are readily available.

The supernatants of all three isolates were foundto be cyto- as well as genotoxic. With metabolite concentrations in the low micromolar range, the overall cytotoxicity is comparable to that of the tumorigenic dibenzo[*a,l*]pyrene which features $EC_{50}$-values of 0.8 and 0.4 µM in HaCaT and HepG2 cells, respectively (data not shown). Similarly, the DNA-damaging potential comes close to that of B[*a*]P or MMS, the latter of which being a typical inducer of direct DNA damage (Lundin et al. 2005). The accumulation of toxic metabolites for *B. licheniformis* 2C and *M. luteus* 1B is in concordance with their trait as partial degraders, while the full degrader *M. luteus* 1D only shows transient excretion. Although the higher cytotoxicity

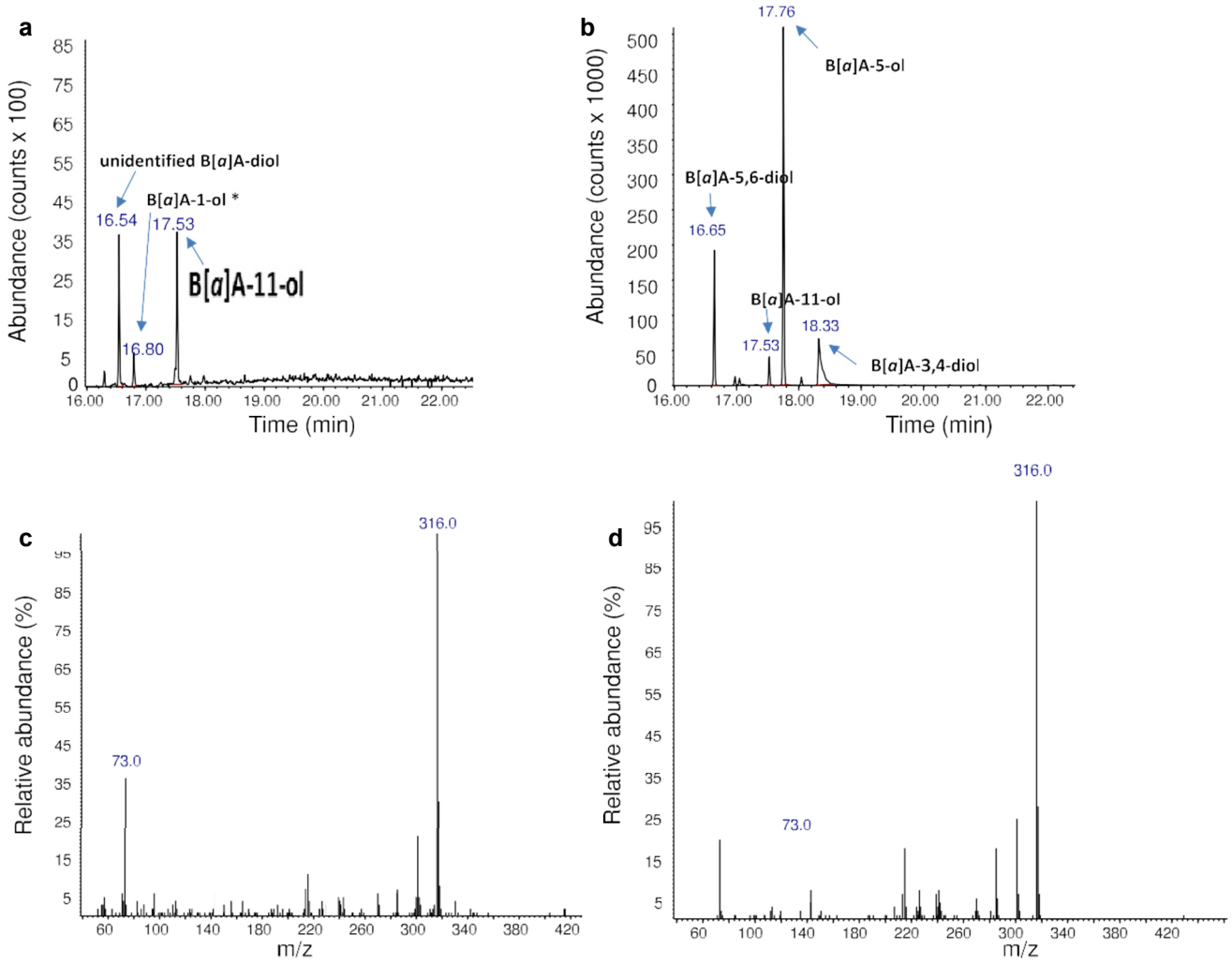


**Fig. 4** GC-MS chromatogram of B[*a*]A-11-ol (m/z = 316; retention time = 17.53 min) metabolically formed from B[*a*]P by *M. luteus* 1D (**a**), compared to the chromatogram of synthetic B[*a*]A-11-ol as part of a calibration mix (**b**). Also shown are the corresponding full-scan mass spectra for B[*a*]A-11-ol as metabolite (**c**) and as synthetic compound (**d**), respectively. *Qualitative identification based on chromatographic behaviour and properties as described by Grova et al. (2011)

in HepG2 cells indicates a contributory role of eukaryotic phase I metabolism all effects were also clearly visible with HaCaT or primary NHEK cells, both of which only feature a limited metabolic competence (Bauer et al. 1995; Gotz et al. 2012; Oesch et al. 2014). The results therefore strongly indicate an inherent toxicity of the excreted metabolites even without further metabolism. Indeed B[*a*]P, B[*a*]P-7,8-dione and B[*a*]A are known for their cyto- toxic potential with $EC_{50}$ values in the mid-nanomolar to mid-micromolar range (Behrens et al. 2001; Burczynski and Penning 2000; Creusot et al. 2015; Kim et al. 1998; Shimada 2006). Yet, tests with the single substances at the concentrations equivalent to those in the correspond- ing supernatants found them only to be weakly toxic. This strongly indicates mixture effects, an observation also strengthened by the fact that the effect of the reconstituted.supernatant of *M. luteus* 1D was close to that observed with the actual supernatants. Likewise genotoxicity could not be attributed to one particular analyte but appeared to be result of co-exposure. This is supported further by the Ames test, which indicated mutagenicity for some of the supernatants but not for single substances. This comes at little surprise as the Ames is known to be less sensitive par-ticularly for substances with low solubility (Lah et al. 2008;Wu et al. 2009). Meanwhile when used at their peak con- centrations, the toxicity of the overall metabolite mixture inthe comet assay came close to that of the original bacterial supernatants.

This is the first time that the skin microbiome's metabolism of PAHs such as B[*a*]P and its toxicological potential has been analysed. The data clearly show the metabolites formed to be cyto- and genotoxic at the concentrations

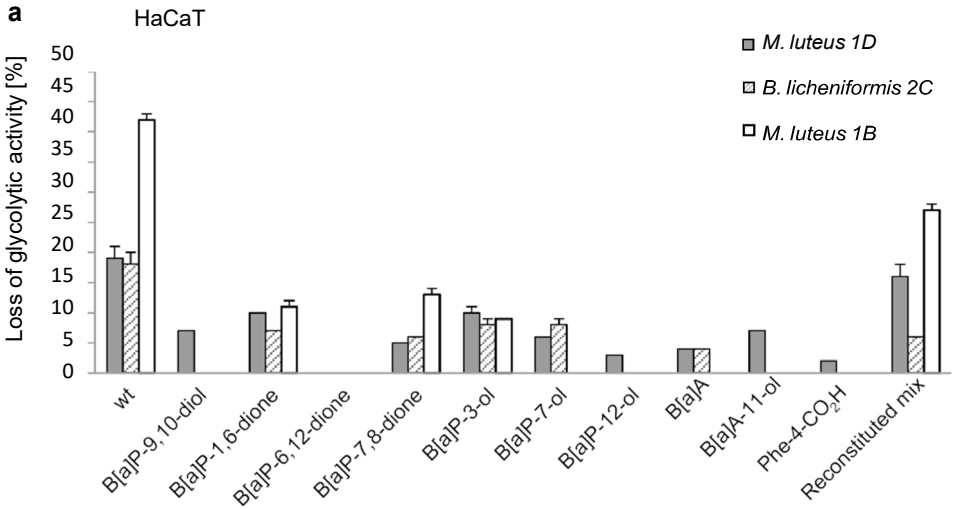


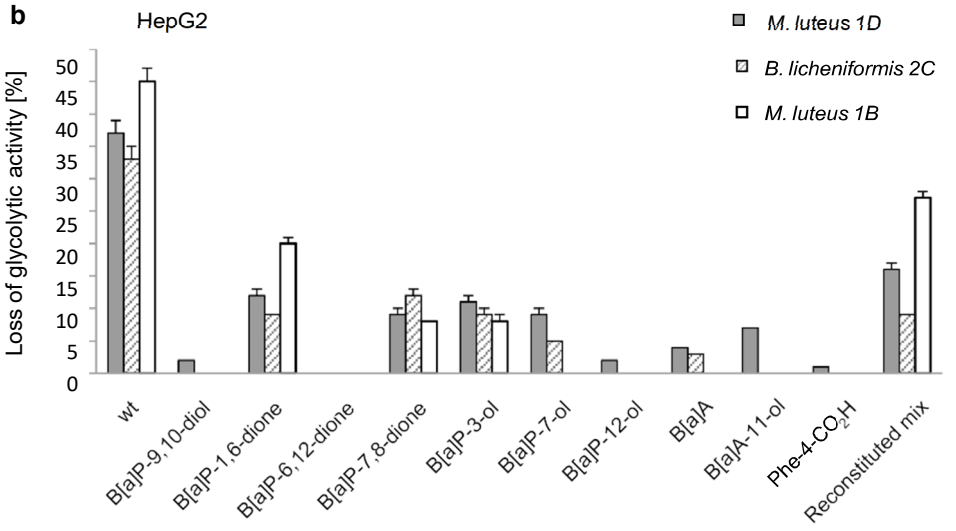


**Fig. 5** Cytotoxicity of bacterial B[*a*]P metabolites in HaCaT (**a**) or HepG2 (**b**) cells. An MTT assay was used to evaluate the cytotoxic potential (reduction of cellular glycolytic activity) of single metabolites and supernatants. Whereas "wt" denotes original culture supernatants of cultures grown on B[*a*]P-containing minimal medium, isolate-specific mixtures of identified metabolites in concentrations as excreted are referred to as "reconstituted". Please refer to Table 4 for details. All data shown represent the mean of three biological replicates with $p < 0.01$

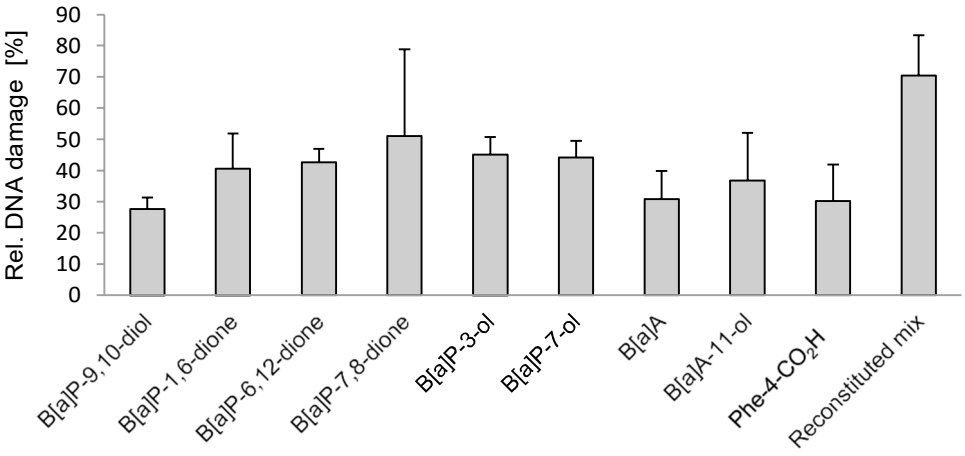


**Fig. 6** Relative genotoxicity of identified B[*a*]P-metabolites. The results show levels of relative DNA damage in HaCaT cells after 48 h of substance treatment. To maximise the sensitivity of the assay, metabolites were used at their highest excreted concentrations (please refer to Table 4) and as defined mixture thereof ("reconstituted mix"). The results show levels of DNA damage relative to MMS as positive control

excreted. Skin migration and penetration of high- and mid-molecular weight PAHs is strongly size-dependent and can reach up to 30% for four- and five-ring systems (Hutzler, personal communication; Paschke et al. 2014). Given the similarity of these substances to the bacterial metabolites, it is likely that similar values apply. Genes involved in

bacterial B[*a*]P-degradation can be detected *in situ* as can transcripts of the 16s-RNA genes of the organisms involved (with copy numbers of up to 20,000 copies/cm$^2$) (data not shown). In this context, exposure of the human host to bacterial B[*a*]P metabolites as potential carcinogens becomes only a question of B[*a*]P availability and concurrent microbial or eukaryotic metabolism. The toxicological impact of the microbiome's metabolism hence clearly deserves more attention in the future.

**Acknowledgements** Juliane Sowada and Lisa Lemoine contributed equally to this manuscript. The authors acknowledge intramural funding at the German Federal Institute for Risk Assessment (BfR), Grant 1322-469 and funding of Juliane Sowada by the FAZIT foundation (Frankfurt, Germany). Furthermore, the authors particularly want to thank Marlies Sagmeister and Thorsten Buhrke for their assistance with the Ames Test. Equally acknowledged is the experimental and technical assistance of Doris Genkinger, Bettina Hoffmann and Fiona Fölster.



## References

Baird WM, Hooven LA, Mahadevan B (2005) Carcinogenic polycyclic aromatic hydrocarbon-DNA adducts and mechanism of action. Environ Mol Mutagen 45(2–3):106–114. doi:10.1002/em.20095

Bauer E, Guo Z, Ueng YF, Bell LC, Zeldin D, Guengerich FP (1995) Oxidation of benzo[*a*]pyrene by recombinant human cytochrome P450 enzymes. Chem Res Toxicol 8(1):136–142

Behrens A, Schirmer K, Bols NC, Segner H (2001) Polycyclic aromatic hydrocarbons as inducers of cytochrome P4501A enzyme activity in the rainbow trout liver cell line, RTL-W1, and in primary cultures of rainbow trout hepatocytes. Environ Toxicol Chem 20(3):632–643

Brezna B, Khan AA, Cerniglia CE (2003) Molecular characterization of dioxygenases from polycyclic aromatic hydrocarbon-degrading *Mycobacterium* spp.. FEMS Microbiol Lett 223(2):177–183

Brezna B, Kweon O, Stingley RL et al (2006) Molecular characterization of cytochrome P450 genes in the polycyclic aromatic hydrocarbon degrading *Mycobacterium vanbaalenii* PYR-1. Appl Microbiol Biotechnol 71(4):522–532. doi:10.1007/s00253-005-0190-8

Brinkmann J, Stolpmann K, Trappe S et al (2013) Metabolically competent human skin models: activation and genotoxicity of benzo[*a*]pyrene. Toxicol Sci 131(2):351–359. doi:10.1093/toxsci/kfs316

Buhrke T, Kibellus A, Lampen A (2013) *In vitro* toxicological characterization of perfluorinated carboxylic acids with different carbon chain lengths. Toxicol Lett 218(2):97–104. doi:10.1016/j.toxlet.2013.01.025

Burczynski ME, Penning TM (2000) Genotoxic polycyclic aromatic hydrocarbon *ortho*-quinones generated by aldo-keto reductases induce CYP1A1 via nuclear translocation of the aryl hydrocarbon receptor. Cancer Res 60(4):908–915

Cerniglia CE, Heitkamp MA (1990) Polycyclic aromatic hydrocarbon degradation by *Mycobacterium*. Methods Enzymol 188:148–153

Clemente JC, Ursell LK, Parfrey LW, Knight R (2012) The impact of the gut microbiota on human health: an integrative view. Cell 148(6):1258–1270. doi:10.1016/j.cell.2012.01.035

Commins BT (1969) Formation of polycyclic aromatic hydrocarbons during pyrolysis and combustion of hydrocarbons. Atmos Environ 3(5):565–572

Costello EK, Lauber CL, Hamady M, Fierer N, Gordon JI, Knight R (2009) Bacterial community variation in human body habitats across space and time. Science 326(5960):1694–1697. doi:10.1126/science.1177486

Costello EK, Carlisle EM, Bik EM, Morowitz MJ, Relman DA (2013) Microbiome assembly across multiple body sites in low-birthweight infants. mBio 4(6):e00782–13 doi:10.1128/mBio.00782-13

Creusot N, Brion F, Piccini B, Budzinski H, Porcher JM, Ait-Aissa S (2015) BFCOD activity in fish cell lines and zebrafish embryos and its modulation by chemical ligands of human aryl hydrocarbon and nuclear receptors. Environ Sci Pollut Res Int 22(21):16393–16404. doi:10.1007/s11356-014-3882-8

Dekant W (2009) The role of biotransformation and bioactivation in toxicity. In: Luch A (ed) Molecular, clinical and environmental toxicology, vol 1. Birkhäuser Publishing, Switzerland, pp 57–86

El Aidy S, van Baarlen P, Derrien M et al (2012) Temporal and spatial interplay of microbiota and intestinal mucosa drive establishment of immune homeostasis in conventionalized mice. Mucosal Immunol 5(5):567–579. doi:10.1038/mi.2012.32

Götz C, Pfeiffer R, Tigges J et al (2012) Xenobiotic metabolism capacities of human skin in comparison with a 3D-epidermis model and keratinocyte-based cell culture as *in vitro* alterna- tives for chemical testing: phase II enzymes. Exp Dermatol 21(5):364–369. doi:10.1111/j.1600-0625.2012.01478.x

Grice EA, Kong HH, Conlan S et al (2009) Topographical and temporal diversity of the human skin microbiome. Science 324(5931):1190–1192. doi:10.1126/science.1171700

Grova N, Salquebre G, Schroeder H, Appenzeller BM (2011) Determination of PAHs and OH-PAHs in rat brain by gas chromatography tandem (triple quadrupole) mass spectrometry. Chem Res Toxicol 24(10):1653–1667. doi:10.1021/tx2003596

Haritash AK, Kaushik CP (2009) Biodegradation aspects of polycyclic aromatic hydrocarbons (PAHs): a review. J Hazard Mater 169(1–3):1–15. doi:10.1016/j.jhazmat.2009.03.137

Kerr CA, Grice DM, Tran CD et al (2015) Early life events influence whole-of-life metabolic health via gut microflora and gut permeability. Crit Rev Microbiol 41(3):326–340. doi:10.3109/1040841x.2013.837863

Kim JH, Stansbury KH, Walker NJ, Trush MA, Strickland PT, Sut- ter TR (1998) Metabolism of benzo[*a*]pyrene and benzo[*a*]pyr- ene-7,8-diol by human cytochrome P450 1B1. Carcinogenesis 19(10):1847–1853

Lah B, Vidic T, Glasencnik E, Cepeljnik T, Gorjanc G, Marinsek-Logar R (2008) Genotoxicity evaluation of water soil leachates by Ames test, comet assay, and preliminary *Tradescantia* micronucleus assay. Environ Monit Assess 139(1–3):107–118. doi:10.1007/s10661-007-9819-7

Lin Q, Xiao-Chen L, Bo Y et al (2016) Quantitative analysis of 3-OH B[*a*]P and (+)-*anti*-BPDE as biomarkers of B[*a*]P exposure in rats. Biomed Chromatogr 30(3):474–483. doi:10.1002/bmc.3574

Lorentzen RJ, Ts'o PO (1977) Benzo[*a*]yrenedione/benzo[*a*]pyrenediol oxidation-reduction couples and the generation of reactive reduced molecular oxygen. Biochemistry 16(7):1467–1473

Luch A (2005) Nature and nurture—lessons from chemical carcinogenesis. Nat Rev Cancer 5(2):113–125. doi:10.1038/nrc1546

Luch A (2009) On the impact of the molecule structure in chemical carcinogenesis. EXS 99:151–179

Luch A, Baird WM (2010) Carcinogenic polycyclic aromatic hydrocarbons. In: McQueen CA (ed) Comprehensive toxicology, 2nd edition. Academic Press, Oxford, pp 85–123

Lundin C, North M, Erixon K et al (2005) Methyl methanesulfonate (MMS) produces heat-labile DNA damage but no detect- able in vivo DNA double-strand breaks. Nucleic Acids Res 33(12):3799–3811. doi:10.1093/nar/gki681

Morillo E, Romero AS, Maqueda C et al (2007) Soil pollution by PAHs in urban soils: a comparison of three European cities. J Environ Monit 9(9):1001–1008. doi:10.1039/b705955h

Oesch F, Fabian E, Guth K, Landsiedel R (2014) Xenobiotic-metabolizing enzymes in the skin of rat, mouse, pig, guinea pig, man, and in human skin models. Arch Toxicol 88(12):2135–2190. doi:10.1007/s00204-014-1382-8

Paschke M, Hutzler C, Brinkmann J, Henkler F, Luch A (2014) Polycyclic aromatic hydrocarbons in newspaper inks: migration, metabolism, and genotoxicity in human skin. Polycyl Aromat Hydrocarb 35(1):32–40 doi:10.1080/10406638.2014.900643

Peng RH, Xiong AS, Xue Y et al (2008) Microbial biodegradation of polyaromatic hydrocarbons. FEMS Microbiol Rev 32(6):927–955. doi:10.1111/j.1574-6976.2008.00127.x

SanMiguel A, Grice EA (2015) Interactions between host factorsand the skin microbiome. Cell Mol Life Sci 72(8):1499–1515. doi:10.1007/s00018-014-1812-z

Shimada T (2006) Xenobiotic-metabolizing enzymes involved in activation and detoxification of carcinogenic polycyclic aromatic hydrocarbons. Drug Metab Pharmacokinet 21(4):257–276

Souza T, Jennen D, van Delft J, van Herwijnen M, Kyrtoupolos S, Kleinjans J (2016) New insights into BaP-induced toxicity: role of major metabolites in transcriptomics and contribution to hepatocarcinogenesis. Arch Toxicol 90(6):1449–1458. doi:10.1007/s00204-015-1572-z

Sowada J, Schmalenberger A, Ebner I, Luch A, Tralau T (2014) Degradation of benzo[*a*]pyrene by bacterial isolates from human skin. FEMS Microbiol Ecol 88(1):129–139. doi:10.1111/1574-6941.12276

Sulc M, Indra R, Moserova M et al (2016) The impact of indi-vidual cytochrome P450 enzymes on oxidative metabolism of benzo[*a*]pyrene in human livers. Environ Mol Mutagen 57(3):229–235. doi:10.1002/em.22001

Tarnow P, Hutzler C, Grabiger S, Schon K, Tralau T, Luch A (2016) Estrogenic activity of mineral oil aromatic hydrocarbons used in printing inks. PLoS One 11(1):e0147239. doi:10.1371/journal.pone.0147239

Tralau T, Sowada J, Luch A (2015) Insights on the human microbiome and its xenobiotic metabolism: what is known about its effects on human physiology? Expert Opin Drug Metab Toxicol 11(3):411–425. doi:10.1517/17425255.2015.990437

Veiga-Fernandes H, Mucida D (2016) Neuro-immune interac-tions at barrier surfaces. Cell 165(4):801–811. doi:10.1016/j.cell.2016.04.041

Wallace BD, Redinbo MR (2013) The human microbiome is a source of therapeutic drug targets. Curr Opin Chem Biol 17(3):379– 384. doi:10.1016/j.cbpa.2013.04.011

Wu JC, Hseu YC, Chen CH, Wang SH, Chen SC (2009) Comparative investigations of genotoxic activity of five nitriles in the comet assay and the Ames test. J Hazard Mater 169(1–3):492–497. doi:10.1016/j.jhazmat.2009.03.121

## 3.2. Microbially competent 3D skin: a test system that reveals insight into host–microbe interactions and their potential toxicological impact

**Lisa Lemoine,** Ralf Dieckmann, Sascha Al Dahouk, Szilvia Vincze, Andreas Luch & Tewes Tralau

This chapter was published on 17 July 2020:

Archives of Toxicology 94, 3487–3502 (2020)

DOI: 10.1007/s00204-020-02841-z

Link: https://doi.org/10.1007/s00204-020-02841-z

Involvement of the author within this publication: Project planning (70%), project execution (90%), data analysis (90%), writing of the manuscript (70%).

Supplementary materials for the following publication are detailed in Annex II.

https://doi.org/10.1007/s00204-020-02841-z

IN VITRO SYSTEMS

# Microbially competent 3D skin: a test system that reveals insight into host–microbe interactions and their potential toxicological impact

Lisa Lemoine[1,2] · Ralf Dieckmann[3] · Sascha Al Dahouk[3] · Szilvia Vincze[3] · Andreas Luch[1,2] · Tewes Tralau[4]

Received: 9 March 2020 / Accepted: 9 July 2020 / Published online: 17 July 2020


**Abstract**
The skin`s microbiome is predominantly commensalic, harbouring a metabolic potential far exceeding that of its host. While there is clear evidence that bacteria-dependent metabolism of pollutants modulates the toxicity for the host there is still a lack of models for investigating causality of microbiome-associated pathophysiology or toxicity. We now report on a biologically characterised microbial–skin tissue co-culture that allows studying microbe–host interactions for extended periods of time in situ. The system is based on a commercially available 3D skin model. In a proof-of-concept, this model was colonised with single and mixed cultures of two selected skin commensals. Two different methods were used to quantify the bacteria on the surface of the skin models. While *Micrococcus luteus* established a stable microbial–skin tissue co-culture, *Pseudomonas oleovorans* maintained slow continuous growth over the 8-day cultivation period. A detailed skin transcriptome analysis showed bacterial colonisation leading to up to 3318 significant changes. Additionally, FACS, ELISA and Western blot analyses were carried out to analyse secretion of cytokines and growth factors. Changes found in colonised skin varied depending on the bacterial species used and comprised immunomodulatory functions, such as secretion of IL-1α/β, Il-6, antimicrobial peptides and increased gene transcription of IL-10 and TLR2. The colonisation also influenced the secretion of growth factors such as VFGFA and FGF2. Notably, many of these changes have already previously been associated with the presence of skin commensals. Concomitantly, the model gained first insights on the microbiome's influence on skin xenobiotic metabolism (i.e., CYP1A1, CYP1B1 and CYP2D6) and olfactory receptor expression. The system provides urgently needed experimental access for assessing the toxicological impact of microbiome-associated xenobiotic metabolism in situ.

Keywords Microbial–skin tissue co-culture · Skin model · Commensals · Transcriptional changes · Method development

## Introduction

In terms of bacterial numbers and population density our skin comes second to the gut, harbouring more than 200 different bacterial genera with an overall population density between 1 million and 1 billion cells per $cm^2$ (Grice et al. 2008, 2009;Ross et al. 2019). Set into relation this is a significant part of our microbiome, which as such not only outnumbers us cell- and genomewise, but also features a metabolic potential far exceeding our own in terms of biochemistry as well as genetic flexibility (Possemiers et al. 2011; Sender et al. 2016; Tralau et al. 2015; Yadav et al. 2018). While still in its relative infancy and thus maybe at time overstated our understanding of the microbiome's impact on host biology continues to increase steadily. This is not the least thanks to massive parallel sequencing, metabolomics, metaproteomics and stable isotope probing-based

Electronic supplementary material The online version of this article (https://doi.org/10.1007/s00204-020-02841-z) contains supplementary material, which is available to authorized users.

Lisa Lemoine
Lisa.Lemoine@bfr.bund.de

[1] Department of Chemical and Product Safety, German Federal Institute for Risk Assessment (BfR), Max-Dohrn-Strasse 8-10, 10589 Berlin, Germany

[2] Department of Biology, Chemistry, Pharmacy, Institute of Pharmacy, Freie Universität Berlin, Berlin, Germany

[3] Department of Biological Safety, German Federal Institute for Risk Assessment (BfR), Diedersdorfer Weg 1, 12277 Berlin, Germany

[4] Department of Food Safety, German Federal Institutefor Risk Assessment (BfR), Max-Dohrn-Strasse 8-10, 10589 Berlin, Germany

approaches (Berry and Loy 2018; Isaac et al. 2019; Lamichhane et al. 2018; Turnbaugh et al. 2007). However, due to the limited choice of suitable in vitro models current studies mostly rely on analyses in situ, culture-independent approaches or, despite their restricted applicability, mouse models (Staley et al. 2017; Wang and Donovan 2015). The picture emerging from these studies shows an intricate relationship between the human host and its microbial colonists, the biological implications of which include commen- salic functions such as vitamin and amino acid synthesisor immune modulation as was well as pathophysiologies such as allergies, chronic diseases, behavioural disorders or toxification of xenobiotics (Clemente et al. 2012; Platzek et al. 1999; Sowada et al. 2017; Tralau et al. 2015). The mechanisms underlying the latter are diverse and include substance-induced shifts of host microbiota composition, microbiome-catalysed chemical modifications or metabolism of xenobiotics as well as microbiome induced changes of the hosts gene expression (Collins and Patterson 2020). Traditionally, most research on microbial influence on xenobiotic metabolism has focused on the gut. Respective examples comprise more than thirty commercially available drugs, including blockbusters such as paracetamol (Clayton et al. 2009; Sousa et al. 2008; Tralau et al. 2015). At times harmless or merely affecting efficacy the corresponding consequences can also prove fatal. This has been tragically the case for sorivudine, highlighting the pressing need for a more systematic and better understanding of any potential microbial impact on toxification of drugs and chemicals (Sousa et al. 2008). Given the high metabolic potential of the various microbiomes and the fact that exposure to xenobiotics also occurs outside the gut it would be naïve, however, to restrict the search for such microbiome-associated substance-induced pathophysiologies to the gut. Indeed and albeit less well investigated in terms of potential microbiome interactions many active ingredients are, for example, also applied to skin.

Yet, detailed and systematic analysis of commensalic metabolism and its effects on host biology is often hampered as there is a lack of model systems able to emulate host–microbiome biology under controlled conditions, particularly if the aim is to move beyond the state of community analysis or measurement of basic metabolite patterns. With only a handful of systems available for the gut this is even more the case for skin. So far there is no microbially competent in vitro model commercially available that would allow skin-microbiome studies for extended periods of time.

Nevertheless, the biological relevance of such models is high and their potential applications extend well beyond toxicology. Modulation of skin inflammation, for example, is functionally dependent on commensals and the progress of inflammation depends, amongst others, on innate immune factors such as β-defensins and cathelicidin (Christensen and Bruggemann 2014; Gallo and Hooper 2012; Lai et al. 2010; Percoco et al. 2013). Released by keratinocytes in order to kill or inactivate pathogens (Lai and Gallo 2009), the expression of these antimicrobial peptides (AMPs) depends on commensal Toll-like receptor 2 (TLR2)-activation (Lai et al. 2010). Likewise, skin commensals have been shown to induce and control T cell responses in mouse models (Linehan et al. 2018; Schommer and Gallo 2013). Effects observed include increased production of pro-inflammatory molecules such as interferon-γ (INFγ) and interleukin (IL)-17A with the regulatory factors involved [IL-1α, IL-1β, IL-6, Transforming Growth Factor (TGF)-β] being partly induced or regulated by skin commensals (Feehley and Nagler 2014; Hasegawa et al. 2012; Naik et al. 2012; Veldhoen et al. 2008). These cytokines are also essential for the expression of various AMPs (Huang et al. 2002; Steinz et al. 2014). However, the mechanisms underlying the respective microbial immune-modulatory function are only partly understood. Particularly bacterially triggered modulations of toll-like receptor (TLR) responses extend the link into cellular signalling cascades beyond immediate immune reactions as the physiological implications of the IL-1R/TLR superfamily not only extend to inflammation regulation but also resistance to epithelial injury and epithelial homeostasis (Barton and Medzhitov 2003; Dunne and O'Neill 2003; Kubinak and Round 2012; Lopez-Castejon and Brough 2011).

Beyond extensively characterised immunomodulation dysbiosis of the skin's microbiome has been associated with conditions such as atopic dermatitis or allergies and recent work highlighted the potential of skin commensals to form highly carcinogenic by-products from benzo[*a*]pyrene and other polycyclic aromatic hydrocarbons (Platzek et al. 1999; Sowada et al. 2014; Stingley et al. 2010). Yet, for many of the observed microbial dysbalances it still remains unclear if they are cause or rather consequence of the respective condition (Tralau et al. 2015). Even the presumably more straightforward hazard of carcinogenic metabolites remains challenging to assess, not the least due to the aforementioned lack of suitable model systems (Sowada et al. 2014, 2017). We now report on the development of a test system designed to study skin–microbe interactions in situ. The system relies on a commercially available 3D skin model, that is EpiDermFT™ from MatTek, which consists of epidermal and dermal layers, that are mitotically and metabolically active and exhibit in vivo-like morphological and growth characteristics which are uniform and highly reproducible. Moreover, the model was previously pre-validated for metabolically competent toxicity testing in vitro (Brinkmann et al. 2013; Hu et al. 2010) and genotoxicity testing using micronucleus and COMET assays (Pfuhler et al. 2014). In a proof-of-concept, this model has now been colonised using two previously isolated skin isolates, namely *Micrococcus*

*luteus* 1B and *Pseudomonas oleovorans* 1C (Sowada et al. 2014). The selection of these organisms followed practical considerations and with the intended later application of studying potential microbiome-mediated substance toxification in mind. Both species are biologically relevant (Chiller et al. 2001; Wang et al. 2019), have an established potential for xenobiotic metabolism (Egea et al. 2017; Hanafy et al. 2016; Sowada et al. 2014; Viggor et al. 2020) and have been isolated repeatedly from healthy volunteers at different sites (Khayyira et al. 2020; Sowada et al. 2014; Steglinska et al. 2019; Wang et al. 2019). Amongst the skin's Micrococcaceae *M. luteus* is the predominant species (Chiller et al. 2001). It is considered essential for the population balance of the skin's microbiome (Epstein 2015) and usually accounts for 20–80% of the micrococci isolated (Davis 1996). Correspondingly *P. oleovorans* belongs to the Proteobacteria which make up to 34% of the whole skin microbiome (Kim et al. 2018). Lastly, both organisms bring the added bonus of being aerobes belonging to different Gram-categories which eases their laboratory handling.

The aim of this work was to develop a microbially competent skin model that provides access to microbe–host interactions and the toxicological impact of microbiome-mediated metabolism of xenobiotics under near in vivo conditions. Any such model has to be functional for at least 1 week in order to also pick up on slow or delayed xenobiotic modulations. Model functionality thus crucially depends on comparing its biology with what has been reported for commensalic skin interactions previously.

## Results

Two representative skin commensals were tested for sta- ble colonisation of commercially available 3D skin mod- els in a proof of concept study. Based on its performance in toxicological prevalidation studies the model of choice was EpiDermFT™ as distributed by MatTek (Brinkmannet al. 2013). The model was tested with two bacterial strains,the Gram-negative *P. oleovorans* and the Gram-positive *M. luteus*, both of which were previously isolated from healthy volunteers (Sowada et al. 2014).

### Establishment of stable microbial–skin tissue co-cultures

First tests focused on establishing microbial–skin tissue co-cultures using single strains or a mixed culture. Following bacterial inoculation the corresponding skin models were maintained over a period of 8 days with sampling performed on days 0, 4 and 8. Microbial–skin tissue co-culture formation and stability was followed by colony counts and strain-specific qPCR. Single cultures as well as the mixed culture viable colony counts (CFU/cm$^2$) showed microbial–skin tissue co-culture establishment to occur during the first 4 days with bacterial cell numbers of *M. luteus* remaining largely stable thereafter (Fig. 1a). However, in both culture scenarios (single vs. mixed culture) *P. oleovorans* repeatedly reached higher cell numbers. In the mixed culture this resulted in *P. oleovorans* outcompeting *M. luteus,* the lat- ter growing in lower numbers than when cultured alone (Fig. 1b, c). Strain-specific real-time quantitative PCR (datanot shown) confirmed this data.

Microscopy and Gram-staining was concomitantly used to visualise bacterial colonisation in situ. The respective slides showed *M. luteus* to exclusively stay on the surface of the skin, whereas *P. oleovorans* appears partially to penetrate into the (epi)dermal layers (Supplementary Fig. S3a). Moreover, and in line with the CFU-data the slides visually confirmed *P. oleovorans* to outnumber *M. luteus* in microbial–skin tissue co-culture (Supplementary Fig. S3b). None of the recordings indicated any cross-contamination or foreign contamination with microorganisms. This was also confirmed by supplementary 16S-PCR and sequencing.

### Impact of bacterial co-colonisation on skin model biology

Next the impact of microbial co-colonisation on the skin models was assessed. For this purpose, Human Clariom™ S assays were subsequently used to record transcriptomic profiles of models colonised with *M. luteus* or *P. oleovorans*. The assay provides a transcriptomic snapshot of a core-set of 20,000 well-annotated genes, thus allowing a basic functional assessment of the skin's global gene expression and molecular network interactions prior and after microbial colonisation. Co-colonisation had a clear effect on the skin with principal component analysis differentiating the untreated controls from the microbially competent models (Fig. 2a). In total 313 and 3318 transcripts were found to be specifically affected by the presence of *M. luteus* and *P. oleovorans*, respectively (Fig. 2b).

Preliminary functional IPA analysis indicated reduced cell death and moderate effects on cell growth, proliferation and tissue development, including vasculogenesis (Supplementary Fig. S4). Although the underlying transcriptional changes occurred with both strains, the effectual tendencies were more pronounced with *P. oleovorans*. In depth analysis showed most of the affected transcripts to relate to immune functions with the AMPs defensin β 4A and B being amongst the most differentially regulated genes (Fig. 3a). Befittingly increased levels of defensin β 4A were also detected in the culture supernatant (Fig. 3b). Other AMPs such as Cathelicidin-related antimicrobial peptides (CAMP) or RNase7 were not found to be differentially expressed. Nevertheless, IPA analysis showed high activity of CAMP-regulated transcripts

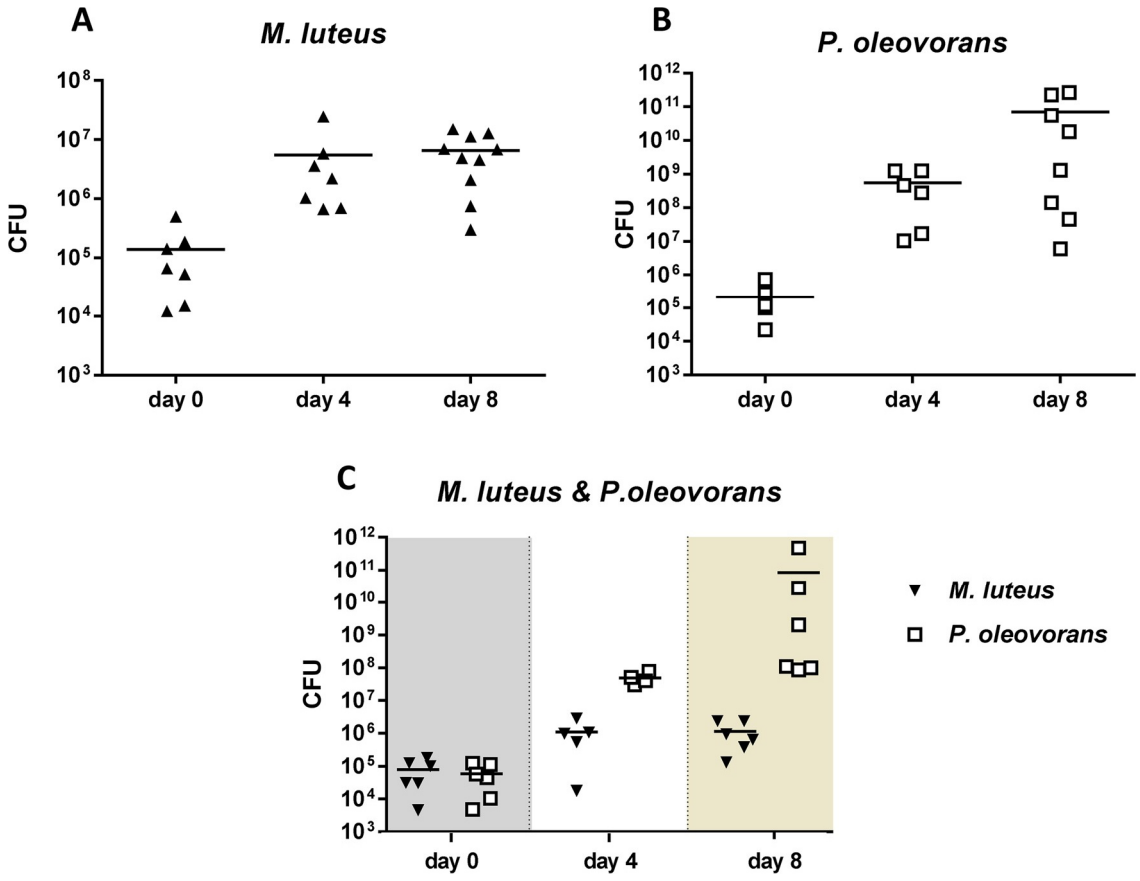


Fig. 1 Plate counts from skin models on day 0, 4 and 8 of bacterial colonisation. The panels depict the results recorded for *Micrococcus luteus* (**a**), *Pseudomonas oleovorans* (**b**) and the mixed culture (**c**), respectively. Each point represents an independent experiment with the horizontal bars indicating the corresponding arithmetic mean. *CFU* colony-forming units

($p = 6.73 \times 10^{-10}$), indicating some activation of the corresponding molecular pathways.

The co-colonised models generally featured increased transcription of *TLR2* with *P. oleovorans* also inducing *TLR6*. Expression of *TLR3* was repressed though and while the stress- and immune-responsive NF-κB pathway clearly reacted differently to *M. luteus* or *P. oleovorans* it nevertheless failed to provide any clear functional response on transcriptional level (Supplementary Fig. S5a).

Taken together the transcriptional responses of the co-colonised models thus indicate a state of increased immune competence. This was further confirmed by the expression patterns of various pro- and anti-inflammatory cytokines including IL1-α, IL1-β, IL-10 and TGF-β. Again, the observed cytokine patterns showed some strain-specific induction, particularly for *P. oleovorans* (Fig. 3a). Pro-tein secretion was in line with the gene expression data except for Macrophage migration inhibitory factor (MIF) and Monocyte chemoattractant protein **(**MCP)-1, both of which were recorded at elevated levels in the presence of *P. oleovorans* but failed to show matching transcriptional induction (Fig. 3a–c). Interestingly, exposure to *P. oleovorans* also induced partial expression of signalling pathways of triggering receptors expressed on myeloid cells (TREMs) (Supplementary Fig. S5b and c). Amongst other functions these receptors act as important immune modulators and are known to be activated by commensal and pathogenic bacteria (Varanat et al. 2017; Wu et al. 2011). Overall, the transcriptional response of combined pro- and anti-inflammatory effects mirrors the reaction against commensals in vivo (Kubinak and Round 2012; Meisel et al. 2018; Nutsch and Hsieh 2012).

Apart from triggering increased immune competence microbial co-colonisation also had marked transcriptional effects on many genes of the fibroblast growth factor family (FGF2, 4, 5 and 12), the vascular endothelial growth fac- tor family (VFGFA and VFGFC), the transforming growth factor beta family (TGFB1 and TGFBI), and the insulin- like growth factor-binding protein family (IGFBP1, 3, 2and 5) (Fig. 4a). Again, some of these effects were rather strain specific with *P. oleovorans* tending to produce a more pronounced response. Altogether the transcriptional

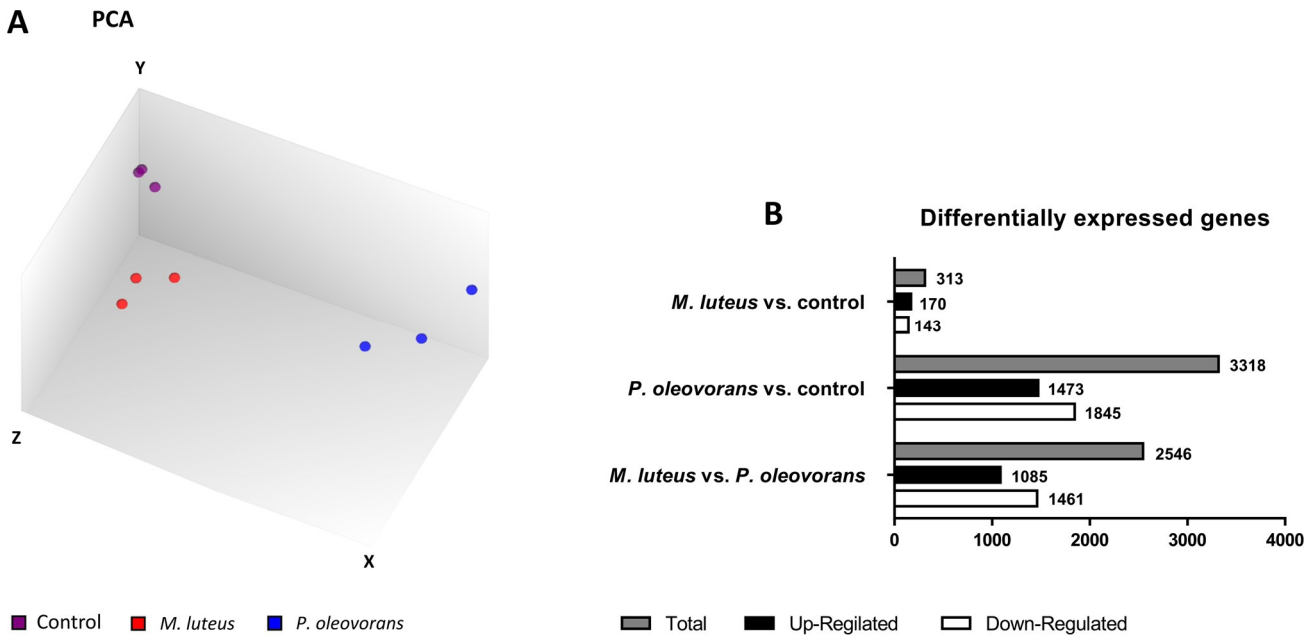


Fig. 2 Transcriptional response of EpiDermFT™ models on day 8 of microbial colonisation. Mapping 81.4% of the available transcripts PCA shows clear separation of the untreated control from tissues colonised with *M. luteus* or *P. oleovorans* (**a**). Number of differentially expressed genes in skin colonised with *M. luteus*, *P. oleovorans* and the mixed culture (**b**). All experiments were conducted in triplicate

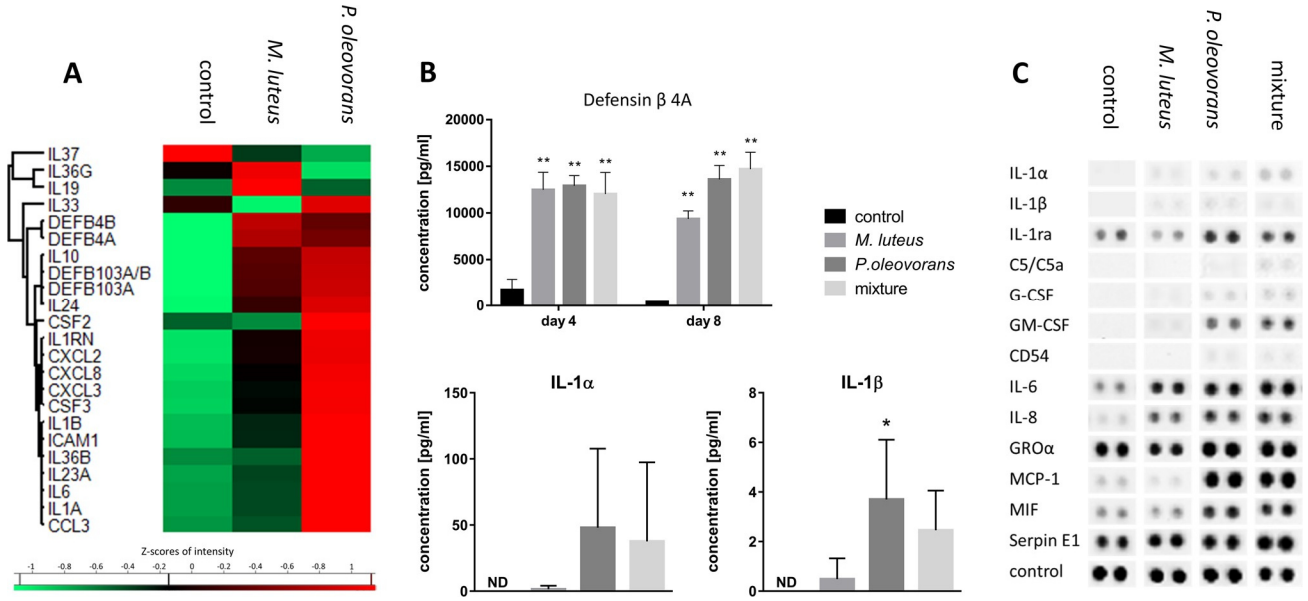


Fig. 3 Expression of various cytokines and defensins in microbially competent skin models. The cluster map records the transcriptional state at day 8 of microbial colonisation as indicated (**a**). Shown are the gene symbols and Z-scores of significantly differentially expressed genes with an $F$ value < 0.05 across at least three independent experiments. Concomitant excretion of defensin β 4A and IL-1α/β into the supernatant was quantified using an ELISA and FACS analysis, respectively (**b**). Shown are mean concentrations with errorbars indicating standard deviation. All values are significant within $*p < 0.05$ or $**p < 0.01$, values labelled "ND" were not detectable. Similarly, cytokine excretion into the supernatant was verified qualitatively using a proteome profiler array (**c**)

effects seemed to be representative of the model's priming towards more fine-tuned differentiation rather than indicating functional differentiation as such, for effects on protein expression were far less pronounced (Fig. 4b, c). The

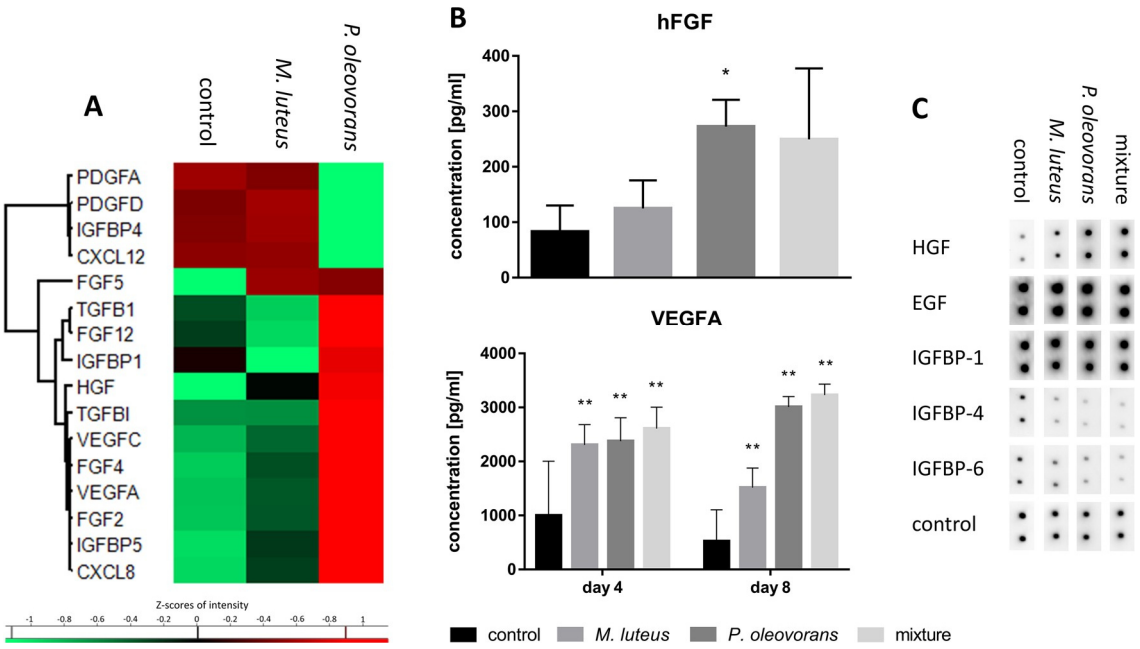


Fig. 4 Expression of cellular growth factors in microbially competent skin models, colonised as indicated. The cluster map records the transcriptional state at day 8 of microbial colonisation (**a**). Shown are the gene symbols and Z-scores of significantly differentially expressed genes with an $F$ value < 0.05 across at least three independent experiments. Concomitant excretion of hFGF and VEGFA into the supernatant was quantified using an ELISA (**b**). Shown are mean concentrations with error bars indicating standard deviation. All values are significant within $*p < 0.05$ or $**p < 0.01$. Expression of growth factors into the supernatant was further verified qualitatively using a proteome profiler array (**c**)

latter only related well for selected transcripts such as the microbially induced expression of VFGFA and hepatocyte growth factor (HGF), or the downregulation of IGFBP6 and IGFBP4, respectively.

Commensal communities are also known to induce strong differential expression of many olfactory receptors (ORs). With about 400 members this receptor family is expressed throughout the body, regulating physiological cell functions well beyond olfaction. In skin this includes keratinocyte proliferation, migration, and re-epithelialisation of keratinocytes (Cheret et al. 2018; Denda 2014). Markedly microbial–skin tissue co-culture with *P. oleovorans* or *M. luteus* led to 77 or 15 differentially regulated ORs (Supplementary Fig. S6), with the functional implications remaining unclear though.

## Impact on metabolic competence

In light of the intended use for toxicological studies the colonised skin models were further analysed with respect to transcription of various cytochrome P450-dependent monooxygenases (CYPs), an enzyme class that represent the mainstay in phase I metabolism (Fig. 5a, b). Of the 63 CYPs examined almost 30% were transcriptionally affected in microbial–skin tissue co-culture, with most of the responses being strain specific to various degrees. However, amongst the six CYPs characteristic for skin metabolism (i.e., CYP1A1, CYP1B1,CYP2B6, CYP2E1, CYP2D6, and CYP3A) only CYP1A1and CYP2D6 were subject to some additional induction in the presence of *P. oleovorans*, with transcript levels rising 1.7-fold and 2.4-fold compared to the uncolonised control. This trend was also confirmed by quantitative RT-PCR. Taken together the results show that while co-colonisation adds an additional layer of microbial metabolism with poten-tially biasing effects on the skin's inherent CYP-mediated phase I capacity, its impact is likely to remain moderate.

## Discussion

The human microbiome is an integral part of our (patho) physiology. Yet, an overwhelming part of microbiome research still concentrates on the description of microbial communities and their population dynamics (Round and Palm 2018; Sazal et al. 2020; Walter et al. 2020). Contrastingly and with hardly any in vitro systems available studying the underlying mechanisms and causality of host–microbe interactions remains a major challenge. For the gut Human Microbiota-Associated Mice (HMA) often continue to be a preferred system, despite all technical limitations and ethical issues. With only 15% of gut bacterial lineages shared compositional differences of the intestinal microbiomes in man and mice far exceed those within species (Ley et al.).

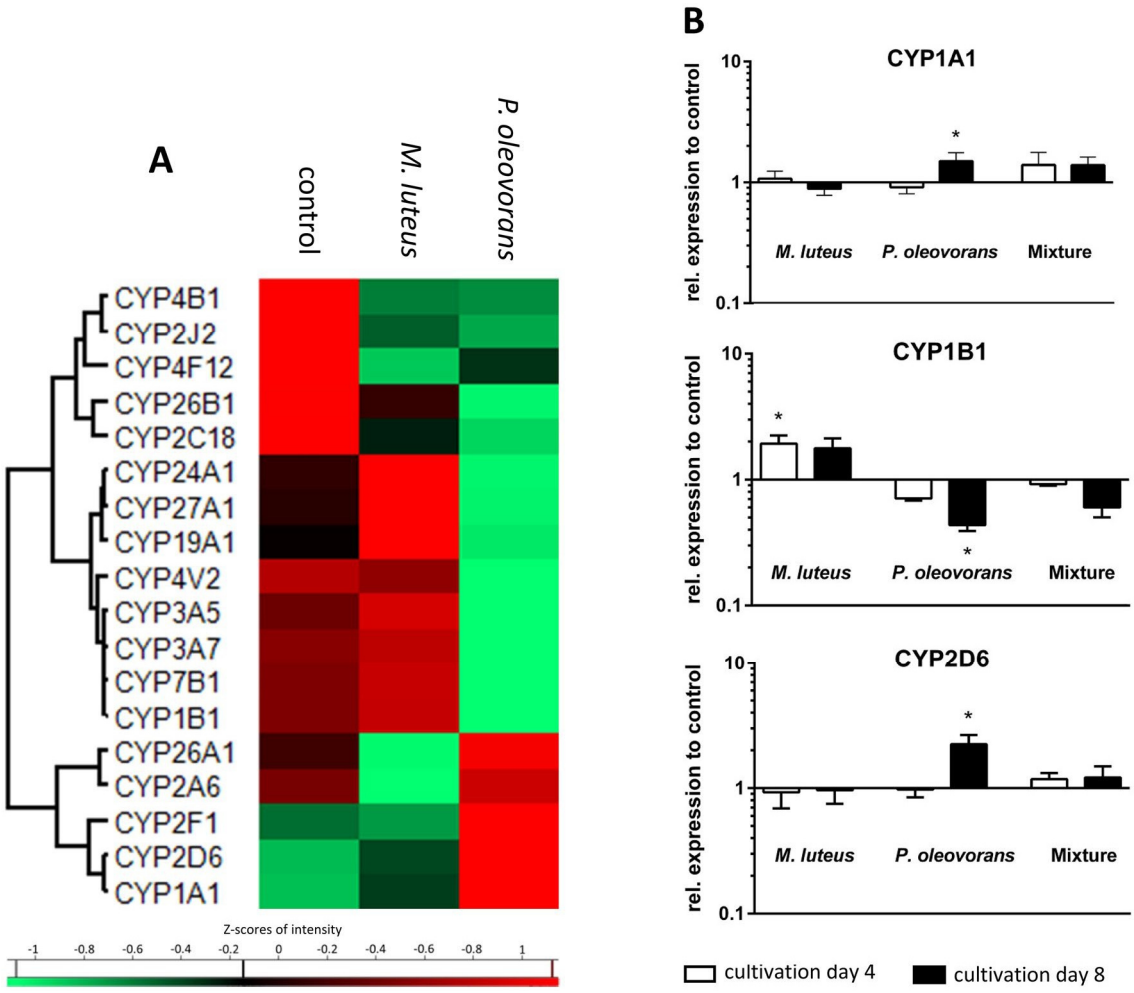


Fig. 5 Expression of various cytochrome P450-dependent monooxygenases (CYPs) involved in phase I metabolism in the skin with the cluster map recording the transcriptional state at day 8 of microbial colonisation (**a**). Shown are the gene symbols and Z-scores of significantly differentially expressed genes with an $F$ value < 0.05 across at least three independent experiments. Expression of key transcripts was quantified further using RT-PCR (**b**)

2005) and consequently humanised systems tend to suffer from poor long-term stability (Rawls et al. 2006). Alternatively, bioreactors have hence been used as a simple and effective method to study microbial metabolism and community dynamics under various dietary and xenobiotic influences (Guzman-Rodriguez et al. 2018). Yet, as with other techniques these systems are also subject to limitations such as culturability, long-term stability and lack of direct intestinal interaction (Guzman-Rodriguez et al. 2018; Vrancken et al. 2019). The problem becomes even more evident when moving to commensal communities outside the gut. Rodent skin for example not only features its own species-specific microbiome, but also is profoundly different in terms of physiology and metabolism (Gerber Peter et al. 2014; Oesch et al. 2014).

For toxicological and mechanistic studies of the skin, human 3D skin models have hence long been tools of choice, albeit lacking any microbial competence in situ (Rademacher et al. 2018). Systems used to study the pathophysiology of skin–microbe interactions (i.e., during infectious or inflammatory settings) comprise cell cultures with added bacterial endotoxins (Kampfer et al. 2017; Lai et al. 2009), two-dimensional cell cultures in the presence of live pathogens or the odd three-dimensional approach with bacteria added to the culture medium (Barrila et al. 2017; Mason et al. 1998; Mohiti-Asli et al. 2014). Addi- tionally, there is a stratum corneum model from van der Krieken et al. (2016), where bacteria are applied to the apical surface of dead corneocytes or a model from deBreij et al. (2012), where an epidermal skin equivalentis colonised by *Acinetobacter* species. While the latter models come close to the in vivo situation, at least struc- turally, they nevertheless lack the option to study micro- bial interaction with living keratinocytes and fibroblasts.

There are also studies on colonising 3D skin equivalents which feature dermis, epidermis and a fully differentiated stratum corneum as well as surface contact with ambient air. However, these models have not been pre-validatedfor toxicity studies. Also, the colonisation in these studies has been limited to 48–120 h. Yet, the studies of Sowadaet al. (2017) show that at least for PAHs microbe-mediated toxicity occurs predominantly at time-points later than5 days. Moreover, the aforementioned models often lack a detailed biochemical characterisation (Bojar 2015; Cadau et al. 2017; Holland et al. 2008; Maboni et al. 2017; Popov et al. 2014).

For our studies we used MatTek's full thickness skin model EpiDermFT™. Together with fully functionalbarrier properties and a metabolic complexity close to that of in vivo skin this model has a proven track recordas reliable testing system for skin toxicity (Black et al. 2010; Brinkmann et al. 2013; Wills et al. 2016). The suc- cessful microbial colonisation reported in this study is a major functional amendment as it provides, to the bestof our knowledge, the first testing system for assessing "longer term" skin-microbiome interactions in situ. Theskin models were efficiently colonised with commensal communities of *M. luteus* and *P. oleovorans*, with the letter performing slightly better than the first. Following inoculation microbial–skin tissue co-cultures took up to4 days to establish and remained stable at least until day8 with colony counts similar to what is reported for skinin vivo (up to $10^9$ CFU/cm$^2$) (Ross et al. 2019; Tralau et al.2015). In general, *P. oleovorans* was repeatedly observedto grow to higher cell counts compared to *M. luteus* both in single and mixed microbial–skin tissue co-culture. For some experiments this resulted in cell counts of up to $10^{11}$ cells/cm$^2$ for *P. oleovorans* on day 8. This is possibly due to an increased robustness against nutrient limitation and this organism's ability to colonise not only the stratumcorneum but to penetrate into the epidermis and dermis, particularly in absence of a fully functional immune response. This growth behaviour matches that reported for other *Pseudomonas* spp. in human skin biopsies (Nakatsuji et al. 2013). In contrast, *M. luteus* cell counts were slightly reduced in mixed microbial–skin tissue co-cultures probably due to its dependence on a more restricted range of carbon sources (Young et al. 2010). What is more, is that 3D skin models such as EpiDermFT™ do not have sweat glands or hair follicles. This limits the choice of naturally available nutrients to peptides and lipids, restricting access to urea, ammonia, vitamins or sugars (Scharschmidt and Fischbach 2013). However, the latter will at least partially be compensated for by diffusion of glucose from the cell culture medium into the dermal and epidermal layers of the model (Khalil et al. 2006; Ullah et al. 2018). This provides some selectional advantage for the more invasive *P. oleovorans* as even a thin stratum corneum layer constitutes a considerable barrier for passive diffusion (Ullah et al. 2018).

Transcriptional influence of the skin microbiome on its host is well established, although little understood and thus of high interest (Duckney et al. 2013; Linehan et al. 2018; Ridaura et al. 2018; Wanke et al. 2011). The extent and impact are community specific, something also seen in our models where *P. oleovorans* influenced the transcription of nearly 3300 genes. That is nearly tenfold the number of transcripts affected by *M. luteus* and in the same order of magnitude what is seen in germ-free mice in response to microbial colonisation (Meisel et al. 2018). Part of this gene response is likely to be the consequence of *P. oleovorans* penetrating the epidermal barrier and its relatively high cell count of up to $10^{11}$ CFU/cm$^2$ on the eighth day of cultivation. With *P. oleovorans* being an opportunistic pathogen an immunogenic response is inherently necessary to maintain a healthy commensal community. Duckney et al. (2013) reported a strong and predominantly inflammatory response in skin models when mimicking complete barrier breakdown. The effects observed in our colonised models are less acute and rather in line with what is seen for commensal communities in vivo. For example, similar to what is seen in host–microbiome animal studies both organisms lead to increased gene expression of β-defensins DEFB3A and DEFB4A (Lai et al. 2010; Rademacher et al. 2019). These β-defensins are critical but not exclusive for host defence, with induction of *DEFB3A* relying, amongst other things, on activation of TLR2 (Shin and Choi 2010). Befittingly we also see increased levels of *TLR2* expression in the skin subsequent to microbial colonisation. The increase was significantly more pronounced in skin models colonised with *P. oleovorans*, together with a slight but significant upregulation of TLR 6. Induction of TLR2 by LPS from *Pseudomonas* species has been shown earlier (Shin et al. 2013). Homo- or heterodimers of TLR2 or TLR2/TLR6 are capable of discriminating various lipopeptides (Takai et al. 2014) and are involved in immune modulation, including elicitation of cytokine secretion and promotion of regulatory T (Treg) cell (Nawijn et al. 2013; Netea et al. 2008; van Maren et al. 2008) and Th17 cell responses (DePaolo et al. 2012; Reynolds et al. 2010; Xu et al. 2017; Zhao et al. 2015). Results from preliminary screens with THP-1 cells further support this as exposure to medium from microbially competent models leads to secretion of IL-23, a cytokine crucial for Th17 development and adaptive immunity (Supplementary Fig. S7) (McGeachy et al. 2009; Zielinski et al. 2012). Various TLRs have been implicated to modulate the immune responses to commensals in vitro (Kubinak and Round 2012; Maier et al. 2018; Ren et al. 2016) as well as in vivo (Oppong et al. 2013; Round et al. 2011), often promoting mutually beneficial microbe–host interactions. Amongst the respective target cytokines are

IL-1α, IL-1β, IL-6 (Hasegawa et al. 2012; Naik et al. 2012; Ren et al. 2016) and IL-10 (Cosseau et al. 2008; Jun et al. 2017; Neish 2009), all of which we found to be elevated in the presence of *P. oleovorans* and *M. luteus*. The transcription of these cytokines is partly subject to TREM-1 signalling, which was significantly induced in models colonised with *P. oleovorans* (Lagler et al. 2009; Rai and Agrawal 2017; Tessarz and Cerwenka 2008). Commensalic influence on IL-1 signalling is known to modulate effector T cell responses. The corresponding modulation and fine-tuning of immune responses is essential for a functioning host–microbiome relationship as well as for maintaining a healthy skin (Naik et al. 2012; Park and Lee 2017). In fact, maturation of IL-1α and IL-1β crucially depends on commensal presence (Lopez-Castejon and Brough 2011; Naik et al. 2012). Indeed microbial–skin tissue co-cultures with both organisms showed an increase in gene expression and excretion for both cytokines. Other genes of the interleukin-1 family were also upregulated, including IL-33 and IL-36β for *P. oleovorans* and IL-36γ for *M. luteus*. Similarly the observed expression of anti-inflammatory messengers such as IL-10 and TGF-β has been linked to commensal colonisation and associated immune tolerance (Fung et al. 2016; Meiselet al. 2018; Ueda et al. 2010). Altogether the response of the co-colonised models thus is very much similar to what is observed in vivo, with increased immunomodulation and immunotolerance, respectively (Nutsch and Hsieh 2012). Similarly, many of the aforementioned transcription factors and genes found to be transcriptionally affected by co-colonisation match those seen in skin development and differentiation in vivo. Examples include the host angiogenesis transcription factor Ephrin-A1 as well as the growth factors FGF2, HGF, PTGER4, VEGFA and VEGFC or ORs such as OR2A7 (Linehan et al. 2018; Sajib et al. 2018; Stappenbeck et al. 2002). The latter is known to play an important role in various processes of the skin, including keratinocyte proliferation (Tsai et al. 2017). The regulation of ORs by human commensals has so far been little studied. Pluznick et al. (2013) showed critical involvement of OR51E2 in intestinal host–microbiome signalling. In our skin models this receptor was upregulated in the presence of *P. oleovorans*. Interestingly, seven of the genes from the OR family were differentially regulated in both microbial–skin tissue co-cultures. Continuatively, it seems worthwhile to assess the general role of ORs in skin-microbiome signalling in more detail.

Colonisation of the skin models also had a marked influence on CYP expression with almost 30% of CYPs affected, including the toxicologically relevant CYP1A1. In mice CYP1A1-facilitated detoxification of carcinogens has been implicated to rely on TLR2-dependent signalling (Do et al. 2012). Therefore, the differential expression of TLR2 with *P. oleovorans* is likely also causal for this organism's marked induction of CYP1A1. While little is known for skin, the overall microbial influence on CYP expression in the gut has been reported previously. This includes CYP3A, CYP2C9, CYP1A and CYP2D6, for which microbial metabolites can either serve as substrates, inductors or inhibitors (Claus et al. 2011; Tralau et al. 2015). Biological pathway analysis also implicated microbial influence of both organisms on other key processes such as proliferation, keratinocyte differentiation and apoptosis. In general, *P. oleovorans* seems to have a greater influence on processes pertained to cellular movement of the dermis (fibroblasts and connective tissue), whereas *M. luteus* rather influences keratinocyte movement. This is probably due to the different habitats of the organisms. So far, little is known about the influence of microorganisms on cell proliferation and differentiation in the skin. However, our results confirm that the balance between epidermal proliferation and differentiation is altered in response to microbial colonisation (Meisel et al. 2018). The underlying pathways involve signalling of MAPK and NF-κB as well as IL-1 and DEFB3/4A, all of which we found to be affected (Eller et al. 1995; Nishimura et al. 2004; Preciado et al. 2005).

Currently, the model is limited to a selected number of species as it has not been tested for entire swabs or community stamps. As such it will also always be limited to the cultivation bias inherited by all growth-based models. This is not the least because it carries the inherent limitations of MatTek's EpiDermFT™ such as the absence of sweat glands and selections glands, both of which contribute to the nutrient pool of natural skin communities. However, the microbially mediated changes in the skin matched what is known from other skin studies and mouse models. This is true for the observed alterations in gene expression such as the IL-1 family, the secretion of antimicrobial peptides and the predicted influence on skin differentiation and proliferation. As an extendable microbial–skin tissue co-culture system this model hence provides a good system for studying selected skin host–microbiome interactions including microbiome-mediated substance toxification in situ over extended periods of time.

## Materials and methods

### Chemicals and media

If not mentioned otherwise chemicals were purchased at purities greater than 98% from Sigma-Aldrich (Taufkirchen, Germany) or Carl Roth (Karlsruhe, Germany), respectively. Media for the 3D skin models were sourced from MatTek (Ashland, MA) while molecular reagents and kits were routinely obtained from Qiagen (Hilden, Germany) and Invitek (STRATEC Molecular GmbH, Berlin, Germany). Primers were purchased from Metabion (Martinsried, Germany).

## Bacterial isolates and bacterial growth

Microbial–skin tissue co-cultures were set up using two previously enriched skin-commensals, that is *Micrococcus luteus* 1B and *Pseudomonas oleovorans* 1C (Sowada et al. 2014). When not applied on the surface of the skin models bacteria were routinely grown as shake flask cultures in lysogeny broth (LB) at 200 rpm and 32 °C. Growth was routinely monitored using optical density (OD, $\lambda = 600$ nm) and correlated to colony-forming units (CFU) as established by serial plate counts (PC) as required. Cells used for skin model inoculation were harvested at an $OD_{600}$ of 0.4–0.9 with 7.500 g for 8 min and washed once in PBS (MatTek, Ashland, MA, USA). The pellet was subsequently re-dissolved in 15 µl PBS and $10^4$–$10^6$ cells used for skin inoculation.

## Whole-genome sequencing (WGS)

For each isolate a single colony grown on LB agar was inoculated in liquid LB and cultivated under shaking conditions at 150 rpm and 37 °C for 22 ± 2 h. Subsequent extraction of DNA was performed using the PureLink® Genomic DNA Mini Kit (Invitrogen, Carlsbad, CA, USA). Sequencing libraries were then prepared with the Nextera XT DNA Sample Preparation Kit (Illumina, San Diego, CA, USA) according to the manufacturer's protocol. Paired-end sequencing performed in 2 × 301 cycles on an Illumina MiSeq benchtop using the MiSeq Reagent v3 600-cycle Kit (Illumina).

## Tissue culture

Skin models (EpiDermFT™) were obtained from Mat- Tek (Ashland, MA, USA). Three days before shipment the models are started to cultivated in antibiotic-free medium. Upon arrival the models were directly transferred into six-well plates (Greiner Bio-One, Frickenhausen, Germany)and allowed to recover overnight in 2.5 ml of antibiotic-freeEPI-100-MM-ABF at 37 °C and 5% $CO_2$ as recommended by the manufacturer. Following recovery the models were then subjected to bacterial inoculation or solvent treatment, respectively. Models were subsequently maintained at 37 °C in a humidified atmosphere of 5% $CO_2$ for up to 8 days with culture media being exchanged daily, following the recommendations of the manufacturer who warrants culture stability for up to 2 weeks. Tissues and media not used upon completion were harvested, shock-frozen in liquid $N_2$ and stored at − 80 °C as appropriate. Model sections to be used for bacterial staining were transferred into embedding medium prior to freezing.

The medium of microbial–skin tissue co-culture models was checked daily for contamination by sampling for possible bacterial growth by $OD_{600}$-measurements and plating. Follow-up experiments were only carried out if the medium was free of contamination.

Please note that it is highly recommended to use different plates for different microbial–skin tissue co-cultures. This minimises the risk of cross-contamination. Also, the volume of the bacterial inoculum applied topically should not exceed 15 µl.

## Bacterial quantification: skin models

Bacterial growth in microbial–skin tissue co-culture was quantified using PC or strain-specific quantitative PCR (ss-qPCR) (as described in the supplementary section Method S1), respectively. For the PC bacterial imprints were obtained from the surface of the skin models using2 $cm^2$ of velvet cloth. The cloth was soaked in sterile PBS and applied with gentle pressure to the surface of the skin model before being subsequently transferred into 1 ml of sterile PBS. Following incubation in a thermomixer (Eppen-dorf, Hamburg, Germany) at room temperature for 30 min at 6000 rpm the velvet was wrung out and 100 µl of the bacterial PBS-suspension were used to set up serial dilutionson LB agar. After 24 h at 37 °C bacterial counts were then recorded as CFU/ml.

In order to preclude the possibility of a contamination with other microorganisms, we have performed a PCR with 16S-rRNA gene-specific primers (Tralau et al. 2011) with the DNA of the individual models, followed by sequencing of the PCR products at Eurofins (Ebersberg, Germany).

## Bacterial staining of co-colonised skin models

For bacterial stains frozen model sections (~ 1 $cm^2$) were cut in a cryomicrotome at − 20 °C. Slices were set to measure 5 µm in diameter and then subjected to standard Gram-staining using the Gram stain tissue kit (Sigma, St. Louis, MO, USA). Staining was performed according to the manufacturer's instructions relying on precooled acetone (− 20 °C, 20 min) as fixation agent. The results were recorded using a standard Axio Observer A1 microscope (Zeiss, Oberkochen, Germany).

## THP-1 cell culture

THP-1 cells were obtained from Leibniz Institute DSMZ—German Collection of Microorganisms and Cell Cultures (Braunschweig, Germany). Growth was routinely performed using RPMI 1640 medium (PAN-Biotec, Aidenbach, Germany) supplemented with 10% (v/v) FBS (Biochrom, Berlin, Germany), HEPES; 10 mM, l-glutamine (2 mM), sodium pyruvate (1 mM) and penicillin/streptomycin (100 U/ml) (PAN-Biotec). For routine cell culture

cells were seeded at $1 \times 10^5$ cells per ml into T75 flasks at 37 °C, 5% $CO_2$ and 95% humidity and passaged every 3–4 days.

Cells used for cytokine arrays were seeded into 96-well plates at a density of $0.5 \times 10^6$ cells per 96 well plate and left to rest for 24 h before being subjected to treatmentwith supernatants from the respective skin models for another 24 h.

## mRNA analysis

Total RNA was recovered subsequent to cell harvesting with a TissueLyser II (Qiagen, Hilden, Germany) using a TRIzol-based protocol (Chomczynski and Sacchi 1987). Briefly, following cellular disruption at 20 Hz for 3 min, total RNA was extracted using TRIzol™ Reagent (Invit- rogen) according to the manufacturer's instructions. The RNA-integrity (RIN) was analysed with an Agilent 2100 Bioanalyzer System (Agilent Technologies, Waldbronn, Germany) and the Agilent RNA 6000 Nano Kit (Agilent Technologies, Waldbronn, Germany) as described by the manufacturer. Following quality assessment samples were either stored at − 80 °C or directly used for quantitative RT-PCR or microarray analysis, respectively.

Microarray analysis was performed using triplicate Human Clariom™ S assays (Applied Biosystems, Foster City, CA, USA) at ATLAS Biolabs (Berlin, Germany). The corresponding RNA-samples all featured a RIN-score > 7. Subsequent data evaluation and interpretation was then carried out in house, relying on the Transcriptome Analysis Console 4.0.1.36 (TAC) (Applied Biosystems, Foster City, CA, USA) (± 2 fold-change; $p < 0.05$) and Ingenuity Pathway Analysis (IPA) (QIAGEN Inc., https://www.qiagenbioinformatics.com/ products/ingenuity-pathway-analysis, Qiagen, Hilden, Germany) software pack- ages. The latter was used with its core analysis module using ± 1.5-fold-change and $p < 0.05$ as cut-off values.

Concomitant analysis of gene-specific expression was performed using quantitative RT-PCR. In brief 500 ng of mRNA were reversely transcribed using oligo-dT primers and the Omniscript® Reverse Transcription Kit (Qiagen, Hilden, Germany). Subsequent amplification and detection of transcript levels relied on gene-specific primers (Supplementary Table S2) together with Fast SYBR® Green Master Mix (Applied Biosystems, Thermo Fisher Scientific, Darmstadt, Germany) as instructed by the manufacturer. All experiments were carried out in triplicate with *GAPDH* as house-keeping control and using a 7500 Fast Real-time cycler by Applied Biosystems (Thermo Fisher Scientific, Darmstadt, Germany). Relative transcript levels were calculated based on $c_T$-values using the 7500 Fast SDS Software.

## Quantification of secreted factors

Cytokine secretion of microbially competent skin and THP-1 cells was measured using a Proteome Profiler™ Human Cytokine Array Panel A (R&R Systems, Abingdon, UK). Il-1α and β were additionally quantified in microbial–skin tissue co-culture using a custom human 7-plex panel (Biolegend, London, UK) and FACS. Growth factor secretion was measured using the Human Growth Factor Array C1 (RayBiotech, Peachtree Corners, GA, USA). Levels of VEGFA and Defensin β4A or hFGF were determined with ELISA kits from RayBiotech, Inc. (Norcross, GA, USA) or USCN Life Science (Wuhan, China) according to the manufacturer's protocol, respectively.

## Western blot

Expression of selected proteins in skin models was verified using Western blotting. For protein extraction skin tissues in PBS (250 µl) were lysed with a TissueLyser II (Qiagen, Hilden, Germany) operated for 5 min at 20 Hz in in presence of Protease Inhibitor Cocktail Set III (3 µl, Merck, Darmstadt, Germany). Extracts equivalent to 30 µg of total protein were then subjected SDS-PAGE and transferred to nitrocellulose membranes following standard protocols. Primary antibodies against TREM-1 (sc-293450), DAP12 (sc-166084) and GAPDH (ab-9485) were used (Santa Cruz Biotechnology, Santa Cruz, CA, USA; Abcam, Cambridge, Great Britain) for subsequent immunostaining, followed by visualisation with appropriate horseradish peroxidase-coupled secondary antibodies (Santa Cruz Biotechnology) and enhanced chemo-luminescence (34078; Thermo Scientific, Waltham, MA, USA) for detection.

## Statistical analysis

All experiments were performed with at least three biological replicates. Data are presented as mean ± SD. GraphPad Prism 6 (Statcon, Witzenhausen, Germany) was used for statistical data processing with analyses of multiple groups by one-way ANOVA with Dunnett's multiple comparisons test or ordinary two-way ANOVA being performed as appropriate. All results are statistically significant within $p < 0.05$ unless stated otherwise.

Acknowledgements Open Access funding provided by Projekt DEAL. The authors acknowledge intramural funding at the German Federal Institute for Risk Assessment (BfR). Equally acknowledged is the experimental and technical assistance of Nils Dommershausen, Julian Tharman, Jane Kowall and Thomas Fischer.

Author contributions TT and LL conceived and designed the experiments. LL performed the sampling, experimental work and analysed

the data. SAD, RD and SV performed the genome sequencing and established the qPCR for bacterial quantification. AL provided conceptual input. LL, TT and AL wrote the manuscript with all authors approving the final version.

Funding This work was supported by Federal Institute for Risk Assessment Grant 1322-656.

Availability of data and material Raw and processed data files are deposited in the Gene Expression Omnibus (GEO) data repository GSE98877 Super Series upon publication.

## Compliance with ethical standards

Conflict of interest The authors declare that they have no competing interests.

Ethics approval Their suppliers have represented in writing that they are strictly regulated by and comply with German federal government standards.

Consent to participate Skin models as obtained from MatTek rely on ethically sourced materials from accredited institutes and are subject to strict donor consent.



## References

Barrila J, Yang J, Crabbe A et al (2017) Three-dimensional organotypic co-culture model of intestinal epithelial cells and macrophages to study *Salmonella enterica* colonization patterns. NPJ Microgravity 3:10. https://doi.org/10.1038/s41526-017-0011-2

Barton GM, Medzhitov R (2003) Toll-like receptor signaling pathways. Science 300(5625):1524–1525. https://doi.org/10.1126/science.1085536

Berry D, Loy A (2018) Stable-isotope probing of human and animal microbiome function. Trends Microbiol 26(12):999–1007. https://doi.org/10.1016/j.tim.2018.06.004

Black AT, Hayden PJ, Casillas RP et al (2010) Expression of proliferative and inflammatory markers in a full-thickness human skin equivalent following exposure to the model sulfur mustard vesicant, 2-chloroethyl ethyl sulfide. Toxicol Appl Pharmacol 249(2):178–187. https://doi.org/10.1016/j.taap.2010.09.005

Bojar RA (2015) Studying the human skin microbiome using 3D in vitro skin models. Appl In Vitro Toxicol 1(2):165–171. https://doi.org/10.1089/aivt.2015.0002

Brinkmann J, Stolpmann K, Trappe S et al (2013) Metabolically competent human skin models: activation and genotoxicity of benzo[*a*]pyrene. Toxicol Sci 131(2):351–359. https://doi.org/10.1093/toxsci/kfs316

Cadau S, Valla-Dury L, Cenizo V et al (2017) Studying microbiote competition and skin interaction using organotypic 3D skin models. Adv Tissue Eng Regen Med Open Access 2(5):00041. https://doi.org/10.15406/atroa.2017.02.00041

Cheret J, Bertolini M, Ponce L et al (2018) Olfactory receptor OR2AT4 regulates human hair growth. Nat Commun 9(1):3624. https://doi.org/10.1038/s41467-018-05973-0

Chiller K, Selkin BA, Murakawa GJ (2001) Skin microflora and bacterial infections of the skin. J Investig Dermatol Symp Proc 6(3):170–174. https://doi.org/10.1046/j.0022-202x.2001.00043.x

Chomczynski P, Sacchi N (1987) Single-step method of RNA isolation by acid guanidinium thiocyanate-phenol-chloroform extraction. Anal Biochem 162(1):156–159. https://doi.org/10.1006/abio.1987.9999

Christensen GJ, Bruggemann H (2014) Bacterial skin commensals and their role as host guardians. Benef Microbes 5(2):201–215. https://doi.org/10.3920/BM2012.0062

Claus SP, Ellero SL, Berger B et al (2011) Colonization-induced host-gut microbial metabolic interaction. mBio 2(2):e00271-10. https://doi.org/10.1128/mBio.00271-10

Clayton TA, Baker D, Lindon JC, Everett JR, Nicholson JK (2009) Pharmacometabonomic identification of a significant host-microbiome metabolic interaction affecting human drug metabolism. Proc Natl Acad Sci USA 106(34):14728–14733. https://doi.org/10.1073/pnas.0904489106

Clemente JC, Ursell LK, Parfrey LW, Knight R (2012) The impact of the gut microbiota on human health: an integrative view. Cell 148(6):1258–1270. https://doi.org/10.1016/j.cell.2012.01.035

Collins SL, Patterson AD (2020) The gut microbiome: an orchestrator of xenobiotic metabolism. Acta Pharm Sin B 10(1):19–32. https://doi.org/10.1016/j.apsb.2019.12.001

Cosseau C, Devine DA, Dullaghan E et al (2008) The commensal *Streptococcus salivarius* K12 downregulates the innate immune responses of human epithelial cells and promotes host-microbe homeostasis. Infect Immun 76(9):4163–4175. https://doi.org/10.1128/IAI.00188-08

Davis CP (1996) Medical microbiology: general concepts study guide, 4th edn. University of Texas Medical Branch at Galveston, Galveston

de Breij A, Haisma EM, Rietveld M et al (2012) Three-dimensional human skin equivalent as a tool to study *Acinetobacter baumannii* colonization. Antimicrob Agents Chemother 56(5):2459–2464. https://doi.org/10.1128/AAC.05975-11

Denda M (2014) Newly discovered olfactory receptors in epider-mal keratinocytes are associated with proliferation, migration, and re-epithelialization of keratinocytes. J Investig Dermatol 134(11):2677–2679. https://doi.org/10.1038/jid.2014.229

DePaolo RW, Kamdar K, Khakpour S, Sugiura Y, Wang W, Jabri B (2012) A specific role for TLR1 in protective T(H)17 immunity during mucosal infection. J Exp Med 209(8):1437–1444. https://doi.org/10.1084/jem.20112339

Do KN, Fink LN, Jensen TE, Gautier L, Parlesak A (2012) TLR2 controls intestinal carcinogen detoxication by CYP1A1. PLoS One 7(3):e32309. https://doi.org/10.1371/journal.pone.0032309

Duckney P, Wong HK, Serrano J, Yaradou D, Oddos T, Stamatas GN (2013) The role of the skin barrier in modulating the effects of common skin microbial species on the inflammation, differentiation and proliferation status of epidermal keratinocytes. BMC Res Notes 6:474. https://doi.org/10.1186/1756-0500-6-474

Dunne A, O'Neill LA (2003) The interleukin-1 receptor/Toll-like receptor superfamily: signal transduction during inflamma- tion and host defense. Sci STKE 2003(171):re3. https://doi.org/10.1126/stke.2003.171.re3

Egea TC, da Silva R, Boscolo M et al (2017) Diuron degradation by bacteria from soil of sugarcane crops. Heliyon 3(12):e00471. https://doi.org/10.1016/j.heliyon.2017.e00471

Eller MS, Yaar M, Ostrom K, Harkness DD, Gilchrest BA (1995) A role for interleukin-1 in epidermal differentiation: regulation by expression of functional versus decoy receptors. J Cell Sci 108(8):2741–2746

Epstein E (2015) Disposal and management of solid waste: pathogens and diseases. Taylor & Francis Group, Boca Raton

Feehley T, Nagler CR (2014) Cellular and molecular pathways through which commensal bacteria modulate sensitization to dietary antigens. Curr Opin Immunol 31:79–86. https://doi.org/10.1016/j.coi.2014.10.001

Fung TC, Bessman NJ, Hepworth MR et al (2016) Lymphoid-tissue-resident commensal bacteria promote members of the IL-10 cytokine family to establish mutualism. Immunity 44(3):634–646. https://doi.org/10.1016/j.immuni.2016.02.019

Gallo RL, Hooper LV (2012) Epithelial antimicrobial defence of the skin and intestine. Nat Rev Immunol 12(7):503–516. https://doi.org/10.1038/nri3228

Gerber Peter A, Buhren Bettina A, Schrumpf H, Homey B, Zlotnik A, Hevezi P (2014) The top skin-associated genes: a comparative analysis of human and mouse skin transcriptomes. Biol Chem 395:577

Grice EA, Kong HH, Renaud G et al (2008) A diversity profile of the human skin microbiota. Genome Res 18(7):1043–1050. https://doi.org/10.1101/gr.075549.107

Grice EA, Kong HH, Conlan S et al (2009) Topographical and temporal diversity of the human skin microbiome. Science (New York, NY) 324(5931):1190–1192. https://doi.org/10.1126/science.1171700

Guzman-Rodriguez M, McDonald JAK, Hyde R et al (2018) Using bioreactors to study the effects of drugs on the human microbiota. Methods 149:31–41. https://doi.org/10.1016/j.ymeth.2018.08.003

Hanafy RA, Couger MB, Baker K et al (2016) Draft genome sequence of *Micrococcus luteus* strain O'Kane implicates metabolic versatility and the potential to degrade polyhydroxy- butyrates. Genom Data 9:148–153. https://doi.org/10.1016/j.gdata.2016.08.006

Hasegawa M, Kamada N, Jiao Y, Liu MZ, Nunez G, Inohara N (2012) Protective role of commensals against *Clostridium difficile* infection via an IL-1beta-mediated positive-feedback loop. J Immunol 189(6):3085–3091. https://doi.org/10.4049/jimmunol.1200821

Holland DB, Bojar RA, Jeremy AHT, Ingham E, Holland KT (2008) Microbial colonization of an in vitro model of a tis- sue engineered human skin equivalent—a novel approach. FEMS Microbiol Lett 279(1):110–115. https://doi.org/10.111 1/j.1574-6968.2007.01021.x

Hu T, Khambatta ZS, Hayden PJ et al (2010) Xenobiotic metabolism gene expression in the EpiDermin vitro 3D human epidermis model compared to human skin. Toxicol In Vitro 24(5):1450–1463. https://doi.org/10.1016/j.tiv.2010.03.013

Huang GT, Zhang HB, Kim D, Liu L, Ganz T (2002) A model for antimicrobial gene therapy: demonstration of human beta-defensin 2 antimicrobial activities in vivo. Hum Gene Ther 13(17):2017–2025. https://doi.org/10.1089/10430340260395875

Isaac NI, Philippe D, Nicholas A, Raoult D, Eric C (2019) Metaproteomics of the human gut microbiota: challenges and contributions to other OMICS. Clin Mass Spectrom 14:18–30. https://doi.org/10.1016/j.clinms.2019.06.001

Jun JC, Jones MB, Oswald DM et al (2017) T cell-intrinsic TLR2 stimulation promotes IL-10 expression and suppressive activity by CD45RbHi T cells. PLoS One 12(7):e0180688. https://doi.org/10.1371/journal.pone.0180688

Kampfer AAM, Urban P, Gioria S, Kanase N, Stone V, Kinsner-Ovaskainen A (2017) Development of an in vitro co-culture model to mimic the human intestine in healthy and diseased state. Toxicol In Vitro 45(Pt 1):31–43. https://doi.org/10.1016/j.tiv.2017.08.011

Khalil E, Kretsos K, Kasting GB (2006) Glucose partition coefficient and diffusivity in the lower skin layers. Pharm Res 23(6):1227–1234. https://doi.org/10.1007/s11095-006-0141-9

Khayyira AS, Rosdina AE, Irianti MI, Malik A (2020) Simultaneous profiling and cultivation of the skin microbiome of healthy young adult skin for the development of therapeutic agents. Heliyon 6(4):e03700. https://doi.org/10.1016/j.heliyon.2020.e03700

Kim H-J, Kim H, Kim JJ et al (2018) Fragile skin microbiomes in megacities are assembled by a predominantly niche-based process. Sci Adv 4(3):e1701581. https://doi.org/10.1126/sciadv.1701581

Kubinak JL, Round JL (2012) Toll-like receptors promote mutu-ally beneficial commensal-host interactions. PLoS Pathog 8(7):e1002785. https://doi.org/10.1371/journal.ppat.1002785

Lagler H, Sharif O, Haslinger I et al (2009) TREM-1 activationalters the dynamics of pulmonary IRAK-M expression in vivo and improves host defense during pneumococcal pneumonia. J Immunol 183(3):2027–2036. https://doi.org/10.4049/jimmunol.0803862

Lai Y, Gallo RL (2009) AMPed up immunity: how antimicrobial peptides have multiple roles in immune defense. Trends Immunol 30(3):131–141. https://doi.org/10.1016/j.it.2008.12.003

Lai Y, Di Nardo A, Nakatsuji T et al (2009) Commensal bacteria regulate Toll-like receptor 3-dependent inflammation after skin injury. Nat Med 15(12):1377–1382. https://doi.org/10.1038/nm.2062

Lai Y, Cogen AL, Radek KA et al (2010) Activation of TLR2 by a small molecule produced by Staphylococcus epidermidis increases antimicrobial defense against bacterial skin infections. J Investig Dermatol 130(9):2211–2221. https://doi.org/10.1038/jid.2010.123

Lamichhane S, Sen P, Dickens AM, Oresic M, Bertram HC (2018) Gut metabolome meets microbiome: a methodological perspective to understand the relationship between host and microbe. Methods 149:3–12. https://doi.org/10.1016/j.ymeth.2018.04.029

Ley RE, Backhed F, Turnbaugh P, Lozupone CA, Knight RD, Gordon JI (2005) Obesity alters gut microbial ecology. Proc Natl Acad Sci USA 102(31):11070–11075. https://doi.org/10.1073/pnas.0504978102

Linehan JL, Harrison OJ, Han SJ et al (2018) Non-classical immu- nity controls microbiota impact on skin immunity and tissue repair. Cell 172(4):784–796 e18 https://doi.org/10.1016/j.cell.2017.12.033

Lopez-Castejon G, Brough D (2011) Understanding the mechanism of IL-1beta secretion. Cytokine Growth Factor Rev 22(4):189–195. https://doi.org/10.1016/j.cytogfr.2011.10.001

Maboni G, Davenport R, Sessford K et al (2017) A novel 3D skin explant model to study anaerobic bacterial infection. Front Cell Infect Microbiol 7(404):404. https://doi.org/10.3389/fcimb.2017.00404

Maier E, Anderson RC, Altermann E, Roy NC (2018) Live *Faecalibacterium prausnitzii* induces greater TLR2 and TLR2/6 activation than the dead bacterium in an apical anaerobic co-culture system. Cell Microbiol 20(2):e12805. https://doi.org/10.1111/cmi.12805

Mason KM, Bigley NJ, Fink PS (1998) Development of a novel in vitro co-culture system for studying host response to native bacterial antigens. J Immunol Methods 211(1–2):147–158. https://doi.org/10.1016/s0022-1759(97)00200-7

McGeachy MJ, Chen Y, Tato CM et al (2009) The interleukin 23 receptor is essential for the terminal differentiation of interleukin 17-producing effector T helper cells in vivo. Nat Immunol 10(3):314–324. https://doi.org/10.1038/ni.1698

Meisel JS, Sfyroera G, Bartow-McKenney C et al (2018) Commensal microbiota modulate gene expression in the skin. Microbiome 6(1):20. https://doi.org/10.1186/s40168-018-0404-9

Mohiti-Asli M, Pourdeyhimi B, Loboa EG (2014) Skin tissue engineering for the infected wound site: biodegradable PLA nanofibers and a novel approach for silver ion release evaluated in a 3D coculture system of keratinocytes and *Staphylococcus aureus*. Tissue Eng Part C Methods 20(10):790–797. https://doi.org/10.1089/ten.TEC.2013.0458

Naik S, Bouladoux N, Wilhelm C et al (2012) Compartmentalized control of skin immunity by resident commensals. Science 337(6098):1115–1119. https://doi.org/10.1126/science.1225152

Nakatsuji T, Chiang HI, Jiang SB, Nagarajan H, Zengler K, Gallo RL (2013) The microbiome extends to subepidermal compartments of normal skin. Nat Commun 4:1431. https://doi.org/10.1038/ncomms2441

Nawijn MC, Motta AC, Gras R, Shirinbak S, Maazi H, van Oosterhout AJ (2013) TLR-2 activation induces regulatory T cells and long-term suppression of asthma manifestations in mice. PLoS One 8(2):e55307. https://doi.org/10.1371/journal.pone.0055307

Neish AS (2009) Microbes in gastrointestinal health and disease. Gastroenterology 136(1):65–80. https://doi.org/10.1053/j.gastro.2008.10.080

Netea MG, van de Veerdonk F, Verschueren I, van der Meer JW, Kullberg BJ (2008) Role of TLR1 and TLR6 in the host defense against disseminated candidiasis. FEMS Immunol Med Microbiol 52(1):118–123. https://doi.org/10.1111/j.1574-695X.2007.00353.x

Nishimura M, Abiko Y, Kurashige Y et al (2004) Effect of defensin peptides on eukaryotic cells: primary epithelial cells, fibroblasts and squamous cell carcinoma cell lines. J Dermatol Sci 36(2):87–95. https://doi.org/10.1016/j.jdermsci.2004.07.001

Nutsch KM, Hsieh CS (2012) T cell tolerance and immunity to commensal bacteria. Curr Opin Immunol 24(4):385–391. https://doi.org/10.1016/j.coi.2012.04.009

Oesch F, Fabian E, Guth K, Landsiedel R (2014) Xenobiotic-metabolizing enzymes in the skin of rat, mouse, pig, guinea pig, man, and in human skin models. Arch Toxicol 88(12):2135–2190. https://doi.org/10.1007/s00204-014-1382-8

Oppong GO, Rapsinski GJ, Newman TN, Nishimori JH, Biesecker SG, Tukel C (2013) Epithelial cells augment barrier function via activation of the Toll-like receptor 2/phosphatidylinositol 3-kinase pathway upon recognition of *Salmonella enterica* serovar *Typhimurium curli* fibrils in the gut. Infect Immun 81(2):478–486. https://doi.org/10.1128/IAI.00453-12

Park YJ, Lee HK (2017) The role of skin and orogenital microbiota in protective immunity and chronic immune-mediated inflammatory disease. Front Immunol 8(1955):1955. https://doi.org/10.3389/fimmu.2017.01955

Percoco G, Merle C, Jaouen T et al (2013) Antimicrobial peptides and pro-inflammatory cytokines are differentially regulated across epidermal layers following bacterial stimuli. Exp Dermatol 22(12):800–806. https://doi.org/10.1111/exd.12259

Pfuhler S, Fautz R, Ouedraogo G et al (2014) The Cosmetics Europe strategy for animal-free genotoxicity testing: project status update. Toxicol In Vitro 28(1):18–23. https://doi.org/10.1016/j.tiv.2013.06.004

Platzek T, Lang C, Grohmann G, Gi US, Baltes W (1999) Formation of a carcinogenic aromatic amine from an azo dye by human skin bacteria in vitro. Hum Exp Toxicol 18(9):552–559. https://doi.org/10.1191/096032799678845061

Pluznick JL, Protzko RJ, Gevorgyan H et al (2013) Olfactory receptor responding to gut microbiota-derived signals plays a role in renin secretion and blood pressure regulation. Proc Natl Acad Sci USA 110(11):4410–4415. https://doi.org/10.1073/pnas.1215927110

Popov L, Kovalski J, Grandi G, Bagnoli F, Amieva MR (2014) Three-dimensional human skin models to understand *Staphylococcus aureus* skin colonization and infection. Front Immunol 5:41. https://doi.org/10.3389/fimmu.2014.00041

Possemiers S, Bolca S, Verstraete W, Heyerick A (2011) The intestinal microbiome: a separate organ inside the body with the metabolic potential to influence the bioactivity of botanicals. Fitoterapia 82(1):53–66. https://doi.org/10.1016/j.fitote.2010.07.012

Preciado D, Caicedo E, Jhanjee R et al (2005) *Pseudomonas aeruginosa* lipopolysaccharide induction of keratinocyte proliferation, NF-kappa B, and cyclin D1 is inhibited by indomethacin. J Immunol 174(5):2964–2973. https://doi.org/10.4049/jimmunol.174.5.2964

Rademacher F, Simanski M, Glaser R, Harder J (2018) Skin microbiota and human 3D skin models. Exp Dermatol 27(5):489–494. https://doi.org/10.1111/exd.13517

Rademacher F, Simanski M, Hesse B et al (2019) *Staphylococcus epidermidis* activates aryl hydrocarbon receptor signaling in human keratinocytes: implications for cutaneous defense. J Innate Immun 11(2):125–135. https://doi.org/10.1159/000492162

Rai V, Agrawal DK (2017) The role of damage- and pathogen-associated molecular patterns in inflammation-mediated vulnerability of atherosclerotic plaques. Can J Physiol Pharmacol 95(10):1245–1253. https://doi.org/10.1139/cjpp-2016-0664

Rawls JF, Mahowald MA, Ley RE, Gordon JI (2006) Reciprocal gut microbiota transplants from zebrafish and mice to germ-free recipients reveal host habitat selection. Cell 127(2):423–433. https://doi.org/10.1016/j.cell.2006.08.043

Ren C, Zhang Q, de Haan BJ, Zhang H, Faas MM, de Vos P (2016) Identification of TLR2/TLR6 signalling lactic acid bacteria for supporting immune regulation. Sci Rep 6:34561. https://doi.org/10.1038/srep34561

Reynolds JM, Pappu BP, Peng J et al (2010) Toll-like receptor 2 signaling in CD4(+) T lymphocytes promotes T helper 17 responses and regulates the pathogenesis of autoimmune disease. Immunity 32(5):692–702. https://doi.org/10.1016/j.immuni.2010.04.010

Ridaura VK, Bouladoux N, Claesen J et al (2018) Contextual control of skin immunity and inflammation by Corynebacterium. J Exp Med 215(3):785–799. https://doi.org/10.1084/jem.20171079

Ross AA, Rodrigues Hoffmann A, Neufeld JD (2019) The skin microbiome of vertebrates. Microbiome 7(1):79. https://doi.org/10.1186/s40168-019-0694-6

Round JL, Palm NW (2018) Causal effects of the microbiota on immune-mediated diseases. Sci Immunol 3(20):eaao1603. https://doi.org/10.1126/sciimmunol.aao1603

Round JL, Lee SM, Li J et al (2011) The Toll-like receptor 2 pathway establishes colonization by a commensal of the human microbiota. Science 332(6032):974–977. https://doi.org/10.1126/science.1206095

Sajib S, Zahra FT, Lionakis MS, German NA, Mikelis CM (2018) Mechanisms of angiogenesis in microbe-regulated inflammatory and neoplastic conditions. Angiogenesis 21(1):1–14. https://doi.org/10.1007/s10456-017-9583-4

Sazal MR, Stebliankin V, Mathee K, Narasimhan G (2020) Causal inference in microbiomes using intervention calculus. BioRxiv. https://doi.org/10.1101/2020.02.28.970624

Scharschmidt TC, Fischbach MA (2013) What lives on our skin: ecology, genomics and therapeutic opportunities of the skin microbiome. Drug Discov Today Dis Mech 10(3–4):e83–e89. https://doi.org/10.1016/j.ddmec.2012.12.003

Schommer NN, Gallo RL (2013) Structure and function of the human skin microbiome. Trends Microbiol 21(12):660–668. https://doi.org/10.1016/j.tim.2013.10.001

Sender R, Fuchs S, Milo R (2016) Revised estimates for the number of human and bacteria cells in the body. PLoS Biol 14(8):e1002533. https://doi.org/10.1371/journal.pbio.1002533

Shin JE, Choi Y (2010) *Treponema denticola* suppresses expression of human beta-defensin-2 in gingival epithelial cells through inhibition of TNFalpha production and TLR2 activation. Mol Cells 29(4):407–412. https://doi.org/10.1007/s10059-010-0048-5

Shin HS, Lee JH, Paek SH, Jung YW, Ha UH (2013) Pseudomonas aeruginosa-dependent upregulation of TLR2 influences host responses to a secondary *Staphylococcus aureus* infection. Pathog Dis 69(2):149–156. https://doi.org/10.1111/2049-632X.12074

Sousa T, Paterson R, Moore V, Carlsson A, Abrahamsson B, Basit AW (2008) The gastrointestinal microbiota as a site for the biotransformation of drugs. Int J Pharm 363(1–2):1–25. https://doi.org/10.1016/j.ijpharm.2008.07.009

Sowada J, Schmalenberger A, Ebner I, Luch A, Tralau T (2014) Degradation of benzo[*a*]pyrene by bacterial isolates from human skin. FEMS Microbiol Ecol 88(1):129–139. https://doi.org/10.1111/1574-6941.12276

Sowada J, Lemoine L, Schon K, Hutzler C, Luch A, Tralau T (2017) Toxification of polycyclic aromatic hydrocarbons by commensal bacteria from human skin. Arch Toxicol 91(6):2331–2341. https://doi.org/10.1007/s00204-017-1964-3

Staley C, Kaiser T, Beura LK et al (2017) Stable engraftment of human microbiota into mice with a single oral gavage following antibiotic conditioning. Microbiome 5(1):87. https://doi.org/10.1186/s40168-017-0306-2

Stappenbeck TS, Hooper LV, Gordon JI (2002) Developmental regulation of intestinal angiogenesis by indigenous microbes via Paneth cells. Proc Natl Acad Sci USA 99(24):15451–15455. https://doi.org/10.1073/pnas.202604299

Steglinska A, Jachowicz A, Szulc J et al (2019) Factors influencing microbiological biodiversity of human foot skin. Int J Environ Res Public Health 16(18):3503. https://doi.org/10.3390/ijerph16183503

Steinz K, Schubert S, Harder J, Gerdes S, Mrowietz U, Glaser R (2014) Bacterial soft tissue infection in psoriasis despite induction of epidermal antimicrobial peptides. Exp Dermatol 23(11):862–864. https://doi.org/10.1111/exd.12538

Stingley RL, Zou W, Heinze TM, Chen H, Cerniglia CE (2010) Metabolism of azo dyes by human skin microbiota. J Med Microbiol 59(Pt 1):108–114. https://doi.org/10.1099/jmm.0.012617-0

Takai T, Chen X, Xie Y et al (2014) TSLP expression induced via Toll-like receptor pathways in human keratinocytes. Methods Enzymol 535:371–387. https://doi.org/10.1016/B978-0-12-397925-4.00021-3

Tessarz AS, Cerwenka A (2008) The TREM-1/DAP12 pathway. Immunol Lett 116(2):111–116. https://doi.org/10.1016/j.imlet.2007.11.021

Tralau T, Yang EC, Tralau C, Cook AM, Küpper FC (2011) Why two are not enough: degradation of *p*-toluenesulfonate by a bacterial community from a pristine site in Moorea, French Polynesia. FEMS Microbiol Lett 316(2):123–129. https://doi.org/10.1111/j.1574-6968.2010.02207.x

Tralau T, Sowada J, Luch A (2015) Insights on the human microbiome and its xenobiotic metabolism: what is known about its effects on human physiology? Expert Opin Drug Metab Toxicol 11(3):411–425. https://doi.org/10.1517/17425255.2015.990437

Tsai T, Veitinger S, Peek I et al (2017) Two olfactory receptors-OR2A4/7 and OR51B5-differentially affect epidermal proliferation and differentiation. Exp Dermatol 26(1):58–65. https://doi.org/10.1111/exd.13132

Turnbaugh PJ, Ley RE, Hamady M, Fraser-Liggett CM, Knight R, Gordon JI (2007) The human microbiome project. Nature 449(7164):804–810. https://doi.org/10.1038/nature06244

Ueda Y, Kayama H, Jeon SG et al (2010) Commensal microbiota induce LPS hyporesponsiveness in colonic macrophages via the production of IL-10. Int Immunol 22(12):953–962. https://doi.org/10.1093/intimm/dxq449

Ullah S, Hamade F, Bubniene U et al (2018) In-vitro model for assessing glucose diffusion through skin. Biosens Bioelectron 110:175–179. https://doi.org/10.1016/j.bios.2018.03.039

van der Krieken DA, Ederveen TH, van Hijum SA et al (2016) An in vitro model for bacterial growth on human stratum cor-neum. Acta Derm Venereol 96(7):873–879. https://doi.org/10.2340/00015555-2401

van Maren WW, Jacobs JF, de Vries IJ, Nierkens S, Adema GJ (2008) Toll-like receptor signalling on Tregs: to suppress or not to suppress? Immunology 124(4):445–452. https://doi.org/10.1111/j.1365-2567.2008.02871.x

Varanat M, Haase EM, Kay JG, Scannapieco FA (2017) Activation of the TREM-1 pathway in human monocytes by periodontal pathogens and oral commensal bacteria. Mol Oral Microbiol 32(4):275–287. https://doi.org/10.1111/omi.12169

Veldhoen M, Hirota K, Westendorf AM et al (2008) The aryl hydrocarbon receptor links TH17-cell-mediated autoimmunity to environmental toxins. Nature 453(7191):106–109. https://doi.org/10.1038/nature06881

Viggor S, Jõesaar M, Soares-Castro P et al (2020) Microbial metabolic potential of phenol degradation in wastewater treatment plant of crude oil refinery: analysis of metagenomes and characterization of isolates. Microorganisms 8(5):652. https://doi.org/10.3390/microorganisms8050652

Vrancken G, Gregory AC, Huys GRB, Faust K, Raes J (2019) Synthetic ecology of the human gut microbiota. Nat Rev Microbiol 17(12):754–763. https://doi.org/10.1038/s41579-019-0264-8

Walter J, Armet AM, Finlay BB, Shanahan F (2020) Establishing or exaggerating causality for the gut microbiome: lessons from human microbiota-associated rodents. Cell 180(2):221–232. https://doi.org/10.1016/j.cell.2019.12.025

Wang M, Donovan SM (2015) Human microbiota-associated swine: current progress and future opportunities. ILAR J 56(1):63–73. https://doi.org/10.1093/ilar/ilv006

Wang Q, Cui S, Zhou L et al (2019) Effect of cosmetic chemical preservatives on resident flora isolated from healthy facial skin. J Cosmet Dermatol 18(2):652–658. https://doi.org/10.1111/jocd.12822

Wanke I, Steffen H, Christ C et al (2011) Skin commensals amplify the innate immune response to pathogens by activation of distinct signaling pathways. J Investig Dermatol 131(2):382–390. https://doi.org/10.1038/jid.2010.328

Wills JW, Hondow N, Thomas AD et al (2016) Genetic toxicity assessment of engineered nanoparticles using a 3D in vitro skin model (EpiDerm). Part Fibre Toxicol 13(1):50. https://doi.org/10.1186/s12989-016-0161-5

Wu M, Peng A, Sun M et al (2011) TREM-1 amplifies corneal inflammation after Pseudomonas aeruginosa infection by modulating Toll-like receptor signaling and Th1/Th2-type immune responses. Infect Immun 79(7):2709–2716. https://doi.org/10.1128/IAI.00144-11

Xu C, Lu Y, Zheng X et al (2017) TLR2 expression in peripheral CD4 + T cells promotes Th17 response and is associated with disease aggravation of hepatitis B virus-related acute-on- chronic liver failure. Front Immunol 8(1609):1609. https://doi.org/10.3389/fimmu.2017.01609

Yadav M, Verma MK, Chauhan NS (2018) A review of metabolic potential of human gut microbiome in human nutrition. Arch Microbiol 200(2):203–217. https://doi.org/10.1007/s00203-017-1459-x

Young M, Artsatbanov V, Beller HR et al (2010) Genome sequence of the Fleming strain of *Micrococcus luteus*, a simple free-living actinobacterium. J Bacteriol 192(3):841–860. https://doi.org/10.1128/JB.01254-09

Zhao RR, Yang XF, Dong J et al (2015) Toll-like receptor 2 promotes T helper 17 cells response in hepatitis B virus infection. Int J Clin Exp Med 8(5):7315–7323

Zielinski CE, Mele F, Aschenbrenner D et al (2012) Pathogen-induced human TH17 cells produce IFN-gamma or IL-10 and are regulated by IL-1beta. Nature 484(7395):514–518. https://doi.org/10.1038/nature10957

## 3.3. Commensal-related changes in the epidermal barrier function lead to alterations in the benzo[a]pyrene metabolite profile and its distribution in 3D-skin

**Lisa Lemoine,** Dilan Bayrambey, Alexander Roloff, Christoph Hutzler, Andreas Luch & Tewes Tralau

This chapter was published on 28 September2021:

mBio. 2021 Oct 26;12(5):e0122321

DOI: 10.1128/mBio.01223-21

Link: https://doi.org/10.1128/mBio.01223-21

Involvement of the author within this publication: Project planning (80%), project execution (90%), data analysis (90%), writing of the manuscript (80%).

Supplementary materials for the following publication are detailed in Annex III.

# Commensal-related changes in the epidermal barrier function lead to alterations in the benzo[*a*]pyrene metabolite profile and its distribution in 3D-skin

Lisa Lemoine[1,2*], Dilan Bayrambey[3], Alexander Roloff[3], Christoph Hutzler[3], Andreas Luch[2,3] and Tewes Tralau[1]

[1] German Federal Institute for Risk Assessment (BfR), Department of Pesticides Safety, Max-Dohrn-Strasse 8-10, 10589 Berlin, Germany

[2] Institute of Pharmacy, Department of Biology, Chemistry, Pharmacy, Freie Universität Berlin, Berlin, Germany

[3] German Federal Institute for Risk Assessment (BfR), Department of Chemical & Product Safety, Max-Dohrn-Strasse 8-10, 10589 Berlin, Germany

[*]correspondence should be addressed to Lisa.Lemoine@bfr.bund.de
ORCID: 0000-0003-2492-7866

**KEYWORDS**

co-culture, skin model, commensals, benzo[*a*]pyrene, metabolites, skin barrier, GC/MS, BPDE DNA adducts

## ABSTRACT

Polycyclic aromatic hydrocarbons (PAH) such as benzo[*a*]pyrene (B[*a*]P) are among the most abundant environmental pollutants, resulting in continuous exposure of human skin and its microbiota. Yet, effects of the latter on B[*a*]P toxicity, absorption, metabolism and distribution in humans remain unclear. Here, we demonstrate that skin microbiota do metabolize B[*a*]P on and in human skin *in situ,* using a recently developed commensalic skin model. In this model microbial metabolism leads to high concentrations of known microbial B[*a*]P metabolites on the surface as well as in the epidermal layers. In contrast to what was observed for uncolonized skin, B[*a*]P and its metabolites were subject to altered rates of skin penetration and diffusion, resulting in up to 58 % reduction of metabolites recovered from basal culture medium. The results indicate the reason for this altered behavior to be a microbial induced strengthening of the epidermal barrier. Concomitantly, colonized models showed decreased formation and penetration of the ultimate carcinogen B[*a*]P-7,8-dihydrodiol-9,10-epoxide (BPDE), leading, in consequence, to fewer BPDE-DNA adducts formed. Befittingly, transcript and expression levels of key proteins for repairing environmentally induced DNA-damage such as XPC were also found to be reduced in the commensalic models, as was expression of B[*a*]P-associated cytochrome P450-dependent monooxygenases (CYPs). The results show that the microbiome can have significant effects on the toxicology of external chemical impacts. The respective effects rely on a complex interplay between microbial as well as host metabolism and microbe-host interactions all of which cannot be adequately assessed using single-system studies.


## IMPORTANCE

Exposure to xenobiotics has repeatedly been associated with adverse health effects. While the majority of reported cases still relates to direct substance effects, there is increasing evidence that microbiome-dependent metabolism of xenobiotic substances likewise has direct adverse effects on the host. This can be due to microbial biotransformation of compounds, interaction between the microbiota and the host's endogenous detoxification enzymes or altered xenobiotic bioavailability. Yet, there are hardly any studies addressing the complex interplay of such interactions *in situ*. Less so in human test systems. Using a recently developed microbially competent 3D-skin model we here show for the first time how commensal influence on skin physiology and gene transcription paradoxically modulates PAH-toxicity.

## INTRODUCTION

The skin is one of our largest organs and as a physical and metabolic barrier our frontline of defence against environmental impacts, physical as well as chemical in nature [1]. Moreover, it harbors a unique ecosystem of 10 to 100 trillion bacteria, fungi and viruses, which together make up the skin microbiota [2-4]. Living in a complex interplay this microbiota relies to a good part on the few nutrients it can source the stratum corneum (SC) as well as sebaceous, eccrine and apocrine secretions [5]. However, with the skin being a chronically nutrient-poor environment particularly the microbial commensals have to rely on the use of external carbon and energy sources in form of xenobiotics [6,7]. Given the preferred growth of commensals in and on the SC, major xenobiotic sources of additional nutrients comprise re-occurring environmental exposures, from air-borne pollutants to cosmetic ingredients or topically applied pharmaceuticals [8].

There is abundant evidence that the human microbiome can modulate exposure-response relationships of xenobiotic chemicals through some general mechanisms that could directly or indirectly affect toxicity [9]. Respective mechanisms include direct metabolic conversions as well indirect transformations. The latter include deconjugation of host-generated metabolites, modulation of epithelial barrier permeability; as well as regulation or alteration of endogenous host metabolism [9-14].

Among the most widespread environmental xenobiotics are polycyclic aromatic hydrocarbons (PAHs). Their ubiquitous occurrence leads to constant human exposure at low to medium levels [15,16]. Toxicologically of particular interest are the potentially carcinogenic, high-molecular-weight representatives such as benzo[*a*]pyrene (B[*a*]P) [17,18]. With regard to the latter it actually is the oxidative metabolic activation by cytochrome P450-dependent monooxygenases (CYPs) during human phase-I-metabolism that can trigger the formation of some of the most potent genotoxic carcinogens known to man [19]. For the metabolic activation or B[*a*]P two of the most important enzymes involved in the formation of the ultimately reactive species are CYP1A1 and CYP1B1 [20]. The resulting electrophilic metabolite B[*a*]P-7,8-dihydrodiol-9,10-epoxide (BPDE) is prone to DNA-adduct formation, preferentially at nucleophilic guanine residues leading to the formation of dG-N2-BPDE [21]. While the formation of the biologically dysfunctional dG-N2-BPDE makes BPDE such a strong genotoxin, overall toxicity will strongly depend on any phase-I- and phase-II-detoxification preceding actual adduct formation as well as on the rate of DNA-repair [22]. It should be noted, however, that before being subject to host metabolism, PAHs obviously first need to pass the epidermis which is a highly functional physico-chemical barrier [23].

Exposure to PAHs will predominantly first occur on the skin with human commensalic microbes hence being the first point of (metabolic) contact [24,25]. Previous studies from our lab have shown a ubiquitous potential of the commensal microbiome for B[*a*]P-degradation., Some of the bacterial Genes for the

respective underlying metabolic pathways were identified and shown to be detectable *in situ* on human skin, as were the associated bacteria. Concomitantly carbon limited batch cultures showed the corresponding bacterial metabolism of B[*a*]P to result in the formation and excretion of highly cytotoxic and genotoxic metabolites [26,27]. Similar observations have been reported for the intestinal microbiota where commensals are known to either directly metabolise xenobiotic substances as well as impacting on the hosts capacity for xenobiotic metabolism by affecting phase-I and phase-II enzymes [28-30].

While these studies deliver valuable insights into the various facetted aspects of how commensalic metabolism of xenobiotics can influence host toxicity they fall short of addressing the complex and facetted interplay systemically. The reasons for this is commensal species specificity together with a lack of suitable model systems. For skin we therefore recently reported the development of a new commensal 3D skin model [31]. We now applied this model to investigate commensal B[*a*]P-metabolism and its potential toxicologically relevant effects *in situ*. These results provide insights into the complex interplay between microbial-induced xenobiotic metabolism of B[*a*]P as a pro-carcinogen and the host organ skin under near *in vivo* conditions (see Scheme S1 for experimental set up). The data indicate a complex pattern of host-microbe interactions that were not accessible in previous single systems studies.

## MATERIAL AND METHODS

*Chemicals and media*

Gas chromatography–mass spectrometry (GC/MS)–grade solvents were purchased from Thermo Fisher Scientific (Waltham, MA, USA). All other chemicals were sourced from Sigma-Aldrich (St. Louis, MO, USA) unless otherwise noted. EpiDermFT™ tissue models with the following LOTs 29346, 25358, 25392, 29308, 29388 and associated maintenance medium were sourced from MatTek (Ashland, MA, USA). Analytical standards were purchased from MRIGlobal Chemical Carcinogen Repository (Kansas City, MO, USA): B[*a*]P, 7-OH-B[*a*]P, 9-OH-B[*a*]P, B[*a*]P-*trans*-7,8-dihydrodiol(+/-), B[*a*]P-*trans*-9,10-dihydrodiol(+/-), B[*a*]P-1,6-dione, B[*a*]P-6,12-dione, B[*a*]P-7,8-dione, B[*a*]P-*r*-7,*t*-8,*t*-9,*c*-10-tetrahydrotetrol, benzo[*a*] anthracene-*cis*-5,6-dihydrodiol (B[*a*]A-*cis*-5,6-dihydrodiol), 5-Methylchrysene-*r*-1,*t*-2,3,*c*-4-tetrahydrotetrol and deuterated B[*a*]P-$D_{12}$. 3-OH-B[*a*]P, 3-OH-B[*a*]P-$^{13}C_6$ and B[*a*]P-1,6-dione were acquired from Toronto Research Chemicals (North York, ON, Canada).

*Bacterial isolates and bacterial growth*

Co-cultures were set up *as previously described* with $10^4$ – $10^6$ cells of *Micrococcus luteus* (*M. luteus*) 1B and/or *Pseudomonas oleovorans* (*P. oleovorans*) 1C used for skin inoculation [31].

Beforehand, to determine the B[*a*]P metabolites of *P. oleovorans,* the latter was cultured in minimal medium (MM) supplemented with 100 µM B[*a*]P as previously described for *M. luteus* by Sowada, et al. [27]. Cell harvesting was performed daily over a period of 2 weeks. For later analytical examination, 25 mL of the bacterial culture supernatant was frozen and stored at -20 °C.

*Tissue viability assay for selection of the applied B[a]P concentration*

As basis for our co-culture we used the full-thickness skin model EpiDermFT™ from MatTek (Ashland, MA, USA). Directly after delivery, the models were transferred into six-well plates (Greiner Bio-One, Frickenhausen, Germany) with 2.5 mL of antibiotic-free EPI-100-MM-ABF maintenance medium and cultivated for 24 h to recover at 37 °C and 5 % $CO_2$ as recommended by the manufacturer. Before treatment of the actual microbial skin tissue co-culture with B[*a*]P, we first evaluated 3 different concentrations of B[*a*]P (5 nM/$cm^2$, 50 nM/$cm^2$ und 500 nM/$cm^2$) and determined their influence on tissue viability via an MTT assay. A high B[*a*]P concentration can promote bacterial use as a food source, but could impair the viability of the skin cells and thus inhibiting its B[*a*]P metabolism. The MTT assay was

performed using MatTek's MTT Concentrate, MTT Diluent and MTT Extractant according to manufactures instructions. The skin models (1 $cm^2$ diameter) were treated daily with one of the 3 B[*a*]P concentrations prepared in acetone of analytical grade or solvent control (pure acetone), respectively. Acetone was chosen as the deposition vehicle due to its successful use in other skin B[*a*]P metabolism studies [32-34]. The cell culture media was exchanged daily and the MTT assay was carried out after 3 and 7 days of B[*a*]P treatment, respectively. With moderate viability losses of 15 % after 7 days of B[*a*]P application, the mean concentration of 50 nM/$cm^2$ was chosen for further experiments (Fig. S1).

*Tissue culture and bacterial quantification*

The EpiDermFT™ were routinely cultivated and subjected to bacterial inoculation or solvent treatment as described earlier [31]. Bacterial inoculation of the respective models was performed using three droplets of bacterial suspension at a volume of 5 µl each with the droplets set evenly spaced across the model surface and then left to dry. 24 h after establishing the co-culture of the B[*a*]P-degrading skin commensals, 50 nM/$cm^2$ B[*a*]P was applied as evenly as possible on the surface of the skin tissues (diameter 1 $cm^2$). Identical amounts of solvent were applied in control experiments. This procedure was repeated daily at the same time during the cultivation period of 8 days stopping 24 h before harvesting the EpiDermFT™ models. In total, each model was treated with B[*a*]P for 7 consecutive days, resulting in a total concentration of 350 nmol/skin model. Tissues and the daily collected basal cell culture medium were separately stored at −80°C until further processing.

Bacterial growth in co-culture was quantified using plate counts, since there was no significant added value in using Quantitative (q)PCR additionally [31]. As in our previous experiments, viable colony counts (CFU/$cm^2$) showed stable quantities for *M. luteus* from day 4 of cultivation (Fig. S2A and C), while these of *P. oleovorans* increased slightly and were on average slightly higher. As reported previously *M. luteus* appeared to grow exclusively on the SC while *P. oleovorans* also penetrates into the dermis, although to a small extent (approximately ≤ 10 %) [31]. The cell numbers shown in Fig. 2 refer to that on the skin surface. In general, the B[*a*]P application had no significant influence on cell numbers (Fig. S2C). The selection of *P. oleovorans* and *M. luteus* as models for commensal B[*a*]P-degraders followed both, biological as well a practical, considerations [31]. Briefly, the selection covers species of both Gram variants as well as two of the major phyla of the skin´s microbiome. Both species are biologically relevant and have been repeatedly isolated from healthy subjects at different skin sites [26]. Moreover, they are easily distinguishable from each other on agar plates and have a well-established potential for xenobiotic metabolism [26,35].

*Transcriptome analysis*

In order to gain insight into microbial-related changes in the skin´s gene expressions after B[*a*]P application, the skin tissues were examined as previously described by microarray analysis [31]. For this purpose, total RNA was recovered subsequent to cell harvesting with a TissueLyser II (Qiagen, Hilden, Germany). The RNA was isolated with a TRIzol-based protocol using the TRIzol® reagent (Thermo Scientific, Waltham, MA, USA) as described earlier [36]. Microarray analysis was performed using duplicates of controls (uncolonized skin, *M. lueus*/ *P .oleovorans* skin tissue co-culture) and triplicates of treatments (B[*a*]P treatment and *M. luteus*/*P .oleovorans* with B[*a*]P application) within Human Clariom™ S assays (Applied Biosystems, Foster City, CA, USA) at ATLAS Biolabs (Berlin, Germany). Data evaluation and interpretation was done using the Transcriptome Analysis Console 4.0.1.36 (TAC) (Applied Biosystems, Foster City, CA, USA) ($p \leq 0.05$).

*Immunofluorescence*

To investigate changes in the epidermal barrier function we snap -froze the skin tissues on day 8 of the cultivation in Tissue-Tek O.C.T. compound (Sakura Finetek, Torrance, CA, USA) using liquid nitrogen and stored these at −80 °C until use. Tissues were cut in 7 µm-thick sections at −20 °C using the cryostat Microm HM 550 and mounted on Super-Frost slides (both from Thermo Fisher Scientific, Waltham, MA, USA). Subsequently, cryosections were fixed for 10 min with ice-cold Methanol (-20 °C). Antibody staining was performed according to Hering, et al. [37]. The following antibodies were used: rabbit Ab against Cytokeratin 10 (18343-1-AP), Involucrin (55328-1-AP; Proteintech Group, Rosemont, IL, USA), as well as mouse AB against Filaggrin (NBP2-53245-20; Novus Biologicals, Littleton, CO, USA) and E-cadherin (33-4000; Thermo Scientific, Waltham, MA, USA) in a concentration of 5 µg/mL. The appropriate secondary antibodies conjugated to Alexa594 (red) (MolecularProbes, Eugene, OR) were applied (1:400 in phosphate buffered saline with 0.1 % Tween (PBST)) followed by Hoechst 33258 (Sigma-Aldrich, St. Louis, MO, USA) (1 µg/mL in Dulbecco's phosphate-buffered solution (DPBS)) application for counterstaining the nuclei. Sections were embedded in mounting media and analyzed in biological triplicates using the LSM700 confocal microscope (Carl Zeiss, Oberkochen, Germany).

*Western Blot*

To determine potential changes in protein levels, western blot analysis of selected proteins was carried out. The latter were isolated in 100 µL of an Urea buffer (8M, pH 8.5) combined with lysis using a TissueLyser II (Qiagen, Hilden, Germany) operated for 5 min at 20 Hz. The cell residues were separated by

centrifugation at 10000 rcf for 10 min. Total protein concentration was evaluated using the BCA Assay (Thermo Fisher Scientific, Darmstadt, Germany). In general, 20 µg of total protein were then subjected to SDS-PAGE and transferred to nitrocellulose membranes following standard protocols. Primary antibodies against CYP1A1 (ABIN1872160; Antibodies-online Inc. Limerick, PA, USA), CYP1B1 (ABIN3184162), XPC (ABIN2855495), XPG (ABIN3187504) and glyceraldehyde 3-phosphate dehydrogenase (GAPDH) (ABIN2666338) were used for subsequent immunostaining, followed by visualization with appropriate horseradish peroxidase-coupled secondary antibodies (Santa Cruz Biotechnology) and enhanced chemo-luminescence (34078; Thermo Scientific, Waltham, MA, USA) for detection in the Fusion FX6 Edge (Vilber Lourmat, Eberhardzell, Deutschland).

*Gas chromatography online-coupled to mass spectrometry (GC-MS)*

*Analysis of P. oleovorans* B[*a*]P *metabolites*

To assess the bacterial influence on the human B[*a*]P metabolism, knowledge of the identity of the corresponding microbial B[*a*]P degradation products is crucial. For this reason, we analyzed the B[*a*]P metabolism of *P. oleovorans* via GC/MS strictly following a previously described protocol applied for *M. luteus* [27]. This applies to the extraction, sample preparation, and GC/MS analysis. The verification was done using retention time (RT) and mass spectra (MS) of authentic references.

B[*a*]P *metabolism in microbial skin tissue co-culture*

In order to determine the microbial influence on the B[*a*]P metabolite profile and distribution within the skin, the levels of B[*a*]P and its metabolites were quantified in surface imprint, tissue samples and culture media from 6 biological replicates using GC/MS.

Cell Lysis: Firstly the surface imprint was taken as described earlier [31]. The resulting cell pellet was digested by freeze-thawing. Therefore, three cycles were performed with freezing cells in dry ice/ethanol bath for 10 min and subsequent thawing at room temperature for 10 min as described by de Bruin and Birnboim [38]. For the following metabolite extraction, the lysates were diluted with 750 µL PBS. The lysis of the skin tissues was done mechanically and enzymatically. Prior to cell lysis, epidermis and dermis were separated followed by homogenization with a TissueLyser II for 2×5 min at 20 Hz in 750 µL PBS each and digestion with 1 U/mL LiberaseTH enzymes (Roche, Mannheim, Germany) for 20 min at 37 °C. The cell culture medium was used directly for metabolite extraction.

Metabolite extraction: The surface imprint lysates, the skin tissue lysates and the cell culture media (2.5 mL each) was spiked with a mixture of internal standards (Table 1) at a final concentration of 500 ng/mL (IS 2 = 1.8 µM, IS 3 = 1.9 µM, SI4 = 1.9 µM and IS 5 = 1.6 µM) in dimethyl sulfoxide (DMSO) except for B[*a*]P-$D_{12}$ with 50 µg/mL (IS 1 = 181,1 µM) in DMSO, respectively (Table 1).

**Table 1**: List of the internal standards (IS). Presented are the internal standards used for verification of B[*a*]P metabolite extraction and silylation with the respective retention time (rt/min), together with quantifier and qualifier ions and the designation to the external standards listed in Table 2.

| Substance | rt /min | Quantifier m/z | Qualifier m/z | Designation |
|---|---|---|---|---|
| $D_{12}$-B[*a*]P | 26,6 | 264 | 262 | 1 |
| 3 OH-B[*a*]P-$^{13}$C6 | 34,9 | 346 | 347 | 2 |
| Chrysene 1,4-dione | 29 | 404 | 405 | 3 |
| B[*a*]A-cis-5,6-diol | 22,7 | 406 | 316 | 4 |
| 5- Methylchrysene-1,2,3,4-tetrahydrotetrol | 29,6 | 304 | 394 | 5 |

The latter is due to the high B[*a*]P concentration in the samples, which is above the linear calibration range. In order to determine the B[*a*]P concentration, the samples were additionally measured in 100-fold dilution in DMSO. Prior to extraction with dichloromethane (DCM) (1:7.5 volume ratio), ethanol (EtOH) was added as a disperser[39] (1:2.5 volume ratio). After the addition of EtOH and DCM the samples were vortexed for 1 min. Subsequently, the samples were centrifuged for 15 min at 4 °C and 4000 g for better phase separation. The lower organic phase containing the analytes was separated, the extraction was repeated twice and the combined organic extracts were concentrated to dryness in 1.5 mL Eppendorf tubes using the Concentrator plus (Eppendorf, Hamburg, Germany) at 30 °C. The residues were dissolved in 20 µL *N,O*-bis(trimethylsilyl)-trifluoracetamide (BSTFA) (99 % BSTFA with 1% TMCS) (15222-10X1ML-F; Sigma-Aldrich, St. Louis, MO, USA) as derivatization agent in GC vials (2 mL crimp top; with 300 µL inlet; Agilent Technologies, Santa Clara, CA, USA) to accomplish silylation of functionalized B[*a*]P metabolites (Fig. S3A) at 60 °C for 90 min and shaking at 120 rpm in a water bath. Subsequently, 1 µL of each sample was diluted in 99 µL fresh BSTFA for quantifcation of unmetabolized B[*a*]P via GC/MS.

GC/MS measurements: 1 µL of silylated sample mixture was injected in spitless mode into a gas chromatograph 6890 (Agilent) equipped with an HP-5MS capillary column (30 m length, 250 µm inner diameter, 0.25 µm film thickness, 10 m pre-column, Agilent) coupled to a 5975 mass spectrometric detector (Agilent). Electron impact (EI) ionization was conducted at 70 eV. The data acquisition was

performed in combined single-ion monitoring (SIM)/full scan mode in order to achieve high sensitivity for target analytes while at the same time acquiring information on unknown metabolites which might be included in the samples. The column was operated in constant flow mode (1 mL/min) with helium 5.0 as carrier gas and an oven program ranging from 60 °C (for 1 min) to 260 °C (15 °C/min) to 280 °C (1 °C/min) to 320 °C (25 °C/min and hold for 5 min). The temperature of the transfer line connecting to the mass spectrometer was set to 295 °C. The injector was a cold injection system (Gerstel, Mülheim, Germany) operated with a temperature program starting at 45 °C and ramping to 300 °C at a rate of 12 °C/s.

Metabolite quantification: Metabolites were quantified using MassHunter Quantitative Analysis Software 7.0 (Agilent Technologies, Santa Clara, CA, USA). Untreated skin models or cell culture media were used as blanks. A matrix calibration was performed using skin models or culture medium spiked with defined amounts of the B[*a*]P metabolites under consideration (Table 1). The calibration series was prepared by dilution of stock solutions in DMSO, so that the DMSO concentration in the final solution did not exceed 0.01 %. The concentration range of the standards varied depending on their limit of detection (Table 2).

**Table 2**: List of the external standards (ES). Presented are the external standards as used for identification and quantification of the B[*a*]P metabolites using GC/MS with the respective retention time (rt/min), together with quantifier and qualifier ions and the designation to the corresponding IS. The respective calibration ranges are given in pmol.

| Substance | rt /min | Quantifier m/z | Qualifier m/z | Allocation to IS | Calibration range [pMol] |
|---|---|---|---|---|---|
| B[*a*]P | 26,7 | 252 | 253 | 1 | 2.5-2500 |
| B[*a*]P-3-ol | 34,9 | 340 | 341 | 2 | 3.7-1850 |
| B[*a*]P-7-ol | 34,6 | 340 | 341 | 2 | 3.7-370 |
| B[*a*]P-9-ol | 33,7 | 340 | 341 | 2 | 3.7-370 |
| B[a]P-1,6-dione | 41,8 | 428 | 429 | 3 | 8.9-1780 |
| B[a]P-6,12-dione | 38,5 | 428 | 429 | 3 | 8.9-1780 |
| B[a]P-7,8-dione | 42,2 | 428 | 429 | 3 | 8.9- 1780 |
| B[a]P-7,10-dione | 33,7 | 428 | 429 | 3 | 8.9- 1780 |
| B[a]P-7,8-diol | 35,4 | 430 | 340 | 4 | 17.6-1760 |
| B[a]P-9,10-diol | 28,3 | 430 | 340 | 4 | 17.6-1760 |
| B[*a*]P-7,8,9,10-tetrahydrotetrol | 36,7 | 404 | 191 | 5 | 18.7-1870 |

Calibration curves were checked for linearity and used for quantification of the analytes (Fig. S3B). The B[*a*]P-diones contained in the samples are present in solution in a redox equilibrium with their respective dihydroxy-B[*a*]P counterparts [40]. During the derivatization reaction B[*a*]P-diones get reduced to their corresponding dihydroxy-B[*a*]Ps, which get silylated and subsequently analyzed by GC/MS. Therefore, the ratio between diones and dihydroxy analogs cannot be determined by this method (Fig. S3A). In bacterial

metabolism, B[*a*]P-dihydrodiols can be converted to dihydroxy-B[*a*]P by dihydrodiol dehydrogenases[41,42]. However, since beside the B[*a*]P-7,8-dihydrodiol and the B[*a*]P-9,10-dihydrodiol no other metabolites with the corresponding mass spectra (m/z = 430, m/z = 340) were measured in our experiments, the presence of B[*a*]P-diones is much more likely here. Given a similar concentration of the B[*a*]P-7,8-dihydrodiol in the uncolonized controls and the colonized skin models, but significantly higher concentration of B[*a*]P-7-8-dione in the latter, the presence of the dione can also be assumed.

*BPDE DNA Adduct quantification*

The BPDE-DNA adduct ELISA (STA-357; Cell Biolabs, Inc., San Diego, CA, USA) was performed according to the manufacturer's instructions to compare BPDE-DNA adduct formation in colonized skin and control tissues. Initially, the DNA of the skin models was isolated with a TRIzol-based protocol using the TRIzol® reagent (Thermo Scientific, Waltham, MA, USA) as described earlier [43]. The DNA concentration was determined using the Qubit™ dsDNA HS Assay Kit (Q32851; Thermo Scientific, Waltham, MA, USA) in the Qubit 2.0 Fluorometer (Thermo Scientific, Waltham, MA, USA). The absorbance was measured at 450 nm using a BioTek Synergy Neo2 spectrophotometer (BioTek Instruments; Winooski, VT, USA).

*Statistical analysis*

All experiments were performed with at least three biological replicates if not stated otherwise. Data are presented as means +/- the standard deviation (SD). GraphPad Prism 8 (Statcon, Witzenhausen, Germany) was used for data analysis, illustration and statistical data processing with analyses of multiple groups by one-way ANOVA with Bonferroni's multiple comparisons test or ordinary two-way ANOVA being performed as appropriate. Data of the analytical investigations were normalized by dividing each value of the microbially colonized skin treated with B[*a*]P by the mean value of the respective control tissues treated with the same B[*a*]P stock solution but lacking skin bacteria and multiplying by 100 for the specification in percentages. For the evaluation of the western blot data, the normalization was done by dividing the measurement of all different conditions by the value of the untreated control (no B[*a*]P and no bacteria) starting with the loading control (GAPDH) and then with the respective target. The normalization of data for immunofluorescence measurements was performed on the respective untreated control (no B[*a*]P and no bacteria), which was stained together at the same time as the treatments. For the evaluation of the transcriptome data, the batch effect was included in the case of the B[*a*]P activating genes for comparability with our previous data [31]. The batch affect considers the cultures treated with the same B[*a*]P stock solution. In general, a value of $p \leq 0.05$ was accepted as statistically significant.

## RESULTS

The aim of the study was to investigate the effects of commensal skin colonization on B[*a*]P-metabolism *in situ* using a microbial competent 3D skin model [31]. The model was colonized with two previously isolated skin commensals, namely *M. luetus* 1B and *P. oleovorans* 1C [27,44]. While both organisms have been established using B[*a*]P as sole source of carbon and energy, including the metabolites formed by *M. luteus*, the nature of the metabolites formed by *P. oleovorans* remained unknown [27]. We therefore started with a comprehensive characterization of B[*a*]P-metabolites formed by the latter using carbon-limited batch cultures.

*P. oleovorans B[a]P-metabolites*

The analytical examination of the respective culture supernatants confirmed this strain's ability to partially metabolize B[*a*]P [26]. The dominant metabolites formed were B[*a*]P-1,6-dione, B[*a*]P-7,8-dione, B[*a*]P-7,10-dione and 3-OH-B[*a*]P (Fig. S4A). Altogether a total of 8 metabolites could be identified, 3 of which seem to be specific for this particular organism (Fig. S4B and C). Among them were 8-OH-B[*a*]P, B[*a*]P-7,10-dione and an additional monohydroxylated B[*a*]P, which could not be further specified (Fig. S4D).

*Analytical characterization of commensal B[a]P metabolism* in situ *and effect on BPDE-DNA adduct formation*

With the PAH metabolite patterns of both microorganisms established it was henceforth possible to follow B[*a*]P-metabolism and distribution of resulting metabolites in the colonized skin model. For this purpose, B[*a*]P was topically applied to stably established microbial competent 3D skin cultures for 7 days. Following substance treatment the concentration of B[*a*]P and its metabolites was measured starting from the surface throughout the model on day 8, with analyte levels in the supporting culture medium being monitored over the entire cultivation period (Scheme S1).

The data indicate commensal B[*a*]P-metabolism to occur directly at the surface with the co-colonized models, which also retained higher amounts (2 of 3 were significantly higher) of unmetabolized B[*a*]P compared to uncolonized 3D skin (Fig. S5A). Furthermore, the concentrations of all detected B[*a*]P-diones as well as 3-OH-B[*a*]P were strongly elevated, all of which being established metabolites of at least one of the two commensals. B[*a*]P-7,10-dione was only formed in presence of *P. oleovorans* (Fig. S5B). Notably, concentrations for the eukayrotic B[*a*]P-7,8,9,10-tetrahydrotetrol (B[*a*]P-tetrol; *i.e.*, the hydrolysis product

resulting from *trans*-opening of the epoxide moiety in BPDE) were slightly elevated in presence of *M. luteus*. (Fig. 1A).

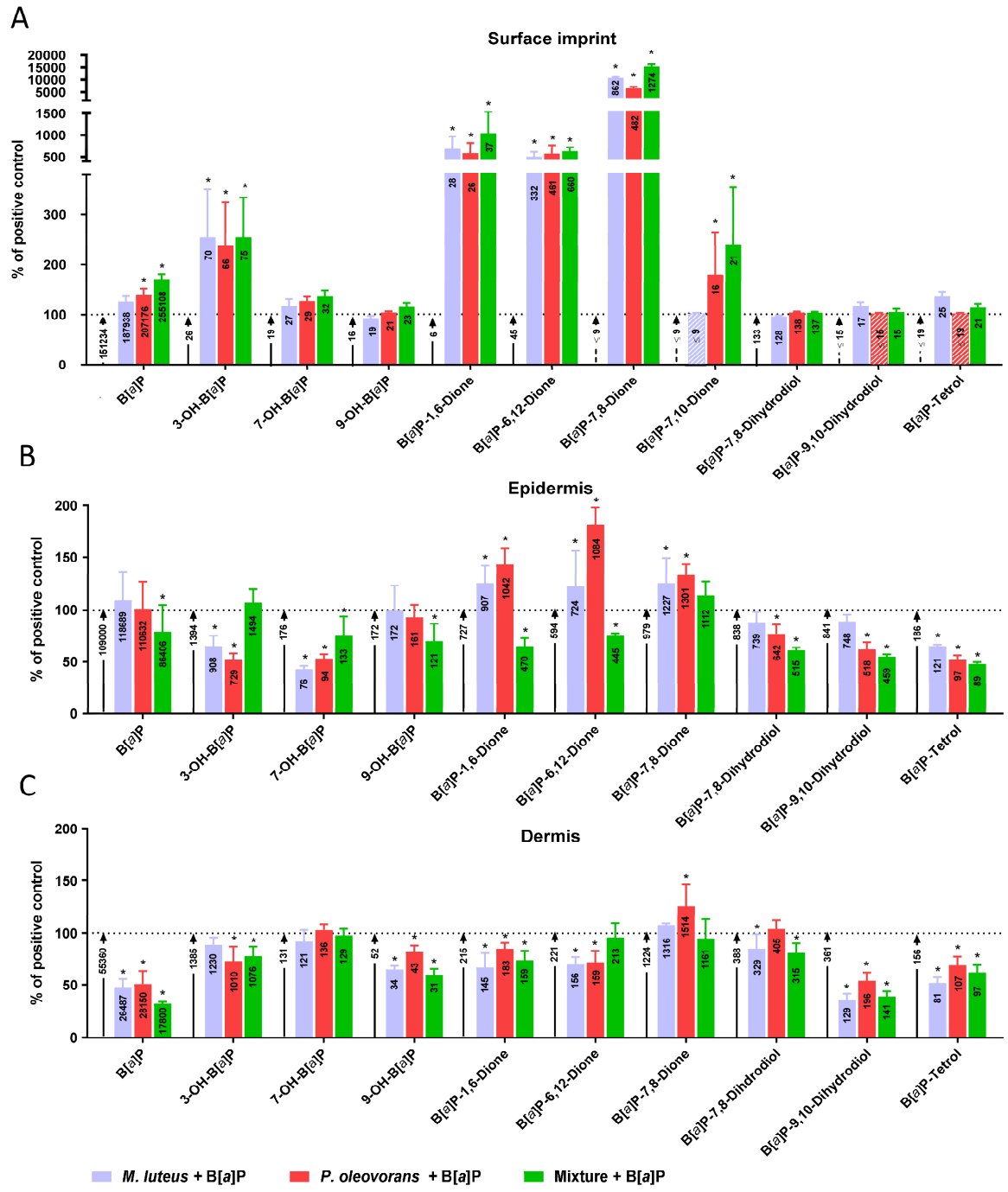


**Fig. 1.** Concentrations of B[*a*]P and its metabolites from the surface imprint (A), epidermis (B) and dermis (C) of microbial skin tissue co-culture colonized as indicated after 7 days of repeated B[*a*]P treatment, respectively, as determined via GC/MS. Each bar represents 6 biological replicates (mean + SD) relative to the B[*a*]P-treated

uncolonized control. Each bar depicts the measured substance concentrations in pmol/skin model. The concentration of the B[*a*]P-treated control lacking microbiota is indicated in the arrow next to the respective bar. If a substance could not be measured, this is indicated as below (≤) the smallest measured concentration in calibration and corresponding columns or arrows are shown dashed. Observed differences are considered to be significant with *$p < 0.05$.

Except for B[*a*]P-7,10-dione all of the above metabolites were also detectable in the epidermis and dermis. The predominant species were B[*a*]P-1,6-dione, B[*a*]P-6,12-dione and B[*a*]P-7,8-dione or just B[*a*]P-7,8-dione , respectively (Fig. 1B and C). For all monitored metabolites there was a clear colonization-dependent impact, indicating a distinct microbiome-mediated effect (Fig. S6A, B and C). In addition, the epidermis of models co-colonized with both organisms tended to contain lower relative concentrations of B[*a*]P-diones when compared to the surface. In the deeper dermal layers this effect was less pronounced.

Notably, commensalic colonizaiton led to significantly reduced levels of B[*a*]P-9,10-diol and B[*a*]P-tetrol throughout all investigated epidermal and dermal samples (Fig. S6D and E). Also, the concentration of unmetabolized B[*a*]P was greatly reduced in the dermis of commensal models, with the strongest effect occurring in the mixed co-culture (Figs. 1B, 1C and S6C).

Several of the metabolites passed through the entire model and were detectable in the basal cell culture medium. Namely these were B[*a*]P-tetrol, B[*a*]P-9,10-diol, B[*a*]P-7,8-diol, 3-OH-B[*a*]P, B[*a*]P-1,6-dione, B[*a*]P-6,12-dione and 7-OH-B[*a*]P (Table S1A) which initially appeared 24 h and 48 h after the first application of B[*a*]P onto the model surface, respectively. The corresponding concentrations increased in a time-dependent manner until reaching a plateau phase from day five onwards with the samples of the colonized models featuring significantly lower levels of B[*a*]P and B[*a*]P-metabolites (Fig. S6F). This effect was particularly pronounced with *M. luteus*.

In concordance with this and to what was found for B[*a*]P-9,10-diol and B[*a*]P-tetrol, that is the significant reduction of metabolite levels in the microbial colonized models, BPDE-DNA adducts were also found to be strongly reduced in models subjected to commensalic colonization (Fig. 2). Meanwhile controls without B[*a*]P showed no BPDE-DNA formation, irrespective of their microbial competence.

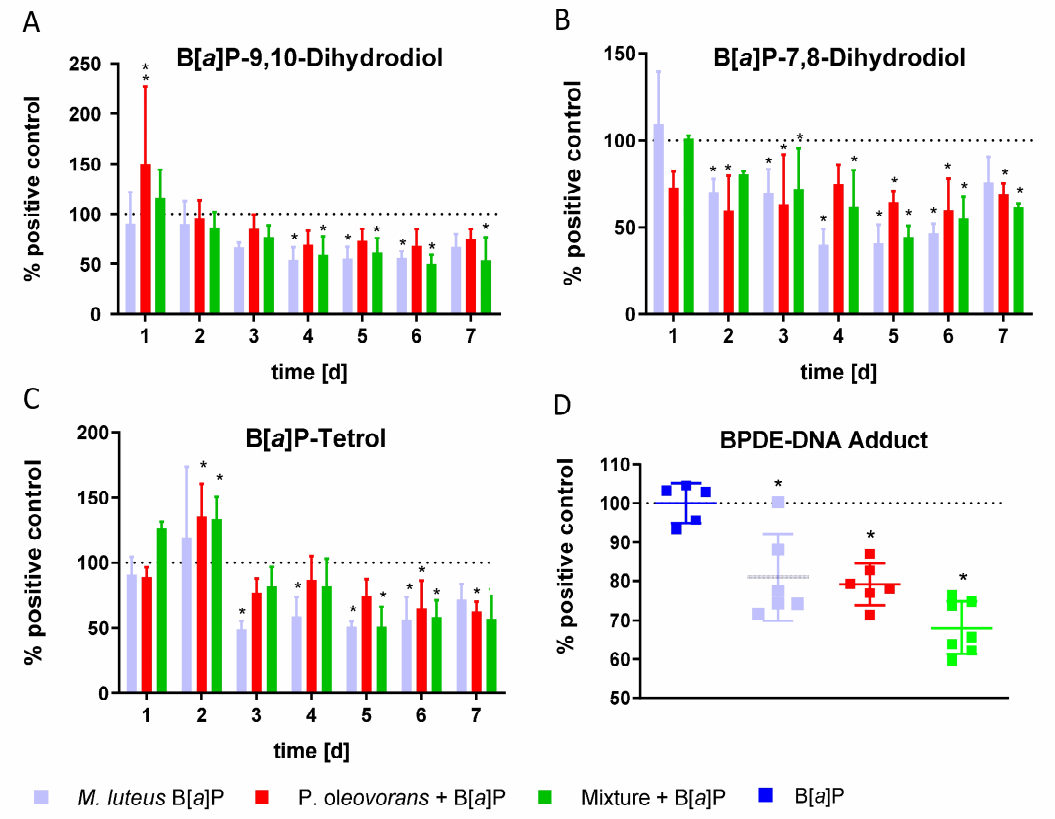


**Fig. 2.** Concentrations of 3 representative B[*a*]P metabolites in the basal culture medium of microbial skin tissue co-cultures over 7 days of repeated B[*a*]P-treatment as determined via GC/MS. Each bar represents 6 biological replicates (A) B[*a*]P-7,8-dihydrodiol, (B) B[*a*]P-9,10-dihydrodiol and (C) B[*a*]P-tetrol (mean + SD) as percentage of the B[*a*]P-treated uncolonized control. Part (D) reports the number of BPDE-DNA adducts of the microbial skin tissue co-cultures colonized as indicated compared to the B[*a*]P-treated control lacking microbiota. Epidermis and dermis were examined as a whole. Observed differences are considered to be significant with *$p < 0.05$.

*Commensalic impact on skin function*

The potential functional impact of commensal B[*a*]P-metabolism on the host and skin function was studied using transcriptomic assays. The respective Clariom™ S system records the activity of more than 20,000 well-annotated transcripts, hence providing coverage of most of the functionally annotated genes. Compared to uncolonized controls, treatment of colonized models with B[*a*]P significantly affected more than 2500 transcripts, while substance treatment alone had an effect on 1300 transcripts (Fig. S7). When compared against all treatment groups, 10 of the 17 most influenced transcripts strikingly encode proteins that play a role in epidermal differentiation, all of which were repressed in co-colonized models as well as

after treatment with B[*a*]P (Fig. 3). This includes several epidermal differentiation complex (EDC) genes such as FLG, loricrin and caspase 14.

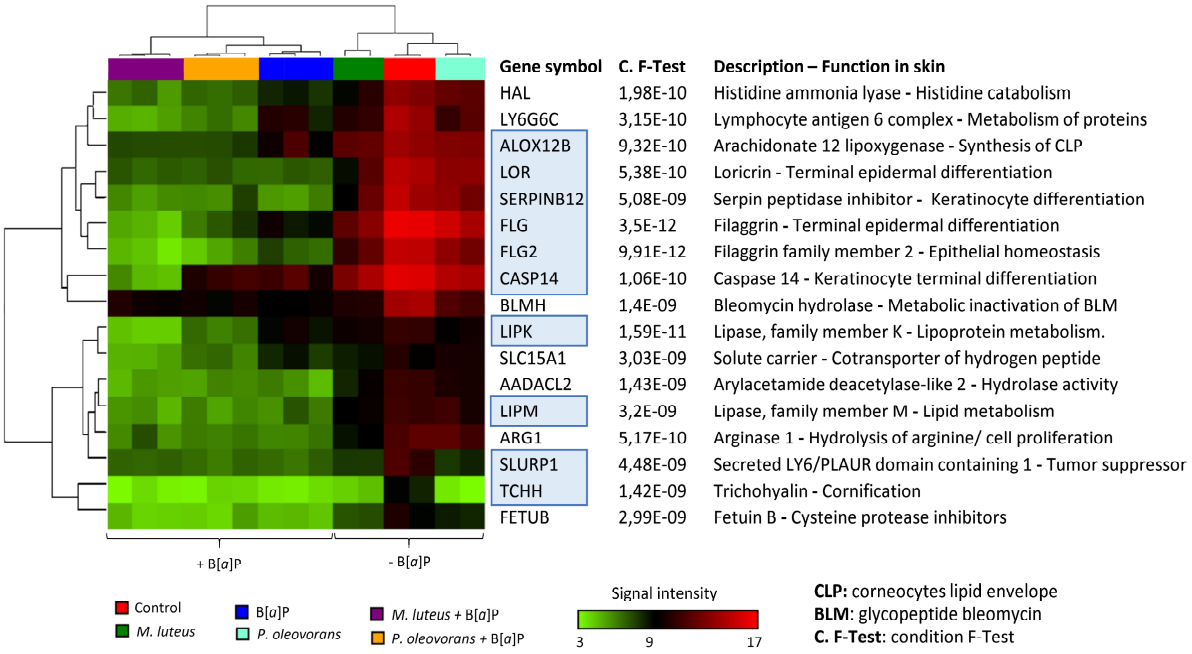


**Fig. 3.** Hierarchical clustering of the 17 most significantly regulated genes according to the conditions F-Test in microbial skin tissue co-culture with and without B[*a*]P treatment. Shown are the signal intensities of the transcripts measured using Clariom™ S microarray analysis. Ten of these 17 genes code for proteins that are related to epidermal differentiation and are marked in blue. In addition, a description and their most likely function in the skin is presented for each gene listed.

The results of the transcriptome analysis strongly imply a potential commensal influence on skin differentiation, particularly following substance treatment. Subsequent analysis therefore focused on the fluorescent visualization of various functional markers for different stages of differentiation as well as a tight junction (TJ) marker (Fig. 4A and S8). In the B[*a*]P-exposed models, bacterial colonisation led to a strong increase for the late differentiation markers FLG and IVL, with a particularly strong increase for *P. oleovorans* and mixed skin tissue (Fig. 4A and B).

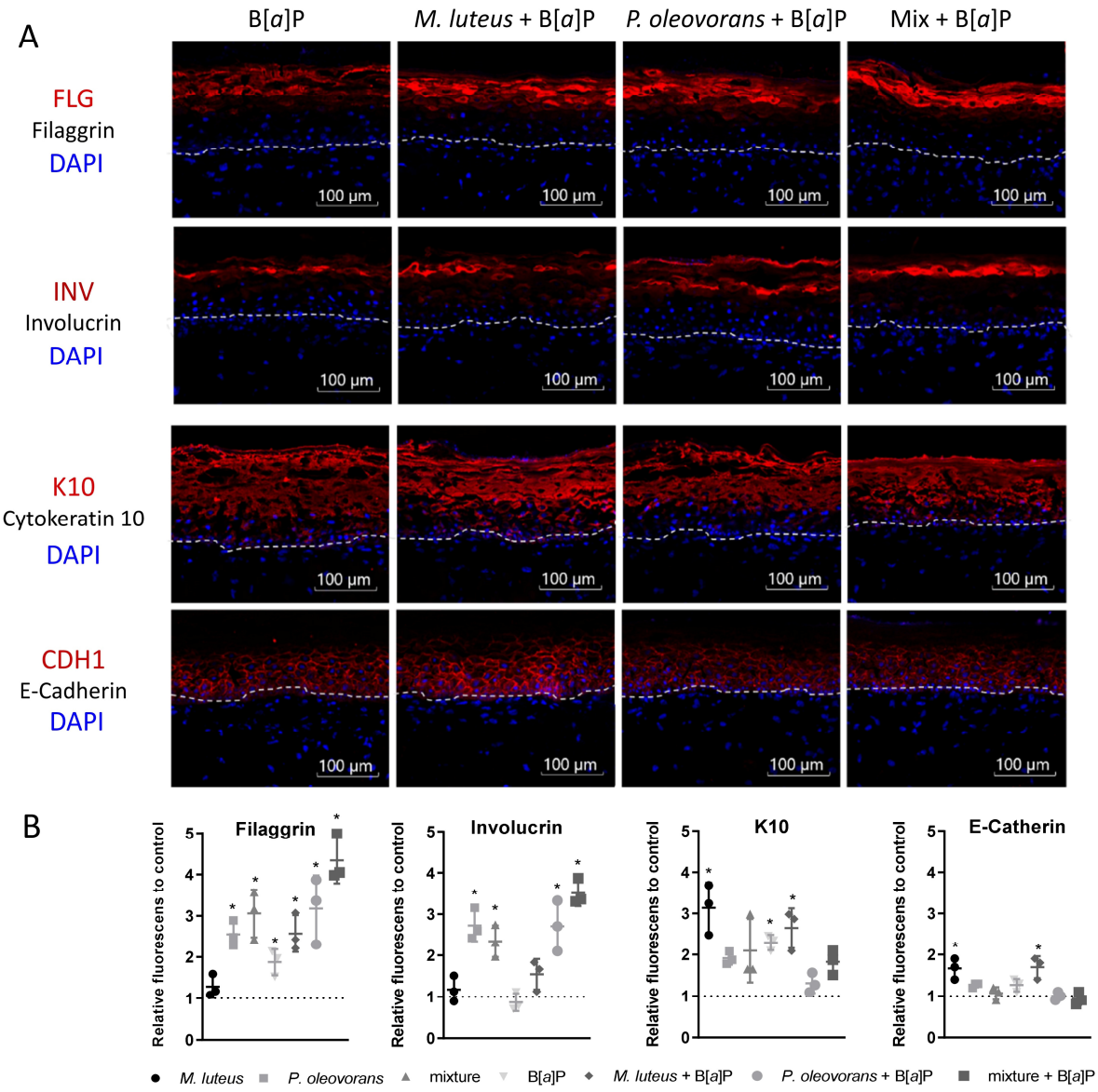


**Fig. 4.** Expression of epidermal differentiation markers in microbial skin tissue co-cultures with and without B[*a*]P treatment. (A) Exemplary shown is an immunostaining of selected differentiation markers and a tight junction marker of skin sections of microbial competent skin models, colonized as indicated with B[*a*]P treatment. All antibody stains are shown in red and the cell nuclei are shown in blue stained with DAPI. The dashed line indicates the course of the basal laminar (B) Summary of the immunostaining of 3 biological replicates relative to the uncolonized skin including all controls without B[*a*]P application. Observed differences are considered to be significant with *$p < 0.05$.

In light of the skin's dual function as a physico-chemical barrier we further investigated the commensal impact on the expression of several key proteins involved in human B[*a*]P-metabolism. Enzymatic expression of CYP1A1 was found to be decreased in the commensal models following treatment with

B[*a*]P, while there was no clear effect on CYPs 1B1, 1A2 or epoxide hydrolase 1. Contrastingly, both microorganisms led to increased expression of the regulatory co-factor ARNT, even in absence of B[*a*]P (Fig. 5A and B).

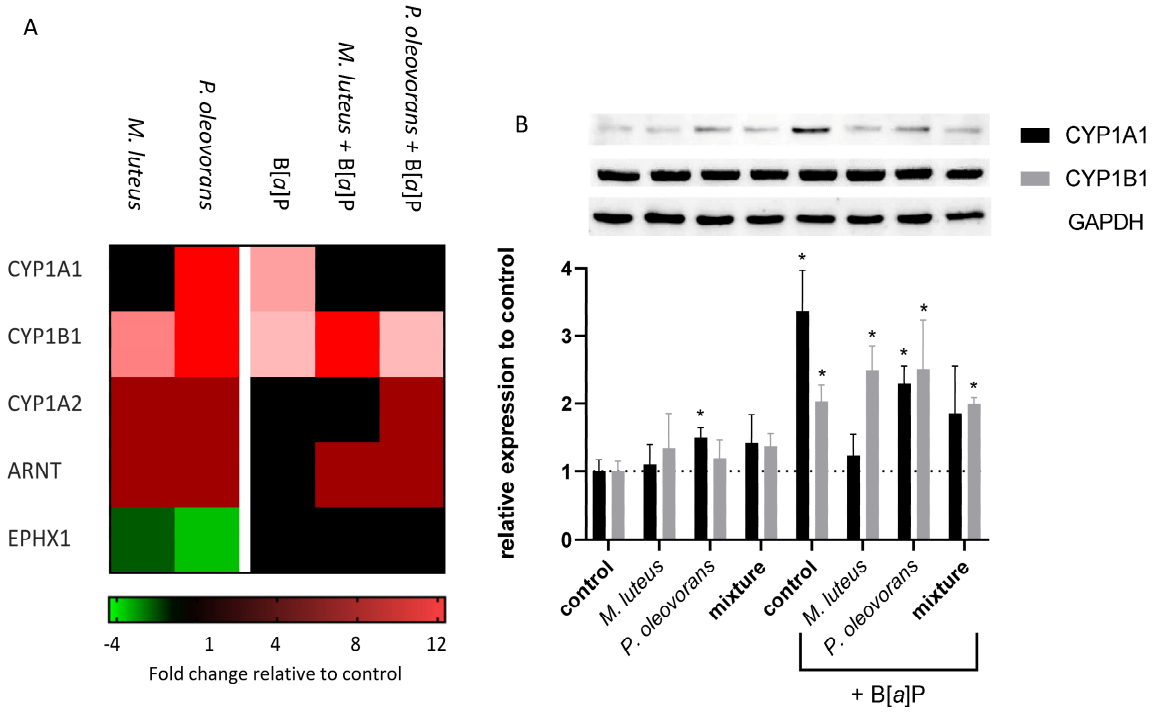


**Fig. 5.** Expression of enzymes involved in B[*a*]P activation in microbial skin tissue co-culture. The cluster map records the fold change compared to uncolonized skin at day 8 of microbial colonisation as indicated (A). Shown are the gene symbols of significantly differentially expressed genes with a P value ≤ 0.05. (B) Exemplary shown is an immunoblot of total protein of microbial skin tissue co-culture, colonized as indicated, as well as the summary of the immunoblots of 3 biological replicates relative to the uncolonized skin. Observed differences are considered to be significant with *p < 0.05.

Metabolic activation of B[*a*]P in eukaryotes can lead to the formation of bulky DNA adducts that can be repaired by the nucleotide excision repair pathway (NER). The treatment of 3D skin models with B[*a*]P resulted in an increase in the expression of xeroderma pigmentosum, complementation group C (XPC) and G (XPG) proteins, both of which are typical representatives of this repair pathway (Fig. 6B). Following B[*a*]P treatment, however, their gene and protein expression was significantly reduced in microbial colonized skin tissue compared to the control treated with B[*a*]P only (Fig. 6A and B).

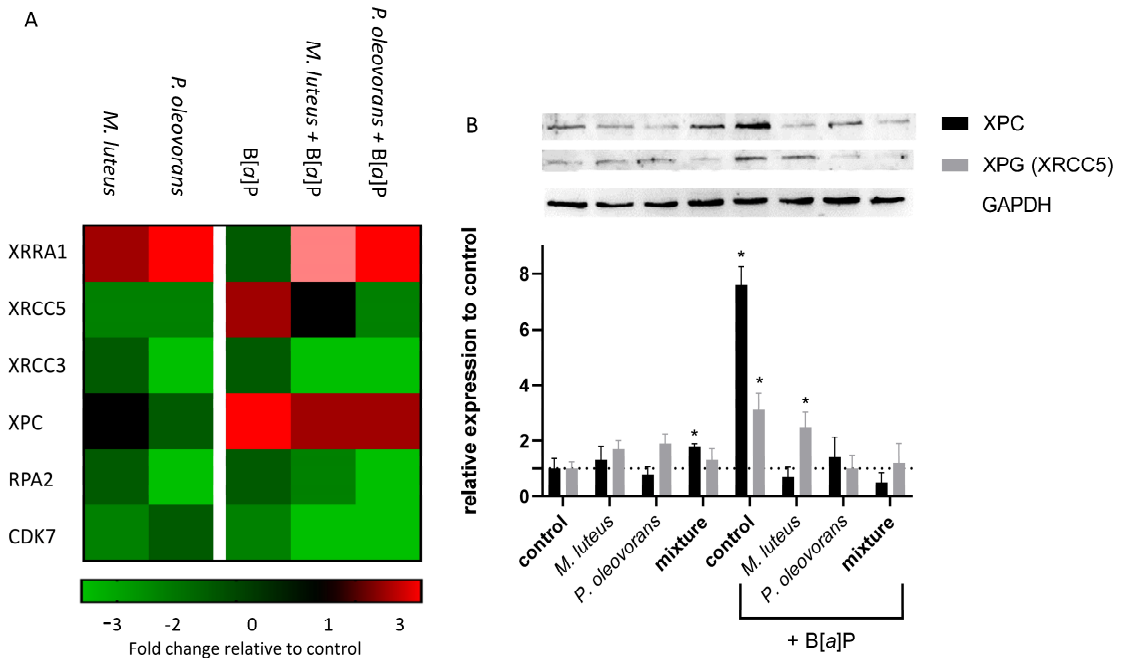


**Fig. 6.** Expression of enzymes of the nucleotide excision repair (NER) pathway in microbial skin tissue co-culture. The cluster map records the fold change compared to uncolonized skin at day 8 of microbial colonization as indicated (A). Shown are the gene symbols of significantly differentially expressed genes with a *P* value < 0.05. Exemplary shown is an immunoblot of total protein of microbial skin tissue co-culture, colonized as indicated, as well as the summary of the immunoblots of 3 biological replicates relative to the uncolonized skin control (B). Observed differences are considered to be significant with *p < 0.05.

## DISCUSSION

Growing evidence suggests potential chemical-associated effects of microbiome-host interactions on human health [7,44,45]. Yet, toxicity studies are still largely conducted without particular consideration of the microbiota [46]. At best the microbiota is considered a systemic compartment when testing toxicity *in vivo*. Yet, neither does this consider the high species specificity of microbiota, nor does this acknowledge that even without this species specificity the microbiota of laboratory animals is strongly impacted by the artificial environment the animals are housed in and thus hardly representative [31]. In the context of risk assessment of xenobiotic exposure this not only is scientifically unsatisfying but also carries a true risk of missing relevant health effects. However, apart from a partial lack of awareness for this issue another major point has been a lack of appropriate models to systematically study such effects. This is true for the gut, but also for the skin [7,47]. For dermal environments the recent development of our microbial-competent co-culture model partly overcomes this as it allows to exemplarily study microbial driven modulation of B[*a*]P-metabolism and -toxicity and its effects on the host [31]. The results reassuringly confirm the previously observed commensal metabolism of B[*a*]P to also occur *in situ* [26,27]. However, and more importantly, they provide a first glance on the corresponding metabolite patterns along skin layers and how this potentially affects host toxicity in a complex and hitherto unexpected manner.

Skin colonization lead to an accumulation of unmetabolized B[*a*]P and bacterial metabolites including B[*a*]P-1,6-dione, B[*a*]P-6,12-dione, B[*a*]P-7,8-dione B[*a*]P-7,10-dione and 3-OH-B[*a*]P [27] on the skin surface and, partially, in the epidermis. The strong increase of these commensal metabolites points to microbiotic recruitment of B[a]P as a source of carbon and energy and is in line with previous *in vitro* studies [26,48]. This is particularly evident in the case of B[*a*]P-7,10-dione, which, being a metabolite of *P. oleovorans,* occurred exclusively on the surface of the correspondingly colonized skin-models. Yet, the identification of B[*a*]P-tetrol and B[*a*]P-9,10-dihydrodiol on the surface of skin harbouring *M. luteus* shows concomitant human phase-I metabolism to occur as neither of the two metabolites occurred in bacterial batch cultures [27]. Notably, when assessed throughout their various compartments the colonized models showed a slight overall decrease of B[*a*]P metabolites compared to uncolonized skin (~ 4.5 %), which was significant for a majority of the metabolites. This included B[*a*]P-tetrol where the respective strong reduction consequently points to less BPDE-DNA adducts being formed beforehand, an effect most pronounced in presence of *P. oleovorans* and its mixed co-culture. Likewise the expression of key enzymes of the NER (XPC and XPG) was reduced in microbial skin tissue co-cultures. In addition, the amount of B[*a*]P-tetrol as well as other metabolites passing through the model into the basal medium was significantly reduced in the commensal models, with *M. luteus* leading to nearly 50 % reduction. This indicative beneficiary commensal effect is in

contrast to what was observed previously with batch cultures where bacterial metabolism of B[*a*]P actually enhanced B[*a*]P-mediated genotoxicity [27]. Given that the colonized models show production of the same metabolites *in situ* the here observed effect came somehow as a surprise.

Altogether the results therefore strongly point to commensally induced changes in skin metabolism and/or barrier function. Overall the analytical results of the uncolonized skin models match those of a previous study by Brinkmann, et al. [32] who showed that MatTek's EpiDermFT™ metabolizes B[*a*]P to form typical human metabolites. However, in the uncolonized models only a small fraction of B[*a*]P is metabolized due to the low or absent metabolic activity of corneocytes. Only about 5.2 % of the applied B[*a*]P was metabolized with the remaining B[*a*]P accumulating on the skin surface and in the epidermis (Table S1B). Since lipophilic compounds steadily penetrate the skin by passive diffusion, this induces the build-up of a substance reservoir [49]. Befittingly, for the uncolonized models the major amount of the B[*a*]P was indeed found to be metabolized in the metabolically active epidermis. In agreement with Bourgart, et al. [33] the more hydrophilic metabolites such as B[*a*]P-tetrol, B[*a*]P-7,8-diol, and B[*a*]P-9,10-diol subsequently penetrated throughout the entire skin while B[*a*]P predominantly remained in the upper layers [33]. Meanwhile, the colonized models are also metabolically active but feature increased accumulation of B[*a*]P and known bacterial metabolites on the surface as well as showing an altered layer-specific decrease. On the transcriptomic level this was accompanied by strong changes for key transcripts involved in epidermal differentiation.

The general observation of commensals influencing skin differentiation matches previous results from other studies, including animals [50]. The most strongly altered transcripts include LIPM and LIPK, both of which have an essential function in lipid metabolism of the most differentiated epidermal layers [51]. Another heavily affected transcript is CASP14, which is a predominant caspase in the epidermal SC and is required for cornification [52]. The reduced transcript levels are in line with the age of the models at the time of sampling. Instead, selected corresponding protein markers of skin differentiation revealed to be elevated. Such an apparent commensal related strengthening of the skin barrier has indeed been observed before, although not in a toxicological context and without such a strong modulatory effect on systemic substance metabolism and availability [53,54]. Our results show that *P. oleovorans* had a particularly strong influence promoting terminal differentiation as exemplified by an increase in the expression of FLG and IVL. In contrast, colonization with *M. luteus* leads to less pronounced changes, showing a slight but significant enhancing effect on FLG, K10 and the TJ marker E-cadherin. Simultaneous colonization of the 3D skin models with both organisms revealed the greatest increases in expression of INV and FLG, supporting the finding by Loomis, et al. [54] that FLG expression is more strongly enhanced by multiple

commensals than by a single species. The high amount of unmetabolized B[*a*]P on the surface of the mixed microbial skin tissue co-cultures suggests that FLG and IVL particularly contribute to a reduction in the diffusion of chemicals into the skin. This is in agreement with the results of Joensen, et al. [55] who showed that loss-of-function mutations of FLG lead to increased internal exposure to phthalate metabolites. INV is also important for skin permeability to chemicals with a triple knockout of IVL, envoplakin, and periplakin resulting in a defective epidermal barrier [56]. Moreover, tissue permeability is regulated by TJs and keratin filaments [57], whose expression can be enhanced by the presence of commensal and probiotic strains [58]. In our models *M. luteus* particularly induced E-cadherin and K10. It seems reasonable to assume that the resulting strengthening of the epidermis is causative for the respective strong effects on metabolite concentrations in the dermis and basal cell culture medium, respectively. At the same time, commensally induced increased terminal differentiation of the SC (*i.e.*, as seen for *P. oleovorans*) promotes the accumulation of B[*a*]P on the skin surface, thus reducing the rate of epidermal skin-type B[*a*]P metabolism. As this strongly affects levels of B[*a*]P-9,10-diol, B[*a*]P -7,8-diol and BPDE this would obviously reduce the number of BPDE-DNA adducts in general.

The altered barrier function also systemically affected key genes of human phase-I metabolism. Effects were seen particularly for the AhR signaling pathway, namely ARNT, CYP1B1 and CYP1A1, with the effect being particularly strong on the latter. Although CYP1A1 expression is increased in co-culture with *P. oleovorans*, it is significantly reduced after repeated B[*a*]P application in all studied microbial co-cultures compared to uncolonized skin. This is likely attributed to the lower amount of B[*a*]P penetrating the SC which in turn reduces the available concentration in the metabolically active part of the epidermis. In the context of B[*a*]P-toxification the commensal influence on the skin barrier hence apparently outweighs any microbially-induced changes in CYP expression. Our results clearly show that commensals are able to metabolize as well as potentially toxify B[*a*]P on and in human skin. However, with regard to B[*a*]P-genotoxicity the microbial effects on host skin differentiation have a strong modulating beneficial influence due to an enhanced physico-chemical barrier function. This latter alterations cause a commensal-related reduction of the toxicity of B[*a*]P especially by inhibiting the uptake of this procarcinogen and its subsequent metabolic activation. The microbial influence on epithelial permeability and integrity has important implications for the absorption, metabolism, and distribution of xenobiotics and environmental pollutants such as B[*a*]P. Overall the results demonstrate the respective microbe-host interactions to have much more complex effects on substance toxification and metabolism than previously inferred from studies on single systems. Depending on the particular substance and circumstances this could lead to either over- or underestimation of toxicity, both of which should be avoided. Therefore there

is an urgent need to address the effect of the microbiome on potential systemic host toxicity more systematically. Given the species specificity of the microbiome this has to be implemented using commensally competent testing systems that are specific for the human host.

## ABBREVIATIONS

**3D**: Three-dimensional

**AhR**: Aryl hydrocarbon receptor

**ARNT**: Aryl hydrocarbon receptor nuclear translocator

**B[*a*]A**: Benzo[*a*]anthracene

**B[*a*]P**: Benzo[*a*]pyrene

**B[*a*]P-tetrol**: B[*a*]P-*r*-7,*t*-8,*t*-9,*c*-10-tetrahydrotetrol

**BPDE**: Benzo[*a*]pyrene-7,8-diol-9,10-epoxide

**Bsc**: Below the smallest measured concentration in calibration

**BSTFA**: *N,O-bis*(trimethylsilyl)-trifluoracetamide

**CFU**: Colony forming unit

**CYP**: Cytochromes P450-dependent monooxygenase

**DCM**: Dichloromethane

**DMSO**: Dimethyl sulfoxide

**EDC**: Epidermal differentiation complex

**EPHX**: Epoxide hydrolase

**EtOH**: Ethanol

**FLG**: Filaggrin

**GAPDH**: Glyceraldehyde 3-phosphate dehydrogenase

**GC/MS**: Gas chromatography–mass spectrometry

**GST**: Glutathione transferase

**IVL**: Involucrin

**MM**: Minimal medium

**MS**: Mass spectra

**NER**: Nucleotide excision repair

**PAH**: Polycyclic aromatic hydrocarbon

**RIN**: RNA-integrity

**SC**: Stratum corneum

**SULT**: Sulfotransferase

**TJs**: Tight junctions

**TLR**: Toll-like Receptor

**RT**: Retention time

**TAC**: Transcriptome Analysis Console

**XPC**: Xeroderma pigmentosum, complementation group C

**XPG**: Xeroderma pigmentosum, complementation group G

## DECLARATIONS

*Ethics approval and consent to participate*

Skin models as obtained from MatTek rely on ethically sourced materials from accredited institutes and are subject to strict donor consent. Their suppliers have represented in writing that they are strictly regulated by and comply with U.S. federal government standards.

*Consent for publication*

Not applicable.

*Availability of data and material*

Raw and processed data files are deposited in the Gene Expression Omnibus (GEO) data repository GSE171720. Super Series upon publication.

*Competing interests*

The authors declare that they have no competing interests.

*Funding*

This work was supported by the German Federal Institute for Risk Assessment (BfR) Grant 1322-664.

*Authors' contributions*

LL and TT conceived and designed the experiments. LL performed the sampling, experimental work and analyzed the data. DB helped with experimental work. AR and CH contributed to the planning of the analytical investigations and their evaluation. AL provided conceptual input. LL, TT and AL drafted the manuscript with input from all authors, who also approved the final version.

*Acknowledgements*

The authors acknowledge intramural funding at the German Federal Institute for Risk Assessment (BfR). Equally acknowledged is the experimental and technical assistance of Tessa Höper, Henrig Hering, Nils Dommershausen, Julian Tharman, and Bettina Hoffmann.

**REFERENCES**


1 Korkina, L. Metabolic and redox barriers in the skin exposed to drugs and xenobiotics. *Expert Opinion on Drug Metabolism & Toxicology* **12**, 377-388, doi:10.1517/17425255.2016.1149569 (2016).

2 Ley, R. E., Peterson, D. A. & Gordon, J. I. Ecological and evolutionary forces shaping microbial diversity in the human intestine. *Cell* **124**, 837-848, doi:10.1016/j.cell.2006.02.017 (2006).

3 Qin, J. *et al.* A human gut microbial gene catalogue established by metagenomic sequencing. *Nature* **464**, 59-65, doi:10.1038/nature08821 (2010).

4 Sender, R., Fuchs, S. & Milo, R. Revised Estimates for the Number of Human and Bacteria Cells in the Body. *PLoS Biol* **14**, e1002533, doi:10.1371/journal.pbio.1002533 (2016).

5 Scharschmidt, T. C. & Fischbach, M. A. What Lives On Our Skin: Ecology, Genomics and Therapeutic Opportunities Of the Skin Microbiome. *Drug Discov Today Dis Mech* **10**, e83-e89, doi:10.1016/j.ddmec.2012.12.003 (2013).

6 Chen, Y. E., Fischbach, M. A. & Belkaid, Y. Skin microbiota-host interactions. *Nature* **553**, 427-436, doi:10.1038/nature25177 (2018).

7 Tralau, T., Sowada, J. & Luch, A. Insights on the human microbiome and its xenobiotic metabolism: what is known about its effects on human physiology? *Expert Opin. Drug Metab. Toxicol.* **11**, 411-425, doi:10.1517/17425255.2015.990437 (2015).

8 Lange-Asschenfeldt, B. *et al.* Distribution of Bacteria in the Epidermal Layers and Hair Follicles of the Human Skin. *Skin pharmacology and physiology* **24**, 305-311, doi:10.1159/000328728 (2011).

9 Abdelsalam, N. A., Ramadan, A. T., ElRakaiby, M. T. & Aziz, R. K. Toxicomicrobiomics: The Human Microbiome vs. Pharmaceutical, Dietary, and Environmental Xenobiotics. *Front Pharmacol* **11**, 390-390, doi:10.3389/fphar.2020.00390 (2020).

10 Martin, A. M., Sun, E. W., Rogers, G. B. & Keating, D. J. The Influence of the Gut Microbiome on Host Metabolism Through the Regulation of Gut Hormone Release. *Front Physiol* **10**, 428-428, doi:10.3389/fphys.2019.00428 (2019).

11 Koppel, N., Maini Rekdal, V. & Balskus, E. P. Chemical transformation of xenobiotics by the human gut microbiota. *Science (New York, N.Y.)* **356**, eaag2770, doi:10.1126/science.aag2770 (2017).

12 Hayes, C. L. *et al.* Commensal microbiota induces colonic barrier structure and functions that contribute to homeostasis. *Scientific Reports* **8**, 14184, doi:10.1038/s41598-018-32366-6 (2018).

13 Hausmann, C. *et al.* Reconstructed Human Epidermis Predicts Barrier-Improving Effects of Lactococcus lactis Emulsion in Humans. *Skin Pharmacol Physiol* **32**, 72-80, doi:10.1159/000495255 (2019).

14 Claus, S. P., Guillou, H. & Ellero-Simatos, S. The gut microbiota: a major player in the toxicity of environmental pollutants? *npj Biofilms and Microbiomes* **2**, 16003, doi:10.1038/npjbiofilms.2016.3 (2016).

15 Baklanov, A. *et al.* Integrated systems for forecasting urban meteorology, air pollution and population exposure. *Atmos Chem Phys* **7**, 855-874, doi:DOI 10.5194/acp-7-855-2007 (2007).

16 Manzetti, S. Polycyclic Aromatic Hydrocarbons in the Environment: Environmental Fate and Transformation. *Polycycl Aromat Comp* **33**, 311-330, doi:10.1080/10406638.2013.781042 (2013).

17 Geier, M. C. *et al.* Comparative developmental toxicity of a comprehensive suite of polycyclic aromatic hydrocarbons. *Arch Toxicol* **92**, 571-586, doi:10.1007/s00204-017-2068-9 (2018).

18 Bamforth, S. M. & Singleton, I. Bioremediation of polycyclic aromatic hydrocarbons: current knowledge and future directions. *Journal of Chemical Technology & Biotechnology* **80**, 723-736, doi:10.1002/jctb.1276 (2005).

19 Luch, A. & Baird, W. M. in *The Carcinogenic Effects of Polycyclic Aromatic Hydrocarbons* 19-96 (2005).

20 Baird, W. M., Hooven, L. A. & Mahadevan, B. Carcinogenic polycyclic aromatic hydrocarbon-DNA adducts and mechanism of action. *Environ. Mol. Mutagen.* **45**, 106-114, doi:10.1002/em.20095 (2005).

21 Jernstrom, B. & Graslund, A. Covalent binding of benzo[a]pyrene 7,8-dihydrodiol 9,10-epoxides to DNA: molecular structures, induced mutations and biological consequences. *Biophys Chem* **49**, 185-199, doi:10.1016/0301-4622(93)e0087-l (1994).

22 Uno, S. *et al.* Oral exposure to benzo[a]pyrene in the mouse: detoxication by inducible cytochrome P450 is more important than metabolic activation. *Mol Pharmacol* **65**, 1225-1237, doi:10.1124/mol.65.5.1225 (2004).

23 Marks, R. The stratum corneum barrier: the final frontier. *J Nutr* **134**, 2017S-2021S, doi:10.1093/jn/134.8.2017S (2004).

24 Marczynski, B. *et al.* Occupational exposure to polycyclic aromatic hydrocarbons and DNA damage by industry: a nationwide study in Germany. *Arch Toxicol* **83**, 947-957, doi:10.1007/s00204-009-0444-9 (2009).

25 VanRooij, J. G., De Roos, J. H., Bodelier-Bade, M. M. & Jongeneelen, F. J. Absorption of polycyclic aromatic hydrocarbons through human skin: differences between anatomical sites and individuals. *J Toxicol Environ Health* **38**, 355-368, doi:10.1080/15287399309531724 (1993).

26 Sowada, J., Schmalenberger, A., Ebner, I., Luch, A. & Tralau, T. Degradation of benzo[*a*]pyrene by bacterial isolates from human skin. *FEMS Microbiol. Ecol.* **88**, 129-139, doi:10.1111/1574-6941.12276 (2014).

27 Sowada, J. *et al.* Toxification of polycyclic aromatic hydrocarbons by commensal bacteria from human skin. *Arch Toxicol* **91**, 2331-2341, doi:10.1007/s00204-017-1964-3 (2017).

28 Toda, T. *et al.* Intestinal flora induces the expression of Cyp3a in the mouse liver. *Xenobiotica* **39**, 323-334, doi:10.1080/00498250802651984 (2009).

29 Meinl, W., Sczesny, S., Brigelius-Flohe, R., Blaut, M. & Glatt, H. Impact of gut microbiota on intestinal and hepatic levels of phase 2 xenobiotic-metabolizing enzymes in the rat. *Drug Metab Dispos* **37**, 1179-1186, doi:10.1124/dmd.108.025916 (2009).

30 Defois, C. *et al.* Environmental Pollutant Benzo[a]Pyrene Impacts the Volatile Metabolome and Transcriptome of the Human Gut Microbiota. *Frontiers in Microbiology* **8**, doi:10.3389/fmicb.2017.01562 (2017).

31 Lemoine, L. *et al.* Microbially competent 3D skin: a test system that reveals insight into host-microbe interactions and their potential toxicological impact. *Arch Toxicol* **94**, 3487-3502, doi:10.1007/s00204-020-02841-z (2020).

32 Brinkmann, J. *et al.* Metabolically competent human skin models: activation and genotoxicity of benzo[*a*]pyrene. *Toxicol. Sci.* **131**, 351-359, doi:10.1093/toxsci/kfs316 (2013).

33 Bourgart, E. *et al.* A realistic human skin model to study benzo[a]pyrene cutaneous absorption in order to determine the most relevant biomarker for carcinogenic exposure. *Archives of Toxicology* **93**, 81-93, doi:10.1007/s00204-018-2329-2 (2019).

34 Jacques, C. *et al.* Disposition and biotransformation of 14C-Benzo(a)pyrene in a pig ear skin model: ex vivo and in vitro approaches. *Toxicol Lett* **199**, 22-33, doi:10.1016/j.toxlet.2010.08.001 (2010).

35 Jaiswal, S. K., Agarwal, S. M., Thodum, P. & Sharma, V. K. SkinBug: an artificial intelligence approach to predict human skin microbiome-mediated metabolism of biotics and xenobiotics. *iScience* **24**, 101925, doi:https://doi.org/10.1016/j.isci.2020.101925 (2021).

36 Chomczynski, P. & Sacchi, N. Single-step method of RNA isolation by acid guanidinium thiocyanate-phenol-chloroform extraction. *Anal Biochem* **162**, 156-159, doi:10.1006/abio.1987.9999 (1987).

37 Hering, H. *et al.* TatS: a novel in vitro tattooed human skin model for improved pigment toxicology research. *Archives of Toxicology* **94**, 2423-2434, doi:10.1007/s00204-020-02825-z (2020).

38 de Bruin, O. M. & Birnboim, H. C. A method for assessing efficiency of bacterial cell disruption and DNA release. *BMC Microbiology* **16**, 197, doi:10.1186/s12866-016-0815-3 (2016).

39 Sadeghi, R., Kobarfard, F., Yazdanpanah, H., Eslamizad, S. & Bayat, M. Validation of an Analytical Method for Determination of 13 priority polycyclic aromatic hydrocarbons in mineral water using dispersive liquid-liquid microextraction and GC-MS. *Iran J Pharm Res* **15**, 157-168 (2016).

40 Song, Y. & Buettner, G. R. Thermodynamic and kinetic considerations for the reaction of semiquinone radicals to form superoxide and hydrogen peroxide. *Free Radic Biol Med* **49**, 919-962, doi:10.1016/j.freeradbiomed.2010.05.009 (2010).

41 Ostrem Loss, E. M. *et al.* Cytochrome P450 Monooxygenase-Mediated Metabolic Utilization of Benzo[<em>a</em>]Pyrene by <em>Aspergillus</em> Species. *mBio* **10**, e00558-00519, doi:10.1128/mBio.00558-19 (2019).

42 Moody, J. D., Freeman, J. P., Fu, P. P. & Cerniglia, C. E. Degradation of Benzo[<em>a</em>]pyrene by <em>Mycobacterium vanbaalenii</em>

PYR-1. *Applied and Environmental Microbiology* **70**, 340, doi:10.1128/AEM.70.1.340-345.2004 (2004).

43 Chomczynski, P. A reagent for the single-step simultaneous isolation of RNA, DNA and proteins from cell and tissue samples. *Biotechniques* **15**, 532-534, 536-537 (1993).

44 Collins, S. L. & Patterson, A. D. The gut microbiome: an orchestrator of xenobiotic metabolism. *Acta Pharmaceutica Sinica B* **10**, 19-32, doi:https://doi.org/10.1016/j.apsb.2019.12.001 (2020).

45 Tralau, T. & Luch, A. The human microbiome, from Achilles armour to Nessus' shirt. *Archives of Toxicology* **91**, 2699-2701, doi:10.1007/s00204-017-1951-8 (2017).

46 Licht, T. R. & Bahl, M. I. Impact of the gut microbiota on chemical risk assessment. *Current Opinion in Toxicology* **15**, 109-113, doi:https://doi.org/10.1016/j.cotox.2018.09.004 (2019).

47 Riebeling, C., Luch, A. & Tralau, T. Skin toxicology and 3Rs—Current challenges for public health protection. *Experimental Dermatology* **27**, 526-536, doi:10.1111/exd.13536 (2018).

48 Juhasz, A. L. & Naidu, R. Bioremediation of high molecular weight polycyclic aromatic hydrocarbons: a review of the microbial degradation of benzo[a]pyrene. *International Biodeterioration & Biodegradation* **45**, 57-88, doi:https://doi.org/10.1016/S0964-8305(00)00052-4 (2000).

49 Chu, I., Dick, D., Bronaugh, R. & Tryphonas, L. Skin reservoir formation and bioavailability of dermally administered chemicals in hairless guinea pigs. *Food and Chemical Toxicology* **34**, 267-276, doi:https://doi.org/10.1016/0278-6915(95)00112-3 (1996).

50 Meisel, J. S. *et al.* Commensal microbiota modulate gene expression in the skin. *Microbiome* **6**, 20-20, doi:10.1186/s40168-018-0404-9 (2018).

51 Toulza, E. *et al.* Large-scale identification of human genes implicated in epidermal barrier function. *Genome Biology* **8**, R107, doi:10.1186/gb-2007-8-6-r107 (2007).

52 Fischer, H. *et al.* Stratum corneum-derived caspase-14 is catalytically active. *FEBS Lett* **577**, 446-450, doi:10.1016/j.febslet.2004.10.046 (2004).

53 Landemaine, L., Cenizo, V., Lemaire, G. & Portes, P. 961 Colonization of a 3D skin model with a complete microbiota is more beneficial to the skin barrier than with Staphylococcus epidermidis alone. *Journal of Investigative Dermatology* **138**, S163, doi:https://doi.org/10.1016/j.jid.2018.03.973 (2018).

54 Loomis, K. H. *et al.* A mixed community of skin microbiome representatives influences cutaneous processes more than individual members. *Microbiome* **9**, 22, doi:10.1186/s40168-020-00963-1 (2021).

55 Joensen, U. N. *et al.* Associations of filaggrin gene loss-of-function variants with urinary phthalate metabolites and testicular function in young Danish Men. *Environ Health Perspect* **122**, 345-350, doi:10.1289/ehp.1306720 (2014).

56 Sevilla, L. M. *et al.* Mice deficient in involucrin, envoplakin, and periplakin have a defective epidermal barrier. *The Journal of cell biology* **179**, 1599-1612, doi:10.1083/jcb.200706187 (2007).

57 Jensen, J. M., Schütze, S., Neumann, C. & Proksch, E. Impaired cutaneous permeability barrier function, skin hydration, and sphingomyelinase activity in keratin 10 deficient mice. *J Invest Dermatol* **115**, 708-713, doi:10.1046/j.1523-1747.2000.00103.x (2000).

58 Ulluwishewa, D. *et al.* Regulation of tight junction permeability by intestinal bacteria and dietary components. *J Nutr* **141**, 769-776, doi:10.3945/jn.110.135657 (2011).

# 4. Discussion

## 4.1. Skin toxicity of commensal B[*a*]P metabolites

### 4.1.1. Selection of representative B[*a*]P-degrading skin commensals

The human skin microbiome contains numerous PAH-degrading bacteria that are able to use B[*a*]P as their sole source of energy and carbon, as shown by Sowada, et al. [254]. The ability to metabolize PAHs is a universal feature of the skin microbiome, with genes identified in this context being detectable *in situ* on the skin, as are the associated bacteria. The degradation of B[*a*]P occurs via various pathways, metabolizing it partially or completely (Chapter 3.1). Metabolites formed in this process have a prolonged residence time on the skin due to the temperature-induced slow bacterial growth and metabolism[256]. For the four skin isolates characterized in more detail in this thesis 1B (partial degrader, closely related to *M. luteus*), 1C (partial degrader, closely related to *P. oleovorans*), 2C (partial degrader, closely related to *B. licheniformis*), and 1D (total degrader, closely related to *M. luteus*) the growth rate with B[*a*]P as nutrient source was between 0.12 and 0.18 $d^{-1}$. This results in a retention time of bacterial B[*a*]P metabolites of about 3 days under ideal cultivation conditions (28-30 °C), leading to an as yet incalculable risk to human health. In order to evaluate this risk, we carried out the toxicological characterization and analytical identification of the bacterial B[*a*]P metabolites of the above-mentioned organisms as part of this work.

The reason for the selection of these four skin commensals from the 21 B[*a*]P-degrading isolates was based on various considerations. The selection covers full and partial B[a]P degraders, species of both Gram variants and three of the major phyla of the skin´s microbiome Actinobacteria (*M. luteus*), Firmicutes (*B. licheniformis*), and Proteobacteria (*P. oleovorans*)[55]. The selected species are biologically relevant, have been repeatedly isolated from healthy subjects at different skin sites, and have demonstrated potential for xenobiotic metabolism[254,257-266]. The decision to use two representatives of the species *M. luteus* was driven by the fact that of all B[*a*]P-degrading skin isolates, 11 were closely related to *M. luteus.* This is despite the fact that, although it is a typical skin representative, it only makes up 4 % of commensals on average [254]. This suggests a special role for *M. luteus* species in highly PAH-exposed human skin. This was confirmed in a recent study of Leung, et al. [267] that showed that differences in PAH exposure to human skin have profound effects on skin microbial community composition, with a correlation between PAH levels and relative abundance of *M. luteus*. In addition to the two *M. luteus* species (1B and 1D) we used the *B. licheniformis* (2C) for the toxicological characterization studies. For the subsequent analytical

identification of the metabolites, we additionally examined *P. oleovorans* (1C), because in particular pseudomonads from the skin microbiome are thought to be able to carry out the oxidation of B[*a*]P (by naphthalene-,2-dioxygenase)[268].

### 4.1.2. Cyto-and genotoxicity of commensal B[*a*]P metabolites

The *M. luteus* (1B), *M. luteus* (1D), and *B. licheniformis* (2C) were grown in enrichment cultures with 100 µM B[*a*]P as the sole energy and carbon source. HaCaT cells, NHEK, and the liver cell line HepG2 were treated with the supernatant samples collected daily. The liver cells were used due to their higher metabolic activity to detect further possible modulation of toxicity by human xenobiotic metabolism[269]. The secreted metabolites from the only B[*a*]P full metabolizer *M. luteus* (1D) showed transient cytotoxicity to the human cells, rather suggesting in the long term a detoxification of B[*a*]P after the intermediate generation of highly toxic metabolites. These cytotoxic metabolites showed even enhanced toxicity to the liver cell line, suggesting their further toxification by human phase-I metabolism. The latter is, among others, responsible for the toxification of the pro-carcinogen B[*a*]P in humans[192]. The two partial B[*a*]P degraders *M. luteus* (1B) and *B. licheniformis* (2C) secrete cytotoxic B[*a*]P metabolites throughout the whole cultivation period starting from the fifth day of cultivation, leading to their accumulation. As seen for the full metabolizer further toxification in human metabolism occurs, proving the higher cytotoxicity of their cell-free supernatants on liver cells. The strong increase of the CYP1A1 gene expression of HaCaT cells treated with the cell free bacterial supernatants confirms the assumption that the human xenobiotic metabolism further processes the bacterial B[*a*]P metabolites. Analytical investigations have shown that in the late logarithmic growth phase of the bacteria, only about 5 µg of the B[*a*]P were left in the supernatants[254]. This argues against a B[*a*]P-induced increase in the CYP1A1 expression level or cytotoxicity.

The bacterial metabolites excreted during degradation additionally exhibit significant genotoxic potential on HaCaT cells and NHEK. While the studies of both *M. luteus* species showed relative DNA damage of up to 50 %, the DNA damage induced by the cell free supernatant of *B. licheniformis* was only the half.

For the identification and quantification of the bacterial metabolites in the supernatants by GC/MS, we added the partial B[*a*]P metabolizer *P. oleovorans* (1C). In the supernatants of these four B[*a*]P degraders we identified a total of thirteen excreted metabolites. Six of these have also been previously detected in eukaryotes (i.e., B[*a*]P-9,10-dihdrodiol, B[*a*]P-1,6-dione, B[*a*]P-6,12-dione, B[*a*]P-7,8-dione, 3-OH-B[*a*]P and 7-OH-B[*a*]P), whereas B[*a*]P-7-10-diol, B[*a*]P-8-ol, B[*a*]P-12-ol, B[*a*]A, B[*a*]A-11-ol, and Phe-4-CO2H appear to be specific to prokaryotic metabolism (Chapter 3.1 and 3.3). Accordingly, the only three-ring

metabolite (i.e. Phe-4-$CO_2H$) was detected in the supernatants of the fully degrading *M. luteus* (1D), whereas the tree partial degraders *B. licheniformis* (2C), *M. luteus* (1B) and *P. oleovorans* (1C) showed only four- and five-ring systems, respectively. Some of these substances are already known as bacterial B[*a*]P metabolites, including B[*a*]P-9,10-dihydrodiol formed by *Sphingomonas yanoikuyae* and *Mycobacterium* sp. strain RJGII-135[229,270]. In addition, the 3-OH-B[*a*]P, 7-OH-B[*a*]P, and B[*a*]P-1,6-dione are among the known bacterial metabolites, as summarized by Ubani, et al. [249]. Consistent with our findings of the metabolites of the full metabolizer *M. luteus* (1D), the *S. yanoikuyae* is capable of degrading B[*a*]A via the intermediates of B[*a*]P-diols[240]. It is also known that the degradation of B[*a*]P by *Microbacterium* sp. M.CSW3 involves the intermediate phenanthrene, which matches the metabolite Phe-4-$CO_2H$ we found and suggests a similar B[*a*]P degradation pathway of *M. luteus* (1D)[242].

To determine which of the metabolites were responsible for previously regarded cyto- as well as genotoxicity, the metabolites were tested as pure substances and mixtures (reconstructed supernatants) and the resulting toxicity was compared to that of the cell free bacterial supernatants. The concentrations of the individual commensal metabolites detected were in the lower µM range with none of them causing cyto- or genotoxic effect that was equivalent to that of the cell free bacterial supernatants. In contrast, the results with the reconstituted supernatants showed significantly higher cyto- and genotoxicity, indicating a synergistic effect of the compounds on toxicity, but these were still lower than those of the supernatants per se. This is most likely due to the fact that not all excreted metabolites could be identified, so that further, potentially toxicity-increasing intermediates must be expected. In addition, there were metabolites that could be determined qualitatively but not quantitatively, including various OH-B[*a*]P and the B[*a*]A-1-ol. Additionally a B[a]A-diol was also detected by mass spectrometry but could not yet be categorized. The difficulties in identifying the metabolites were mainly due to their very low concentrations, unstable intermediates and the lack of the required reference substances.

In general, for both cyto- and genotoxicity, the cell free supernatants and the reconstructed supernatants of *M. luteus* (1B) showed the strongest effect. However, neither the latter nor the other skin commensals examined, form the B[*a*]P-7,8-dihydrodiol produced during the eukaryotic activation of B[*a*]P, nor the highly carcinogenic BPDE generated by its epoxidation. Since it is mainly the BPDE that leads to DNA adduct formation in eukaryotes, the genotoxicity of the bacterial intermediates must have a different origin[208]. The latter could be due, among others, to the B[*a*]P-7,8-dione detected in the culture supernatant of all skin isolates investigated. According to studies by Flowers, et al. [271], the B[*a*]P-7,8-dione shows a strong genotoxic effect on human DNA through the formation of covalent adducts. This leads to a concentration-dependent fragmentation of DNA in the range of 0.05-10 µM, with the 10 µM found in the culture

supernatant of *M. luteus* (1B) being on the upper end, followed by 2 µM formed by *P. oleovorans*. Another study by Shou, et al. [272] confirmed the genotoxic potential of the latter dione with the major adduct formed being a deoxyguanosine adduct.

In summary, in this part of our work we were able to show a direct toxification of B[*a*]P as an example of an environmental pollutant by the human skin microbiome. However, the question of an indirect modulation of toxicity still remains open. The latter can be versatile and includes changes in human xenobiotic metabolism such as the regulation of phase-I and phase-II enzymes, DNA repair mechanisms and substance bioavailability through changes in the epithelial barrier. This all can be influenced by host-microbe interaction[273]. However, while toxicologically relevant, systematic toxicological assessment of microbial substance toxification falls short due to a lack of suitable test systems[144]. The development of our microbial competent skin model enables us to overcome the experimental barrier to study toxicological microbe-host interactions in skin under near-*in vivo* conditions *in situ* (Chapter 3.2).

To ensure that the bacterial metabolites are also quantifiable in a complex biological system, despite the presence of human B[*a*]P metabolism, we used *M. luteus* (1B) and *P. oleovorans* (1C) for the establishment of a microbial skin tissue co-culture. Besides the highest toxicity of the supernatants of *M. luteus* (1B), the analytical investigation showed the highest metabolite concentrations in the supernatants of these two commensals in general as well as the highest amount of the genotoxic B[*a*]P-7,8-dione. The metabolite concentration of the full degrader *M. luteus* (1D) was by far the lowest followed by that of *B. licheniformis* (2C).

## 4.2. Microbial skin tissue co-culture

### 4.2.1. Commensal influence on skin cells

The skin represents a dehydrated, nutrient-poor, acidic environment, with competition for the rare natural carbon and energy sources being that fierce. This contributes to that skin representatives also make use of a variety of external sources, one being the degradation of xenobiotic substances, which may represent a selection advantage[268,274,275]. We therefore set out to investigate whether skin isolates also metabolize B[*a*]P *in situ* in the presence of other natural food sources and whether the microbe-host interaction influences the metabolism and distribution of B[*a*]P. However, this question of toxicological significance is preceded by the question of what functions these skin commensal communities normally fulfil. Only by answering this question we can distinguish microbiome-related changes from substance-related influences at a later stage.

Animal models are of limited use for such problems, as they are difficult to handle and suffer from questionable transferability because of the extraordinarily high species specificity. Due to 85 % differences in gut microbiota between humans and mice, microbial transplants are unstable at best, and harmful at worst[276-278]. In scope of this work we established a long term co-culture system based on a colonized 3D-skin model. The system is based on the commercially available EpiDermFT™ from MatTek which was colonized with the two B[*a*]P degrading skin isolates, *M. luteus* (1B) and *P. oleovorans* (1C)[254]. The EpiDermFT™ provides a valuable *in vitro* approach for evaluation of metabolism and toxicity of cutaneous exposures to xenobiotics, as it shows xenobiotic metabolizing capacity including CYP expression that is representative of human skin[43]. Even more important, it was pre-validated for metabolically competent toxicity testing *in vitro*. This includes the ability to degrade B[*a*]P with the formation of human skin-like metabolite patterns, making it the model of choice for our microbial skin tissue co-culture[46]. For this co-culture, the EpidermFT™ models were colonized with *M. luteus*, *P. oleovorans* or their mixtures with between $10^5$-$10^6$ cells/cm$^2$. This number was chosen according to the average microbial cell counts on human skin *in vivo*[279]. After 4 and 8 days of co-cultivation, the microbial cell counts were determined, respectively. The co-culture with *M. luteus* was stable over the entire cultivation period, while *P. oleovorans* continued to grow until cultivation day 8. At $10^7$ CFU/cm$^2$, the maximum cell count of *M. luteus* was similar to that reported for skin *in vivo* whereas that of *P. oleovorans* with $10^{11}$ CFU/cm2 was higher[279,280]. Microscopic analysis of the co-cultures (Gram stain) shows that *M. luteus* grows almost exclusively on and partly in the SC, whereas *P. oleovorans* also grows in deeper layers. Staining shows an

occurrence in the epidermis and sporadically also in the dermis, which fits with the results of previous studies in which Pseudomonads sp. were repeatedly detected in the dermis *in vivo*[68,69].

A detailed transcriptome analysis showed that microbial colonization affects the transcription of up to 3300 differentially regulated genes in the skin. While some effects were comparable others were dependent on the species used for colonization. Along with the strong and extended growth to the dermis of *P. oleovorans,* the transcriptional changes in its co-culture were also ten times more pronounced than those in the *M. luteus* co-culture. However, in general the number of changes were in line with the study of Meisel, et al. [281], who found 2820 genes differentially regulated in response to microbial colonization of germ free mice. This applies not only to the number of changes, but also to the key findings including the upregulation of genes encoding pro-inflammatory cytokines, as well as key regulatory factors and pathway components for cell growth, angiogenesis/tissue repair or cell adhesion. Moreover, biological functions such as the apoptosis, proliferation and differentiation of skin cells or migration of keratinocytes were also affected. Notably our results were recently confirmed using a co-culture with extended species diversity based on the same 3-D skin model EpidermFT™. Although this study shows that the microbial community has unique and distinct effects on the skin, the biologic processes affected, such as apoptosis, differentiation, etc., are consistent with the changes caused by single species colonization[136].

In addition to the known microbial induced changes in cutaneous gene transcription, we were able to show for the first time its important role in the regulation of olfactory receptors, which has already been shown for the gut microbiome[282]. Interestingly, the microbial influenced OR2A7 for example is known to play an important role in epidermal proliferation and differentiation[283]. Colonization also affected the secretion of growth factors such as VFGFA and FGF2, which have previously been shown to be promoted by commensals and are important for tissue repair[89].

The strong upregulation of immune-specific genes is probably caused by the epidermal barrier breakthrough by *P. oleovorans* 1C, with various Pseudomonas sp. being considered an opportunistic pathogen[284]. Although Pseudomonads sp. are present in the dermis *in vivo*[68,69], the crossing of the epidermal barrier and its high cell counts/cm$^2$ are nevertheless a warning signal for the human immune system. This phenomenon was investigated by Duckney, et al. [285], who added bacteria to the culture medium of an epidermis model to mimic such a penetration, achieving a strong inflammatory response compared to its cultivation on top of the models.

Apart from this, however, both organisms strengthen the human immune defense by stimulating the skin cells to produce AMPs such as β-defensins, which have already been demonstrated for commensals in animal experiments[80,286]. Additionally, they strongly regulate IL-1 family gene expression, which is an

important component of the skin microbiome, to promote effector T-cell responses[133]. In addition to the induction of pro-inflammatory factors, the colonization also led to an increased expression of anti-inflammatory cytokines such as IL-10 and TGF-b, which are necessary for the skin to develop tolerance towards commensals[287-289].

### 4.2.2. Microbial-related changes in skin`s xenobiotic metabolism

In parallel with the confirmation of known immunoregulatory effects of skin commensals, we had also investigated for the first time the influence of the skin`s microbiome on phase-I and phase-II metabolism. Notably co-culture led to transcriptional alteration of almost 30 % of all CYPs investigated. This complements and extends our knowledge from numerous studies on the influence of the gut microbiome on the expression and activity of important drug-metabolising enzymes such as CYPs[74,111,290-292]. The altered CYP expressions that occurred in the co-culture included those of CYP1A1 and CYP1B1, which are of particular importance for B[*a*]P activation[200]. This microbial influence may have been caused by TLR2-dependent signaling, as it was shown that CYP1A1 activation is controlled by TLR2, and colonization with both *M. luteus* and especially *P. oleovorans* led to its increased expression[293]. Interestingly, the AhR, the transcription factor responsible for CYP1A1 and CYP1B1 expression, has also been shown to regulate skin barrier function and repair processes. This process was dependent on commensals microbiota in an animal study with germ-free mice[134]. In this study, the skin isolates were able to restore the skin barrier competence. This barrier plays an important role in the absorption of chemicals and its possible alteration could therefore be of interest in our microbial skin tissue co-culture for B[*a*]P uptake.

## 4.3. Commensal influence on B[*a*]P distribution and toxicity *in situ*

Having previously identified the potential of the skin microbiome's potential for toxification of B[*a*]P (Chapter 3.1), this project now investigates whether this modulation of the toxicity also occur *in situ*. Besides a possible direct bacterial metabolism of B[*a*]P, the effects on toxicity, bioavailability, absorption, metabolism and distribution in the skin *in situ* are still unclear and will be examined here. For this purpose, we treated the colonized skin models over a period of 7 days with 50 nM/cm$^2$ B[*a*]P daily (total quantity of 350 nM/cm$^2$), corresponding to the daily dose to which the skin of coke oven workers and the skin under so-called protective clothing is exposed[179,180].

The colonization of MatTek`s EpidermFT™ which *P. oleovorans* and *M. luteus* led to significant changes in B[*a*]P and its metabolite levels. These were measured analytically (GC/MS) on day 8 of co-cultivation on the skin surface, in the epidermis and dermis, and throughout the duration of cultivation in the basal cell culture medium. On the skin surface, colonization led to increased metabolite concentrations. In particular, 3-OH-B[*a*]P and all B[*a*]P-diones were measurable in higher amounts compared to the un-colonized control, including large amounts of the genotoxic B[*a*]P-7-8-dione[271,272]. These substances are consistent with the bacterial B[*a*]P metabolites previously determined in the enrichment cultures, suggesting microbial B[*a*]P metabolism on the skin *in situ*. Nonetheless, because a large proportion of the metabolites are formed in both eukaryotic and prokaryotic metabolism, precise determination of their origin is not possible. However, there is strong evidence suggesting microbial formation. This is the site of formation, which is also the primary habitat of skin commensals, and the formation of the B[*a*]P-7,10-dione. The latter occurred exclusively on co-cultures with *P. oleovorans* involvement, has been identified as its metabolite, and is not known to be formed in eukaryotic metabolism. Likewise, in the epidermis, the concentration of B[*a*]P-diones were microbial-related increased, but the concentration of B[*a*]P-dihydrodiols and the ultimate carcinogen BPDE (measured as its hydrolysis product resulting from trans-opening of the epoxide moiety the B[*a*]P-7,8,9,10-tetrahydrotetrol) were significantly reduced. In the dermis, this reduction of metabolites was even more pronounced. In the underlying basal cell culture medium, metabolite concentrations were reduced by an average of 40 %. This effect was particularly pronounced in the *M. luteus* co-culture with an overall reduction of about 58 % of all metabolites. The medium's entry of the metabolites in our model represents its passage into the bloodstream *in vivo*, suggesting a strong reduction in the systemic distribution of toxic metabolites.

The concentration gradient described for the metabolites in the colonized skin also applied to the unmetabolized B[*a*]P as its concentration decreases from the surface to the epidermis, and through the dermis to the medium compared to the uncolonized control. On the skin surface its concentration was

particularly high in the colonized models, which is equivalent to its accumulation at the application site. As a lipophilic molecule, B[*a*]P`s penetration into the skin is highly dependent on its biotransformation[294]. This indicates that the penetration was microbial-induced diminished, resulting in the formation of fewer metabolites in the skin itself. Of particular importance was the reduction of the B[*a*]P-tetrol in the epidermis and dermis, as these were consistent with our measurements of the decreased resulting BPDE-DNA adducts. This suggests reduced genotoxicity of B[*a*]P to human skin in the presence of commensals.
The increased concentration of genotoxic metabolites such as B[*a*]P-7,8-diones on the skin surface is expected to play a minor role in this context. The corneocytes present on the skin surface are nucleus-free and therefore not susceptible to DNA adduct formation. In addition, corneocytes regularly *s*hed off the skin as scales, with a complete turnover of corneocyte layer every 2–4 weeks[8,295]. In combination with regular body hygiene, these potentially dangerous metabolites are more likely to be removed from the skin surface rather than causing harm.
The transcription analysis supports the assumption of reduced penetration rate and toxicity of B[*a*]P, since the eukaryotic activation of B[*a*]P is dependent on oxidation by CYP1A1 and its expression was strongly reduced in the colonized models after B[*a*]P treatment compared to uncolonized skin. Additionally, transcription analysis showed significant lower expression of various components of the NER pathway, responsible for the repair of B[*a*]P induced bulky DNA adducts. This applies to XPA as well as XPC, both of which are involved in damage recognition in NER[217]. These were strongly reduced both at transcript and protein level after B[*a*]P treatment in the colonized models compared to uncolonized skin. This strengthens the assumption of a reduced B[*a*]P toxicity in colonized skin.

#### 4.3.1. Microbial-induced strengthening of the skin barrier

Using immunofluorescence analyses, we were able to show that in addition to the existing microbial B[*a*]P metabolism on the skin, a microbial induced change in the epidermal skin barrier could have caused the altered penetration and distribution of B[*a*]P in the skin. This is probably due to the bacterially induced alteration of the epidermal structure, which is a species-specific enhancement of TJ and epidermal differentiation measured in form of increased expression of selected differentiation marker. These markers relate to different stages of epidermal differentiation: K10, early differentiation stage, IVL early terminal differentiation and FLG late terminal differentiation[3]. Their expression was particularly high in the *P. oleovorans* co-cultures, indicating a strengthening of the skin barrier as a whole, maybe as a reaction to its strong growth and penetration depth. Both could be a trigger for the skin to reinforce its barrier and thus keep *P. oleovorans* growth in check. *M. luteus*, on the other hand, tends to increase the formation of

TJs. The differences in metabolite concentrations in the two microbial co-cultures were only minor, but suggest that strengthening of the epidermal differentiation in particular contributes to the accumulation of B[*a*]P on the skin surface. Whereas the enhancement of the TJs reduces the permeability of the skin, which in turn leads to a decrease in the metabolite concentration in the underlying basal cell culture medium. For all microbial co-cultures, however, the final result is that the microbial-induced strengthening of the skin barrier leads to lower concentrations of B[*a*]P, which can be metabolized by the metabolically active skin cells present in the deeper skin layers. As a result, fewer B[*a*]P metabolites are generally formed in the skin, suggesting that microbe-host interaction appears to play a more important role than commensal metabolism on the skin. Consequently, the strengthening of the skin barrier relativizes the formation of genotoxic bacterial metabolites.

## 4.4. Role of the microbiome in toxicity of environmental xenobiotics

There is growing evidence that exposure to xenobiotic pollutants is one of the multiple environmental factors that contribute to the development of various health disorders [111]. The biotransformation of a variety of these chemicals depends on various microbial enzymes of our microbiome. Consequently variations in the latter can also inherently influence their toxicity to the host [110]. Corresponding research especially highlighting the ability of gut microbes to perform diverse chemical transformations including reduction, hydrolysis, the removal of a succinate group, dehydroxylation, acetylation, deacetylation, the cleavage of a N-oxide bounds, proteolysis, denitration, deconjugation, thiazole ring opening, deglycosylation and demethylation on xenobiotic compounds, such as drugs, antibiotics, diet-derived bioactive compounds and environmental pollutants [296,297]. For the latter about 1,500 reactions are currently listed, carried out by 529 microorganisms and affecting about 1,370 compounds [298].

Due to the particularly important role of the gut in human health, microbiome research has so far focused especially on the gut microbiome leaving other areas, such as the skin microbiome only poorly understood. As the body's direct contact with the outside world, the skin also plays a central role in the metabolic exchange of environmental pollutants. Although the composition of the skin microbiome is different from that of the gut, they share many metabolic pathways, such as tryptophan metabolism and the formation of SCFAs, which also suggests an important role of the skin microbiome on human metabolism of xenobiotics [299-301]. A confirmed example of this is the toxification of azo dyes by human skin isolates *in vitro* [302].

Animal models have been used extensively in the past in pharmaceutical and industrial research to predict toxicity in humans. In the absence of adequate alternatives to date, these continue to be accepted,

although analyses suggest that these models are poor predictors of drug safety in humans. Overall, about 89% of new drugs fail in clinical trials, and about half of these failures are due to unexpected human toxicity of drugs that have previously been shown to be safe in animal studies [303]. One reason for this is the large difference in the composition of the microbiome between laboratory animals and humans. Add to that the microbiome of some laboratory animals is even unknown, the effects of which thus cannot be included in the toxicity assessment [304]. The use of germ-free mice colonized with single bacterial species or restricted flora, or more recently the use of human microbiota, now allow us to better assess the impact of the microbiome [305]. For example, comparing germ-free mice with conventional mice allows us to estimate the impact of the microbiome on the toxicity of chemicals. Among others, the microbiome-induced toxicity of bismuth into its toxic volatile derivative, trimethyl bismuth, could thus be demonstrated [306]. However, the reduction in toxicity may also be commensal-induced, as gut bacteria have been shown to be protective against the toxicity of 1,3-dinitrobenzene [307]. Although these techniques are a great achievement, the species-specific differences in microbial composition are so big that many of the results are not readily transferable to humans.

In addition, the influence of the microbiome on the host biology and the resulting consequences for xenobiotic metabolism also play a major role in the toxicity of xenobiotics. Such indirect modification of toxicity includes alteration of the expression of enzymes of phase I or/and phase II metabolism, as well as changes of bioavailability through modification of the epithelial barrier [308]. However, if typical laboratory animals such as mice are compared with humans, important xenobiotic enzymes are missing or differ significantly, so that resulting microbial-induced modifications are also lacking or vary [309]. Although mouse skin, like human skin, consists of three layers, there are considerable differences in the anatomy and physiology of the individual layers, which in turn makes it very difficult to evaluate microbe-induced changes, e.g. in epidermal differentiation [310].

All these circumstances make the use of cells and microorganisms of human origin more appropriate, especially in a 3D tissue structure that provides bacteria with a habitat very close to their real one. The use of commercially available skin models as a basis also allows standardization of the experimental system, providing reproducible results.

# 5. Conclusion and Outlook

Our results show that skin commensals are capable of toxifying environmental pollutants such as B[*a*]P when grown in carbon-limited cultures with B[*a*]P as the sole energy and carbon source *in vitro*. Treatment of cell lines, as well as primary keratinocytes, with the resulting bacterial metabolites shows species-specific increases of cyto- as well as genotoxicity. The development of a co-culture system consisting of skin isolates and a 3D skin model based on human cells allows for the first time to assess the potential effects of this microbial toxification under near *in vivo* conditions *in situ*. The results confirmed microbial B[*a*]P metabolism to also occurs *in situ* hinting that xenobiotics such as B[*a*]P will indeed be used as additional nutrient source when present on human skin. Moreover, the studies also clearly showed the *in vivo* situation not only to be more complex than the original cell culture setup but to feature a paradox response with regard to potential host-toxicity due to microbe-host interactions. In this system epithelial permeability and integrity were strongly influenced by microbial colonization, resulting in implications for the uptake, metabolism, and distribution of B[*a*]P and its metabolites. Other xenobiotics are likely to be subject to similar effects. While bacterial culture supernatants from carbon-limited cultures grown on B[*a*]P were highly genotoxic, the application of B[*a*]P on the colonized models shows that the microbial effects on host skin differentiation have a strong positive modulating influence. The reason is an improved physicochemical barrier function of the skin. This strengthening causes a commensal-induced reduction in the toxicity of B[*a*]P, in particular by inhibiting the uptake of this pro-carcinogen and its subsequent metabolic activation to a carcinogen. Depending on the particular substance and the circumstances, the consideration of individual systems could thus lead to an overestimation or underestimation of toxicity, both of which should be avoided. Overall this work clearly demonstrates that there is an urgent need to more systematically investigate the influence of the microbiome on potential systemic host toxicity. In the long term, such systems and studies will hence principally not only help to identify potential hazards but will also contribute to the improvement of the respective toxicity predictions. Due to the species specificity of the microbiome, such predictions are only useful if they are based on realistic experimental models that are specific to the human host.

One of the major tasks for the future is to further develop our microbial skin tissue co-culture. This primarily refers to the use of whole skin swabs instead of single commensals. In addition to host-commensal interactions, interactions between commensals could also be included. In this regard the development of a stable culture with a constant number and species composition of organisms plays a decisive role. Research findings, especially in the last decade, also show the important role of the

microbiome on the immune function of its host. The extension of the model to include skin-specific immune cells would allow this important aspect to be included in future studies.

The microbiome has received little attention in toxicology. This holds true for the gut but particularly also with regard to skin. This work now clearly demonstrates not only that there is an influence of the skin's microbiome on xenobiotic metabolism and toxification, but that its implications for host biology can only be assessed in sufficiently complex models. Future toxicological research in should thus not only focus on which chemical groups might be affected by such interactions but also focus on systems that address microbiome-mediated toxicity in a species specific manner. Moroever, the respective systems have to be sufficiently complex, yet standardized as to allow assessing microbiome-mediated health risks such as metabolite induced carcinogenicity. The influence of the microbiome on the development of cancer is still poorly understood but current literature and ongoing research projects suggest some involvement[311]. One possible starting point is microbiome-influenced immunoregulatory change. Since the development of cancer also involves a sustained inflammatory response, a connection can be inferred. Special emphasis should be placed on the discovery of mechanisms that lie behind such reactions. For this purpose, new techniques should be established that allow both the human and the microbial systems to be examined at the same time. This thesis delivered the proof of concept of microbiome-mediated toxification of PAHs to occur on skin. I further provides a reliable and highly standardized 3D-skin model to investigate substance-microbiome-host interactions *in situ*. This system among the first of its kind and ideally suited to extend work on the toxicology of the microbiome as outlined above.

# 6. References


1 Abdo, J. M., Sopko, N. A. & Milner, S. M. The applied anatomy of human skin: A model for regeneration. *Wound Medicine* **28**, 100179, doi:https://doi.org/10.1016/j.wndm.2020.100179 (2020).

2 Yannas, I. V. in *Tissue and Organ Regeneration in Adults: Extension of the Paradigm to Several Organs* (ed Ioannis V. Yannas) 89-136 (Springer New York, 2015).

3 Candi, E., Schmidt, R. & Melino, G. The cornified envelope: a model of cell death in the skin. *Nat Rev Mol Cell Biol* **6**, 328-340, doi:10.1038/nrm1619 (2005).

4 Menon, G. K., Lee, S. E. & Lee, S.-H. An overview of epidermal lamellar bodies: Novel roles in biological adaptations and secondary barriers. *Journal of Dermatological Science* **92**, 10-17, doi:https://doi.org/10.1016/j.jdermsci.2018.03.005 (2018).

5 Lopez-Ojeda, W., Pandey, A., Alhajj, M. & Oakley, A. M. in *StatPearls* (StatPearls Publishing Copyright © 2020, StatPearls Publishing LLC., 2020).

6 Menon, G. K., Dryer, L. & Kalafsky, R. in *Skin Aging Handbook* (ed Nava Dayan) 265-290 (William Andrew Publishing, 2009).

7 Colombo, I. *et al.* HaCaT Cells as a Reliable In Vitro Differentiation Model to Dissect the Inflammatory/Repair Response of Human Keratinocytes. *Mediators Inflamm* **2017**, 7435621, doi:10.1155/2017/7435621 (2017).

8 Joost, S. *et al.* Single-Cell Transcriptomics Reveals that Differentiation and Spatial Signatures Shape Epidermal and Hair Follicle Heterogeneity. *Cell Systems* **3**, 221-237.e229, doi:https://doi.org/10.1016/j.cels.2016.08.010 (2016).

9 Sandilands, A., Sutherland, C., Irvine, A. D. & McLean, W. H. I. Filaggrin in the frontline: role in skin barrier function and disease. *Journal of Cell Science* **122**, 1285, doi:10.1242/jcs.033969 (2009).

10 Jacob, J. T., Coulombe, P. A., Kwan, R. & Omary, M. B. Types I and II Keratin Intermediate Filaments. *Cold Spring Harb Perspect Biol* **10**, a018275, doi:10.1101/cshperspect.a018275 (2018).

11 Gu, L.-H. & Coulombe, P. A. Keratin function in skin epithelia: a broadening palette with surprising shades. *Current Opinion in Cell Biology* **19**, 13-23, doi:https://doi.org/10.1016/j.ceb.2006.12.007 (2007).

12 Fuchs, E. Keratins and the skin. *Annu Rev Cell Dev Biol* **11**, 123-153, doi:10.1146/annurev.cb.11.110195.001011 (1995).

13 Ehrlich, F. *et al.* Differential Evolution of the Epidermal Keratin Cytoskeleton in Terrestrial and Aquatic Mammals. *Mol Biol Evol* **36**, 328-340, doi:10.1093/molbev/msy214 (2019).

14 Volksdorf, T. *et al.* Tight Junction Proteins Claudin-1 and Occludin Are Important for Cutaneous Wound Healing. *The American Journal of Pathology* **187**, 1301-1312, doi:https://doi.org/10.1016/j.ajpath.2017.02.006 (2017).

15 Yamate, J. in *Boorman's Pathology of the Rat (Second Edition)* (ed Andrew W. Suttie) 323-345 (Academic Press, 2018).

16 Brandner, J. M. *et al.* Epidermal tight junctions in health and disease. *Tissue Barriers* **3**, e974451, doi:10.4161/21688370.2014.974451 (2015).

17 Tunggal, J. A. *et al.* E-cadherin is essential for in vivo epidermal barrier function by regulating tight junctions. *EMBO J* **24**, 1146-1156, doi:10.1038/sj.emboj.7600605 (2005).

18 Coates, M., Lee, M. J., Norton, D. & MacLeod, A. S. The Skin and Intestinal Microbiota and Their Specific Innate Immune Systems. *Frontiers in Immunology* **10**, doi:10.3389/fimmu.2019.02950 (2019).

19 Pailler-Mattei, C., Nicoli, S., Pirot, F., Vargiolu, R. & Zahouani, H. A new approach to describe the skin surface physical properties in vivo. *Colloids Surf B Biointerfaces* **68**, 200-206, doi:10.1016/j.colsurfb.2008.10.005 (2009).

20 Boer, M., Duchnik, E., Maleszka, R. & Marchlewicz, M. Structural and biophysical characteristics of human skin in maintaining proper epidermal barrier function. *Postepy Dermatol Alergol* **33**, 1-5, doi:10.5114/pdia.2015.48037 (2016).

21 Moreci, R. S. & Lechler, T. Epidermal structure and differentiation. *Current Biology* **30**, R144-R149, doi:https://doi.org/10.1016/j.cub.2020.01.004 (2020).

22 Prost-Squarcioni, C., Fraitag, S., Heller, M. & Boehm, N. [Functional histology of dermis]. *Ann Dermatol Venereol* **135**, 1s5-20, doi:10.1016/s0151-9638(08)70206-0 (2008).

23 Uitto, J., Li, Q. & Urban, Z. The complexity of elastic fibre biogenesis in the skin--a perspective to the clinical heterogeneity of cutis laxa. *Exp Dermatol* **22**, 88-92, doi:10.1111/exd.12025 (2013).

24 Rutter, N. The dermis. *Seminars in Neonatology* **5**, 297-302, doi:https://doi.org/10.1053/siny.2000.0016 (2000).

25 EU: final ban on animal experiments for cosmetic ingredients implemented. *ALTEX* **30**, 268-269 (2013).

26 Colombo, I. *et al.* HaCaT Cells as a Reliable In Vitro Differentiation Model to Dissect the Inflammatory/Repair Response of Human Keratinocytes. *Mediators Inflamm* **2017**, 7435621-7435621, doi:10.1155/2017/7435621 (2017).

27 Boukamp, P. *et al.* Normal keratinization in a spontaneously immortalized aneuploid human keratinocyte cell line. *J Cell Biol* **106**, 761-771, doi:10.1083/jcb.106.3.761 (1988).

28 Micallef, L. *et al.* Effects of extracellular calcium on the growth-differentiation switch in immortalized keratinocyte HaCaT cells compared with normal human keratinocytes. *Exp Dermatol* **18**, 143-151, doi:10.1111/j.1600-0625.2008.00775.x (2009).

29 Seo, M.-D., Kang, T. J., Lee, C. H., Lee, A.-Y. & Noh, M. HaCaT Keratinocytes and Primary Epidermal Keratinocytes Have Different Transcriptional Profiles of Cornified Envelope-Associated Genes to T Helper Cell Cytokines. *Biomol Ther (Seoul)* **20**, 171-176, doi:10.4062/biomolther.2012.20.2.171 (2012).

30 Wiegand, C. & Hipler, U. C. Evaluation of Biocompatibility and Cytotoxicity Using Keratinocyte and Fibroblast Cultures. *Skin Pharmacology and Physiology* **22**, 74-82, doi:10.1159/000178866 (2009).

31 Randall, M. J., Jüngel, A., Rimann, M. & Wuertz-Kozak, K. Advances in the Biofabrication of 3D Skin in vitro: Healthy and Pathological Models. *Frontiers in Bioengineering and Biotechnology* **6**, doi:10.3389/fbioe.2018.00154 (2018).

32 Langhans, S. A. Three-Dimensional in Vitro Cell Culture Models in Drug Discovery and Drug Repositioning. *Frontiers in Pharmacology* **9**, doi:10.3389/fphar.2018.00006 (2018).

33 Antoni, D., Burckel, H., Josset, E. & Noel, G. Three-Dimensional Cell Culture: A Breakthrough in Vivo. *International Journal of Molecular Sciences* **16**, doi:10.3390/ijms16035517 (2015).

34 Suhail, S. *et al.* Engineered Skin Tissue Equivalents for Product Evaluation and Therapeutic Applications. *Biotechnology Journal* **14**, 1900022, doi:https://doi.org/10.1002/biot.201900022 (2019).

35 Kim, H. *et al.* Skin Corrosion and Irritation Test of Nanoparticles Using Reconstructed Three-Dimensional Human Skin Model, EpiDerm<sup>TM</sup>. *ToxicolRes* **32**, 311-316, doi:10.5487/TR.2016.32.4.311 (2016).

36 Catarino, C. M. *et al.* Skin corrosion test: a comparison between reconstructed human epidermis and full thickness skin models. *European Journal of Pharmaceutics and Biopharmaceutics* **125**, 51-57, doi:https://doi.org/10.1016/j.ejpb.2018.01.002 (2018).

37 Pennacchi, P. C. *et al.* Glycated Reconstructed Human Skin as a Platform to Study the Pathogenesis of Skin Aging. *Tissue Eng Part A* **21**, 2417-2425, doi:10.1089/ten.TEA.2015.0009 (2015).

38 Ackermann, K., Borgia, S. L., Korting, H. C., Mewes, K. R. & Schäfer-Korting, M. The Phenion full-thickness skin model for percutaneous absorption testing. *Skin Pharmacol Physiol* **23**, 105-112, doi:10.1159/000265681 (2010).

39 Batheja, P., Song, Y., Wertz, P. & Michniak-Kohn, B. Effects of growth conditions on the barrier properties of a human skin equivalent. *Pharm Res* **26**, 1689-1700, doi:10.1007/s11095-009-9879-1 (2009).

40 Meloni, M., Farina, A. & de Servi, B. Molecular modifications of dermal and epidermal biomarkers following UVA exposures on reconstructed full-thickness human skin. *Photochem Photobiol Sci* **9**, 439-447, doi:10.1039/b9pp00164f (2010).

41 Yunis, R., Albrecht, H., Kalanetra, K. M., Wu, S. & Rocke, D. M. Genomic characterization of a three-dimensional skin model following exposure to ionizing radiation. *J Radiat Res* **53**, 860-875, doi:10.1093/jrr/rrs063 (2012).

42 Jäckh, C. *et al.* Characterization of enzyme activities of Cytochrome P450 enzymes, Flavin-dependent monooxygenases, N-acetyltransferases and UDP-glucuronyltransferases in human reconstructed epidermis and full-thickness skin models. *Toxicol In Vitro* **25**, 1209-1214, doi:10.1016/j.tiv.2011.03.012 (2011).

43 Hu, T. *et al.* Xenobiotic metabolism gene expression in the EpiDerm™ in vitro 3D human epidermis model compared to human skin. *Toxicology in Vitro* **24**, 1450-1463, doi:https://doi.org/10.1016/j.tiv.2010.03.013 (2010).

44 Reisinger, K. *et al.* Validation of the 3D Skin Comet assay using full thickness skin models: Transferability and reproducibility. *Mutat Res Genet Toxicol Environ Mutagen* **827**, 27-41, doi:10.1016/j.mrgentox.2018.01.003 (2018).

45 Schmid, T. E. *et al.* Relative biological effectiveness of pulsed and continuous 20 MeV protons for micronucleus induction in 3D human reconstructed skin tissue. *Radiother Oncol* **95**, 66-72, doi:10.1016/j.radonc.2010.03.010 (2010).

46 Brinkmann, J. *et al.* Metabolically Competent Human Skin Models: Activation and Genotoxicity of Benzo[a]pyrene. *Toxicological Sciences* **131**, 351-359, doi:10.1093/toxsci/kfs316 (2013).

47 Küchler, S. *et al.* 3D-wound healing model: influence of morphine and solid lipid nanoparticles. *J Biotechnol* **148**, 24-30, doi:10.1016/j.jbiotec.2010.01.001 (2010).

48 Letasiova, S. *et al.* Cutaneous wound healing in the EpiDerm-FT full thickness in vitro human skin model. *Toxicology Letters* **196**, S152, doi:https://doi.org/10.1016/j.toxlet.2010.03.524 (2010).

49 Lee, S. *et al.* Predicting full thickness skin sensitization using a support vector machine. *Toxicol In Vitro* **28**, 1413-1423, doi:10.1016/j.tiv.2014.07.002 (2014).

50 Kubilus, J. *et al.* Full Thickness EpiDerm: a dermal-epidermal skin model to study epithelial-mesenchymal interactions. *Altern Lab Anim* **32 Suppl 1A**, 75-82, doi:10.1177/026119290403201s12 (2004).

51 Sanches, P. L. *et al.* Toxicity Evaluation of TiO2 Nanoparticles on the 3D Skin Model: A Systematic Review. *Frontiers in Bioengineering and Biotechnology* **8**, doi:10.3389/fbioe.2020.00575 (2020).

52 Mallampati, R. *et al.* Evaluation of EpiDerm full thickness-300 (EFT-300) as an in vitro model for skin irritation: studies on aliphatic hydrocarbons. *Toxicol In Vitro* **24**, 669-676, doi:10.1016/j.tiv.2009.08.019 (2010).

53 Grice, E. A. *et al.* Topographical and temporal diversity of the human skin microbiome. *Science (New York, N.Y.)* **324**, 1190-1192, doi:10.1126/science.1171700 (2009).

54 Marples, M. J. *The ecology of the human skin*. (1965).

55 Grice, E. A. & Segre, J. A. The skin microbiome. *Nat Rev Microbiol* **9**, 244-253, doi:10.1038/nrmicro2537 (2011).

56 Timm, C. M. *et al.* Isolation and characterization of diverse microbial representatives from the human skin microbiome. *Microbiome* **8**, 58, doi:10.1186/s40168-020-00831-y (2020).

57 Kong, H. H. & Segre, J. A. Skin Microbiome: Looking Back to Move Forward. *Journal of Investigative Dermatology* **132**, 933-939, doi:https://doi.org/10.1038/jid.2011.417 (2012).

58 Prescott, S. L. *et al.* The skin microbiome: impact of modern environments on skin ecology, barrier integrity, and systemic immune programming. *World Allergy Organ J* **10**, 29-29, doi:10.1186/s40413-017-0160-5 (2017).

59 Huttenhower, C. *et al.* Structure, function and diversity of the healthy human microbiome. *Nature* **486**, 207-214, doi:10.1038/nature11234 (2012).

60 Dimitriu, P. A. *et al.* New Insights into the Intrinsic and Extrinsic Factors That Shape the Human Skin Microbiome. *mBio* **10**, e00839-00819, doi:10.1128/mBio.00839-19 (2019).

61 Zmora, N., Suez, J. & Elinav, E. You are what you eat: diet, health and the gut microbiota. *Nature Reviews Gastroenterology & Hepatology* **16**, 35-56, doi:10.1038/s41575-018-0061-2 (2019).

62 Gupta, V. K., Paul, S. & Dutta, C. Geography, Ethnicity or Subsistence-Specific Variations in Human Microbiome Composition and Diversity. *Frontiers in microbiology* **8**, 1162-1162, doi:10.3389/fmicb.2017.01162 (2017).

63 Goodrich, J. K. *et al.* Human genetics shape the gut microbiome. *Cell* **159**, 789-799, doi:10.1016/j.cell.2014.09.053 (2014).

64 Conlon, M. A. & Bird, A. R. The impact of diet and lifestyle on gut microbiota and human health. *Nutrients* **7**, 17-44, doi:10.3390/nu7010017 (2014).

65 Colotti, G. & Rinaldi, T. The central role of gut microbiota in drug metabolism and personalized medicine. *Future Medicinal Chemistry* **12**, 1197-1200, doi:10.4155/fmc-2020-0023 (2020).

66 Findley, K. & Grice, E. A. The Skin Microbiome: A Focus on Pathogens and Their Association with Skin Disease. *PLOS Pathogens* **10**, e1004436, doi:10.1371/journal.ppat.1004436 (2014).

67 Lange-Asschenfeldt, B. *et al.* Distribution of bacteria in the epidermal layers and hair follicles of the human skin. *Skin Pharmacol Physiol* **24**, 305-311, doi:10.1159/000328728 (2011).

68 Bay, L. *et al.* Universal Dermal Microbiome in Human Skin. *mBio* **11**, e02945-02919, doi:10.1128/mBio.02945-19 (2020).

69 Nakatsuji, T. *et al.* The microbiome extends to subepidermal compartments of normal skin. *Nat Commun* **4**, 1431, doi:10.1038/ncomms2441 (2013).

70 Gupta, S. *et al.* Amplicon sequencing provides more accurate microbiome information in healthy children compared to culturing. *Communications Biology* **2**, 291, doi:10.1038/s42003-019-0540-1 (2019).

71 Raymond, F. *et al.* Culture-enriched human gut microbiomes reveal core and accessory resistance genes. *Microbiome* **7**, 56, doi:10.1186/s40168-019-0669-7 (2019).

72 Qv, L. *et al.* Methods for Establishment and Maintenance of Germ-Free Rat Models. *Frontiers in Microbiology* **11**, doi:10.3389/fmicb.2020.01148 (2020).

73 Martin, A. M., Sun, E. W., Rogers, G. B. & Keating, D. J. The Influence of the Gut Microbiome on Host Metabolism Through the Regulation of Gut Hormone Release. *Front Physiol* **10**, 428-428, doi:10.3389/fphys.2019.00428 (2019).

74 Tralau, T., Sowada, J. & Luch, A. Insights on the human microbiome and its xenobiotic metabolism: what is known about its effects on human physiology? *Expert Opinion on Drug Metabolism & Toxicology* **11**, 411-425, doi:10.1517/17425255.2015.990437 (2015).

75 Medzhitov, R. Recognition of microorganisms and activation of the immune response. *Nature* **449**, 819-826, doi:10.1038/nature06246 (2007).

76 Cotter, P. D., Ross, R. P. & Hill, C. Bacteriocins - a viable alternative to antibiotics? *Nat Rev Microbiol* **11**, 95-105, doi:10.1038/nrmicro2937 (2013).

77 Cogen, A. L. *et al.* Selective Antimicrobial Action Is Provided by Phenol-Soluble Modulins Derived from Staphylococcus epidermidis, a Normal Resident of the Skin. *Journal of Investigative Dermatology* **130**, 192-200, doi:https://doi.org/10.1038/jid.2009.243 (2010).

78 Nakatsuji, T. *et al.* Sebum free fatty acids enhance the innate immune defense of human sebocytes by upregulating beta-defensin-2 expression. *The Journal of investigative dermatology* **130**, 985-994, doi:10.1038/jid.2009.384 (2010).

79 Lai, Y. *et al.* Commensal bacteria regulate Toll-like receptor 3-dependent inflammation after skin injury. *Nat Med* **15**, 1377-1382, doi:10.1038/nm.2062 (2009).

80 Lai, Y. *et al.* Activation of TLR2 by a small molecule produced by Staphylococcus epidermidis increases antimicrobial defense against bacterial skin infections. *J Invest Dermatol* **130**, 2211-2221, doi:10.1038/jid.2010.123 (2010).

81 Gallo, R. L. & Hooper, L. V. Epithelial antimicrobial defence of the skin and intestine. *Nat Rev Immunol* **12**, 503-516, doi:10.1038/nri3228 (2012).

82 Percoco, G. *et al.* Antimicrobial peptides and pro-inflammatory cytokines are differentially regulated across epidermal layers following bacterial stimuli. *Exp Dermatol* **22**, 800-806, doi:10.1111/exd.12259 (2013).

83 Seo, S. J., Ahn, S. W., Hong, C. K. & Ro, B. I. Expressions of beta-defensins in human keratinocyte cell lines. *J Dermatol Sci* **27**, 183-191 (2001).

84 Braff, M. H. & Gallo, R. L. Antimicrobial peptides: an essential component of the skin defensive barrier. *Curr Top Microbiol Immunol* **306**, 91-110 (2006).

85 Lai, Y. & Gallo, R. L. Toll-like receptors in skin infections and inflammatory diseases. *Infect Disord Drug Targets* **8**, 144-155 (2008).

86 Lai, Y. & Gallo, R. L. AMPed up immunity: how antimicrobial peptides have multiple roles in immune defense. *Trends Immunol* **30**, 131-141, doi:10.1016/j.it.2008.12.003 (2009).

87 Scharschmidt, Tiffany C. *et al.* A Wave of Regulatory T Cells into Neonatal Skin Mediates Tolerance to Commensal Microbes. *Immunity* **43**, 1011-1021, doi:https://doi.org/10.1016/j.immuni.2015.10.016 (2015).

88 Egawa, G., Honda, T. & Kabashima, K. SCFAs Control Skin Immune Responses via Increasing Tregs. *Journal of Investigative Dermatology* **137**, 800-801, doi:https://doi.org/10.1016/j.jid.2016.12.022 (2017).

89 Linehan, J. L. *et al.* Non-classical Immunity Controls Microbiota Impact on Skin Immunity and Tissue Repair. *Cell* **172**, 784-796 e718, doi:10.1016/j.cell.2017.12.033 (2018).

90 Schommer, N. N. & Gallo, R. L. Structure and function of the human skin microbiome. *Trends Microbiol* **21**, 660-668, doi:10.1016/j.tim.2013.10.001 (2013).

91 Gaffen, S. L., Jain, R., Garg, A. V. & Cua, D. J. The IL-23-IL-17 immune axis: from mechanisms to therapeutic testing. *Nat Rev Immunol* **14**, 585-600, doi:10.1038/nri3707 (2014).

92 van der Fits, L. *et al.* Imiquimod-Induced Psoriasis-Like Skin Inflammation in Mice Is Mediated via the IL-23/IL-17 Axis. *The Journal of Immunology* **182**, 5836, doi:10.4049/jimmunol.0802999 (2009).

93 Naik, S. *et al.* Compartmentalized control of skin immunity by resident commensals. *Science* **337**, 1115-1119, doi:10.1126/science.1225152 (2012).

94 Huang, G. T., Zhang, H. B., Kim, D., Liu, L. & Ganz, T. A model for antimicrobial gene therapy: demonstration of human beta-defensin 2 antimicrobial activities in vivo. *Hum Gene Ther* **13**, 2017-2025, doi:10.1089/10430340260395875 (2002).

95 Dinulos, J. G., Mentele, L., Fredericks, L. P., Dale, B. A. & Darmstadt, G. L. Keratinocyte expression of human beta defensin 2 following bacterial infection: role in cutaneous host defense. *Clin Diagn Lab Immunol* **10**, 161-166 (2003).

96 Harder, J., Meyer-Hoffert, U., Wehkamp, K., Schwichtenberg, L. & Schroder, J. M. Differential gene induction of human beta-defensins (hBD-1, -2, -3, and -4) in keratinocytes is inhibited by retinoic acid. *J Invest Dermatol* **123**, 522-529, doi:10.1111/j.0022-202X.2004.23234.x (2004).

97 Steinz, K. *et al.* Bacterial soft tissue infection in psoriasis despite induction of epidermal antimicrobial peptides. *Exp Dermatol* **23**, 862-864, doi:10.1111/exd.12538 (2014).

98 Arend, W. P., Palmer, G. & Gabay, C. IL-1, IL-18, and IL-33 families of cytokines. *Immunol Rev* **223**, 20-38, doi:10.1111/j.1600-065X.2008.00624.x (2008).

99 Lopez-Castejon, G. & Brough, D. Understanding the mechanism of IL-1beta secretion. *Cytokine Growth Factor Rev* **22**, 189-195, doi:10.1016/j.cytogfr.2011.10.001 (2011).

100 Akira, S., Uematsu, S. & Takeuchi, O. Pathogen recognition and innate immunity. *Cell* **124**, 783-801, doi:10.1016/j.cell.2006.02.015 (2006).

101 Belkaid, Y. & Segre, J. A. Dialogue between skin microbiota and immunity. *Science* **346**, 954, doi:10.1126/science.1260144 (2014).

102 Banerjee, A. & Gerondakis, S. Coordinating TLR-activated signaling pathways in cells of the immune system. *Immunol Cell Biol* **85**, 420-424, doi:10.1038/sj.icb.7100098 (2007).

103 Barton, G. M. & Medzhitov, R. Toll-like receptor signaling pathways. *Science* **300**, 1524-1525, doi:10.1126/science.1085536 (2003).

104 Rakoff-Nahoum, S., Paglino, J., Eslami-Varzaneh, F., Edberg, S. & Medzhitov, R. Recognition of commensal microflora by toll-like receptors is required for intestinal homeostasis. *Cell* **118**, 229-241, doi:10.1016/j.cell.2004.07.002 (2004).

105 Kubinak, J. L. & Round, J. L. Toll-like receptors promote mutually beneficial commensal-host interactions. *PLoS Pathog* **8**, e1002785, doi:10.1371/journal.ppat.1002785 (2012).

106 Devine, D. A., Marsh, P. D. & Meade, J. Modulation of host responses by oral commensal bacteria. *Journal of oral microbiology* **7**, 26941-26941, doi:10.3402/jom.v7.26941 (2015).

107 Lai, Y. & Gallo, R. *Commensal skin bacteria as the probiotic of the cutaneous immune response*. Vol. 5 (2010).

108 Boffetta, P. Human cancer from environmental pollutants: The epidemiological evidence. *Mutation Research/Genetic Toxicology and Environmental Mutagenesis* **608**, 157-162, doi:https://doi.org/10.1016/j.mrgentox.2006.02.015 (2006).

109 Abdelsalam, N. A., Ramadan, A. T., ElRakaiby, M. T. & Aziz, R. K. Toxicomicrobiomics: The Human Microbiome vs. Pharmaceutical, Dietary, and Environmental Xenobiotics. *Front Pharmacol* **11**, 390-390, doi:10.3389/fphar.2020.00390 (2020).

110 Koontz, J. M. *et al.* The Role of the Human Microbiome in Chemical Toxicity. *International Journal of Toxicology* **38**, 251-264, doi:10.1177/1091581819849833 (2019).

111 Claus, S. P., Guillou, H. & Ellero-Simatos, S. The gut microbiota: a major player in the toxicity of environmental pollutants? *npj Biofilms and Microbiomes* **2**, 16003, doi:10.1038/npjbiofilms.2016.3 (2016).

112 Koppel, N., Maini Rekdal, V. & Balskus, E. P. Chemical transformation of xenobiotics by the human gut microbiota. *Science (New York, N.Y.)* **356**, eaag2770, doi:10.1126/science.aag2770 (2017).

113 Koppel, N., Rekdal, V. M. & Balskus, E. P. Chemical transformation of xenobiotics by the human gut microbiota. *Science (New York, N.y.)* **356** (2017).

114 Maurice, C. F., Haiser, H. J. & Turnbaugh, P. J. Xenobiotics shape the physiology and gene expression of the active human gut microbiome. *Cell* **152**, 39-50, doi:10.1016/j.cell.2012.10.052 (2013).

115 Sousa, T. *et al.* The gastrointestinal microbiota as a site for the biotransformation of drugs. *International Journal of Pharmaceutics* **363**, 1-25, doi:10.1016/j.ijpharm.2008.07.009 (2008).

116 Zimmermann, M., Zimmermann-Kogadeeva, M., Wegmann, R. & Goodman, A. L. Mapping human microbiome drug metabolism by gut bacteria and their genes. *Nature* **570**, 462-467, doi:10.1038/s41586-019-1291-3 (2019).

117 Tralau, T. & Luch, A. The human microbiome, from Achilles armour to Nessus' shirt. *Archives of Toxicology* **91**, 2699-2701, doi:10.1007/s00204-017-1951-8 (2017).

118 Zimmermann, M., Zimmermann-Kogadeeva, M., Wegmann, R. & Goodman, A. L. Separating host and microbiome contributions to drug pharmacokinetics and toxicity. *Science (New York, N.Y.)* **363**, eaat9931, doi:10.1126/science.aat9931 (2019).

119 Okuda, H., Ogura, K., Kato, A., Takubo, H. & Watabe, T. A Possible Mechanism of Eighteen Patient Deaths Caused by Interactions of Sorivudine, a New Antiviral Drug, with Oral 5-Fluorouracil Prodrugs. *Journal of Pharmacology and Experimental Therapeutics* **287**, 791 (1998).

120 Segal, J. P. *et al.* The gut microbiome: an under-recognised contributor to the COVID-19 pandemic? *Therapeutic Advances in Gastroenterology* **13**, 1756284820974914, doi:10.1177/1756284820974914 (2020).

121 Lamers, M. M. *et al.* SARS-CoV-2 productively infects human gut enterocytes. *Science* **369**, 50, doi:10.1126/science.abc1669 (2020).

122 Geva-Zatorsky, N. *et al.* Mining the Human Gut Microbiota for Immunomodulatory Organisms. *Cell* **168**, 928-943.e911, doi:10.1016/j.cell.2017.01.022 (2017).

123 Zuo, T. *et al.* Alterations in Gut Microbiota of Patients With COVID-19 During Time of Hospitalization. *Gastroenterology* **159**, 944-955.e948, doi:https://doi.org/10.1053/j.gastro.2020.05.048 (2020).

124 Janda, L., Mihalčin, M. & Šťastná, M. Is a healthy microbiome responsible for lower mortality in COVID-19? *Biologia*, doi:10.2478/s11756-020-00614-8 (2020).

125 Niehues, H. *et al.* 3D skin models for 3R research: The potential of 3D reconstructed skin models to study skin barrier function. *Experimental Dermatology* **27**, 501-511, doi:https://doi.org/10.1111/exd.13531 (2018).

126 Schmid-Wendtner, M. H. & Korting, H. C. The pH of the Skin Surface and Its Impact on the Barrier Function. *Skin Pharmacology and Physiology* **19**, 296-302, doi:10.1159/000094670 (2006).

127 Kennedy, E. A. *et al.* Skin microbiome before development of atopic dermatitis: Early colonization with commensal staphylococci at 2 months is associated with a lower risk of atopic dermatitis at 1 year. *J Allergy Clin Immunol* **139**, 166-172, doi:10.1016/j.jaci.2016.07.029 (2017).

128 Barnard, E., Shi, B., Kang, D., Craft, N. & Li, H. The balance of metagenomic elements shapes the skin microbiome in acne and health. *Scientific Reports* **6**, 39491, doi:10.1038/srep39491 (2016).

129 Tett, A. *et al.* Unexplored diversity and strain-level structure of the skin microbiome associated with psoriasis. *NPJ Biofilms Microbiomes* **3**, 14, doi:10.1038/s41522-017-0022-5 (2017).

130 Hsu, D. K., Fung, M. A. & Chen, H.-L. Role of skin and gut microbiota in the pathogenesis of psoriasis, an inflammatory skin disease. *Medicine in Microecology* **4**, 100016, doi:https://doi.org/10.1016/j.medmic.2020.100016 (2020).

131 Seite, S. & Bieber, T. Barrier function and microbiotic dysbiosis in atopic dermatitis. *Clin Cosmet Investig Dermatol* **8**, 479-483, doi:10.2147/CCID.S91521 (2015).

132 Oh, J. S. & Jang, H. H. Epidermal Differentiation and Skin Barrier. *Kor J Aesthet Cosmetol* **13**, 713-720 (2015).

133 Meisel, J. S. *et al.* Commensal microbiota modulate gene expression in the skin. *Microbiome* **6**, 20-20, doi:10.1186/s40168-018-0404-9 (2018).

134 Uberoi, A. *et al.* Commensal Microbiota Regulates Skin Barrier Function And Repair Via Signaling Through The Aryl Hydrocarbon Receptor. *bioRxiv*, 2020.2012.2005.413096, doi:10.1101/2020.12.05.413096 (2020).

135 Landemaine, L., Cenizo, V., Lemaire, G. & Portes, P. 961 Colonization of a 3D skin model with a complete microbiota is more beneficial to the skin barrier than with Staphylococcus epidermidis alone. *Journal of Investigative Dermatology* **138**, S163, doi:https://doi.org/10.1016/j.jid.2018.03.973 (2018).

136 Loomis, K. H. *et al.* A mixed community of skin microbiome representatives influences cutaneous processes more than individual members. *Microbiome* **9**, 22, doi:10.1186/s40168-020-00963-1 (2021).

137 Jung, Y.-O. *et al.* Lysates of a Probiotic, Lactobacillus rhamnosus, Can Improve Skin Barrier Function in a Reconstructed Human Epidermis Model. *Int J Mol Sci* **20**, 4289, doi:10.3390/ijms20174289 (2019).

138 Holz, C. *et al.* Novel bioactive from Lactobacillus brevis DSM17250 to stimulate the growth of Staphylococcus epidermidis: a pilot study. *Benef Microbes* **8**, 121-131, doi:10.3920/bm2016.0073 (2017).

139 Sultana, R., McBain, A. J. & O'Neill, C. A. Strain-dependent augmentation of tight-junction barrier function in human primary epidermal keratinocytes by Lactobacillus and Bifidobacterium lysates. *Appl Environ Microbiol* **79**, 4887-4894, doi:10.1128/aem.00982-13 (2013).

140 Tsai, C.-C. *et al.* Applications of Lactobacillus rhamnosus spent culture supernatant in cosmetic antioxidation, whitening and moisture retention applications. *Molecules* **18**, 14161-14171, doi:10.3390/molecules181114161 (2013).

141 Ferreira, A. *et al.* Novel cosmetic formulations containing a biosurfactant from Lactobacillus paracasei. *Colloids and Surfaces B: Biointerfaces* **155**, 522-529, doi:https://doi.org/10.1016/j.colsurfb.2017.04.026 (2017).

142 Butler, É., Lundqvist, C. & Axelsson, J. Lactobacillus reuteri DSM 17938 as a Novel Topical Cosmetic Ingredient: A Proof of Concept Clinical Study in Adults with Atopic Dermatitis. *Microorganisms* **8**, doi:10.3390/microorganisms8071026 (2020).

143 Bojar, R. A. Studying the Human Skin Microbiome Using 3D In Vitro Skin Models. *Applied In Vitro Toxicology* **1**, 165-171, doi:10.1089/aivt.2015.0002 (2015).

144 Riebeling, C., Luch, A. & Tralau, T. Skin toxicology and 3Rs-Current challenges for public health protection. *Exp Dermatol* **27**, 526-536, doi:10.1111/exd.13536 (2018).

145 Myles, I. A. *et al.* Transplantation of human skin microbiota in models of atopic dermatitis. *JCI Insight* **1**, doi:10.1172/jci.insight.86955 (2016).

146 Gerber, P. A. *et al.* The top skin-associated genes: a comparative analysis of human and mouse skin transcriptomes. *Biological Chemistry* **395**, 577-591, doi:doi:10.1515/hsz-2013-0279 (2014).

147 Hewitt, N. J. *et al.* Use of human in vitro skin models for accurate and ethical risk assessment: metabolic considerations. *Toxicol Sci* **133**, 209-217, doi:10.1093/toxsci/kft080 (2013).

148 Lundberg, R. *et al.* Human microbiota-transplanted C57BL/6 mice and offspring display reduced establishment of key bacteria and reduced immune stimulation compared to mouse microbiota-transplantation. *Scientific Reports* **10**, 7805, doi:10.1038/s41598-020-64703-z (2020).

149 Brettmann, E. A. & de Guzman Strong, C. Recent evolution of the human skin barrier. *Exp Dermatol* **27**, 859-866, doi:10.1111/exd.13689 (2018).

150 Mason, K. M., Bigley, N. J. & Fink, P. S. Development of a novel in vitro co-culture system for studying host response to native bacterial antigens. *J Immunol Methods* **211**, 147-158, doi:10.1016/s0022-1759(97)00200-7 (1998).

151 Mohiti-Asli, M., Pourdeyhimi, B. & Loboa, E. G. Skin tissue engineering for the infected wound site: biodegradable PLA nanofibers and a novel approach for silver ion release evaluated in a 3D coculture system of keratinocytes and Staphylococcus aureus. *Tissue Eng Part C Methods* **20**, 790-797, doi:10.1089/ten.TEC.2013.0458 (2014).

152 van der Krieken, D. A. *et al.* An In vitro Model for Bacterial Growth on Human Stratum Corneum. *Acta Derm Venereol* **96**, 873-879, doi:10.2340/00015555-2401 (2016).

153 Popov, L., Kovalski, J., Grandi, G., Bagnoli, F. & Amieva, M. R. Three-Dimensional Human Skin Models to Understand Staphylococcus aureus Skin Colonization and Infection. *Front Immunol* **5**, 41, doi:10.3389/fimmu.2014.00041 (2014).

154 Bäsler, K. *et al.* Biphasic influence of Staphylococcus aureus on human epidermal tight junctions. *Ann N Y Acad Sci* **1405**, 53-70, doi:10.1111/nyas.13418 (2017).

155 Dieterich, C. *et al.* In vitro reconstructed human epithelia reveal contributions of Candida albicans EFG1 and CPH1 to adhesion and invasion. *Microbiology* **148**, 497-506, doi:https://doi.org/10.1099/00221287-148-2-497 (2002).

156 Holland, D. B., Bojar, R. A., Jeremy, A. H., Ingham, E. & Holland, K. T. Microbial colonization of an in vitro model of a tissue engineered human skin equivalent--a novel approach. *FEMS Microbiol Lett* **279**, 110-115, doi:10.1111/j.1574-6968.2007.01021.x (2008).

157 Holland, D. B., Bojar, R. A., Farrar, M. D. & Holland, K. T. Differential innate immune responses of a living skin equivalent model colonized by Staphylococcus epidermidis or Staphylococcus aureus. *FEMS Microbiol Lett* **290**, 149-155, doi:10.1111/j.1574-6968.2008.01402.x (2009).

158 Chen, Y. E., Fischbach, M. A. & Belkaid, Y. Skin microbiota-host interactions. *Nature* **553**, 427-436, doi:10.1038/nature25177 (2018).

159 Ghosal, D., Ghosh, S., Dutta, T. K. & Ahn, Y. Current State of Knowledge in Microbial Degradation of Polycyclic Aromatic Hydrocarbons (PAHs): A Review. *Frontiers in Microbiology* **7**, doi:10.3389/fmicb.2016.01369 (2016).

160 Sims, R. C. & Overcash, M. R. in *Residue Reviews.* (ed Francis A. Gunther) 1-68 (Springer New York).

161 Samanta, S. K., Singh, O. V. & Jain, R. K. Polycyclic aromatic hydrocarbons: environmental pollution and bioremediation. *Trends in Biotechnology* **20**, 243-248, doi:https://doi.org/10.1016/S0167-7799(02)01943-1 (2002).

162 Blumer, M. Polycyclic aromatic compounds in nature. *Sci Am* **234**, 35-45 (1976).

163 Ciemniak, A. [Polycyclic aromatic hydrocarbons (PAHs) in herbs and fruit teas]. *Rocz Panstw Zakl Hig* **56**, 317-322 (2005).

164 Vu, A. T. *et al.* Polycyclic Aromatic Hydrocarbons in the Mainstream Smoke of Popular U.S. Cigarettes. *Chem Res Toxicol* **28**, 1616-1626, doi:10.1021/acs.chemrestox.5b00190 (2015).

165 Diekmann, A., Giese, U. & Schaumann, I. Polycyclic aromatic hydrocarbons in consumer goods made from recycled rubber material: A review. *Chemosphere* **220**, 1163-1178, doi:https://doi.org/10.1016/j.chemosphere.2018.12.111 (2019).

166 Bartsch, N., Heidler, J., Vieth, B., Hutzler, C. & Luch, A. Skin permeation of polycyclic aromatic hydrocarbons: A solvent-based in vitro approach to assess dermal exposures against benzo[a]pyrene and dibenzopyrenes. *J Occup Environ Hyg* **13**, 969-979, doi:10.1080/15459624.2016.1200724 (2016).

167 Bourgart, E. *et al.* A realistic human skin model to study benzo[a]pyrene cutaneous absorption in order to determine the most relevant biomarker for carcinogenic exposure. *Archives of Toxicology* **93**, 81-93, doi:10.1007/s00204-018-2329-2 (2019).

168 Wilson, S. C. & Jones, K. C. Bioremediation of soil contaminated with polynuclear aromatic hydrocarbons (PAHs): a review. *Environ Pollut* **81**, 229-249, doi:10.1016/0269-7491(93)90206-4 (1993).

169 Marvin, C. H., Lundrigan, J. A., McCarry, B. E. & Bryant, D. W. Determination and genotoxicity of high molecular mass polycyclic aromatic hydrocarbons isolated from coal-tar-contaminated sediment. *Environmental Toxicology and Chemistry* **14**, 2059-2066, doi:https://doi.org/10.1002/etc.5620141208 (1995).

170 Mourón, S. A., Grillo, C. A., Dulout, F. N. & Golijow, C. D. Genotoxic Effects of Benzo[a]pyrene and Dibenzo[a,l]pyrene in a Human Lung Cell Line. *International Journal of Toxicology* **25**, 49-55, doi:10.1080/10915810500488411 (2006).

171 Keith, L. & Telliard, W. ES&T Special Report: Priority pollutants: I-a perspective view. *Environmental Science & Technology* **13**, 416-423, doi:10.1021/es60152a601 (1979).

172 Menzie, C. A., Potocki, B. B. & Santodonato, J. Exposure to carcinogenic PAHs in the environment. *Environmental Science & Technology* **26**, 1278-1284, doi:10.1021/es00031a002 (1992).

173 Siddens, L. K. *et al.* Polycyclic aromatic hydrocarbons as skin carcinogens: comparison of benzo[a]pyrene, dibenzo[def,p]chrysene and three environmental mixtures in the FVB/N mouse. *Toxicol Appl Pharmacol* **264**, 377-386, doi:10.1016/j.taap.2012.08.014 (2012).

174 Honda, M. & Suzuki, N. Toxicities of Polycyclic Aromatic Hydrocarbons for Aquatic Animals. *Int J Environ Res Public Health* **17**, 1363, doi:10.3390/ijerph17041363 (2020).

175 Benmoussa, N., Rebibo, J.-D., Conan, P. & Charlier, P. Chimney-sweeps' cancer—early proof of environmentally driven tumourigenicity. *The Lancet Oncology* **20**, 338, doi:https://doi.org/10.1016/S1470-2045(19)30106-8 (2019).

176 Siemiatycki, J. in *Occupational Cancers* (eds Sisko Anttila & Paolo Boffetta) 1-20 (Springer International Publishing, 2020).

177 Hammond, E. C., Selikoff, I. J., Lawther, P. L. & Seidman, H. Inhalation of benzpyrene and cancer in man. *Ann N Y Acad Sci* **271**, 116-124, doi:10.1111/j.1749-6632.1976.tb23100.x (1976).

178 Meijers, J. M., Swaen, G. M., Slangen, J. J. & van Vliet, C. Lung cancer among Dutch coal miners: a case-control study. *Am J Ind Med* **14**, 597-604, doi:10.1002/ajim.4700140510 (1988).

179 Vanrooij, J. G., Bodelier-Bade, M. M., De Looff, A. J., Dijkmans, A. P. & Jongeneelen, F. J. Dermal exposure to polycyclic aromatic hydrocarbons among primary aluminium workers. *Med Lav* **83**, 519-529 (1992).

180 VanRooij, J. G., Bodelier-Bade, M. M. & Jongeneelen, F. J. Estimation of individual dermal and respiratory uptake of polycyclic aromatic hydrocarbons in 12 coke oven workers. *Br J Ind Med* **50**, 623-632, doi:10.1136/oem.50.7.623 (1993).

181 Hattemer-Frey, H. A. & Travis, C. C. Benzo-a-Pyrene: Environmental Partitioning and Human Exposure. *Toxicology and Industrial Health* **7**, 141-157, doi:10.1177/074823379100700303 (1991).

182 Wester, P. W. *et al.* Carcinogenic activity of benzo[a]pyrene in a 2 year oral study in Wistar rats. *Food Chem Toxicol* **50**, 927-935, doi:10.1016/j.fct.2011.12.003 (2012).

183 Boffetta, P., Jourenkova, N. & Gustavsson, P. Cancer risk from occupational and environmental exposure to polycyclic aromatic hydrocarbons. *Cancer Causes Control* **8**, 444-472, doi:10.1023/a:1018465507029 (1997).

184 Moorthy, B., Chu, C. & Carlin, D. J. Polycyclic aromatic hydrocarbons: from metabolism to lung cancer. *Toxicol Sci* **145**, 5-15, doi:10.1093/toxsci/kfv040 (2015).

185 Jiang, G., Lun, L. & Cong, L. Association between polycyclic aromatic hydrocarbons and human rectal tumor or liver cancer. *The Chinese-German Journal of Clinical Oncology* **11**, 391-394, doi:10.1007/s10330-012-0977-x (2012).

186 Korsh, J., Shen, A., Aliano, K. & Davenport, T. Polycyclic Aromatic Hydrocarbons and Breast Cancer: A Review of the Literature. *Breast Care (Basel)* **10**, 316-318, doi:10.1159/000436956 (2015).

187 Cho, J. *et al.* Association between exposure to polycyclic aromatic hydrocarbons and brain cortical thinning: The Environmental Pollution-Induced Neurological EFfects (EPINEF) study. *Science of The Total Environment* **737**, 140097, doi:https://doi.org/10.1016/j.scitotenv.2020.140097 (2020).

188 Bolden, A. L., Rochester, J. R., Schultz, K. & Kwiatkowski, C. F. Polycyclic aromatic hydrocarbons and female reproductive health: A scoping review. *Reprod Toxicol* **73**, 61-74, doi:10.1016/j.reprotox.2017.07.012 (2017).

189 Burchiel, S. W. in *Encyclopedic Reference of Immunotoxicology* (eds Mario Assenmacher *et al.*) 515-518 (Springer Berlin Heidelberg, 2005).

190 Billiard, S. M., Meyer, J. N., Wassenberg, D. M., Hodson, P. V. & Di Giulio, R. T. Nonadditive effects of PAHs on Early Vertebrate Development: mechanisms and implications for risk assessment. *Toxicological Sciences* **105**, 5-23, doi:10.1093/toxsci/kfm303 (2008).

191 Harris, K. L., Banks, L. D., Mantey, J. A., Huderson, A. C. & Ramesh, A. Bioaccessibility of polycyclic aromatic hydrocarbons: relevance to toxicity and carcinogenesis. *Expert Opin Drug Metab Toxicol* **9**, 1465-1480, doi:10.1517/17425255.2013.823157 (2013).

192 Luch, A. & Baird, W. M. in *The Carcinogenic Effects of Polycyclic Aromatic Hydrocarbons* 19-96 (2005).

193 Croom, E. in *Progress in Molecular Biology and Translational Science* Vol. 112 (ed Ernest Hodgson) 31-88 (Academic Press, 2012).

194 Parkinson, A. & Ogilvie, B. 161-304 (2007).

195 Jancova, P., Anzenbacher, P. & Anzenbacherova, E. Phase II drug metabolizing enzymes. *Biomed Pap Med Fac Univ Palacky Olomouc Czech Repub* **154**, 103-116, doi:10.5507/bp.2010.017 (2010).

196 Bernhardt, R. Cytochrome P450: structure, function, and generation of reactive oxygen species. *Rev Physiol Biochem Pharmacol* **127**, 137-221, doi:10.1007/BFb0048267 (1996).

197 Eilstein, J. *et al.* Xenobiotic metabolizing enzymes in human skin and SkinEthic reconstructed human skin models. *Experimental Dermatology* **24**, 547-549, doi:https://doi.org/10.1111/exd.12694 (2015).

198 Swanson, H. I. Cytochrome P450 expression in human keratinocytes: an aryl hydrocarbon receptor perspective. *Chemico-Biological Interactions* **149**, 69-79, doi:https://doi.org/10.1016/j.cbi.2004.08.006 (2004).

199 Shimada, T. & Fujii-Kuriyama, Y. Metabolic activation of polycyclic aromatic hydrocarbons to carcinogens by cytochromes P450 1A1 and 1B1. *Cancer Sci* **95**, 1-6, doi:10.1111/j.1349-7006.2004.tb03162.x (2004).

200 Gautier, J. C. *et al.* Contribution of human cytochrome P450 to benzo[a]pyrene and benzo[a]pyrene-7,8-dihydrodiol metabolism, as predicted from heterologous expression in yeast. *Pharmacogenetics* **6**, 489-499, doi:10.1097/00008571-199612000-00002 (1996).

201 Schwarz, D., Kisselev, P., Cascorbi, I., Schunck, W.-H. & Roots, I. Differential metabolism of benzo[a]pyrene and benzo[a]pyrene-7,8-dihydrodiol by human CYP1A1 variants. *Carcinogenesis* **22**, 453-459, doi:10.1093/carcin/22.3.453 (2001).

202 Hakkola, J. *et al.* CYP Induction and Xeno-Sensing Receptors PXR, CAR, AHR and PPARα at the Crossroads of Toxicokinetics and Toxicodynamics. *Basic & Clinical Pharmacology & Toxicology* **123 Suppl 5**, doi:10.1111/bcpt.13004 (2018).

203 Merches, K., Haarmann-Stemmann, T., Weighardt, H., Krutmann, J. & Esser, C. AHR in the skin: From the mediator of chloracne to a therapeutic panacea? *Current Opinion in Toxicology* **2**, 79-86, doi:https://doi.org/10.1016/j.cotox.2017.02.002 (2017).

204 Nebert, D. W. *et al.* Role of the aromatic hydrocarbon receptor and [Ah] gene battery in the oxidative stress response, cell cycle control, and apoptosis. *Biochem Pharmacol* **59**, 65-85, doi:10.1016/s0006-2952(99)00310-x (2000).

205 Moserova, M. *et al.* Analysis of benzo[a]pyrene metabolites formed by rat hepatic microsomes using high pressure liquid chromatography: optimization of the method. *Interdisciplinary toxicology* **2**, 239-244, doi:10.2478/v10102-009-0024-0 (2009).

206 Baird, W. M., Hooven, L. A. & Mahadevan, B. Carcinogenic polycyclic aromatic hydrocarbon-DNA adducts and mechanism of action. *Environ. Mol. Mutagen.* **45**, 106-114, doi:10.1002/em.20095 (2005).

207 Allmann, S. *et al.* Benzo[a]pyrene represses DNA repair through altered E2F1/E2F4 function marking an early event in DNA damage-induced cellular senescence. *Nucleic Acids Research* **48**, 12085-12101, doi:10.1093/nar/gkaa965 (2020).

208 Jernström, B. & Gräslund, A. Covalent binding of benzo[a]pyrene 7,8-dihydrodiol 9,10-epoxides to DNA: molecular structures, induced mutations and biological consequences. *Biophysical Chemistry* **49**, 185-199, doi:https://doi.org/10.1016/0301-4622(93)E0087-L (1994).

209 Takeshita, T. & Kanaly, R. A. In vitro DNA/RNA Adductomics to Confirm DNA Damage Caused by Benzo[a]pyrene in the Hep G2 Cell Line. *Frontiers in Chemistry* **7**, doi:10.3389/fchem.2019.00491 (2019).

210 Ling, H. *et al.* Crystal structure of a benzo[a]pyrene diol epoxide adduct in a ternary complex with a DNA polymerase. *Proc Natl Acad Sci U S A* **101**, 2265-2269, doi:10.1073/pnas.0308332100 (2004).

211 Hargis, J. C., Schaefer, H. F., Houk, K. N. & Wheeler, S. E. Noncovalent interactions of a benzo[a]pyrene diol epoxide with DNA base pairs: insight into the formation of adducts of (+)-BaP DE-2 with DNA. *J Phys Chem A* **114**, 2038-2044, doi:10.1021/jp911376p (2010).

212 Kress, J. M. *et al.* Human primary endothelial cells are impaired in nucleotide excision repair and sensitive to benzo[a]pyrene compared with smooth muscle cells and pericytes. *Sci Rep* **9**, 13800, doi:10.1038/s41598-019-49953-w (2019).

213 Hu, Z. H. & Wells, P. G. Modulation of Benzo[a]pyrene Bioactivation by Glucuronidation in Lymphocytes and Hepatic Microsomes from Rats with a Hereditary Deficiency in Bilirubin UDP-Glucuronosyltransferase. *Toxicol Appl Pharmacol* **127**, 306-313, doi:https://doi.org/10.1006/taap.1994.1166 (1994).

214 Arlt, V. M. *et al.* Metabolic activation of benzo[ a ]pyrene in vitro by hepatic cytochrome P450 contrasts with detoxification in vivo : experiments with hepatic cytochrome P450 reductase null mice. *Carcinogenesis* **29**, 656-665, doi:10.1093/carcin/bgn002 (2008).

215 Hoeijmakers, J. H. DNA damage, aging, and cancer. *N Engl J Med* **361**, 1475-1485, doi:10.1056/NEJMra0804615 (2009).

216 Schärer, O. D. Nucleotide excision repair in eukaryotes. *Cold Spring Harb Perspect Biol* **5**, a012609-a012609, doi:10.1101/cshperspect.a012609 (2013).

217 Perlow, R. A. *et al.* DNA Adducts from a Tumorigenic Metabolite of Benzo[a]pyrene Block Human RNA Polymerase II Elongation in a Sequence- and Stereochemistry-dependent Manner. *Journal of Molecular Biology* **321**, 29-47, doi:https://doi.org/10.1016/S0022-2836(02)00593-4 (2002).

218 Tapias, A. *et al.* Ordered Conformational Changes in Damaged DNA Induced by Nucleotide Excision Repair Factors*. *Journal of Biological Chemistry* **279**, 19074-19083, doi:https://doi.org/10.1074/jbc.M312611200 (2004).

219 Sugasawa, K. *et al.* A multistep damage recognition mechanism for global genomic nucleotide excision repair. *Genes Dev* **15**, 507-521, doi:10.1101/gad.866301 (2001).

220 Kropachev, K. *et al.* The sequence dependence of human nucleotide excision repair efficiencies of benzo[a]pyrene-derived DNA lesions: insights into the structural factors that favor dual incisions. *Journal of molecular biology* **386**, 1193-1203, doi:10.1016/j.jmb.2008.12.082 (2009).

221 Araujo, S. J. & Kuraoka, I. Nucleotide excision repair genes shaping embryonic development. *Open Biol* **9**, 190166, doi:10.1098/rsob.190166 (2019).

222 Zhang, X.-X., Cheng, S.-P., Zhu, C.-J. & Sun, S.-L. Microbial PAH-Degradation in Soil: Degradation Pathways and Contributing Factors. *Pedosphere* **16**, 555-565, doi:10.1016/s1002-0160(06)60088-x (2006).

223 Ghosal, D., Ghosh, S., Dutta, T. K. & Ahn, Y. Current State of Knowledge in Microbial Degradation of Polycyclic Aromatic Hydrocarbons (PAHs): A Review. *Front Microbiol* **7**, 1369, doi:10.3389/fmicb.2016.01369 (2016).

224 Lu, C. *et al.* A PAH-degrading bacterial community enriched with contaminated agricultural soil and its utility for microbial bioremediation. *Environ Pollut* **251**, 773-782, doi:10.1016/j.envpol.2019.05.044 (2019).

225 Haritash, A. K. & Kaushik, C. P. Biodegradation aspects of polycyclic aromatic hydrocarbons (PAHs): a review. *J. Hazard. Mater.* **169**, 1-15, doi:S0304-3894(09)00549-4 [pii]
10.1016/j.jhazmat.2009.03.137 [doi] (2009).

226 Peng, R. H. *et al.* Microbial biodegradation of polyaromatic hydrocarbons. *FEMS Microbiol. Rev.* **32**, 927-955, doi:FMR127 [pii]
10.1111/j.1574-6976.2008.00127.x [doi] (2008).

227 Gupta, S., Pathak, B. & Fulekar, M. H. Molecular approaches for biodegradation of polycyclic aromatic hydrocarbon compounds: a review. *Reviews in Environmental Science and Bio/Technology* **14**, 241-269, doi:10.1007/s11157-014-9353-3 (2015).

228 Kweon, O. *et al.* Polycyclic aromatic hydrocarbon metabolic network in *Mycobacterium vanbaalenii* PYR-1. *Journal of bacteriology* **193**, 4326-4337, doi:10.1128/JB.00215-11 (2011).

229 Moody, J. D., Freeman, J. P., Fu, P. P. & Cerniglia, C. E. Degradation of benzo[*a*]pyrene by *Mycobacterium vanbaalenii* PYR-1. *Applied and environmental microbiology* **70**, 340-345 (2004).

230 Willison, J. C. Isolation and characterization of a novel sphingomonad capable of growth with chrysene as sole carbon and energy source. *FEMS microbiology letters* **241**, 143-150, doi:10.1016/j.femsle.2004.10.012 (2004).

231 Abo-State, M. A. M., Riad, B. Y., Bakr, A. A. & Abdel Aziz, M. F. Biodegradation of naphthalene by Bordetella avium isolated from petroleum refinery wastewater in Egypt and its pathway. *Journal of Radiation Research and Applied Sciences* **11**, 1-9, doi:https://doi.org/10.1016/j.jrras.2017.10.001 (2018).

232 Ni'matuzahroh *et al.* Biodegradation of naphthalene and phenanthren by Bacillus subtilis 3KP. *AIP Conference Proceedings* **1854**, 020026, doi:10.1063/1.4985417 (2017).

233 Lee, Y., Lee, Y. & Jeon, C. O. Biodegradation of naphthalene, BTEX, and aliphatic hydrocarbons by Paraburkholderia aromaticivorans BN5 isolated from petroleum-contaminated soil. *Scientific Reports* **9**, 860, doi:10.1038/s41598-018-36165-x (2019).

234 Pourbabaee, A. A., Shahriari, M. H. & Garousin, H. Biodegradation of phenanthrene as a model hydrocarbon: Power display of a super-hydrophobic halotolerant enriched culture derived from a saline-sodic soil. *Biotechnology Reports* **24**, e00388, doi:https://doi.org/10.1016/j.btre.2019.e00388 (2019).

235 Okere, U. V., Cabrerizo, A., Dachs, J., Jones, K. C. & Semple, K. T. Biodegradation of phenanthrene by indigenous microorganisms in soils from Livingstone Island, Antarctica. *FEMS microbiology letters* **329**, 69-77, doi:10.1111/j.1574-6968.2012.02501.x (2012).

236 Ike, P. T. L., Birolli, W. G., dos Santos, D. M., Porto, A. L. M. & Souza, D. H. F. Biodegradation of anthracene and different PAHs by a yellow laccase from Leucoagaricus gongylophorus. *Environmental Science and Pollution Research* **26**, 8675-8684, doi:10.1007/s11356-019-04197-z (2019).

237 Jacques, R. J. S. *et al.* Anthracene biodegradation by Pseudomonas sp. isolated from a petrochemical sludge landfarming site. *International Biodeterioration & Biodegradation* **56**, 143-150, doi:https://doi.org/10.1016/j.ibiod.2005.06.005 (2005).

238 Mihelcic, J. R. & Luthy, R. G. Microbial degradation of acenaphthene and naphthalene under denitrification conditions in soil-water systems. *Appl Environ Microbiol* **54**, 1188-1198, doi:10.1128/aem.54.5.1188-1198.1988 (1988).

239 Mallick, S. Biodegradation of acenaphthene by Sphingobacterium sp. strain RTSB involving trans-3-carboxy-2-hydroxybenzylidenepyruvic acid as a metabolite. *Chemosphere* **219**, 748-755, doi:https://doi.org/10.1016/j.chemosphere.2018.12.046 (2019).

240 Nzila, A. & Musa, M. M. Current Status of and Future Perspectives in Bacterial Degradation of Benzo[a]pyrene. *Int J Environ Res Public Health* **18**, doi:10.3390/ijerph18010262 (2021).

241 Moody, J. D., Freeman, J. P., Fu, P. P. & Cerniglia, C. E. Degradation of Benzo[<em>a</em>]pyrene by <em>Mycobacterium vanbaalenii</em>

PYR-1. *Applied and Environmental Microbiology* **70**, 340, doi:10.1128/AEM.70.1.340-345.2004 (2004).

242 Qin, W. *et al.* Biodegradation of benzo(a)pyrene by Microbacterium sp. strain under denitrification: Degradation pathway and effects of limiting electron acceptors or carbon source. *Biochemical Engineering Journal* **121**, 131-138, doi:https://doi.org/10.1016/j.bej.2017.02.001 (2017).

243 Schneider, J., Grosser, R., Jayasimhulu, K., Xue, W. & Warshawsky, D. Degradation of pyrene, benz[a]anthracene, and benzo[a]pyrene by Mycobacterium sp. strain RJGII-135, isolated from a former coal gasification site. *Applied and environmental microbiology* **62**, 13-19 (1996).

244 Rentz, J. A., Alvarez, P. J. J. & Schnoor, J. L. Benzo[a]pyrene degradation by Sphingomonas yanoikuyae JAR02. *Environmental Pollution* **151**, 669-677, doi:https://doi.org/10.1016/j.envpol.2007.02.018 (2008).

245 Juhasz, A. L., Britz, M. L. & Stanley, G. A. Degradation of high molecular weight polycyclic aromatic hydrocarbons by Pseudomonas cepacia. *Biotechnology Letters* **18**, 577-582, doi:10.1007/BF00140206 (1996).

246 Bhatt Kamlesh, K., Lily Madhuri, K., Joshi, G. & Dangwal, K. in *Turkish Journal of Biochemistry* Vol. 43 693 (2018).

247 Chen, S.-H. & Aitken, M. D. Salicylate Stimulates the Degradation of High-Molecular Weight Polycyclic Aromatic Hydrocarbons by Pseudomonas saccharophila P15. *Environmental Science & Technology* **33**, 435-439, doi:10.1021/es9805730 (1999).

248 Nzila, A. *et al.* Degradation of benzo[a]pyrene by halophilic bacterial strain Staphylococcus haemoliticus strain 10SBZ1A. *PLOS ONE* **16**, e0247723, doi:10.1371/journal.pone.0247723 (2021).

249 Ubani, O., Atagana, H. & Thantsha, M. Biological degradation of oil sludge: A review of the current state of development. *AFRICAN JOURNAL OF BIOTECHNOLOGY* **12**, 6544-6567, doi:10.5897/AJB11.1139 (2013).

250 Gibson, D. T. *Beijerinckia* sp. strain B1: a strain by any other name. *Journal of Industrial Microbiology and Biotechnology* **23**, 284-293, doi:10.1038/sj/jim/2900715 (1999).

251 Cerniglia, C. E. & Heitkamp, M. A. Polycyclic aromatic hydrocarbon degradation by *Mycobacterium*. *Methods Enzymol.* **188**, 148-153 (1990).

252 Boonchan, S., Britz, M. L. & Stanley, G. A. Degradation and Mineralization of High-Molecular-Weight Polycyclic Aromatic Hydrocarbons by Defined Fungal-Bacterial Cocultures. *Applied and environmental microbiology* **66**, 1007, doi:10.1128/AEM.66.3.1007-1019.2000 (2000).

253 Sowada, J. *et al.* Toxification of polycyclic aromatic hydrocarbons by commensal bacteria from human skin. *Archives of Toxicology* **91**, 2331-2341, doi:10.1007/s00204-017-1964-3 (2017).

254 Sowada, J., Schmalenberger, A., Ebner, I., Luch, A. & Tralau, T. Degradation of benzo[a]pyrene by bacterial isolates from human skin. *FEMS Microbiol Ecol* **88**, 129-139, doi:10.1111/1574-6941.12276 (2014).

255 Kanehisa, M., Goto, S., Sato, Y., Furumichi, M. & Tanabe, M. KEGG for integration and interpretation of large-scale molecular data sets. *Nucleic Acids Res* **40**, D109-114, doi:10.1093/nar/gkr988 (2012).

256 Chandler, M., Bird, R. E. & Caro, L. The replication time of the Escherichia coli K12 chromosome as a function of cell doubling time. *Journal of Molecular Biology* **94**, 127-132, doi:https://doi.org/10.1016/0022-2836(75)90410-6 (1975).

257 Wang, Q. *et al.* Effect of cosmetic chemical preservatives on resident flora isolated from healthy facial skin. *Journal of Cosmetic Dermatology* **18**, 652-658, doi:https://doi.org/10.1111/jocd.12822 (2019).

258 Khayyira, A. S., Rosdina, A. E., Irianti, M. I. & Malik, A. Simultaneous profiling and cultivation of the skin microbiome of healthy young adult skin for the development of therapeutic agents. *Heliyon* **6**, e03700, doi:https://doi.org/10.1016/j.heliyon.2020.e03700 (2020).

259 Steglińska, A. *et al.* Factors Influencing Microbiological Biodiversity of Human Foot Skin. *Int J Environ Res Public Health* **16**, doi:10.3390/ijerph16183503 (2019).

260 O'Sullivan, J. N., Rea, M. C., O'Connor, P. M., Hill, C. & Ross, R. P. Human skin microbiota is a rich source of bacteriocin-producing staphylococci that kill human pathogens. *FEMS Microbiol Ecol* **95**, doi:10.1093/femsec/fiy241 (2019).

261 Chiller, K., Selkin, B. A. & Murakawa, G. J. Skin Microflora and Bacterial Infections of the Skin. *Journal of Investigative Dermatology Symposium Proceedings* **6**, 170-174, doi:https://doi.org/10.1046/j.0022-202x.2001.00043.x (2001).

262 Viggor, S. *et al.* Microbial Metabolic Potential of Phenol Degradation in Wastewater Treatment Plant of Crude Oil Refinery: Analysis of Metagenomes and Characterization of Isolates. *Microorganisms* **8**, doi:10.3390/microorganisms8050652 (2020).

263 Egea, T. C. *et al.* Diuron degradation by bacteria from soil of sugarcane crops. *Heliyon* **3**, e00471, doi:https://doi.org/10.1016/j.heliyon.2017.e00471 (2017).

264 Hanafy, R. A. *et al.* Draft genome sequence of Micrococcus luteus strain O'Kane implicates metabolic versatility and the potential to degrade polyhydroxybutyrates. *Genomics Data* **9**, 148-153, doi:https://doi.org/10.1016/j.gdata.2016.08.006 (2016).

265 Tang, J. *et al.* Isolation, identification, and fenvalerate-degrading potential of Bacillus licheniformis CY-012. *Biotechnology & Biotechnological Equipment* **32**, 574-582, doi:10.1080/13102818.2018.1438210 (2018).

266 Arena, M., Abbate, C., Fukushima, K. & Gennari, M. Degradation of poly (lactic acid) and nanocomposites by Bacillus licheniformis. *Environ Sci Pollut Res Int* **18**, 865-870, doi:10.1007/s11356-011-0443-2 (2011).

267 Leung, M. H. Y. *et al.* Changes of the human skin microbiota upon chronic exposure to polycyclic aromatic hydrocarbon pollutants. *Microbiome* **8**, 100, doi:10.1186/s40168-020-00874-1 (2020).

268 Jaiswal, S. K., Agarwal, S. M., Thodum, P. & Sharma, V. K. SkinBug: an artificial intelligence approach to predict human skin microbiome-mediated metabolism of biotics and xenobiotics. *iScience* **24**, 101925, doi:10.1016/j.isci.2020.101925 (2021).

269 van Eijl, S. *et al.* Elucidation of Xenobiotic Metabolism Pathways in Human Skin and Human Skin Models by Proteomic Profiling. *PLOS ONE* **7**, e41721, doi:10.1371/journal.pone.0041721 (2012).

270 Gibson, D. T., Mahadevan, V., Jerina, D. M., Yogi, H. & Yeh, H. J. Oxidation of the carcinogens benzo [a] pyrene and benzo [a] anthracene to dihydrodiols by a bacterium. *Science* **189**, 295, doi:10.1126/science.1145203 (1975).

271 Flowers, L., Bleczinski, W. F., Burczynski, M. E., Harvey, R. G. & Penning, T. M. Disposition and Biological Activity of Benzo[a]pyrene-7,8-dione. A Genotoxic Metabolite Generated by Dihydrodiol Dehydrogenase. *Biochemistry* **35**, 13664-13672, doi:10.1021/bi961077w (1996).

272 Shou, M., Harvey, R. G. & Penning, T. M. Reactivity of benzo[a]pyrene-7,8-dione with DNA. Evidence for the formation of deoxyguanosine adducts. *Carcinogenesis* **14**, 475-482, doi:10.1093/carcin/14.3.475 (1993).

273 Collins, S. L. & Patterson, A. D. The gut microbiome: an orchestrator of xenobiotic metabolism. *Acta Pharm Sin B* **10**, 19-32, doi:10.1016/j.apsb.2019.12.001 (2020).

274 Byrd, A. L., Belkaid, Y. & Segre, J. A. The human skin microbiome. *Nature Reviews Microbiology* **16**, 143-155, doi:10.1038/nrmicro.2017.157 (2018).

275 Koppel, N., Maini Rekdal, V. & Balskus, E. P. Chemical transformation of xenobiotics by the human gut microbiota. *Science* **356**, eaag2770, doi:10.1126/science.aag2770 (2017).

276 Ley, R. E. *et al.* Obesity alters gut microbial ecology. *Proc Natl Acad Sci U S A* **102**, 11070-11075, doi:10.1073/pnas.0504978102 (2005).

277 Rawls, J. F., Mahowald, M. A., Ley, R. E. & Gordon, J. I. Reciprocal gut microbiota transplants from zebrafish and mice to germ-free recipients reveal host habitat selection. *Cell* **127**, 423-433, doi:10.1016/j.cell.2006.08.043 (2006).

278 Lundberg, R. Humanizing the gut microbiota of mice: Opportunities and challenges. *Lab Anim* **53**, 244-251, doi:10.1177/0023677218787554 (2019).

279 Ross, A. A., Rodrigues Hoffmann, A. & Neufeld, J. D. The skin microbiome of vertebrates. *Microbiome* **7**, 79, doi:10.1186/s40168-019-0694-6 (2019).

280 Tralau, T., Sowada, J. & Luch, A. Insights on the human microbiome and its xenobiotic metabolism: what is known about its effects on human physiology? *Expert Opin. Drug Metab. Toxicol.* **11**, 411-425, doi:10.1517/17425255.2015.990437 (2015).

281 Meisel, J. S. *et al.* Commensal microbiota modulate gene expression in the skin. *Microbiome* **6**, 20, doi:10.1186/s40168-018-0404-9 (2018).

282 Pluznick, J. L. *et al.* Olfactory receptor responding to gut microbiota-derived signals plays a role in renin secretion and blood pressure regulation. *Proceedings of the National Academy of Sciences* **110**, 4410, doi:10.1073/pnas.1215927110 (2013).

283 Tsai, T. *et al.* Two olfactory receptors—OR2A4/7 and OR51B5—differentially affect epidermal proliferation and differentiation. *Experimental Dermatology* **26**, 58-65, doi:https://doi.org/10.1111/exd.13132 (2017).

284 ParÉ, J. A., Sigler, L., Rosenthal, K. L. & Mader, D. R. in *Reptile Medicine and Surgery (Second Edition)* (ed Douglas R. Mader) 217-238 (W.B. Saunders, 2006).

285 Duckney, P. *et al.* The role of the skin barrier in modulating the effects of common skin microbial species on the inflammation, differentiation and proliferation status of epidermal keratinocytes. *BMC Res Notes* **6**, 474, doi:10.1186/1756-0500-6-474 (2013).

286 Rademacher, F. *et al.* Staphylococcus epidermidis Activates Aryl Hydrocarbon Receptor Signaling in Human Keratinocytes: Implications for Cutaneous Defense. *J Innate Immun*, 1-11, doi:10.1159/000492162 (2018).

287 Ueda, Y. *et al.* Commensal microbiota induce LPS hyporesponsiveness in colonic macrophages via the production of IL-10. *Int Immunol* **22**, 953-962, doi:10.1093/intimm/dxq449 (2010).

288 Cohen-Poradosu, R., McLoughlin, R. M., Lee, J. C. & Kasper, D. L. Bacteroides fragilis-stimulated interleukin-10 contains expanding disease. *J Infect Dis* **204**, 363-371, doi:10.1093/infdis/jir277 (2011).

289 Fung, T. C. *et al.* Lymphoid-Tissue-Resident Commensal Bacteria Promote Members of the IL-10 Cytokine Family to Establish Mutualism. *Immunity* **44**, 634-646, doi:10.1016/j.immuni.2016.02.019 (2016).

290 Jourová, L. *et al.* Gut Microbiome Alters the Activity of Liver Cytochromes P450 in Mice With Sex-Dependent Differences. *Frontiers in Pharmacology* **11**, doi:10.3389/fphar.2020.01303 (2020).

291 Nichols, R. G., Peters, J. M. & Patterson, A. D. Interplay Between the Host, the Human Microbiome, and Drug Metabolism. *Human Genomics* **13**, 27, doi:10.1186/s40246-019-0211-9 (2019).

292 Walsh, J. *et al.* Gut microbiome-mediated modulation of hepatic cytochrome P450 and P-glycoprotein: impact of butyrate and fructo-oligosaccharide-inulin. *Journal of Pharmacy and Pharmacology* **72**, 1072-1081, doi:https://doi.org/10.1111/jphp.13276 (2020).

293 Do, K. N., Fink, L. N., Jensen, T. E., Gautier, L. & Parlesak, A. TLR2 Controls Intestinal Carcinogen Detoxication by CYP1A1. *PLOS ONE* **7**, e32309, doi:10.1371/journal.pone.0032309 (2012).

294 Kao, J., Patterson, F. K. & Hall, J. Skin penetration and metabolism of topically applied chemicals in six mammalian species, including man: An in vitro study with benzo[a]pyrene and testosterone. *Toxicology and Applied Pharmacology* **81**, 502-516, doi:https://doi.org/10.1016/0041-008X(85)90421-1 (1985).

295 Wilhelm, K. P., Saunders, J. C. & Maibach, H. I. Increased stratum corneum turnover induced by subclinical irritant dermatitis. *British Journal of Dermatology* **122**, 793-798, doi:https://doi.org/10.1111/j.1365-2133.1990.tb06268.x (1990).

296 Kang, M. J. *et al.* The effect of gut microbiota on drug metabolism. *Expert Opin. Drug Metab. Toxicol.* **9**, 1295-1308, doi:10.1517/17425255.2013.807798 (2013).

297 Sousa, T. *et al.* The gastrointestinal microbiota as a site for the biotransformation of drugs. *Int J Pharm* **363**, 1-25, doi:10.1016/j.ijpharm.2008.07.009 (2008).

298 Haiser, H. J. & Turnbaugh, P. J. Developing a metagenomic view of xenobiotic metabolism. *Pharmacol Res* **69**, 21-31, doi:10.1016/j.phrs.2012.07.009 (2013).

299 Yu, J. *et al.* A tryptophan metabolite of the skin microbiota attenuates inflammation in patients with atopic dermatitis through the aryl hydrocarbon receptor. *J Allergy Clin Immunol* **143**, 2108-2119.e2112, doi:10.1016/j.jaci.2018.11.036 (2019).

300 Sanford, J. A., O'Neill, A. M., Zouboulis, C. C. & Gallo, R. L. Short-Chain Fatty Acids from <em>Cutibacterium acnes</em> Activate Both a Canonical and Epigenetic Inflammatory Response in Human Sebocytes. *The Journal of Immunology* **202**, 1767, doi:10.4049/jimmunol.1800893 (2019).

301 Keshari, S. *et al.* Butyric Acid from Probiotic Staphylococcus epidermidis in the Skin Microbiome Down-Regulates the Ultraviolet-Induced Pro-Inflammatory IL-6 Cytokine via Short-Chain Fatty Acid Receptor. *Int J Mol Sci* **20**, 4477, doi:10.3390/ijms20184477 (2019).

302 Platzek, T., Lang, C., Grohmann, G., Gi, U. S. & Baltes, W. Formation of a carcinogenic aromatic amine from an azo dye by human skin bacteria in vitro. *Human & Experimental Toxicology* **18**, 552-559, doi:10.1191/096032799678845061 (1999).

303 Van Norman, G. A. Limitations of Animal Studies for Predicting Toxicity in Clinical Trials: Is it Time to Rethink Our Current Approach? *JACC: Basic to Translational Science* **4**, 845-854, doi:https://doi.org/10.1016/j.jacbts.2019.10.008 (2019).

304 Xiang, Z. *et al.* A glance at the gut microbiota of five experimental animal species through fecal samples. *Scientific Reports* **10**, 16628, doi:10.1038/s41598-020-73985-2 (2020).

305 Park, J. C. & Im, S.-H. Of men in mice: the development and application of a humanized gnotobiotic mouse model for microbiome therapeutics. *Experimental & Molecular Medicine* **52**, 1383-1396, doi:10.1038/s12276-020-0473-2 (2020).

306 Michalke, K. *et al.* Role of Intestinal Microbiota in Transformation of Bismuth and Other Metals and Metalloids into Volatile Methyl and Hydride Derivatives in Humans and Mice. *Applied and Environmental Microbiology* **74**, 3069, doi:10.1128/AEM.02933-07 (2008).

307 Philbert, M. A., Gray, A. J. & Connors, T. A. Preliminary investigations into the involvement of the intestinal microflora in CNS toxicity induced by 1,3-dinitrobenzene in male F-344 rats. *Toxicol Lett* **38**, 307-314, doi:10.1016/0378-4274(87)90013-0 (1987).

308 Collins, S. L. & Patterson, A. D. The gut microbiome: an orchestrator of xenobiotic metabolism. *Acta Pharmaceutica Sinica B* **10**, 19-32, doi:https://doi.org/10.1016/j.apsb.2019.12.001 (2020).

309 Fay, M. J. *et al.* Xenobiotic Metabolism in Mice Lacking the UDP-Glucuronosyltransferase 2 Family. *Drug Metab Dispos* **43**, 1838-1846, doi:10.1124/dmd.115.065482 (2015).

310 Wong, V. W., Sorkin, M., Glotzbach, J. P., Longaker, M. T. & Gurtner, G. C. Surgical Approaches to Create Murine Models of Human Wound Healing. *Journal of Biomedicine and Biotechnology* **2011**, 969618, doi:10.1155/2011/969618 (2011).

311 Sepich-Poore, G. D. *et al.* The microbiome and human cancer. *Science* **371**, eabc4552, doi:10.1126/science.abc4552 (2021).

# 7. List of publications

## 7.1. Publications integrated in the cumulative dissertation

1. Sowada, J., **Lemoine, L.,** Schön, K. et al. Toxification of polycyclic aromatic hydrocarbons by commensal bacteria from human skin. *Arch Toxicol* **91**, 2331–2341 (2017).
2. **Lemoine, L**., Dieckmann, R., Al Dahouk, S. et al. Microbially competent 3D skin: a test system that reveals insight into host–microbe interactions and their potential toxicological impact. *Arch Toxicol* **94**, 3487–3502 (2020).
3. **Lemoine, L**., Bayrambey, D., Roloff, A. et al. Commensal-related changes in the epidermal barrier function lead to alterations in the benzo[*a*]pyrene metabolite profile and its distribution in 3D-skin. *mBio* **12**, e01223-01221 (2021).

**Talks**

1. 46$^{th}$ EEMGS/30$^{th}$ GUM meeting: Microbially competent skin - a new skin model for testing genotoxicity in situ. 18 - 21 March 2018, Potsdam, Germany.
2. 3$^{rd}$ German Pharm-Tox Summit (DGPT): Colonising 3D skin - a novel test system to study host-microbe skin toxicity. 28 February 2018, Göttingen, Germany.
3. 2$^{nd}$ German Pharm-Tox Summit (DGPT): Influence of commensal benzo[*a*]pyrene (B[*a*]P) metabolism on UV-damage repair. 06 April 2017, Heidelberg, Germany.

**Poster**

1. **Lemoine, L**, Luch, A., Tralau, T, Colonizing 3D-skin - Impact on cutaneous gene transcription. 4$^{th}$ German Pharm-Tox Summit (DGPT), 25 - 28 February 2019, Stuttgart, Germany.
2. Tralau, T, Luch, A., **Lemoine, L**, Microbiome-mediated PAH- and azo dye-toxification and its impact on the human host. Metabolomics and Human Health Gordon Research Conference, 3 - 8 February 2019, Ventura CA,USA.
3. **Lemoine, L**, Luch, A., Tralau, T, Influence of commensal benzo[a]pyrene metabolism on skin UV-damage repair, 1$^{th}$ German Pharm-Tox Summit, 29 February - 3 March 2016, Berlin, Germany.

# Annex I

# Supplementary Data

## Toxification of polycyclic aromatic hydrocarbons by commensal bacteria from human skin

Juliane Sowada, **Lisa Lemoine**, Karsten Schön, Christoph Hutzler, Andreas Luch & Tewes Tralau

This chapter was published on 04 April 2017:
Archives of Toxicology 91, 2331–2341 (2017)
DOI: 10.1007/s00204-017-1964-3
Link: https://doi.org/10.1007/s00204-017-1964-3

**Sowada *et al*, supplementary material**

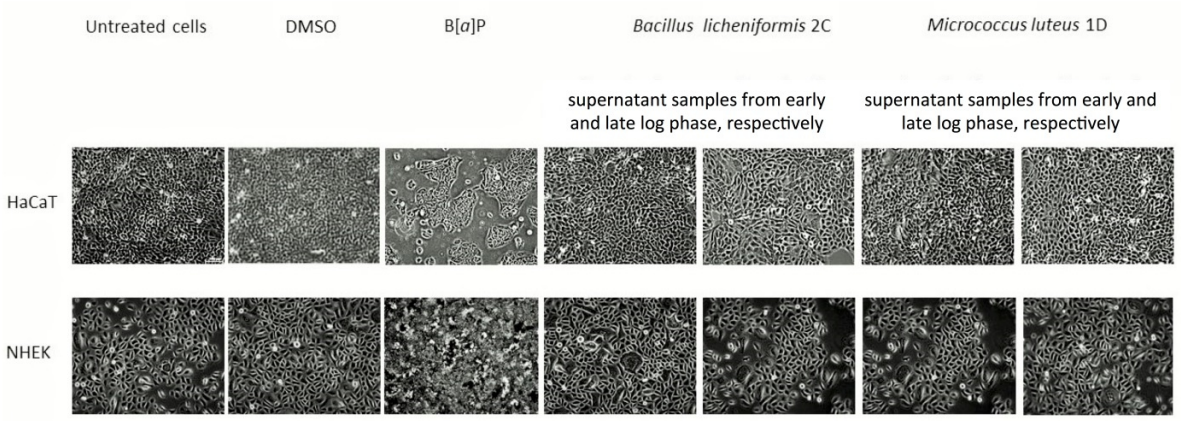


**Fig. S1.** Selected images of HaCaT and NHEK cells after treatment with bacterial supernatants as indicated. Cytotoxicity led to slower growth and pronounced differences in morphology, especially for HaCaT cells. Abbreviations: DMSO, dimethyl sulfoxide; B[*a*]P, benzo[*a*]pyrene.

**a**

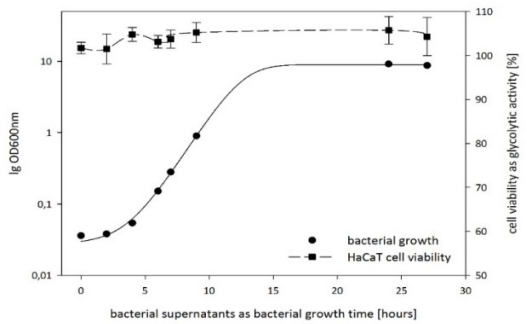


**b**

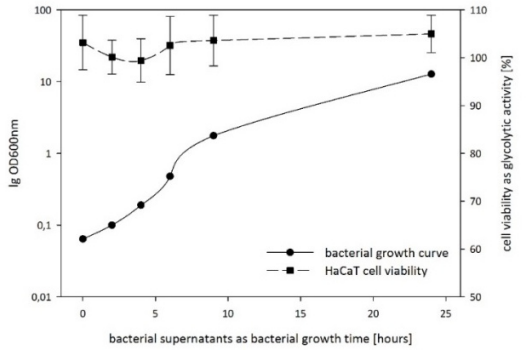


**c**

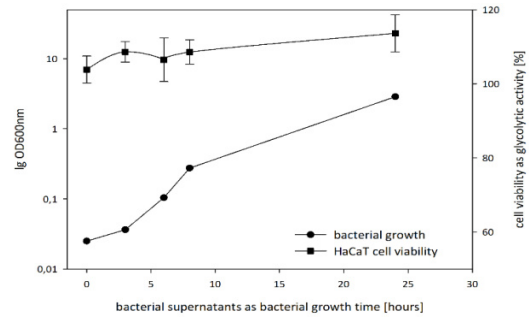


**Fig. S2.** Negative controls for MTT assays with bacterial supernatants from lysogeny broth cultures of *M. luteus* 1D (**a**), *B. licheniformis* 2C (**b**) and *M. luteus* 1B (**c**), respectively. Data shown represent the mean of three biological replicates with $p < 0.01$.

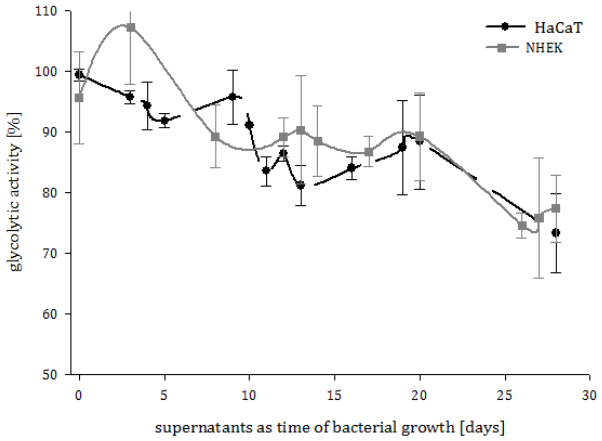


**Fig. S3.** Cytotoxicity of bacterial supernatants excreted by the partial degrader *B. licheniformis* 2C during growth on 100 µM B[*a*]P. Supernatants were added to HaCaT and NHEK cells as indicated and cellular glycolytic activity recorded after 48 h using an MTT assay. Data shown represent the mean of four biological replicates with $p < 0.01$. Negative controls comprised bacterial minimal medium or supernatants from lysogeny broth cultures.

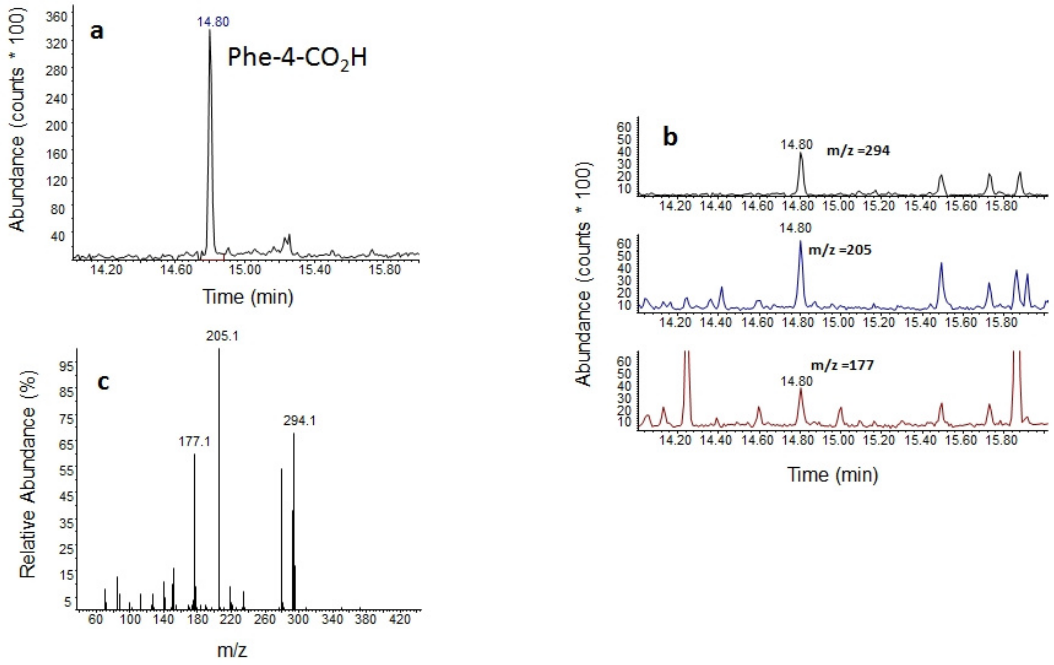


**Fig. S4.** GC-MS ion chromatograms of m/z = 294, m/z = 205 and m/z =177 indicating metabolically formed phenanthrene (Phe)-4-$CO_2H$ from *M. luteus* 1D. Shown are the chromatograms of the synthetic standard at the retention time of 14.80 min (**a**); together with the metabolites as excreted (most characteristic ion chromatograms, retention time of 14.80 min) (**b**); and the corresponding mass spectrum of the standard compound (**c**).

**Table S1.** Summary of the results of the reverse mutation assay according to Ames. The test was performed using *Salmonella typhimurium* TA95 and TA1535 as well as *Escherichia coli* WP2 *uvrA* suitable for detecting frameshift mutations (*S. typhimurium* TA95) and base-pair substitions (*S. typhimurium* TA1535 and *E. coli* WP2 *uvrA*), respectively. Bacterial supernatants were tested in absence or presence of S9-mix as indicated. Unless stated otherwise test results were considered to be positive once the number of revertant colonies equalled at least three times the count of the corresponding solvent control (induction factor ≥ 3). Data shown represent the mean of three biological replicates. Also tested were the identified metabolites (Table 4) without the addition of S9-mix. However, at their maximally excreted concentrations they did not induce clear reverse mutations, neither did the reconstituted mix.

| | ***TA98*** ***-/+ S9*** | ***TA1535*** ***-/+ S9*** | ***WP2 uvrA*** ***-/+ S9*** |
|---|---|---|---|
| Solvent control (DMSO) | -/- | -/- | -/- |
| Negative control (MM) | -/- | -/- | -/- |
| 2-Nitrofluorene [4 µg/plate] | +/+ | | |
| Sodium azide [1.5 and 4 µg/plate] | | +/+ | |
| 4-Nitrochinoline-n-oxide [1 µg/plate] | | | +/+ |
| Bacterial supernatant *M.luteus* 1D | -/- | -/- | -/- |
| Bacterial supernatant *B.licheniformis* 2C | -/- | -/+ | -/- |
| Bacterial supernatant *M.luteus* 1B | +/+ | +/+ | (+/+)[#] |

[#] induction factors of 2.7 and 2.9, respectively

# Annex II

# Supplementary Data

## Microbially competent 3D skin: a test system that reveals insight into host–microbe interactions and their potential toxicological impact

**Lisa Lemoine**, Ralf Dieckmann, Sascha Al Dahouk, Szilvia Vincze, Andreas Luch & Tewes Tralau

This chapter was published on 17 July 2020:
Archives of Toxicology 94, 3487–3502 (2020)
DOI: 10.1007/s00204-020-02841-z
Link: https://doi.org/10.1007/s00204-020-02841-z

# Supplementary Material

**Method S1**

*Bacterial quantification*

For strain specific quantitative PCR (ss-qPCR) total genomic DNA was isolated from the remaining solution using the RTP® Bacteria DNA Mini Kit (Invitek, STRATEC Molecular GmbH, Berlin, Germany). Prior to ss-qPCR, purity of DNA was estimated using a Nanodrop-1000 Spectrophotometer (Thermo Fisher Scientific, Darmstadt, Germany) and the amount obtained quantified by fluorometry (QuBit 4 Fluorometer, Thermo Fisher Scientific, Darmstadt, Germany).

Primer design

Strain-specific primers were designed for both strains using the WGS data. Sequence alignments and primer design were carried out using the Primer Express (version 3.0.1; Applied Biosystems, Foster City, CA, USA) and *in silico* primer specificity by BLAST in conjunctin with the Accelrys (version 2.5; San Diego, California). The primers selected for further use were 5'- CAT GGC ACC AGC GAA ACC -3' (forward) and 5'- CTG CTA CTA CCC CTA CTG ATA TTT TCT CT -3' (reverse) for *M. luteus* and 5'- GTA TCC GCA CCG TCT ACA CC -3' (forward) and 5'- CAA TGC CTC CAG ATC CAC CA -3' (reverse) for *P. oleovorans*, targeting a 90 bp intergenic region and a 110 bp region of a 2-acylglycerophosphoethanolamine acyltransferase, respectively.

Assessment of assay specificity and efficiency

Specificity of both primer pairs was assessed by performing end point PCR with DNA obtained from pure cultures of *M. luteus* and *P. oleovorans* as well as by analysis of the melting curve. Standard curves were generated for both bacterial species using serial dilutions of genomic DNA containing $2 \times 10^1$ - $2 \times 10^6$ copies of the target gene per reaction. Quantitative (q)PCR was performed on a CFX96 Touch™ Real-Time PCR Detection System (Bio-Rad Laboratories, Hercules, CA, USA) using the SsoAdvanced™ Universal SYBR® Green mix (Bio-Rad Laboratories, Munich, Germany). Amplification reactions were performed in technical triplicates using 5 µl of template DNA in 25 µL of reaction volume with Biorad Hard-Shell® 96-Well PCR plates and 80 nM of forward and reverse primers, respectively (initial denaturation at 95 °C for 5 min, followed by 40 cycles of 95 °C for 15 s and 61 °C for 30 s and an incremental melting curve from 50 °C to 95 °C at 0.5 °C/5 s).

Linear relationship between quantification cycle ($C_q$) and log input DNA copy number was evaluated based on three biological replicates and amplification efficiencies (E) calculated based on the slope of standard curve ($E=10^{-1/slope}-1$).

Ss-qPCR

The corresponding amount of *M. luteus* and *P. oleovorans* was subsequently tested for each sample in technical replicates on a 96 well plate. Genomic DNA containing 2 x $10^6$ copies of the target gene served as internal quantification control. Negative controls containing water instead of template were included in each run. Running conditions resembled those used for the generation of standard curves. A reaction was considered positive if the exponential amplification curve exceeded the threshold within 40 cycles. The quantification cycle ($C_q$) was then defined as the cycle number at which the sample fluorescence crossed the threshold. Genome copy numbers were calculated based on representative standard curves for each sample.

**Supplementary Table S2.** Primers used for quantitative RT-PCR.

| Primer | Sequence forward | Sequence reverse |
|---|---|---|
| **CYP1A1** | 5'-TCC AAG AGT CCA CCC TTC C-3' | 5'-AAG CAT GAT CAG TGT AGG GAT CT-3' |
| **CYP2D6** | 5`-AAG AAG TCG CTG GAG CAG TG-3' | 5`-TTG TCC AAG AGA CCG TTG GG-3' |
| **CYP1B1** | 5`-TGG ATT TGG AGA ACG TAC CG-3' | 5`-CCA CGA CCT GAT CCA ATT CT-3' |
| **GAPDH** | 5`-CTC TGC TCC TCC TGT TCG AC-3' | 5`-ACG ACC AAA TCC GTT GAC TC-3' |

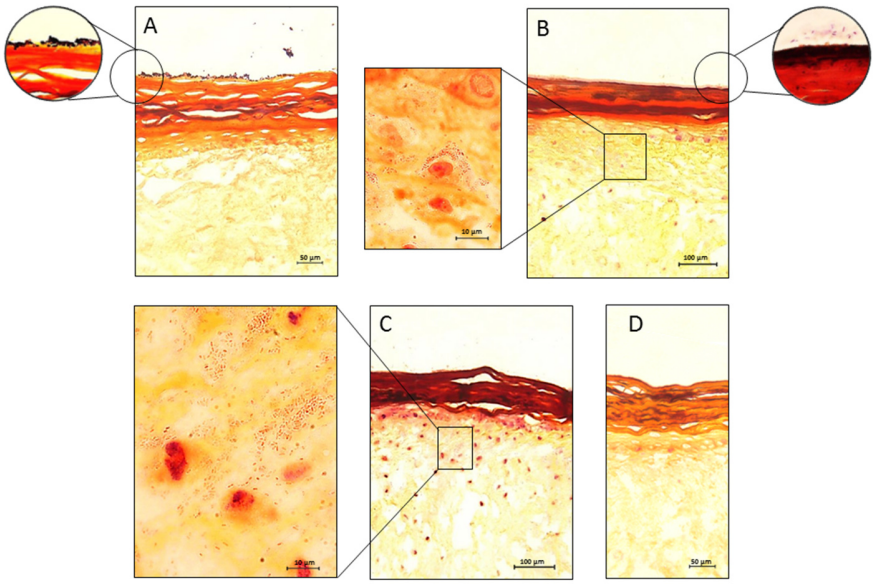


**Supplementary Figure S3.** Gram staining of tissue sections of models colonised (A) with *M. luteus*, (B) *P. oleovorans*, (C) a mixture thereof and an untreated control (D). All samples were collected at day 8.

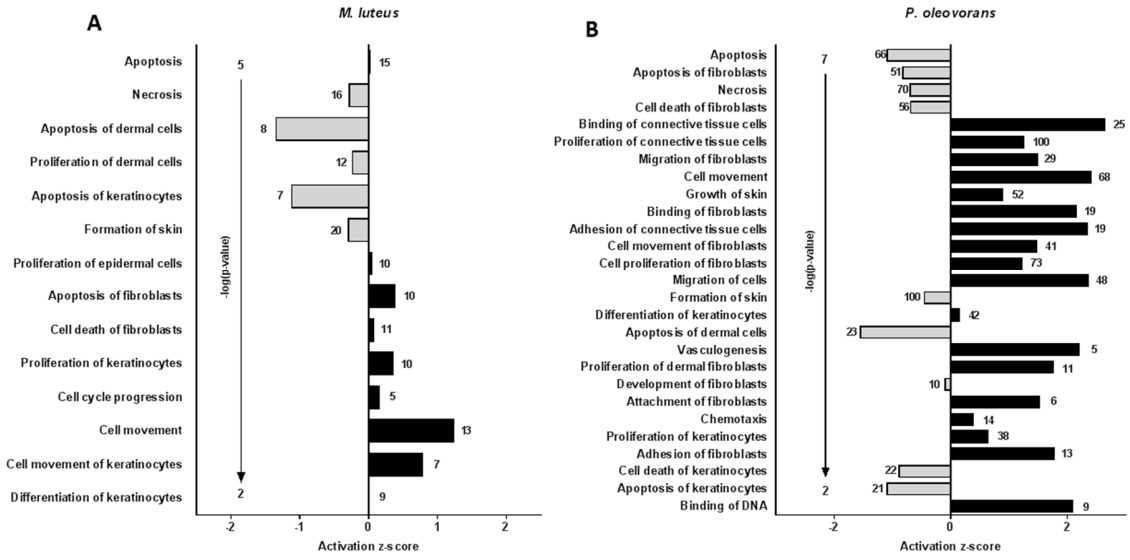


**Supplementary Figure S4.** Functional IPA-analysis of skin models colonised with (A) *M. luteus* and (B) *P. oleovorans*. The activation Z-score indicates an increase or decrease of the corresponding transcriptional pools, with the number of affected transcripts quoted next to each bar.

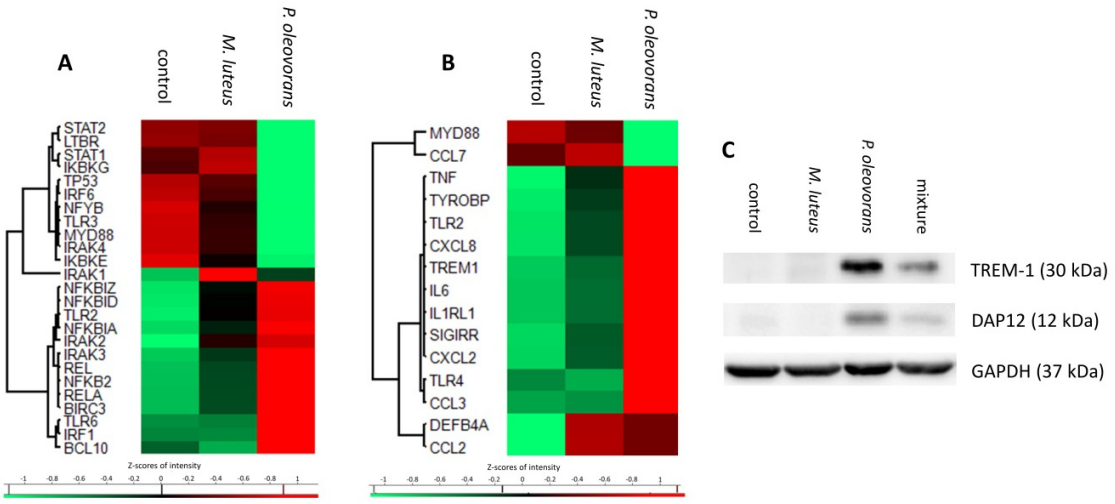


**Supplementary Figure S5.** Transcriptional cluster maps of the NFκB pathway (A) and TREM-signalling related genes (B) in microbially competent skin models at day 8 of microbial colonisation. Shown are the gene symbols and Z-scores of significantly differentially expressed genes with an F-value < 0.05 across three independent experiments. (C) Exemplary shown is an immunoblot of total protein of microbially competent skin models, colonised as indicated.

| | *P. oleovorans* | | *M. luteus* | |
|---|---|---|---|---|
| **Gene Symbol** | **Fold Change** | **P-value** | **Fold Change** | **P-value** |
| AC171558.1 | 1.79 | 0.0069 | 1.28 | 0.2808 |
| OMP | 2.01 | 0.0064 | 1.01 | 0.9862 |
| OR1A1 | 2.01 | 0.0430 | 1.27 | 0.1219 |
| OR1E1 | 1.45 | 0.0324 | 1.07 | 0.9323 |
| OR1F1 | 2.16 | 0.0269 | 1.36 | 0.3600 |
| OR1J4 | 2.79 | 0.0011 | 2.03 | 0.0428 |
| OR1N1 | 1.7 | 0.0040 | 1.32 | 0.0523 |
| OR1N2 | 1.76 | 0.0036 | 1.35 | 0.1463 |
| OR1S1 | 2.02 | 0.0423 | 1.25 | 0.6662 |
| OR2A7; ARHGEF34P | -1.58 | 0.0209 | -1.37 | 0.1797 |
| OR2A25 | 1.68 | 0.0312 | 1.09 | 0.7259 |
| OR2AP1 | 1.79 | 0.0141 | 1.4 | 0.1018 |
| OR2J2 | 2.42 | 0.0048 | 1.02 | 0.8699 |
| OR2M3 | 1.73 | 0.0376 | 1.3 | 0.7766 |
| OR2M4 | -1.65 | 0.0422 | -2.22 | 0.0178 |
| OR2T2 | 1.84 | 0.0086 | 1.23 | 0.8239 |
| OR2T4 | 1.87 | 0.0076 | -1.11 | 0.7499 |
| OR2T27 | 2.19 | 0.0046 | 1.18 | 0.6003 |
| OR2T35 | 1.71 | 0.0227 | -1.07 | 0.7544 |
| OR2V2 | 2.2 | 0.0093 | 1.3 | 0.2170 |
| OR2Y1 | 2.04 | 0.0089 | 1.93 | 0.0898 |
| OR3A4P; OR3A5P | 1.85 | 0.0042 | 1.46 | 0.0552 |
| OR4A16 | 1.71 | 0.0483 | 1.06 | 0.9652 |
| OR4C3 | 2.68 | 0.0010 | 1.45 | 0.2553 |
| OR4C45 | 1.73 | 0.0433 | 1.11 | 0.6251 |
| OR4D2 | 2.23 | 0.0102 | 1.37 | 0.2484 |
| OR4E2 | 1.78 | 0.0488 | 1.19 | 0.7440 |
| OR4F3 | 1.12 | 0.2879 | -1.75 | 0.0158 |
| OR4F5 | 1.69 | 0.0190 | -1.03 | 0.9798 |
| OR4F15 | 1.85 | 0.0356 | 2.23 | 0.0979 |
| OR4K15 | 1.16 | 0.6018 | -1.31 | 0.0398 |
| OR4M2 | 1.08 | 0.4247 | 1.21 | 0.0474 |
| OR4M2; AC171558.2 | 1.69 | 0.0340 | 1.29 | 0.2340 |
| OR4P4 | 2.39 | 0.0039 | 1.07 | 0.8226 |
| OR4Q3 | 1.88 | 0.0016 | 1.09 | 0.5529 |
| OR4X1 | 1.42 | 0.0404 | -1.05 | 0.9860 |
| OR5AK2 | 1.82 | 0.0408 | -1.19 | 0.6512 |
| OR5AP2 | 1.75 | 0.0258 | 1.33 | 0.2311 |
| OR5AS1 | 1.46 | 0.0164 | 1.04 | 0.6689 |

| | | | | |
|---|---|---|---|---|
| OR5H1 | 1.56 | 0.0268 | 1.17 | 0.3041 |
| OR5H6 | 1.72 | 0.0280 | 2.06 | 0.0264 |
| OR5M1 | 2.01 | 0.0037 | -1.02 | 0.9225 |
| OR5M8 | 2.04 | 0.0266 | 1.3 | 0.1823 |
| OR5M9 | 1.7 | 0.0064 | 1.1 | 0.5617 |
| OR5P2 | -15.8 | 3.74E-05 | -2.41 | 0.0324 |
| OR5P2 | -5.84 | 0.0005 | -3.27 | 0.0114 |
| OR5P3 | -2.01 | 0.0061 | -2.02 | 0.0203 |
| OR5P3 | -4.15 | 0.0012 | -1.68 | 0.1121 |
| OR5R1 | 1.15 | 0.1591 | -1.39 | 0.0376 |
| OR6C3 | 2.5 | 0.0207 | 1.73 | 0.2329 |
| OR6C70 | 1.37 | 0.0417 | 1.3 | 0.1876 |
| OR6K2 | 3.28 | 0.0098 | 1.08 | 0.5145 |
| OR6K6 | -1.25 | 0.3533 | -1.38 | 0.0405 |
| OR6M1 | 1.56 | 0.0226 | 1.03 | 0.7031 |
| OR6Q1 | 3.35 | 0.0008 | 1.18 | 0.4992 |
| OR6X1 | 2.31 | 0.0008 | 1 | 0.9155 |
| OR7A5 | 1.95 | 0.0044 | 1.04 | 0.7636 |
| OR7E24 | 2.97 | 0.0018 | 1.56 | 0.3432 |
| OR7G1 | 1.98 | 0.0011 | 1.32 | 0.1336 |
| OR8B3 | -1.51 | 0.3317 | -2.07 | 0.0181 |
| OR8B12 | 1.8 | 0.0098 | 1.72 | 0.1877 |
| OR8S1 | 1.78 | 0.0098 | 1.18 | 0.2960 |
| OR9A2 | 2.04 | 0.0204 | 1.19 | 0.3365 |
| OR9G4 | 1.56 | 0.0263 | -1.01 | 0.3899 |
| OR9I1 | 1.99 | 0.0101 | 1.14 | 0.5733 |
| OR9Q1 | 4.89 | 0.0002 | -1.2 | 0.7552 |
| OR9Q2 | 5.09 | 1.37E-05 | -1.58 | 0.0379 |
| OR10AC1 | 1.76 | 0.0034 | -1.09 | 0.7708 |
| OR10C1 | 1.9 | 0.0087 | 1.14 | 0.5509 |
| OR10J4 | 1.84 | 0.0145 | 1.23 | 0.1774 |
| OR10S1 | 1.61 | 0.0212 | 1.13 | 0.4626 |
| OR12D1 | 1.85 | 0.0085 | 1.19 | 0.6590 |
| OR13A1 | 1.69 | 0.0344 | -1.02 | 0.7281 |
| OR14C36 | 1.5 | 0.0111 | -1.58 | 0.3706 |
| OR51E2 | 1.52 | 0.0332 | -1.03 | 0.9894 |
| OR51F1 | 1.51 | 0.0221 | -1 | 0.6906 |
| OR51H1 | 2.28 | 0.0081 | 1.15 | 0.4326 |
| OR51L1 | 1.61 | 0.0348 | 1.9 | 0.1414 |
| OR52E1 | -2.08 | 0.0386 | -1.6 | 0.0463 |
| OR52E2 | 1.94 | 0.0044 | 1.08 | 0.7729 |
| OR52H1 | 1.65 | 0.0644 | 1.63 | 0.0200 |

| | | | | |
|---|---|---|---|---|
| OR52N5 | 1.66 | 0.0223 | 1.23 | 0.2946 |
| OR52R1 | 1.61 | 0.0265 | 1.25 | 0.1126 |
| OR56A1 | 1.83 | 0.0389 | 1.99 | 0.0909 |

**Supplementary Figure S6**. List of olfactory receptors for which co-colonisation led to altered gene expression. Shown are fold changes relative to the control and the respective p-values. Upregulated genes are highlighted in red and downregulated genes in green ($p < 0.05$).

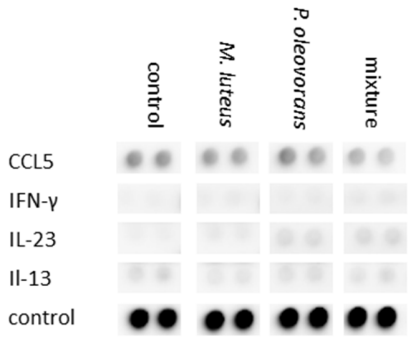


**Supplementary Figure S7.** Cytokine excretion of THP-1 cells treated with day 8-supernatant from microbially competent skin, colonised as indicated.

# Annex III

# Supplementary Data

## Commensal-related changes in the epidermal barrier function lead to alterations in the benzo[a]pyrene metabolite profile and its distribution in 3D-skin

**Lisa Lemoine**, Dilan Bayrambey, Alexander Roloff, Christoph Hutzler, Andreas Luch & Tewes Tralau

This chapter was published on 28 September2021:

mBio. 2021 Oct 26;12(5):e0122321

DOI: 10.1128/mBio.01223-21

Link: https://doi.org/10.1128/mBio.01223-21

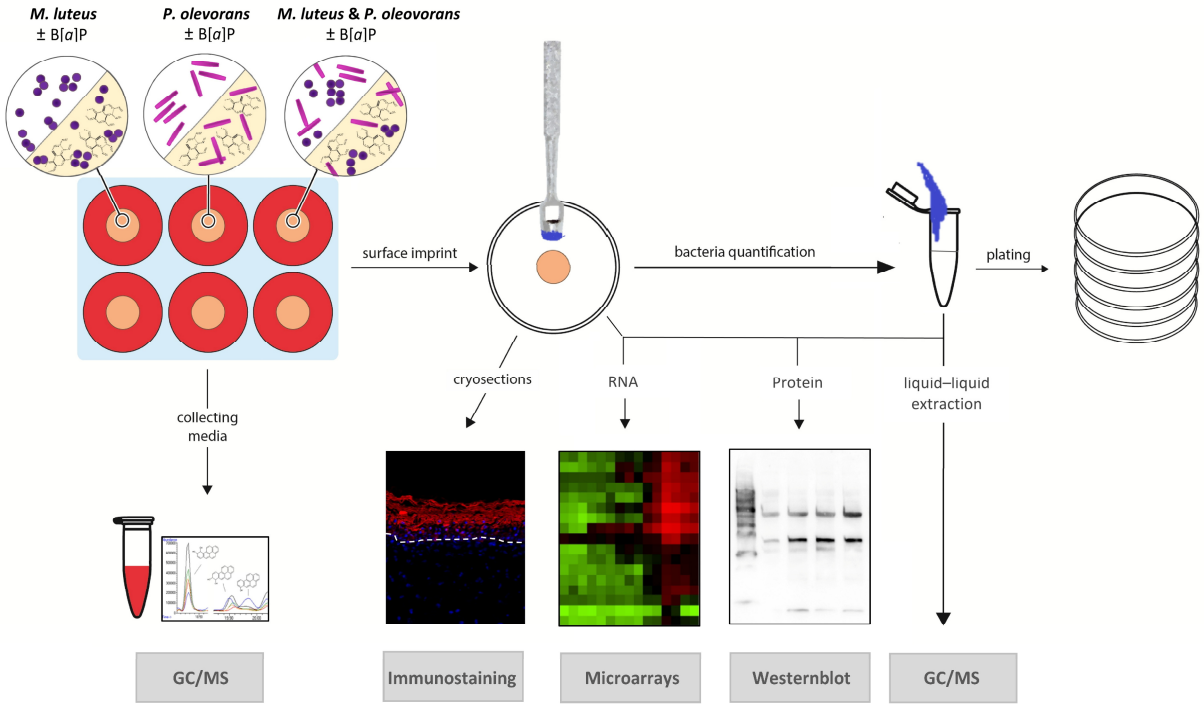


**Supplementary Scheme S1.** The experimental setup and study design. A surface imprint for bacterial quantification as well as for chemical analysis and the examination of the skin models themselves took place on day 8 of cultivation. Sampling of the medium, on the other hand, was done daily.

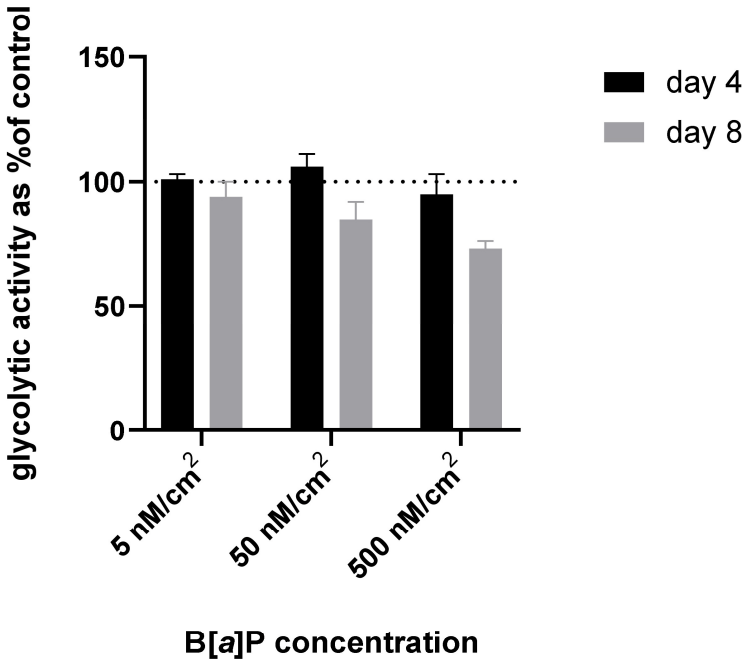


**Supplementary Fig. S1.** Glycolytic activity of MatTek`s EpiDermFT™ after 4 and 7 days of B[*a*]P application (3D-skin was treated with 3 different B[*a*]P concentrations as indicated).

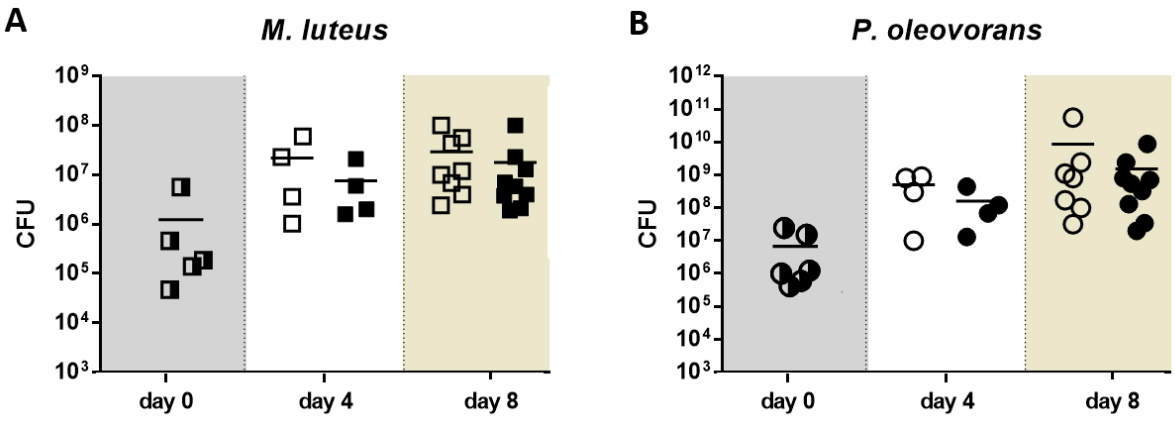


C

| Spezies / CFU | T0 | ± [%] | T4 | ± [%] | T8 | ± [%] |
|---|---|---|---|---|---|---|
| *M. luteus* | 4.87E+05 | 185 | 3.07E+07 | 156 | 1.22E+07 | 133 |
| *P. oleovorans* | 1.97E+05 | 116 | 2.65E+08 | 71 | 5.69E+09 | 124 |
| *M. luteus* + B[*a*]P | 4.87E+05 | 185 | 9.57E+06 | 123 | 6.89E+06 | 193 |
| *P. oleovorans* + B[*a*]P | 1.97E+05 | 116 | 2.60E+08 | 99 | 2.62E+09 | 187 |



**Supplementary Fig. S2.** Plate counts of skin models on day 0, 4 and 8 of bacterial colonization with and without B[*a*]P treatment. The individual points show the cell counts of one microbial skin tissue co-culture each for *M. luteus* (A) and *P. oleovorans* (B). The horizontal bars show the median of all measured values. The mean values of the plate counts of the mixed co-culture (C) are shown in a table with a range of variation in %. The respective plate counts on day 0 serve as starting culture for all co-cultures with and without subsequent B[*a*]P treatment.

A

silylated derivative of the 8-hydroxy-benzo[*a*]pyrene

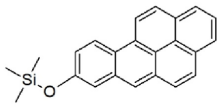

Formula Weight: 340.1 g/mol

Molecular Formula: $C_{23}H_{20}OSi$

di-silylated derivative of the 7,8-dihydroxy-benzo[*a*]pyrene analogon of the benzo[*a*]pyrene-7,8-dione

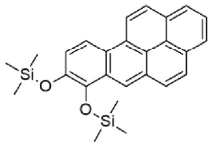

Formula Weight: 428.2 g/mol

Molecular Formula: $C_{26}H_{28}O_2Si_2$

di-silylated derivative of the benzo[*a*]pyrene-7,8-dihydrodiol

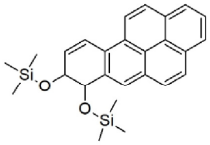

Formula Weight: 430.1 g/mol

Molecular Formula: $C_{26}H_{30}O_2Si_2$

tetra-silylated derivative of the benzo[*a*]pyrene-7,8-9,10-tetrahydrotetrol

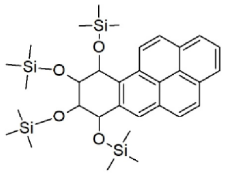

Formula Weight: 609.0 g/mol

Molecular Formula: $C_{32}H_{48}O_4Si_4$

tetra-silylated derivative of the benzo[*a*]pyrene-7,8-9,10-tetrahydrotetrol

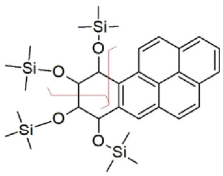

$C_{24}H_{28}O_2Si_2$
404.1628 Da

Dominant fragment peak (404.1 m/z)

B

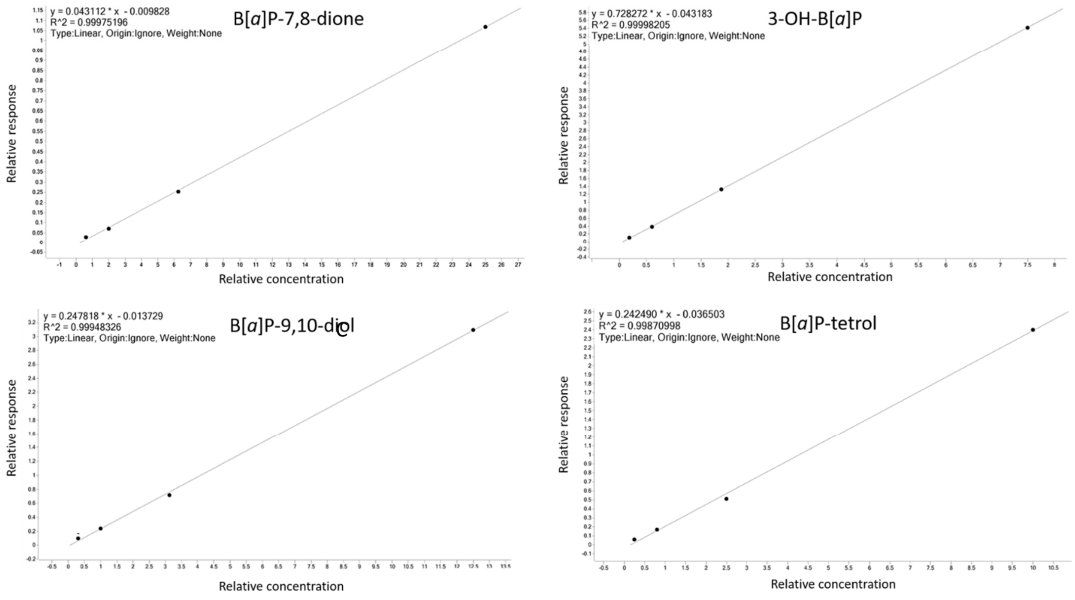

**Supplementary Fig. S3.** Structural formulas, molecular weights and calibration curves of all investigated substance classes (OH-B[*a*]P, B[*a*]P-diol, B[*a*]P-dione and B[*a*]P-tetrol). Structural formulas and molecular weights of representative metabolites formed during derivatization with BSTFA (*N,O*-bis(trimethylsilyl)-trifluoracetamide) for GC/MS analysis. Shown are the respective silylated compounds (A). For B[*a*]P-tetrol, the dominant fragment formed upon cleavage during ionization is also shown (A). Calibration curves from epidermis treated with external standards are shown as examples (B). Each analyte was quantified in relation to the assigned internal standard (IS) (see Table 1). For the epidermis and dermis, a four-point calibration was performed for cost reasons (matrix calibration). For the medium, an eight-point calibration was conducted.

A

| Substance | rt [min] | Quantifier [m/z] | Qualifier [m/z] | Concentration [nM] |
|---|---|---|---|---|
| **3-OH-B[*a*]P** | 20.2 | 340 | 341 | 385 |
| **7-OH-B[*a*]P** | 19.8 | 340 | 341 | 29 |
| **8-OH-B[*a*]P** | 20.4 | 340 | 341 | 255 |
| **9-OH-B[*a*]P** | 20.1 | 340 | 341 | 53 |
| **X-OH-B[*a*]P*** | 20.5 | 340 | 341 | Nq. |
| **B[*a*]P-1,6-dione** | 21.5 | 428 | 429 | 63 |
| **B[*a*]P-7,8-dione** | 21.7 | 428 | 429 | 2043 |
| **B[*a*]P-7,10-dione** | 20.8 | 428 | 429 | 894 |

*** According to its mass spectrum this substance corresponds to a hydroxylated benzo[*a*]pyrene (OH-B[*a*]P) but the retention time does not match any of the available reference substances (Supplementary Fig.S7C).**

Not quantified = Nq

B

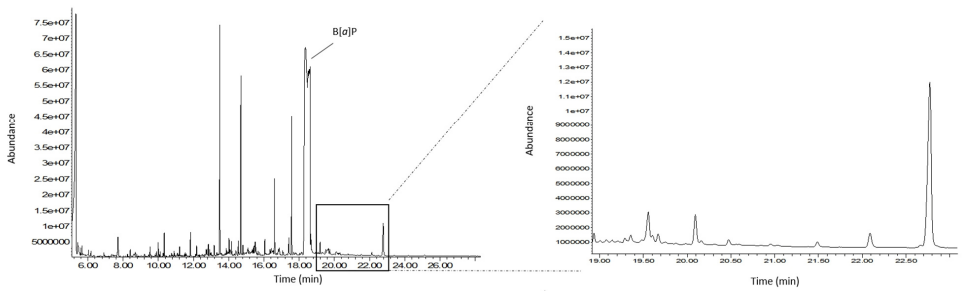


C

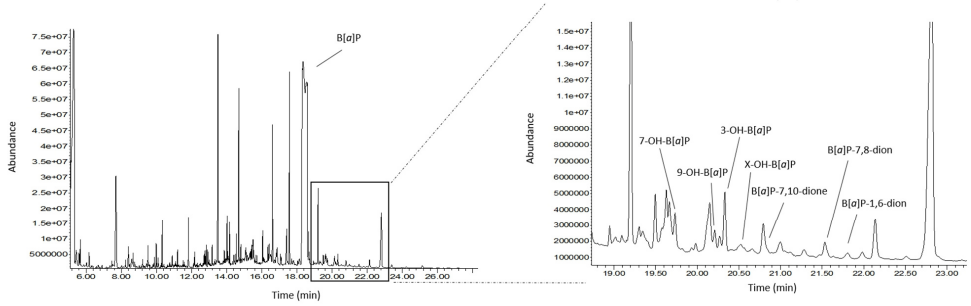


D

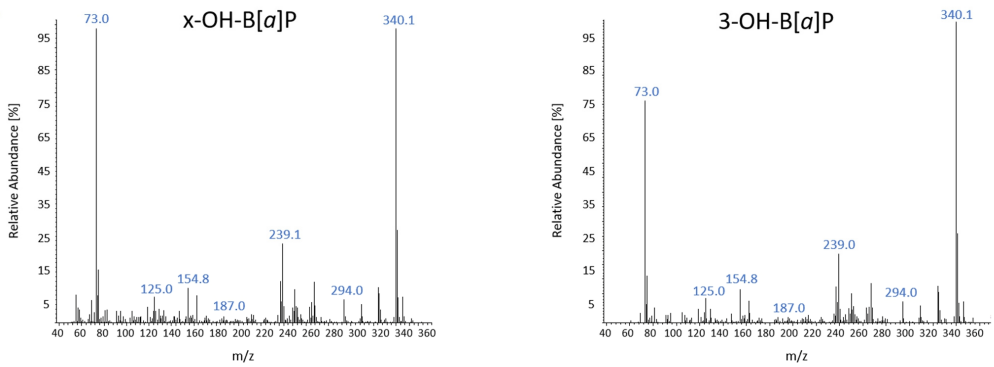

**Supplementary Fig. S4:** The B[*a*]P metabolites of *P. oleovorans*. Presented are the metabolites determined by GC/MS with the respective retention time (rt/min), together with quantifier and qualifier ions and the corresponding concentrations (A). GC/MS chromatograms and corresponding full-scan mass spectra of control (medium with 100 µM B[*a*]P) (B) and metabolites formed by *P. oleovorans* on day 5 of cultivation (C). Mass spectra of the unknown X-OH-B[*a*]P (20.5 min) and (D) the corresponding mass spectrum of the standard compound 3-OH-B[*a*]P (20.2 min).

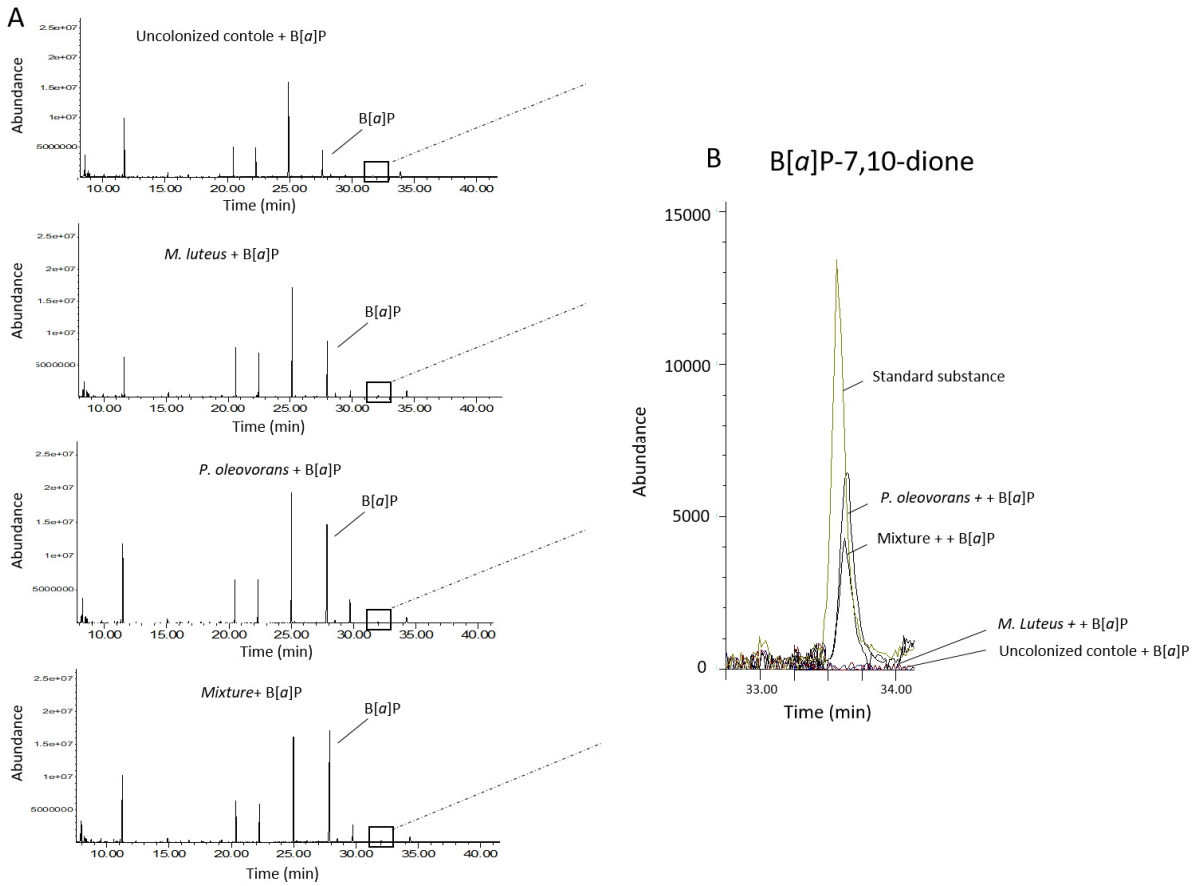


**Supplementary Fig. S5.** GC/MS chromatograms of the surface imprint of co-cultures colonized as indicated and control (A). GC/MS ion chromatograms of m/z = 428 indicating metabolically formed B[*a*]P-7,10-dione from *P. oleovorans* (B).

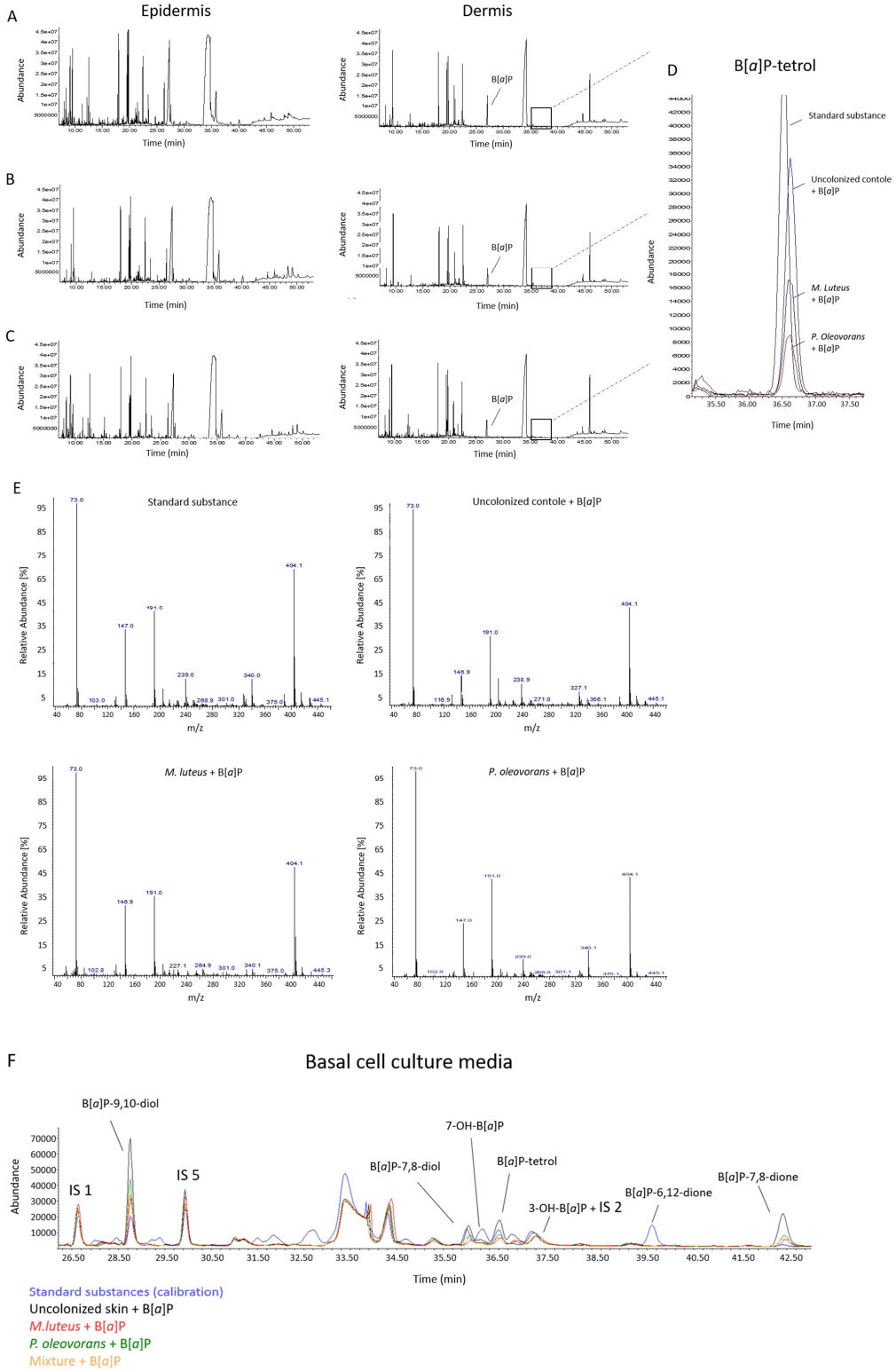
A
Epidermis
Dermis
B[a]P
Abundance
Time (min)
B
C
D
B[a]P-tetrol
Standard substance
Uncolonized contole
+ B[a]P
M. Luteus
+ B[a]P
P. Oleovorans
+ B[a]P
E
Standard substance
Uncolonized contole + B[a]P
M. luteus + B[a]P
P. oleovorans + B[a]P
Relative Abundance [%]
m/z
F
Basal cell culture media
B[a]P-9,10-diol
IS 1
IS 5
B[a]P-7,8-diol
7-OH-B[a]P
B[a]P-tetrol
3-OH-B[a]P + IS 2
B[a]P-6,12-dione
B[a]P-7,8-dione
Standard substances (calibration)
Uncolonized skin + B[a]P
M.luteus + B[a]P
P. oleovorans + B[a]P
Mixture + B[a]P

**Supplementary Fig. S6.** GC/MS chromatograms of the colonized skin models and the basal cell culture medium. Chromatogram of the uncolonized skin treated with B[*a*]P (A), the *M. luteus* (B) and the *P. oleovorans* co-culture (C) on day 8 of cultivation of the epidermis and the dermis. GC/MS ion chromatograms of m/z = 404 indicating metabolically formed B[*a*]P-tetrol. Mass spectra of B[*a*]P-tetrol (36.7 min) injected as analytical standard and extracted from the co-cultures from the dermis (E). GC/MS chromatograms of the basal cell culture medium (F) spiked with standard substances (calibration mixture), of the uncolonized skin treated with B[*a*]P, the *M. luteus* co-culture, the *P. oleovorans* co-culture and the mixed co-culture on day 8 of cultivation. Shown is a section of the superimposed chromatogram from 26.50- 42.50 min. The internal standards (IS) are numbered according to Table 1.

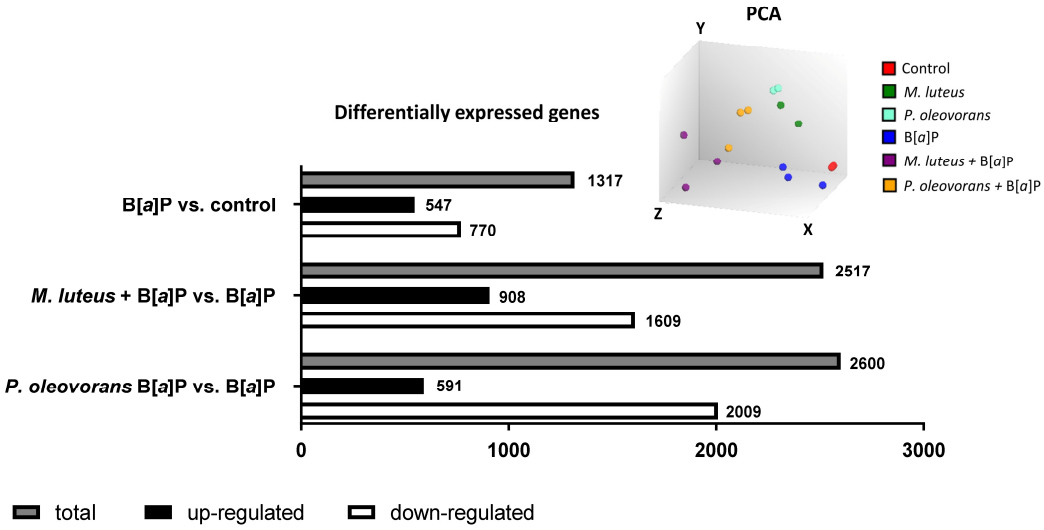


**Supplementary Fig. S7.** Number of differentially expressed genes in skin colonized with *M. luteus*, *P. oleovorans* and their mixture after B[*a*]P application compared to B[*a*]P treatment alone. Additionally the transcriptional response of EpiDermFT™ models on day 8 of microbial colonization with and without B[*a*]P application. Mapping 76.3 % of the available transcripts PCA shows separation of all terms of co-cultivation and controls with and without B[*a*]P treatment.

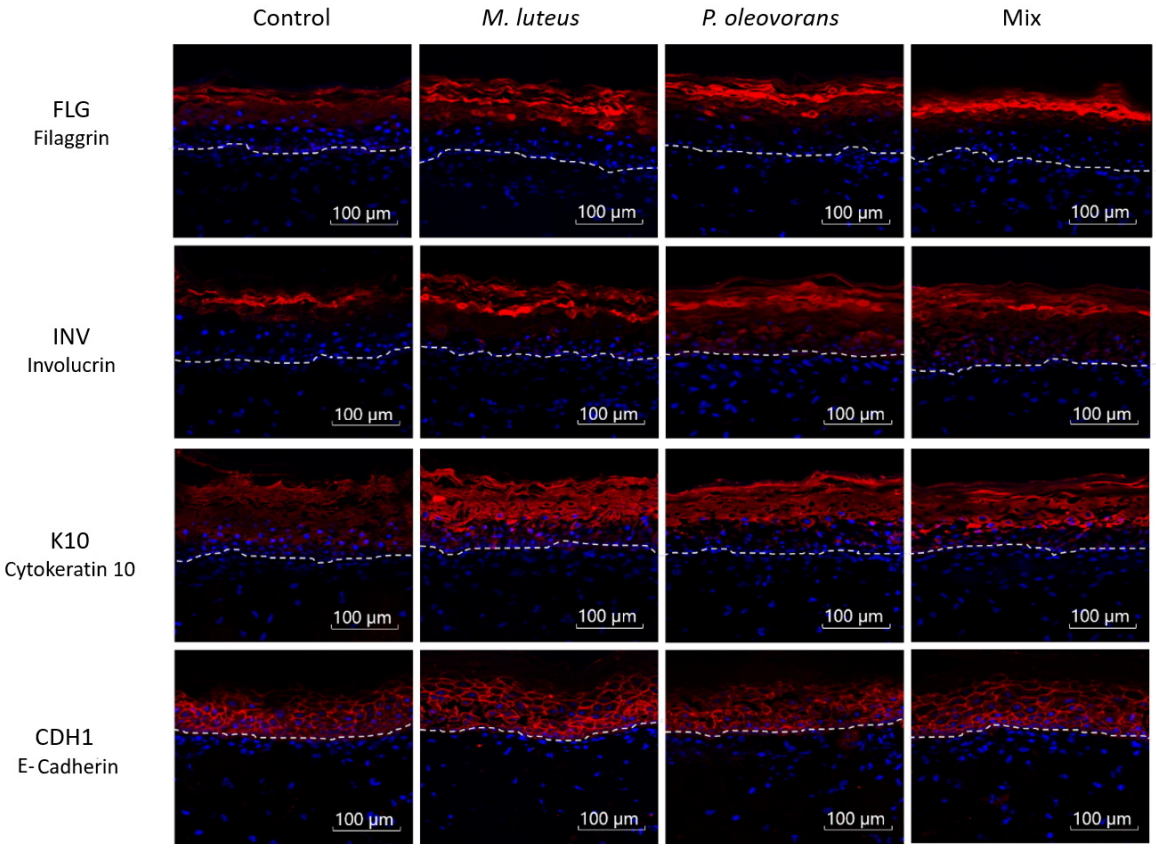


**Supplementary Fig. S8.** Expression of epidermal differentiation markers in microbial skin tissue co-cultures without B[*a*]P treatment. Exemplary shown is an immunostaining of selected differentiation markers and a tight junction marker of skin section of microbial competent skin models, colonized as indicated without B[*a*]P treatment.

**Supplementary Table S1:** B[*a*]P and its metabolites in microbial skin tissue co-culture. (A) Shown is the sum of the concentrations of B[*a*]P and its metabolites in nM excreted into the cell culture medium over the entire cultivation period of 8 days. (B) Amount of B[*a*]P and its metabolites as well as their sums in control tissue, *M. luteus* co-culture, *P. oleovorans* co-culture, and mixed co-culture, each treated with B[*a*]P, as a sum of all compartments (skin surface, epidermis, dermis, and cell culture medium) determined by GC/MS in pmol/skin model. In addition, the corresponding sums of the metabolite concentrations are given in parentheses as a percentage of the amonut of B[*a*]P applied throughout the cultivation period (350 nmol/skin model). Overall, the recovery rate of B[*a*]P and its metabolites relative to the amount of B[*a*]P applied ranged from 95 to 107 %. If a substance could not be detected this is indicated as *below the smallest measured concentration in the calibration* (bsc).

| **A** | **Control** | ***M. luteus*** | ***P. oleovorans*** | **Mixture** |
|---|---|---|---|---|
| **3-OH-B[*a*]P** | 85 | 46 | 55 | 42 |
| **7-OH-B[*a*]P** | 28 | 16 | 22 | 22 |
| **9-OH-B[*a*]P** | bsc | bsc | bsc | bssc |
| **B[*a*]P-1,6-dione** | 21 | 12 | 14 | 11 |
| **B[*a*]P-6,12-dione** | bsc | bsc | bsc | bsc |
| **B[*a*]P-7,8-dione** | 85 | 46 | 57 | 44 |
| **B[*a*]P-7,10-dione** | bsc | bsc | bsc | bsc |
| **B[*a*]P-7,8-dihydrodiol** | 94 | 54 | 91 | 66 |
| **B[*a*]P-9,10-dihydrodiol** | 368 | 206 | 299 | 235 |
| **B[*a*]P-tetrahydrotetrol** | 785 | 474 | 552 | 652 |
| **B[*a*]P** | 30 | 9 | 10 | 15 |

| **B** | **Control** | ***M. luteus*** | ***P. oleovorans*** | **Mixture** |
|---|---|---|---|---|
| **3-OH-B[*a*]P** | 3312 | 2483 | 2133 | 2897 |
| **7-OH-B[*a*]P** | 495 | 320 | 391 | 424 |
| **9-OH-B[*a*]P** | 241 | 225 | 224 | 175 |
| **B[*a*]P-1,6-dione** | 1075 | 1149 | 1340 | 732 |
| **B[*a*]P-6,12-dione** | 861 | 1212 | 1490 | 1318 |
| **B[*a*]P-7,8-dione** | 2710 | 3681 | 3665 | 3812 |
| **B[*a*]P-7,10-dione** | bsc | bcs | 16 | 21 |
| **B[*a*]P-7,8-dihydrodiol** | 1819 | 1314 | 1624 | 1354 |
| **B[*a*]P-9,10-dihydrodiol** | 2572 | 1530 | 2160 | 1719 |
| **B[*a*]P-tetrahydrotetrol** | 5018 | 3084 | 3564 | 4164 |
| **B[*a*]P** | 315624 | 333168 | 345966 | 359401 |
| **Sum** | 333727 | 348165 | 362575 | 376018 |
| **% of applied quantity** | 95 (5.2) | 99 (4.3) | 104 (4.7) | 107 (4.7) |